

https://dspace.org/

Reconstructing locomotor behaviour of Southern African plio-pleistocene cercopithecoids: evidence from functionally-related inner structural arrangement of the trabecular bone

Babutsi, Mosarwa

2023-07

University of the Witwatersrand, Johannesburg

https://hdl.handle.net/10539/42414

Babutsi, Mosarwa. (2023). Reconstructing locomotor behaviour of Southern African plio-pleistocene cercopithecoids: evidence from functionally-related inner structural arrangement of the trabecular bone. [Master's dissertation, University of the Witwatersrand, Johannesburg]. https://hdl.handle.net/10539/42414

Downloaded from a DSpace repository. https://dspace.org/



UNIVERSITY OF THE
WITWATERSRAND,
JOHANNESBURG

RECONSTRUCTING LOCOMOTOR BEHAVIOUR OF SOUTHERN AFRICAN PLIO-PLEISTOCENE CERCOPITHECOIDS: EVIDENCE FROM FUNCTIONALLY-RELATED INNER STRUCTURAL ARRANGEMENT OF THE TRABECULAR BONE

by

Mosarwa Babutsi

(2186441)

ORCID NO: 0000-0001-8341-787X

A dissertation submitted in fulfilment of the requirements for the degree of

Master of Science

in

Palaeontology

in the Faculty of Science, University of the Witwatersrand, Johannesburg, South Africa

Supervisors: Dr Bernhard Zipfel, Dr Amélie Beaudet, Dr Kudakwashe Jakata

16th August 2023

Table of contents

Declaration……1

Abstract……2

Acknowledgement……3

Chapter 1: Introduction……4

1.1 Southern African sites and their cercopithecoids yield ……4

1.2 Rationale of the study……6

1.3 Aim of the study……7

1.4 Hypothesis……7

Chapter 2: Background information……8

2.1 Chronological and geological context……8

2.2 Taxonomic context ……10

2.3 Ecology of extant cercopithecoids……14

2.4 Locomotor behaviour of extant Cercopithecoids……15

2.5 Anatomical framework……16

2.6 Trabecular bone adaptation and functional variation……18

Chapter 3: Materials and method……21

3.1 Materials……21

3.1.1 Fossil specimens ……21

3.1.1.1 Sterkfontein……22

3.1.1.2 Swartkrans ……24

3.1.1.3 Makapansgat ……25

3.1.1.4 Bolt's Farm……25

3.1.1.5 Taung ……25

3.1.2 Extant specimens……26

3.2 Methods……27

3.2.1 Scanning ……27

3.2.2 Reconstruction ……28

3.2.3 Virtual separation of two specimens……29

3.2.4 3D surfaces alignment……..…30
3.2.4.1 Orientation of femoral heads…….....31
3.2.4.2 Orientation of proximal tibia……33
3.2.4.3 Orientation of calcaneus.……...……...…34
3.2.4.4 Orientation of humerus……...…….....35
3.2.5 Virtual segmenting sedimented specimens……...…...…36
3.2.6 Extraction of homologous 2D sections……36
3.2.7 Extraction of homologous volumes of interest (VOI)……..…….…...38
3.2.8 Quantitative analysis of 3D volume…….42
3.2.9 Statistical analysis……...….45
Chapter 4: Results……...…….46
4.1 Description of specimen's external morphologies…….……..……46
4.1.1 Femora…….…….……...…….46
4.1.2 Humeri…….…….……65
4.1.3 Tibiae…….……...68
4.1.4 Calcanei..…….....71
4.2 Description of homologous 2D sections……..75
4.2.1 Femoral…….…….……..…75
4.2.2 Humeral……....……...92
4.2.3 Tibiae…….....95
4.2.4 Calcanei……98
4.3 Result of trabecular bone volumes of interest ……..….104
4.3.1 Fabric anisotropy……...….104
4.3.2 Volume fraction……...……...…110
4.3.3 Bone thickness……....……114
4.3.4 Bone spacing…….….116
Chapter 5: Discussion and conclusion……..…….……120
5.1 Trabecular bone organisations in 2 dimensions and functional interpretations...120
5.2 Trabecular bone organisations in 3 dimensions and functional interpretations...123
5.3 Reconstruction of the palaeoenvironment and palaeohabitats in the Cradle of Humankind World Heritage site…….126
5.4 Inferences and implications for human evolution……..…..128
7.6 Conclusion……...….128

References…….……..……...……....130
Annexture……..……..…….....144
Table A1: Extant femoral heads structural parameters……..144
Table A2: Extant calcanei structural parameters…….……..…….145
Table A3: Extant tibiae structural parameters……146
Table A4: Extant humeri structural parameters……147
Table A5: Fossil femoral heads scan resolutions……...……148
Table A6: Fossil calcanei, humeri and tibiae scan resolutions……...149
Table A7: Extant femoral heads resolutions……..150
Table A8: Extant humerus tibia, and calcaneus resolutions……...150
Table A9: Research budget……....151

Lists of figures

Figure 1.1: location map of study area…….....….6
Figure 2.1: Trabecular and cortical bone……...……...…17
Figure 3.1: Representation of fossil specimens….……...…...….22
Figure 3.2: Nikon XTH/225L CT scanner……..…….28
Figure 3.3: Centre of rotation and beam hardening……...……...29
Figure 3.4: Separating simultaneously scanned specimens…….....…30
Figure 3.5: Landmarking femur eroded head head……..……32
Figure 3.6: Femur head with Landmarks on head and neck contact……...…32
Figure 3.7: Landmarked femur head with ortho slice…….……..…...33
Figure 3.8: Orientation of tibia…….……. ……34
Figure 3.9: Orientating calcaneus specimen within global axes and grids…….34
Figure 3.10: Anterior and posterior view of humerus within global axes and grids ...…..…..35
Figure 3.11: Segmenting sedimented specimens……...…….….36
Figure 3.12: Extracting mediolateral 2D section in femur head……..…….……...37
Figure 3.13: Extracting anteroposterior 2D section in femur head……..…….……...37
Figure 3.14: Medial view of anteroposterior cross section of femur head with scale …….....38
Figure 3.15: Extracting volume of interest in femur head….……..……39
Figure 3.16: Extracting volume of interest with coordinates……..…….39
Figure 3.17: Recording coordinates on humerus head …...……..……...40
Figure 3.18: Volume of interest extracted in different facets of tibia…..…….…….……..40

Figure 3.19: Extracting volume in calcaneus……..…….41
Figure 3.20: Neutral angle of calcaneus……..……...……...…41
Figure 3.21: Adjusting thresholds in ImageJ……..…..……43
Figure 3.22: Calculating trabecular bone volume fraction ……...……...……44
Figure 3.23: Calculating bone thickness and spacing…...…….……..……...44
Figure 4.1: External morphology of 14954M……....……..…..….46
Figure 4.2: External morphology of 16383M ……..……..…….47
Figure 4.3: External morphology of SWP 526……...……48
Figure 4.4: External morphology of SWP 528……...……49
Figure 4.5: External morphology of SWP 529…….……...……50
Figure 4.6: External morphology of SWP 531……...……..…51
Figure 4.7: External morphology of SWP 532……....52
Figure 4.8: External morphology of SWP 533……....53
Figure 4.9: External morphology of SWP 747……....53
Figure 4.10: External morphology of SWP 749……...…...54
Figure 4.11: External morphology of SWP 753……...……...…....55
Figure 4.12: External morphology of SWP 756……...…….....55
Figure 4.13: External morphology of SWP 1009……...……...……..56
Figure 4.14: External morphology of SWP 1011……..……...……...……....57
Figure 4.15: External morphology of SWP 1203……...……...……..57
Figure 4.16: External morphology of SWP 1384…….……...…….....58
Figure 4.17: External morphology of SWP 1698……...……...……..……....59
Figure 4.18 External morphology of SWP 1699……..……..…….....59
Figure 4.19: External morphology of Sts 2050…….……..……....60
Figure 4.20: External morphology of Sts 2259…….……..……....61
Figure 4.21: External morphology of SK 605...…….……...…….....61
Figure 4.22: External morphology of SK 607…….……....….....62
Figure 4.23: External morphology of SK 1513.…….……...……...……...63
Figure 4.24: External morphology of SK 2595…….....63
Figure 4.25: External morphology of Sk14015……...…….....64
Figure 4.26: External morphology of BF 36…….……..…....65
Figure 4.27: External morphology of 1930M…..…….……..……....65
Figure 4.28: External morphology of 1934M……...……..……..…….....66

Figure 4.29: External morphology of SWP 606……...……...66
Figure 4.30: External morphology of SWP 962…….……...……...……...67
Figure 4.31: External morphology of SWP1406……..……...68
Figure 4.32: External morphology of SWP 1141…….……...……...68
Figure 4.33: External morphology of SWP 1546…….……...…...……69
Figure 4.34: External morphology of SWP 1596..…….……...…….....70
Figure 4.35: External morphology of TP 18…….……...…….....70
Figure 4.36: External morphology of 2222M…….……...…...….....71
Figure4.37: External morphology of SWP 537…….……...….....72
Figure 4.38: External morphology of SWP 1146…….……...…….....72
Figure 4.39: External morphology of 1157……..…….……...……....73
Figure 4.40: External morphology of 1161……..……...……...…….....74
Figure 4.41: External morphology of SWP 1207……...…….……...……...….....75
Figure 4.42: Internal structure of 14984M…….……...…….……..76
Figure 4.43: Internal structure of 16383M…….……...…….…….....76
Figure 4.44: Internal structure of SWP 526……...……...……...……..77
Figure 4.45: Internal structure of SWP 528……...…….…..78
Figure 4.46: Internal structure of SWP 529…….……...…..…..78
Figure 4.47: Internal structure of SWP 531…….……...……..79
Figure 4.48: Internal structure of SWP 532…...……...……...…..……..80
Figure 4.49: Internal structure of SWP 533……...……...……...……...……..80
Figure 4.50: Internal structure of SWP 747……...……...……...……...…81
Figure 4.51: Internal structure of SWP 749……...……...……...……...……....82
Figure 4.52: Internal structure of SWP 753…...……...……...……....……..82
Figure 4.53: Internal structure of SWP 756……...……...……...……....……..83
Figure 4.54: Internal structure of SWP 1009……....……...……...……...……84
Figure 4.55: Internal structure of SWP 1011…...……...……...……....…84
Figure 4.56: Internal structure of SWP 1203……..……...……...……...…….85
Figure 4.57: Internal structure of SWP 1384……...……...……...…….86
Figure 4.58: Internal structure of SWP 1698..……...……...…….86
Figure 4.59: Internal structure of SWP 1699..……...……...…….87
Figure 4.60: Internal structure of Sts 2050…..…….……...…….……87
Figure 4.61: Internal structure of Sts 2259…..……...……...……...…..……88

Figure 4.62: Internal structure of Sk 605…..……..……..……...……89
Figure 4.63: Internal structure of Sk 607……..……..……..…..…….89
Figure 4.64: Internal structure of Sk 1513..……..……..……...…….90
Figure 4.65: Internal structure of Sk 2595…..……..……..……..…….91
Figure 4.66: Internal structure of Sk 14015....……..……..…….91
Figure 4.67: Internal structure of Bf 36..……..……..……..……..….92
Figure 4.68: Internal structure of 1930M..……..…...……..……...…93
Figure 4.69: Internal structure of 1934M…....……..…...……..……93
Figure 4.70: Internal structure of SWP 962..……..……..……..…...…….94
Figure 4.71: Internal structure of SWP 606..……..……..……..……94
Figure 4.72: Internal structure of SWP 1406..……..……..……...….95
Figure 4.73: Internal structure of SWP 1546……..……....……...….95
Figure 4.74: Internal structure of SWP 1596..……..…..……..…..…….....…….96
Figure 4.75: Internal structure of SWP 1411……..…….....…….97
Figure 4.76: Internal structure of TP 18..……..……..……...…….....…..….97
Figure 4.77: Internal structure of 2222M.……..……..…...…….....……98
Figure 4.78: Internal structure of SWP 537..……..……..……....…….99
Figure 4.79: Internal structure of SWP 1146……..……..……....…….99
Figure 4.80: Internal structure of SWP 1157……..……..……..…….....…100
Figure 4.81: Internal structure of SWP 1161..……...……..……..…….....……101
Figure 4.82: Internal structure of SWP 1207..…….…….....101
Figure 4.83: Box plot of fossil vs extant femoral heads fabric anisotropy …..……....105
Figure 4.84: Box plot of fossil vs extant calcanei fabric anisotropy …..……...……....107
Figure 4.85: Box plot of fossil vs extant proximal tibiae fabric anisotropy ……..……...….109
Figure 4.86: Box plot of fossil vs extant humeri heads fabric anisotropy..…….…..…….110
Figure 4.87: Box plot of fossil vs extant femoral heads bone volume fraction…....…...….111
Figure 4.88: Box plot of fossil vs extant calcanei volume fraction…….... …..…….…...….112
Figure 4.89: Box plot of fossil vs extant humeri heads volume fraction.…..…...…….113
Figure 4.90: Box plot of fossil vs extant proximal tibiae volume fraction……..…….…….114
Figure 4.91: Box plot of fossil vs extant femoral heads trabecular thickness …..……...….115
Figure 4.92: Box plot of fossil vs extant calcanei trabecular thickness….....……...….116
Figure 4.93: Box plot of fossil vs extant femoral heads trabecular bone spacing …..….....117
Figure 4.94: Box plot of fossil vs extant calcanei trabecular bone spacing……..…..……..118

Figure 5.1: Partially and fully sedimented femoral heads……..…..…….……...121
Figure 5.2: Vertical and arcuate bundles in femur head……..…..…….…...121

List of tables

Table 2.1: Summary of cercopithecoids taxa found in the study area …….……...…...13

Table 2.2: Summary of most quantified trabecular bone structures ……...……..…18

Table 3.1: Sites and material abbreviations ……..…....…21

Table 3.2: Materials from Sterkfontein…..……...…….……...…...23

Table 3.3: Materials from Swartkrans cave ……..…….…..24

Table 3.4: Materials from Makapansgat……..…….25

Table 3.5: Materials from Bolt's Farm…….……25

Table 3.6: Materials from Taung buxton limeworks……25

Table 3.7: Individual extant skeletons…….……...……...……...……26

Table 3.8 Calculated size and position of volume of interest...…….…….…….31

Table 3.9: Calculated bone structural properties…….……...……..……....42

Table 4.1: Summary of fossil specimens with extracted 2D and 3D volumes…….....102

Table 4.2 : Measured parameters in fossil and extant femoral heads……..……..…….105

Table 4.3: Fossil calcanei trabecular bone and mean extant parameters.....106

Table 4.4: Fossil proximal tibiae trabecular bone with extant parameters……..…..…....106

Table 4.5: Fossil proximal humeri trabecular bone with extant mean parameters……108

Table 4.6: Summary of fossil vs extant specimens trabecular bone parameters…….…..…119

Declaration

I declare that this dissertation is my own original and unaided work. It is being submitted for the Degree of Master of Science in Palaeontology at the University of the Witwatersrand, Johannesburg. This work has not been submitted before for any degree or examination at any other University or publication.

Mbabutsi

16th day of August 2023 at Johannesburg, South Africa

ABSTRACT

Because of their abundance in African Plio-Pleistocene hominin-bearing sites and their stratigraphic association with fossil hominins, cercopithecoids represent a relevant "control group" for contextualising hominin evolution. often considered as ecological and biochronological indicators, particularly their ecological sensitivity is valuable in reconstructing southern African hominin bearing site's palaeoenvironment and environmental changes. Since biomechanical loadings on trabecular bone produced throughout locomotor activities shape the structure of the skeleton, particularly at locomotor key joints, the expectation is that investigation of the trabecular bone of fossil cercopithecoids key joints like femur, humerus, Tibia and calcaneus would provide further evidence for eloquent discreet disparity in their locomotor behaviour and reconstructing their paleohabitats. This study used trabecular bone, described as meshwork or sponge with porous network within long bones joints and inside footbones contains red bone marrow. Its preferred orientation in is the basis of Wolff's law, relating bone structures and its ability to adapt to mechanical load alignment in the direction of loading stress, as such recoding informative locomotor signals.

Forty one (41) fossil cercopithecids from the Cradle of Humankind World Heritage sites that include Sterkfontein, Swartkrans, Makapansgat, Taung and Bolt's Farm as well as forty (40) extant cercopithecoids specimens were scanned using a micro-focus X-ray computed tomography (CT) scanner. Trabecular bone parameters that include trabecular bone fabric anisotropy, volume fraction, thickness and spacing were quantified in ImageJ. These Plio-Pleistocene cercopithecoids recorded more arboreal locomotor signals with occasional terrestrial locomotion, suggesting transitional palaeoenvironment from long trees with cool climatic conditions to a more open grass land savanna type with dry climatic conditions believed contributed significantly to extinct of archaic humans and the emergence of the successful *Homo*

Acknowledgements

I would like to acknowledge the following organisations and people for making this study successful; my supervisors, Dr Bernhard Zipfel, Dr Amélie Beaudet and Dr Kudakwashe Jakata for making this research successful by advising and guiding me throughout the research stages. The Ditsong Natural History Museum particularly, Miriam Tawane for giving me permission to access and loan some of fossil specimens. Evolutionary Studies Institute (ESI) collection manager Dr. Sifelani Jirah for accessing fossils and extant collection of monkeys and ultimately loaning for scanning. The South African Nuclear Energy Corporation (NECSA) especially Dr. Frikkie de Beer and Jakobus Hoffman for allocating beam time and scanned extant specimens. Wits Medical school, in particular Dr Brendon Billings and Dr Nicholas Bacci for allowing access into Dart collection and loaning me extant specimens for scanning. A special thank you to Mr Gideon Chinamantira of ESI who played critical role in scanning fossil specimens. This is because he managed to do scanning while he was an MSc students in ESI and sacrificed his time to make this research a success.

I would also like to acknowledge Palaeontological Scientific Trust (PAST) for sponsoring a trip to the University of Cambridge, United Kingdom to go and develop some of my methodology there as well as the University Cambridge for allowing me to use their facilities. Centre of Excellence in Palaeosciences (COE) sponsored trips to Pretoria as well as scanning trips NECSA in Phelandamba. ESI research coordinator Dr Shaw Badenhorst for guiding me in all administration related to my research. A sincere and special thank you to Botswana government through the Department of National Museum and Monuments in the Ministry of Environment and Tourism for giving me study leave as well as funding this study as well as the Botswana Consulate in Pretoria for financial and motivational support.

CHAPTER 1 - INTRODUCTION

1.1 Southern African sites and their cercopithecoids yield

The late Pliocene and early Pleistocene southern African hominins sites, which age about 3.7-2.0 Million years ago (Ma) (Freedman, 1960; Granger *et al*, 2015) are extensively known to have yielded a large fossil assemblage that documents substantial taxonomic diversity in hominins (Gear, 1926; Freedman 1960, 1961, 1976; Vrba, 1975; Brain, 1981; McKee, 1993). The discovery of *Australopithecus africanus* by Dart in 1924, played a critical role in our understanding of early hominins evolution (Dart, 1925). This is so because several researchers (e.g Gear, 1926; Broom, 1938; Broom and Robinson 1947) showed interest in understanding hominin evolution and the emergence of the genus *Homo.*

Apart from hominins, southern African hominin sites yielded a large number of fossil cercopithecids commonly known as Old World monkeys. The fossil remains are dominated by four fossil taxa (Parapapio broomi, Parapapio jonesi, Parapapio whitei, and Cercopithecoides williamsi) which are widely recognised in South Africa (Brain, 1981; McKee, 1993 Clarke, 2008; Wood and Boyle, 2016) and radiated in the Plio-Pleistocene (Bobe *et al*., 2002; Tosi *et al.*, 2005; Elton, 2007; Maslin *et al*., 2014). The significant radiation of cercopithecoids in southern Africa has been attributed to environmental changes during the Plio-Pleistocene, resulting in an intensification of grassland and open environment (Bobe *et al*., 2002; Tosi *et al.*, 2005; Elton, 2007; Maslin *et al*., 2014). This resulted in substantial diversity in both subfamilies, with several species that flourished in the Plio-Pleistocene not making it into the late Pleistocene and Holocene (Tosi *et al.*, 2005).

However, with hominin fossil remains being scarce at most of these sites, coupled with lack of extensive studies involving botanical remains and/or isotope analyses in southern Africa (notwithstanding crucial studies, e.g. Bamford *et al.*, 2010), the assessment of the influence of environmental changes in hominin evolution remains a challenging task. Therefore, the Old World monkeys (cercopithecoids), which represents a vital part of the Plio-Pleistocene ecosystem, represent as an excellent proxy for human evolution (Jablonski and Frost, 2010; Elton, 2001, 2006). Indeed, they share behavioural and ecological similarities with hominins as well as their geographical distribution (Elton, 2006). Although cercopithecoids are often

considered as a ‘control group for human evolution’ by palaeoscientists (Elton, 2006), to date, not much work has been done on fossil cercopithecid postcranial remains from a functional and palaeoenvironmental perspective (Ciochon, 1993; Elton, 2001). This can be tentatively explained by the focus on craniodental remains and the search for new species, (e.g. Gear, 1926; Freedman 1960, 1961, 1957; 1976; McKee, 1993; Gilbert *et al*., 2016).

Although studies like Ciochon (1993) and Elton (2001) used multivariate ecomorphic approach to determine locomotor behaviour and ultimately deduce the palaeoenvironment of cercopithecoids, a study focusing on quantifying trabecular bone is needed. Therefore trabecular bone quantifying studies such as that of Ryan and Walker (2010) have shown that reconstructions of locomotor behaviour of primates mostly depend on the hypothesis of the relationship of bone anatomy, biomechanical function, and the external loads generated during locomotor behaviour (according to the Wolff’s law; Wolff 1986, Ruff *et al.*, 2006). Preserved postcranial material, mainly represented by long bone shafts are limited by their fragmentary nature in the fossil record. Previous studies on extant and fossil primates have revealed that variation observed in trabecular pattern reflects function and relates to locomotion behaviour (Ketcham and Ryan, 2004; Gosman and Ketcham, 2009; Ryan and Walker, 2010). In this context, because of the close relationship between trabecular bone structure and locomotor behaviour, the expectation is that the investigation of functionally-related inner structural arrangement of the trabecular bone of fossil cercopithecoids will provide further evidence about their palaeohabitats and, ultimately, the environment they shared with contemporaneous hominins.

Therefore, the current study focuses on quantifying trabecular bone of cercopithecoids key locomotor joints in view of finding locomotor signals as shown on extant primates by Ketcham and Ryan (2004), Gosman and Ketcham (2009) and Ryan and Walker (2010). Highly aligned trabecular bone fabric anisotropy with compact (thick as well as denser and well connected) trabecular bone is closely associated with loading due to arboreal locomotion while less isotropic trabecular bone with less compact (thin, spaced and loosely connected) trabecular bone is associated with terrestrial locomotion, where the load is evenly distributed (Takechi,1977; Fajardo and Muller 2001; Fajardo *et al*., 2007, Ryan *et al*., 2018).

The study is conducted in five southern African hominin-bearing sites within the Cradle of Humankind World Heritage site, which include three sites of Sterkfontein caves, Swartkrans and Bolt's Farm in the main site, which are about 40 km southwest of Johannesburg as well as the two satellite sites (Limpopo's Mapansgat Limeworks and North West's Taung Buxton-Norlim Limeworks), which are approximately 250 km and 350 km from the main site respectively (Edwards *et al*, 2020). Figure 1.1 below illustrated positional relevant of satellite sites with respect to the main site. The sites are important in human evolution studies because they produced significant amount of fossil hominins as well as hominids.

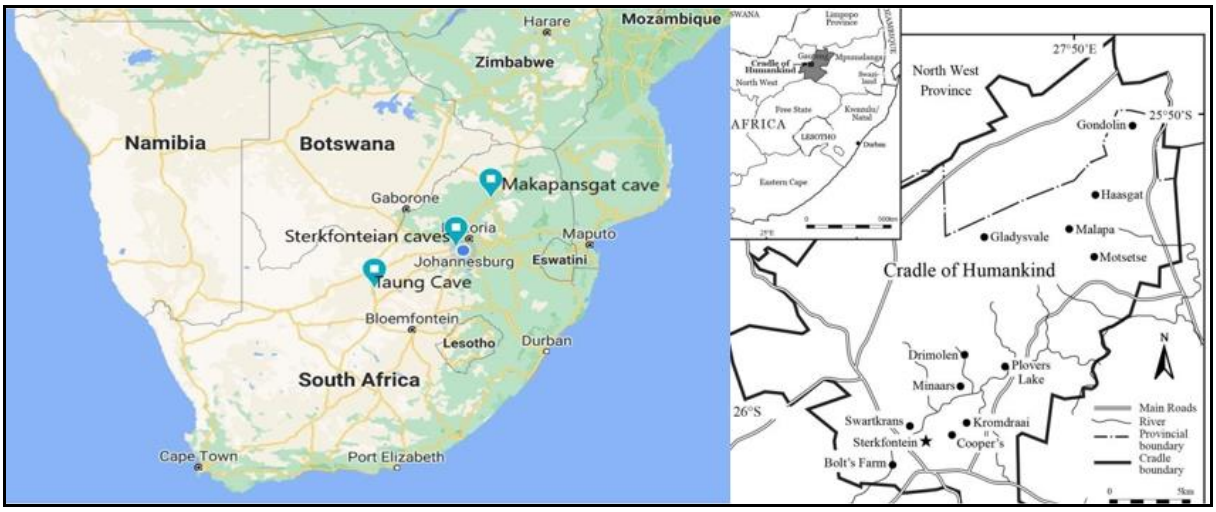

***Figure 1.1*:** Map of the study area **(**adapted from Stratford and Caruana, 2017).

1.2 Rationale of the study

The scarcity and fragmentary nature of hominin fossil remains in most southern Africa sites, as well as lack of isotope analyses resulted in the impact of environmental changes in hominin evolution not well understood. However, due to abundant cercopithecoids remains in these sites, they often preset an excellent proxy for human evolution (Jablonski and Frost, 2010; Elton, 2001, 2006). However, not much work has been done on fossil cercopithecid postcranial remains from a functional and palaeoenvironmental perspective (Ciochon, 1993; Elton, 2001).

It is against this background that this study used Trabecular bone struts in cercopithecoids postcranial and key locomotor joint in search of locomotor signal associated with their palaeoenvironment. Trabecular bone is described as a meshwork or sponge with porous network within long bones joints and inside footbones (Warwick and Williams, 1973; Sukhdeo at al.,

2020). It contains red bone marrow, responsible for producing blood cells (Oftadeh *et al*., 2015). Its preferred orientation in trabecular bone is the basis of Wolff's law, which relates trabecular bone structures and its adaptation to mechanical loading (Ruff *et al,* 2006). Trabecular bone volume fraction and the degree of anisotropy are among the most and usually quantified parameters in trabecular bone study, together with other variables that can provide more comprehensive evidence about variation in shape in trabecular bone (Odgaard *et al*., 1997).therefore, trabecular bone properties are informative for reconstructing locomotor activities and behaviours of extinct life forms (Ryan and Krovitz, 2006; Fajardo *et al*., 2007; Susan, 2018). Therefore, the orientation of trabecular bone struts in relation to the direction of stress has excited research interest and its successful qualitatively and quantitively will yield locomotor signal that will help us to understand hominin evolution by inferring their palaeoenvironment.

1.3 Aim of the study

The main aim of the study is to reconstruct Plio-Pleistocene palaeoenviroment of hominin sites in southern Africa using fossil cercopithecoids palaeo-locomotor behaviour recorded in their trabecular bone.

1.4 Hypothesis

The hypothesis is that quantitatively analysing the structural arrangement of the trabecular bone of cercopithecoid locomotor key joints will reveal functional signal that can be subsequently used to reconstruct locomotor repertoire and palaeohabitats of fossil cercopithecoids as well as the palaeoenvironment shared with hominins.

The hypothesis will achieved by exploring the following three main objectives:

1. To analyse trabecular bone textural and structural properties in key locomotor joints of the fossil cercopithecoids.
2. To functionally interpret the results.
3. To provide further understanding of the paleoenvironment of the Plio-Pleistocene cercopithecoids that coeval with hominins in southern Africa.

CHAPTER 2 - BACKGROUND INFORMATION AND LITERATURE REVIEW

2.1 The chronological and geological context

Most of southern African early hominin sites mostly developed within cave systems which are hosted in the Malmani Dolomite sequence of the Late Achaean (2.6-2.5-billion years) deposited in the intracratonic Transvaal Basin (Button, 1973; Rayner *et al,* 1993; Partridge, 2000). The deposit covers an area roughly 15 000 km and incorporates almost all of the early hominin sites in South Africa (Partridge, 2000).

The Sterkfontein cave deposits were initially divided into a series of six successive Members, from 1 to 6 (Partridge, 1978) but some studies (e.g. Pickering and Kramers, 2010) could not identify all members described by Partridge (1978). However, for this study, I will be dealing with fossiliferous Member 2, Member 4 and Member 5 (Pickering and Kramers, 2010; Granger *et al*., 2015), as opposed to all identified Members of the site because they yielded fossil materials that could be used for this study.

Member 2 consists of an upward fining deposit with dolomite blocks and secondary cave flowstones as well as fossilised primate and carnivore remains (Coke, 1938; Pickering and Kramers, 2010; Granger *et al*, 2015). Pickering and Kramers (2010) used U-Pb and UTh dating technique and dated Member 2 to 2.8-2.6 Ma while recently Granger *at al* (2015) dated Member 2 to 3.67 Ma using isochron burial dating with cosmogenic aluminium-26 and beryllium-10. Sterkfontein Member 4, which has yielded a relatively large number of hominin remains (McKee, 1993) when compared to East African hominin sites, suggest an age of 2.8-2.6 Ma, while Berger *et al,* (2002) used faunal interpretation with archeometric results as well as magnetostratigraphic results suggested a maximum age of 2.5 Ma. Pickering and Kramer (2010) suggested ages of 2.65-2.0 Ma from results of U-Pb and UTh dating technique. However, a more recent cosmogenic nuclide dating by Granger *et al*, (2022), places Sterkfontein Member 4 at 3.6-3.4 Ma, thus much older than previously thought. Sterkfontein Member 5 has moderately calcified strata with reddish-brown clastic fossiliferous deposits with less calcite and clastic material (Pickering and Kramers, 2010; Kuman and Clarke, 2000). This Member is famous for having yielded *Homo ergaster* and *Paranthropus* remains as well as Oldowan and Acheulean stone tools (Granger *et al*., 2015). Pickering and Kramers (2010) determined Member 5 to be less

than 2.0 Ma due to its stratigraphic position relative to member 4. This is corroborated by Granger *et al* (2015), which suggested that Member 5 is 2.0-1.7 Ma.

The deposits of Swartkrans are divided into five breccia components or members (Sutton *et al*., 2009). The current study concerns Member 1, that comprises two sub-units, the Hanging Remnant and Lower Bank (Brain, 1993b; Pickering *et al*., 2012). The significant and classification of these sub-units are thought to be mostly arbitrary since that the Hanging Remnant is an extension of the first deposited Lower Bank (Brain, 1993b; Gibbon *et al*., 2014). Member 1 is the oldest stratigraphic member at Swartkrans and consists of sandy silt with dolomite clasts, chert as well as several stone and artifacts (Brain, 1993b). Vrba (1975) analysed faunal remains at Swartkrans and suggested an age of 2.0-1.5million years while recently Gibbon *et al* (2014) used radiometric dating and suggested an age of 2.19-1.80 million years. However, Kuman *et al* (2021) dated Swartkrans Member 1 to an absolute 2.22 to million years, using an isochron burial dating technique (Kuman *et al*, 2021).

Taung is divided into four deposits, which include the fluvial and aeolian deposited Thabaseek Tufa, the pale reddish-brown to pink clay stone Norlim Tufa, the yellowish-red aeolian sandstone and as well as the siltstone Oxland Tufa and the massive manganese containing Blue Pool Tufa (Peabody, 1954; Marker, 1975; McKee and Kuykendall, 2016).

Though the *Australopithecus africanus* (Taung child) specimen was the first early hominin to be discovered on the continent (e.g. Dart, 1925; Haughton, 1925), the Taung site has been marred by different dates from several studies (e.g. Broom 1946; Peabody, 1954; Cooke, 1970; Freeman, 1970; Partridge, 1973; Delson 1988 and Tobias *et al*, 1993). However, with more studies and comparison with East African sites that were radiometrically dated the Taung site deposits are estimated to be about 2.3 million years old (Delson, 1988).

Makapansgat valley is situated in the Limpopo Provinceand many of its hominin remains were recovered from limework dumps (Partridge, 1982: Rayner *et al*., 1993). Accordingly, precisely infering the palaeodepositional environment of the Makapansgat valley is a challenging task. This site consists of five stratigraphic units called members (Maguire *et al*., 1985; Clad and Rayner, 1989).

The oldest Member 1 contained articulated skeletons in distal area and is dated to 4.19-3.7 Ma (Brook *et al*, 1977; Harries, 2003; Slogett, 2016) from palaeomagnetic investigation, magnetostratigraphy analysis and the review of paleoecological reconstructions respectively. Member 2 consists of silty loam, speleothem pieces, calcite pebbles together with localised bones (Slogett, 2016) with estimated ages of 3.33-2.8 Ma from palaeomagnetic results (Brook *et al*, 1977). Member 3 deposits are sandy silty loam grey breccia with calcite intergrowth, speleothem fragments, pebbles, coprolites and abundant faunal remains (Latham *et al*., 2007) and magnetostratigraphy Edward (dated it to 3.31-3.3 Ma old (Partridge, 2000). Member 4 is characterised by pink matrix supported breccia with dolomite clasts, as well as faunal remains (Latham *et al*., 2007). This Member comprises four stratigraphic units, called beds, with bed A and bed B having similar material to Member 3 but does not have many fossil bones. Patridge (1979) used lithostratigraphic analysis and dated Member 4 to 2.9 Ma (Partridge, 1979). The youngest Member 5 has five (5) beds named A, B, C, D and E. Beds A, B and D contain gravelly material while Bed C is less gravelly. Bed E has the least gravel, comprising mainly silt and loam (Partridge, 1979).

The Bolt's Farm site, situated about 3 km southwest of the Sterkfontein cave, comprises several depositional pockets (Cooke, 1991). Bolt’s Farm fossiliferous breccias are little darker when compared to pinkish Sterkfontein breccias. This makes them more similar in colour to those of Swartkrans and Kromdraai (Cooke, 1991). Edward (2020) when employed chronology combined with uranium (U-PB) together with palaeomagnetic results to date breccias of Bolt’s farm site date to about 3.03-2.61 Ma (Edward *et al*., 2020).

2.2 Taxonomic context

Cercopithecoids are a group of primates often referred to as Old World monkeys. Extant Old World monkeys are known to be the most successful non-human living primate family, thought to account for more than 25% of the living genera of primates (Disotell, 1996). They divided into two distinguished and recognised groups or subfamillies: Cercopithecinae and Colobinae (Disotell, 1996). These subfamilies differ in many aspects, chief among them is the specialised diet with colobinae being herbivorous (leave eating) while cercopithecinae are frugivorous (Disotell, 1996). This family of Old World monkeys include, among others, *Papio* (baboons) and *Macaca* (macaques) (Disotell *et al*., 1992; Disotell, 1996). African cercopithecoids have an

extraordinary fossil record, extending as back as the early and middle Miocene (Jablonski, 2002; Disotell, 1996), with significant contribution from southern African hominin sites.

Southern African hominin sites have produced a significant number of fossil cercopithecoids, including *Parapapio jonesi, Parapapio broomi, Parapapio whitei, Papio izodi, Papio angusticeps, Papio robinsoni, Papio spelaeus, Simopithecus darti, Simopithecus danieli, Cercopithecoides williamsi, Dinopithecus ingens, Procercocebus antiguus* and *Gorgopithecus major* (Freedman 1957; Gilbert *et al*., 2016). The most common of these are three morphologically similar papionin species *Parapapio broomi, Parapapio jonesi* and *Parapapio whitei,* together with the colobine species *Cercopithecoides williamsi*. Indeed, they are found in most southern African hominin sites (Gear, 1926; Freedman 1960, 1961, 1976; Brain, 1981; McKee, 1993).

Sterkfontein Members 2 and 4 yielded three *Parapapio* species (*Parapapio whitei, Parapapio broomi* and *Parapapio jonesi*), recovered from other southern African sites such as Taung, Swartkrans and Bolt's Farm (Brain, 1981; Mokokwe, 2016). *Parapapio broomi* remains were first noted by Jones (1937), while the two other species were discovered by Broom (1940) who concluded that the three closely related species, differing only in size, existed together at the same time in the Sterkfontein valley. This idea was supported by McKee (1991) based on evidence from the stratigraphy of the area, that the three lived concurrently at the same time. Of the three, *Parapapio whitei* is the largest while *Parapapio jonesi* is the smallest (McKee, 1991). Wilkinson (1983) recorded *Cercopithecoides williamsi* in Sterkfontein Member 4.

Although Sterkfontein Member 5 is known to have yielded a number of hominin remains and much less cercopithecoids, StW 53 infill has produced *Cercopithecoides williamsi* and *Theropithecus oswaldi* as well as unidentified *Papio, Parapapio,* and a colobin (Mokokwe, 2016).

Swartkrans Member 1 fossiliferous breccia contained remains of four widely known taxa, which are *Parapapio jonesi, Papio robinsoni, Theropithecus oswaldi* and *Dinopithecus ingens (*Broom, 1940; de Ruiter, 2003). All these remains were recovered in both Hanging Remnant and Lower Bank (de Ruiter, 2003).

The Taung site has produced specimens of *Parapapio antiquus* (Haughton, 1925), now known as *Procercocebus antiquus* (Gilbert *et al*., 2016), while Gear (1926) described the presence of *Papio izodi*. The presence of *Parapapio jonesi,* and *Parapapio whitei* is well documented by Freedman (1961), with McKee (1993) describing *Parapapio broomi* and *Cercopithecoides williamsi* as well at the Taung site.

Makapansgat Members 3 and 4 in Makapansgat valley produced a large number of *Parapapio broomi, Parapapio jonesi, Parapapio whitei, Cercopithecoides williamsi* and *Simopithecus darti* fossils (Freedman, 1960) while *Parapapio broomi, Papio robinsoni* and *Cercopithecoides williamsi*, were recovered from Bolt's Farm (Freedman, 1976; Fourie *et al*, 2008). Table 2.1 below summarises cercopithecoid taxa found from southern African hominin sites.

Table 2.1: Summary of cercopithecoids taxa found in the study area.

Taxon	**Site**	**Member**	**Reference**
Parapapio broomi	Bolt's Farm, Makapansgat, Sterkfontein, Taung	Makapansgat Members 3-4, Sterkfontein Members 2 & 4	Jones, 1937; Broom, 1940; Freedman, 1957; Brain, 1981; Mckee, 1993; Mokokwe, 2016.
Parapapio jonesi,	Makapansgat, Sterkfontein, Swartkrans, Taung	Makapansgat Members 3-4, Sterkfontein Members2 & 4, Swartkrans Member 1	Broom, 1940; Freedman, 1957, 1960; Brain, 1981; Fourie *et al*, 2008; Mokokwe, 2016.
Parapapio whitei	Makapansgat, Sterkfontein, Taung	Makapansgat Members 3-4, Sterkfontein Members 2 & 4	Broom, 1940; Freedman, 1957, 1960, 1961; Brain, 1981; Fourie *et al*, 2008; Mokokwe, 2016.
Papio robinsoni	Bolt's Farm, Swartkrans	Swartkrans Member 1	Jones, 1937; Broom, 1940; Freedman,1961; de Ruiter, 2003
Cercopithecoides willamsi	Bolt's Farm, Sterkfontein, Swartkrans Makapansgat Taung	Sterkfontein Members 2, 4, 5	Broom, 1940; Freedman, 1957, 1960; Fourie *et al*, 2008; McKee, 1993.
Cercopithecus	Sterkfontein	Sterkfontein,	Wilkinson, 1983; Mokokwe, 2016.
Theropithecus oswaldi	Swartkrans, Sterkfontein 5	Swartkrans 1	Broom, 1940; de Ruiter, 2003.
Dinopithecus ingens	Swartkrans	Swartkrans 1	Broom, 1940; de Ruiter, 2003.

Papio izodi	Taung		Gear, 1926.
Procercocebus antiquus	Taung		Gilbert *et al*., 2016.

2.3 Ecology of extant cercopithecoids

Most extant cercopithecoids are found in Africa and Asia, with Barbary Macaques of Gibraltar being the only European native. They are known to occupy an array of environments such as tropical rain forests, savannahs, shrub lands and mountainous territories (Morbeck, 1977; Disotell *et al*, 1992; Disotell, 1996; Elton, 2001, 2007; Jablosnki and Frost, 2010). This trait is recognisable in their early evolutionary history (Elton, 2007). However, they are particularly biased to open terrestrial and seasonal terrain (Jablonski, 2002). Extant cercopithecoids are known to be quadrupedal and can be further classified as arboreal quadrupedal (e.g. colobus monkeys) and terrestrial quadrupedal (e.g. baboons) (Rose,1973).

Southern African cercopithecoids are believed to have mainly radiated due to a surge in grassland and open habitats in Pleistocene environment (Elton, 2006). However, reconstruction of the palaeohabitats in southern African hominin sites is problematic, mainly due to the fossil localities which are primarily in calcareous outcrops of the Malmani Subgroup (Button, 1973). Studies of plant remains (e.g. Bamford *et al*., 2010) recovered remains of *Podocarpus* (*Afrocarpus*) in a coprolite recovered in Malapa site in Cradle of Humankind World Heritage site and dated to 2 Ma. Extant *Podocarpus* species are known to occur in areas of high rainfall, suggesting that the southern African Plio-Pleistocene hominin sites were characterised by Afromontane Forest like with cool and wet conditions (Mckee, 1991; Bamford *et al*., 2010).

Furthermore, the southern African sites have yielded a significant number of *Parapapio* species and more particularly *Parapapio jonesi (*Broom, 1940; Brain, 1981; de Ruiter, 2003), which is thought to be ancestral to modern *Papio* (McKee, 1991). The characteristics of *Parapapio* skeleton indicate an adaption to a broad ranging palaeoenvironment such as savanna and open woodland (Eisernhart, 1974). Some studies (e.g. Elton, 2001) suggests that unlike its extant form, *Cercopithecoides williamsi* was more terrestrial than arboreal. Therefore, this suggest an open savanna type of environment.

In her 2001 paper, Sarah Elton used a multivariate ecomorphic approach and divided cercopithecoids postcranial material Cradle of Humankind World Heritage sites (particularly Sterkfontein, Bolt' s Farm and Swartkrans) to three locomotor classes and habitat preferences. Although this was taxon less study, the result show that cercopithecoids post cranial material could be classified as arboreal quadrupedal, terrestrial quadrupedal and arboreal with occasional terrestrial locomotion. Arboreal locomotion associated with thick forest with tall trees and terrestrial locomotion is attributed to open grassland environment, while mix locomotion is associated transition from thick forest to open grassland (Elton 2001).

Isotopic studies (e.g. Bamford, 1999; Dupont, 2006; Bamford *et al*, 2010) involving analyses of Plio-Pleistocene fossilised micro plant remains. Dupont (2006) and Bamford *et al* (2010) when working on *Podocarpus/Afrocarpus species* concluded that since extant *Podocarpus* species thrive well in cool and wet climatic conditions, the vegetation should have been thicket forest cover with long tress during the Plio-Pleistocene epoch (Bamford, 1999; Dupont, 2006). Bamford *et al* (2010) analysed fossilised *Anastrabe integerrima* as well as *liana Dichapetalum ct. mombuftense* suggested a cooler and moist palaeoenvironment with large trees that offered physical support for liana to climb (Bamford, 1999).

2.4 Locomotor behaviour of extant Cercopithecoids

For us to properly reconstruct locomotor behaviour of Plio-Pleistocene cercopithecoids, we have to examine at the locomotor behaviour of their extant genera. Various studies on locomotion of extant cercopithecoids (e.g., Rose, 1973; Elton, 2001) shows that extant Old Word Monkeys are characteristically quadrupeds. Even though they spent considerable amount of time on terrestrial quadrupedalism locomotion (e.g. *Papio species*), particularly in social activities but often involved in arboreal quadrupedalism when foraging for food and sleeping (Schmidt., 2011). Terrestrial cercopithecoids are those that spend most of their time foraging on the ground and climb up trees for resting or when they want to sleep, such as baboons and mangabeys (Rose, 1973; Elton, 2001, 2007). Thus, most of the time, both their forelimbs and hindlimbs are in contact with the substrate (ground).

The idea that arboreal cercopithecoids climb up trees when looking for food and sleeping is consistent with Rose (1973) that extant cercopithecoids are closely linked to arboreal

quadrupedalism, employing all their fore and hind limbs and supporting themselves when walking on tree branches. These monkeys spend most of their time on branch postural activities, mainly in sitting postures of suspensory behaviour and are known for their incredible leaping capabilities (Morbeck, 1977; Disotell, 1996; Elton, 2001). In fact, Morbeck (1977) described the leaping capabilities of arboreal monkeys as long leaps in which the animal they land first with their forelimbs before hindlimbs could contact substrate. An example is the extant *Chlorocebus* and *colobine*, which are particularly famous for spending much of its time climbing trees (Schmidt, 2011). Arborealism tends to lead to forelimbs specialised in grasping and attaining branches while hindlimbs propel the monkey in motion (Rose, 1973).

2.5 Anatomical framework

There are two types of bone tissues found in the skeleton of vertebrates, i.e., elastic and spongy trabecular bone, and the hard and compact cortical bone as illustrated by figure 2.1 below (Cowin, 2001; Barak *et al*., 2008; Oftadeh *et al*., 2015; Susan, 2018; Sukhdeo *et al*., 2020). Trabecular bone is spongy with numerous pores, and this makes it weaker, resulting in it being more prone to fracture than the cortical bone (Oftadeh *et al*., 2015). Trabecular bone is a meshwork or sponge work of bony trabeculae (Warwick and Williams 1973), consisting of a porous network found within long bones, joints and inside footbones (Warwick and Williams, 1973; Sukhdeo *at al*., 2020).

Trabecular bone contains red bone marrow, which is responsible for producing blood cells (Oftadeh *et al*., 2015). Susan (2018) described trabecular bone as compartments with 20% being bone and the rest being space that is filled with bone marrow and fat, with mosaic of interlocked macroscopic structure mosaic successions of rods and plates which lacks osteonal structures but tend to have preferred orientations (Susan, 2018). The preferred orientation is the basis of Wolff's law, which relates trabecular bone structures and its adaptation to mechanical stress or loading (Ruff *et al*, 2006).

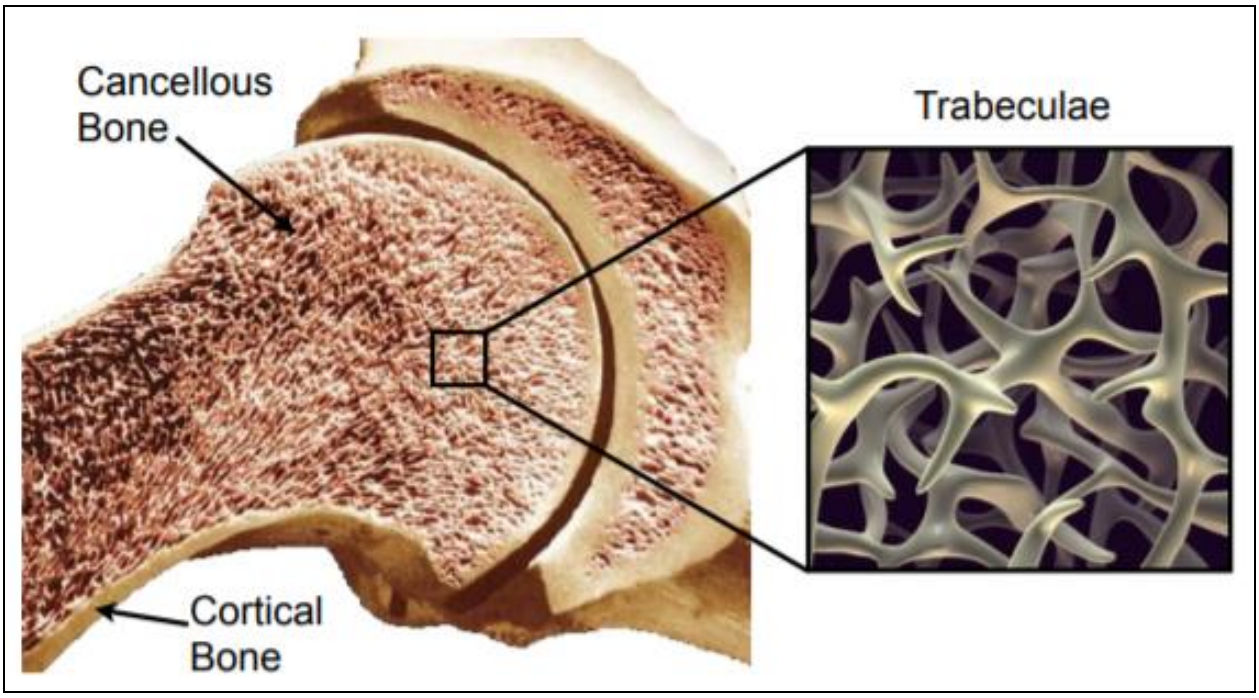

***Figure 2.1*:** An illustration of trabecular (cancellous) bone within cortical bone (Cardiff, 2012).

Trabecular bone architecture is considered isotropic when their strands are randomly orientated with no preferred orientation but are anisotropic when they have preferred orientation (Kuganenthira *et al*., 1996; Odgaard *et al*., 1997), and this degree of alignment is corelated with mechanical load in a certain direction (Odgaard *et al*., 1997). Trabecular bone volume fraction (BV/BT) or bone density and its degree of alignment (anisotropy) are the most informative traits of trabecular bone architecture (Odgaard *et al*., 1997). Therefore, trabecular bone volume fraction and the degree of anisotropy are among the most and usually quantified parameters in trabecular bone study, together with other variables that can provide more comprehensive evidence about variation in shape and trabecular architecture (Table 2.2). Trabecular bone in the femoral head is known to be involved in the load transfer from the joints to the cortex of long bones (Susan, 2018). Trabecular bone properties have been suggested to be particularly informative for reconstructing locomotor activities and behaviours of extinct life forms (Ryan and Krovitz, 2006; Fajardo *et al*., 2007; Susan, 2018). Therefore, the orientation of trabecular bone struts in relation to the direction of stress has excited research interest (Singh, 1978).

Since trabecular bone is spongy and elastic, its structural properties, as described by the trabecular bone volume fraction (BV/BT), trabecular bone fabric anisotropy (DA), trabecular

bone thickness (Tb.Th) and trabecular bone number (Tb.N) (Hodgkinson and Currey, 1990a, b), are believed to account for up to 94% of the variance in the elastic modulus of trabecular bone (Odgaard *et al*., 1997), which confirms that the mechanical behaviour of trabecular bone is mainly controlled by its 3 dimensional architectural arrangement (Cowin, 1997). Therefore, it is clear from these analyses that the arrangement of the 3D structure of trabecular bone exhibits vital and significant information about the elasticity of the structure and, by extension, the mechanical and functional adaptation of the bone to the loads exerted on them.

Table 2.2: Most quantified trabecular bone structures (Adapted from Saers *et al.,* 2019).

Trabecular bone structure	**Description**	**Abbreviation**	**Measurement units**
Trabecular bone volume	Ratio of bone volume to a total of volume of interest	BV/TV	%
Trabecular bone fabric anisotropy	Trabecular bone orientation.	DA	-
Trabecular bone thickness	Average thickness of trabecular bone	Tb.Th	mm
Trabecular bone spacing	Average distance between two trabecular struts	Tb.Sp	mm

2.6 Trabecular bone adaptation and functional variation

The external morphology of a skeleton used to be the main focus of interpretation of palaeofunction and reconstruction of behavioural aspect of an individual fossil specimen (Heiple and Lovejoy, 1971; Rose, 1988; Ward, 2002; Begun and Kivell, 2011). However, while the method provided invaluable information, it has some challenges such as separating phylogeny and function (Sukhdeo *et al*, 2020; Latimer and Lovejoy, 1989; Berger and Tobias, 1996; Ward, 2002; Begun and Kivell, 2011; Kivell, 2016). Therefore, trabecular bone structural arrangement provides us with an important proxy in interpreting and inferring the function and behavioural details of individual recorded during their lifetime (Ruff *et al*., 2006; Kivell, 2016; Barak *et al.,* 2017). This is because trabecular bone has the ability to adjust and adapt to mechanical loading

throughout the life of an individual (Cowin, 2001; Pearson and Lieberman, 2004; Ruff *at al*, 2006), a process which was described by Wolf (1892) but was later referred to as bone functional adaption (Ruff *at al*, 2006).

The idea that trabecular bone can adjust and record load history was however first discovered and published by Roux (Roux, 1881), who recognised that bone structures are capable of responding to confined mechanical stresses and that organisms are capable of adapting their bone structure to the new environment. It is these malleability properties that make its response to reflect loading history more important than cortical bone (Currey, 1968; Lovejoy *et al.,* 2003; Ruff *et al*., 2006).

Based on its variability, some studies like Cowen (2001) and Ruff *et al* (2006) were doubtful about this being a law. However, experimental studies have always documented a correlation of loads and trabecular bone orientation, particularly among primates (Barak *et al*., 2011). In their studies, Barak *et al* (2011) concluded that their results support Wolff's hypothesis that trabecular bone architecture actively adjusts to external stress generated by loading joints (Wolff, 1986, Barak *et al*, 2011).

Several studies have embarked on quantifying trabecular bone properties in primate bones to investigate parameters that can indicate adaptations to local mechanical stress, interpret locomotor signals and, ultimately, reconstruct their locomotor behaviours (e.g Ryan and van Rietbergen, 2005; Ryan and Krovitz, 2006; Ryan and Shaw, 2012). An example could be the study of Ryan and van Rietbergen (2005), which used computed tomography (CT) scanning to determine the mechanical significance of femoral head trabecular bone ion *Galago* and *Loris* and concluded that, notwithstanding substantial variation, general fabric anisotropy of trabecular bone seems to track locomotor behavioural differences. Another study which used the same method is the one of Ryan and Shaw (2012) which evaluated the relationship between inferred locomotor behaviour and trabecular bone structural features. It further characterise the bone architecture in extant primates and recorded fabric struts that reflect adaptation associated with different locomotor signals of human and non-human anthropoid (Ryan and Shaw, 2012).

Ryan and van Rietbergen (2005) found that the architecture of the trabecular bone in primate femoral heads vary along with the locomotor behaviour and these differences are associated with

bone remodelling (the process of bone or skeleton changes) Ryan and Walker (2010) utilised CT scan technology to quantify trabecular bone properties to determine locomotor signals in anthropoid primates. They investigated the effects of differences in the femoral head and humeral heads across taxa categorised by several locomotor behaviours and found that femoral trabecular bone was generally thicker, with higher volume fraction and high fabric anisotropy than humeral trabecular bone in all taxa examined. As such they concluded that trabecular bone of the femoral heads reflects higher forces acting on hip joint as a result of locomotor and postural behaviours (Ryan and Walker, 2010).

Ryan *et al.* (2018) studied variation in the structure of trabecular bone of the femoral head of modern humans, non-human extant hominoids, extant baboons and fossil hominins, and found that anisotropy of the trabecular bone enclosed in the femoral head in fossil hominins, particularly in *Australopithecus*, is similar to that of anatomically modern humans, an indication that they walked similarly to anatomically modern humans.

The study of Ryan and Shaw (2012), which investigated the relationship between inferred locomotor activities and several trabecular bone structural properties in human and non-human primates, improved reconstruction of locomotor behaviour in the fossil record. This was achieved because trabecular bone has ability to respond to loading environment during the lifetime of an individual (Ryan and Krovitz, 2006; Gosman and Ketcham, 2009; Barak and Lieberman, 2011) and results revealed that variations in trabecular bone fabric anisotropy is among vital locomotor signals. Therefore, this supports hypotheses that morphological patterns reflect an adaptation of trabecular bone to a characteristic locomotor style. Therefore, this technique is useful in inferring characteristic locomotor patterns in fossils cercopithecoids.

CHAPTER 3 - MATERIALS AND METHODS

3.1 Materials

3.1.1 Fossil specimens

Fossil material used in this study includes forty one (41) fossil specimens from southern African hominin-bearing sites within the Cradle of Humankind. These include Sterkfontein, Swartkrans, Makapansgat, Taung and Bolt's Farm sites. The fossil specimens are housed at the Evolutionary Studies Institute, University of the Witwatersrand, Johannesburg as well as the Ditsong Museum of Natural History, Pretoria. Table 3.1. below list sites and their associated material abbreviations.

Table 3.1: Sites and material abbreviations

Site	**Specimen abbreviation**
Sterkfontein	Sts and SWP
Swartkrans	SK
Makapansgat	M
Taung	TP
Bolt's Farm	BF

Fossil cercopithecids material for this study are represented by femoral heads, humeral heads, proximal tibiae and calcanei. Figure 3.1 below shows representation of specimens used in this reserch.

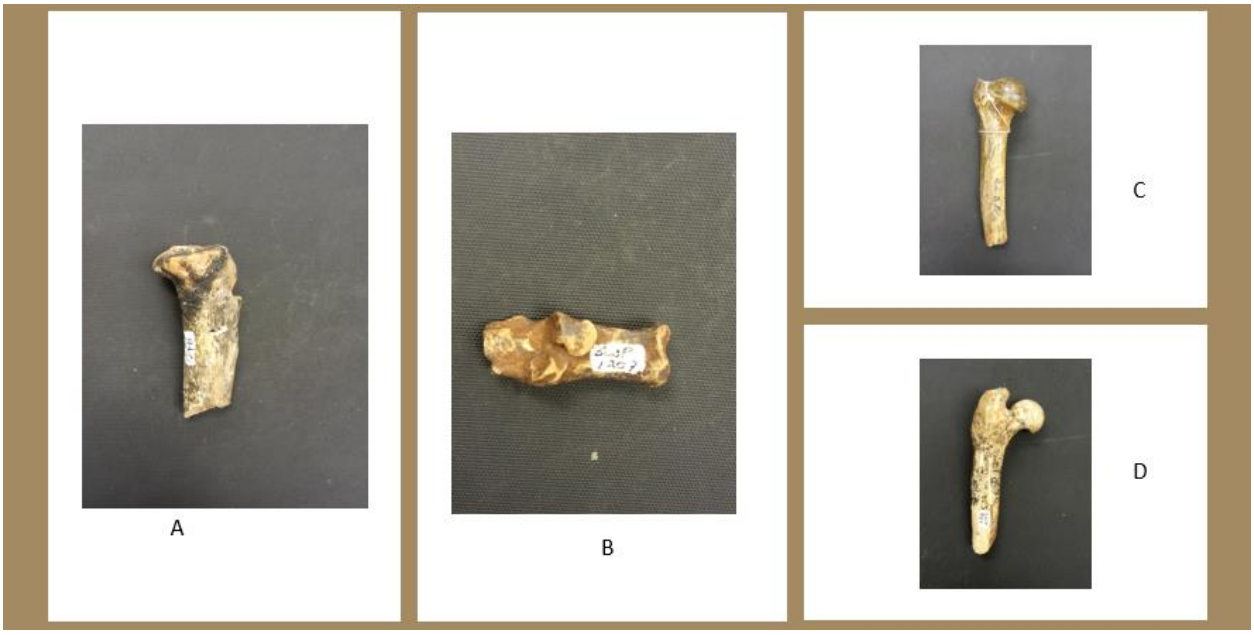

Figure 3.1*:* Samples of locomotor joint bones used in this study include tibia (A), calcaneus(B), humerus (C) and femur (D).

3.1.1.1 Sterkfontein

Specimens labelled '**Sts'** represent specimens discovered prior to 1966 at Sterkfontein and stored at the Ditsong Museum of Natural History in Pretoria, while **SWP** represent specimens discovered at Sterkfontein post 1966 and stored at the University of the Witwatersrand in Johannesburg (Heaton, 2006). Specimens included in this study are from Member 2, Member 4 and Member 5 (Mokokwe, 2016) and included eighteen (18) femora, three (3) humeri, five (5) calcanei and three (3) proximal tibiae. See table 3.2 below for more details.

Table 3.2: Specimens from Sterkfontein, with site member denoted by '**M**'.

Specimen no	Description	Provenance	side	Reference
SWP 526	Proximal femur	M 4	L	Mokokwe, 2016
SWP528	Proximal femur	M 4	L	Mokokwe, 2016
SWP 529	Proximal femur	M 4	L	Mokokwe, 2016
SWP 531	Proximal femur	M 4	R	Mokokwe, 2016
SWP 532	Proximal femur	M 4	R	Mokokwe, 2016
SWP 533	Proximal femur	M 4	R	Mokokwe, 2016
SWP 537	Calcaneus	M 4	L	Mokokwe, 2016
SWP 606	Proximal humerus	M 4	L	Mokokwe, 2016
SWP 747	Proximal femur	M 4	R	Mokokwe, 2016
SWP 749	Proximal femur	M 4	L	Mokokwe, 2016
SWP 753	Proximal femur	M 4	R	Mokokwe, 2016
SWP 756	Proximal femur	M 4	R	Mokokwe, 2016
SWP 962	Proximal humerus	M 4	R	Mokokwe, 2016
SWP 1009	Proximal femur	M 4	L	Mokokwe, 2016
SWP 1011	Proximal femur	M 4	L	Mokokwe, 2016
SWP 1146	Calcaneus	M 4	L	Mokokwe, 2016
SWP 1157	Calcaneus	M 4	L	Mokokwe, 2016
SWP 1161	Calcaneus	M 4	R	Mokokwe, 2016
SWP 1203	Proximal femur	M5	L	Mokokwe, 2016
SWP 1207	Calcaneus	M 4	R	Mokokwe, 2016

SWP 1384	Proximal femur	M 2	R	Mokokwe, 2016
SWP 1406	Proximal humerus	M 2	R	Mokokwe, 2016
SWP 1411	Proximal tibia	M2	L	Mokokwe, 2016
SWP 1546	Proximal tibia	M 2	L	Mokokwe, 2016
SWP 1596	Proximal tibia	M4	R	Mokokwe, 2016
SWP 1698	Proximal femur	M2	L	Mokokwe, 2016
SWP 1699	Proximal femur	M2	L	Mokokwe, 2016
Sts 2050	Proximal femur	M4	L	Brain, 1981
Sts 2259	Proximal femur	M4	L	Brain, 1981

3.1.1.2 Swartkrans

Five (5) cercopithecoid proximal femora from Swartkrans Member 1 are included in this study (Brain, 1981), as table 3.3 below. The specimens are housed at Ditsong Museum of Natural History in Pretoria.

Table 3.3: Materials from Swartkrans cave labelled '**SK**' and with site member denoted by '**M**'.

Specimen no	**Description**	**Provenance**	**side**	**Reference**
SK 605	Proximal femur	M1	L	Brain, 1981
SK 607	Proximal femur	M1	R	Brain, 1981
SK 1513	Proximal femur	M1	R	Brain, 1981
SK 2595	Proximal femur	M1	R	Brain, 1981
SK 14015	Proximal femur	M1	L	Brain, 1981

3.1.1.3 Makapansgat

Two (2) cercopithecoids proximal humeri, one (1) calcaneus and two (2) proximal femora from Makagapansgat Member 4 housed in the Evolutionary Studies Institute in University of the Witwatersrand, Johannesburg were used in the study (table 3.4).

Table 3.4: Makapansgat specimens denoted by '**M**' as well as provenance member denoted by suffix '**M**'.

Specimen no	**Description**	**Provenance**	**side**	**Reference**
1930 M	Proximal humerus	M4	L	Eisenhart, 1974
1934 M	Proximal humerus	M4	L	Eisenhart, 1974
2222 M	Calcaneus	M1	L	Eisenhart, 1974
14934 M	Proximal femur	Undetermined	R	Wits Catalogue
16383 M	Proximal femur	Undetermined	L	Wits Catalogue

3.1.1.4 Bolt's Farm Materials

Bolt's Farm material consist of a single left proximal femur that is stored in University of the Witwatersrand, Johannesburg (table 3.5).

Table 3.5: Material from Bolt's Farm

Specimen no	**Description**	**Provenance**	**side**	**Reference**
BF 36	Proximal femur	Bolt's Farm	L	Wits catalogue

3.6 Materials from Taung Limeworks

Materials from Taung Buxton Limeworks consist of a single right proximal Tibia stored at University of the Witwatersrand, Johannesburg as illustrated by table 3.6 below.

Table 3.6: Material Taung Buxton Limeworks.

Specimen no	**Description**	**Provenance**	**side**	**Reference**
TP 18	Proximal tibia	Taung	R	Wits catalogue

3.1.2 Extant specimens

Forty (40) specimens of wild extant cercopithecoids (*Papio Ursinus*, *Cercopithecoid aethiops* and *Chlorocebus*) from the School of Anatomical Sciences, University of the Witwatersrand were scanned for comparative purposes. Thirteen (13) complete individual monkey skeletons were selected and 26 femoral heads, 6 calcanei, 4 proximal humerus as well as 4 tibiae were scanned (Table 3.7) because they are known to record locomotor signals (Fajardo and Muller, 2001; Ryan and van Rietbergen, 2005; Ryan and Krovitz, 2006; Ryan and Shaw, 2012).

Table 3.7: All 13 individual skeletons with selected body parts.

No	Za Number	Femur	Tibia	Calcaneus	humerus
1	Za 103	Left and right	Left and right	Left and right	Left and right
2	Za 118	Left and right			
3	Za 127	Left and right			
4	Za 128	Left and right			
5	Za 182	Left and right		Left and right	
6	Za 168	Left and right			
7	Za 787	Left and right			
8	Za 791	Left and right		Left	
9	Za 792	Left and right			
10	Za 793	Left and right			
11	Za 891	Left and right	Left and right	Right	Left and right
12	Za 1226	Left and right			
13	Za 1227	Left and right			
Total		**26**	**4**	**7**	**4**

Since the study focuses on locomotor behaviour, it excludes immature specimens as well as specimens with pathological conditions (e.g. osteoarthritis, osteoporosis or osteopenia) or those with trauma since these can affect the skeleton architecture through changes in locomotor activities or movement levels during the animal's life (Ryan and Walker, 2010).

3.2 Methods

Specimens were micro Computed Tomography (CT) scanned to obtain virtual cross-sections of the specimen. The scans were reconstructed in CT Pro 3D and Tagged Image File Format (tiff), files generated in VGStudio for purposes of storing raster graphics images. Tiff stacks were later manipulated (orientated, separated, dimensions taken, extraction of homologous 2D sections as well as extraction of homologous volumes of interest) in Avizo software. The last stage entails computation of trabecular bone parameters in ImageJ, using the BoneJ plugin and parameters were later used in classifying textural and structural properties of the trabecular bone as well as modelling joints loading conditions on fossil remains during their life.

3.2.1 Scanning

Specimens selected were scanned using high-resolution CT scanner facility at the Evolutionary Studies Institute of the University of the Witwatersrand (Nikon XTH/225L), Johannesburg and at the South African Nuclear Energy Cooperation (Nikon Metrology, Metris) in Pelindaba (Figure 3.2). Computed tomography scanner operates on the same principles as a normal or conventional medical X-ray, because it generates numerous images as the specimen is rotated through 360º. Specimens were mounted in an upright position with the distal ends of the femur, tibia and humerus embedded in a rectangular foam block, while calcanei were completely imbedded in the foam block. The foam block was used to secure specimens and prevent gratuitously moving while the sampling stage is being rotated Scanning specimens produces X-ray radiation with 3D data, as such reduces the need for handling actual specimens and facilitate working with virtual specimens created. The resolutions for fossil specimens are from 0.0180 mm to 0.0653 mm (annexture A5-A6) while resolutions for extant specimens are from 0.0216 mm to 0.0695 mm (annexture A7-A8).



***Figure 3.2*:** Nikon XTH/225 Micro-focus X-Ray tomography scanner (https://industry.nikon.com/en-us/products/x-ray-ct/).

3.2.2 Reconstruction of scanned data

Images scanned from different angles were reconstructed in CT Pro 3D software. Scanned data was loaded into CT Pro 3D software. The first step involves finding the *Centre of Rotation* (COR) (figure 3.3). This was done automatically with *accuracy of determination* set at *high quality* and *dual slice section*. Both *upper* and *lower centre of rotation slices* were activated before starting the process. Centre of rotations were followed with the *setup* corrections in the *setup menu*. These were done by adjusting *red lines* to the *densest* part or the darkest part of the specimens. *Beam hardening Pre-sets* 1,2,3 and 4 were selected before pressing the start option at the bottom right of the menu (Figure 3.3). The final reconstruction step is the volume or the Volume of Interest (VOI). Although all previous selected beam hardening can be used, it is usually the first 2 that have highest dark coloured contrast (as such one of them was selected). The Regions of Interests were adjusted in the 0 and 90 display respectively. After adjusting Regions of Interest, data was sent to CT Agent for reconstruction.

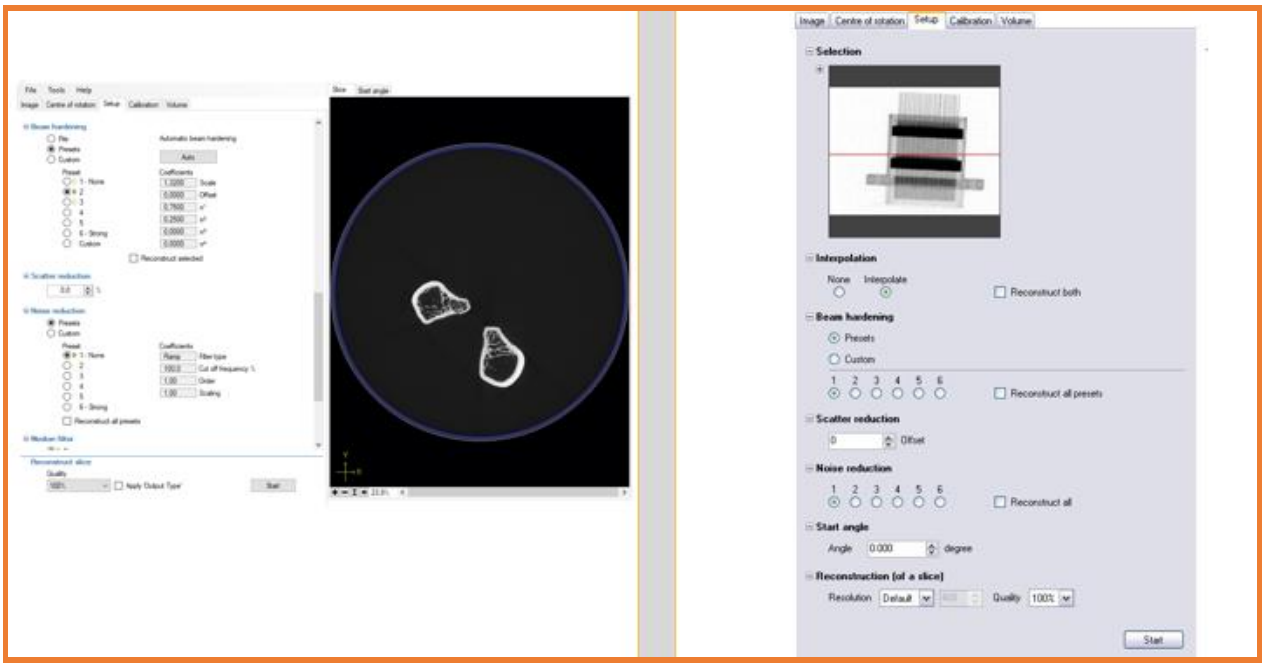

***Figure 3.3*:** Finding centre of rotation (L) and Beam hardening in setup menu (R).

Tiff files were generated in VGStudio Max 2.1 and adjusted to the lowest grey value (unsigned16 bits to reduce memory usage while retaining professional image analyses (VGstudio manual).

3.2.3 Virtual separation of two specimens

When two (2) specimens are scanned simultaneously, they must be separated before they could be processed in Avizo. Separation of specimens scanned together was done by the process of cropping the 3D data from newly created *isosurfaces*, which is the 3D analog of an isoline (Figure 3.4) and cropped data was exported and saved in *Avizo binary .am* format

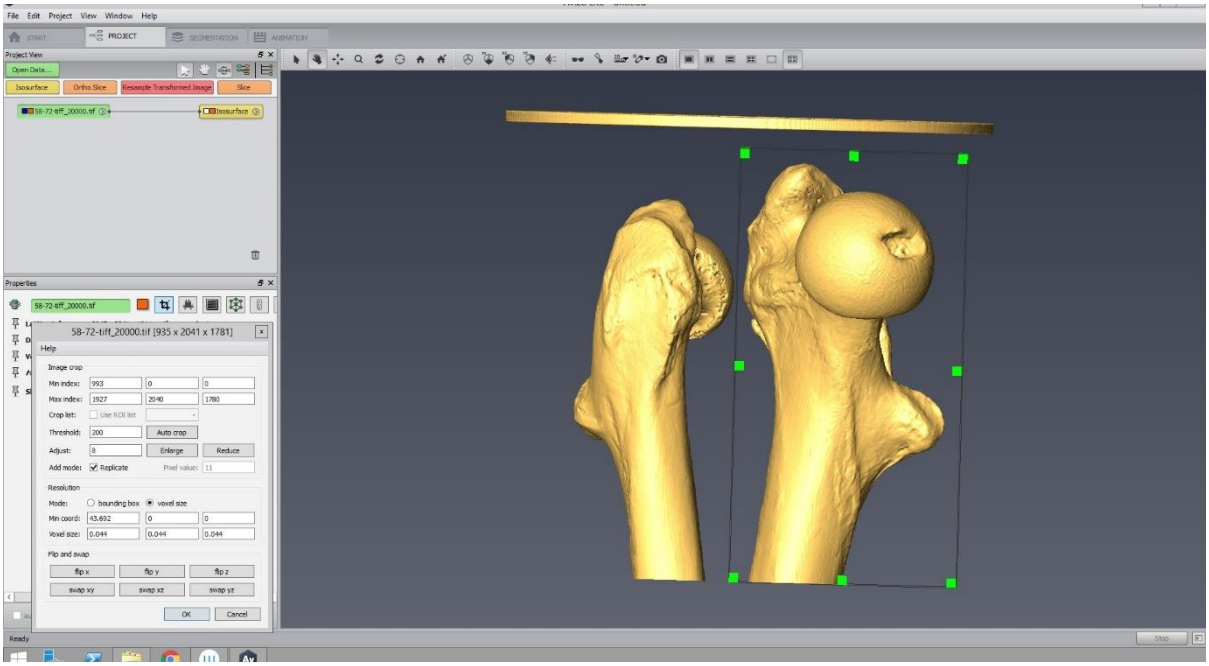

Figure 3.4: Separation of simultaneously scanned specimens.

3.2.4 3D surfaces alignment

To determine homologous positions of sections and volumes of interest to be extracted, the size of concerned specimen (e.g. femoral head) was measured and *Isosurfaces* generated from the *Transformed Avizo files* followed by the creation of *Ortho slices*. Slices were oriented in different directional positions, being *x, y* and *z* planes. Positional coordinates of these different directional views i.e., most anterior view, most posterior view, most medial view, most lateral view, most superior view and lastly most inferior view were recorded in Microsoft excel sheet (table 3.8). This is an important step for computing maximum length in the three directions because these recorded coordinates are useful in calculating the most maximum slice number, centre of slice number, size of volume of interest to be calculated and lastly the position of volume of interest coordination as illustrated in table 3.8 below because all VOIs should be homologous in size and location across individual specimen (Ryan and Ketcham, 2002a, b).

Table 3.8: Calculated centre, size and position of VOI in each specimen.

14954 M						
centre femoral head	med	lat	ant	post	sup	inf
slice number max	222	732	226	896	1001	298
distance in slice number	510		670		703	
center in slice number	477		561		649.5	
distance in mm	15.096		19.832		20.8088	
VOI size						
size (1/6ap) in slice number	117.1667					
size (1/6ap) in mm	3.468133					
position VOI						
coordination in slice number	535.5833	418.4167	619.5833	502.4167	590.9167	708.0833
	117.1667		117.1667		117.1667	
Resolution in mm	0.0296					

3.2.4.1 Orientation of femoral heads

A new project in Avizo was created and *isosurfaces* were generated form the *tiff* files generated earlier. Thresholds were *downsampled* to four (4) average so that the number of polygons being produced are reduced while retaining the original shape of trabeculae. Different *voxel sizes* (resolutions) of individual specimens were entered. Pictures of created images were were taken in different positional views for further physical descriptions (see chapter 4.2 on description of homologous 2 dimensions).

The junction between the femoral head and neck was identified. Some specimens presented a challenge because their cortical bones in the contact area were eroded or missing (figure 3.5). Therefore, for these types of specimens, the jucntion were inferred and landmarked. *Points and lines objects* were created in the project menu bar. From these *points and lines*, *landmarks* were created under the *landmark editor*. *Landmark editor* enabled the addition and deletion or subtraction of *landmarks* (figure 3.6). *Slices* were created under the *display* in the *specimen file*, below the *menu bar*.

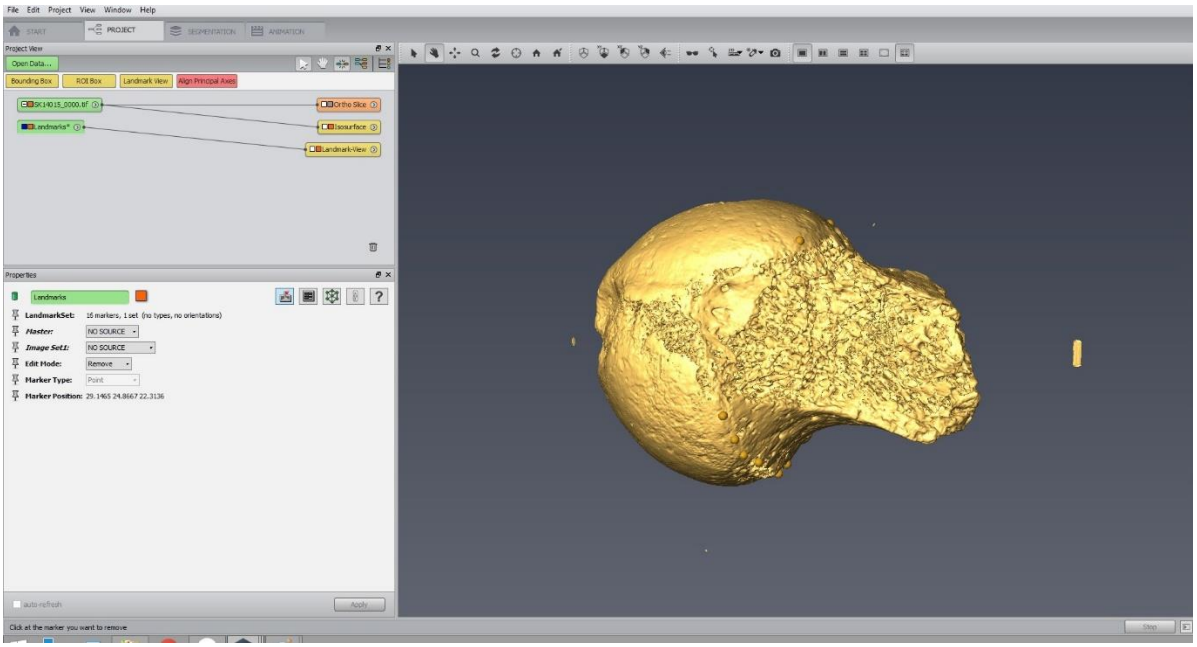

Figure 3.5: Landmarking cortically eroded specimen on the juction between head and neck.

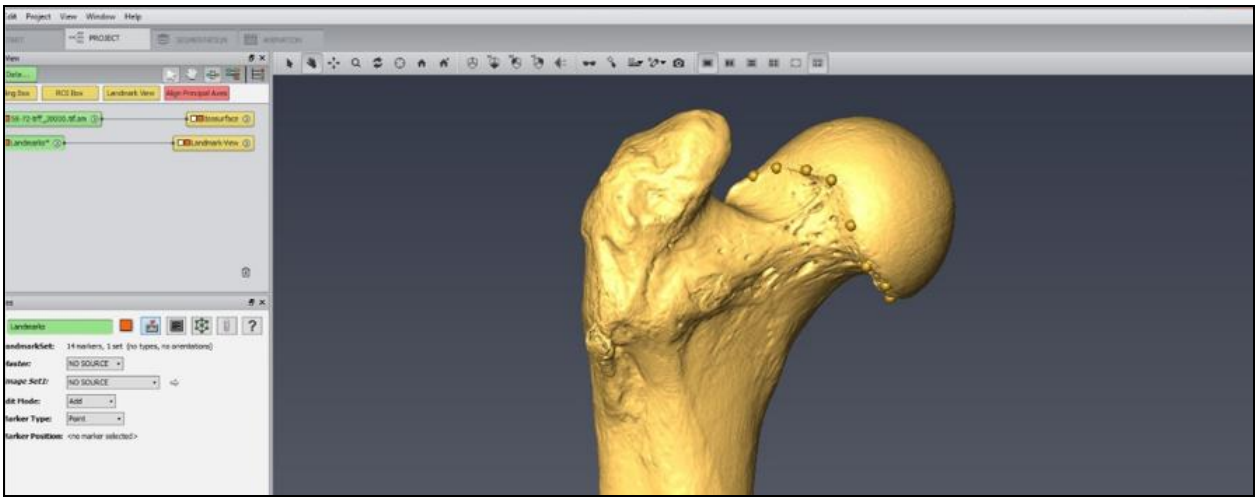

Figure 3.6: Femur head with landmarks on the head and neck junction area.

Slices were made to *fit landmarks* (figure 36) with the *finest sampling*. These *slices* were orientated according to the shape of an individual specimen but not in the conventional vertical and horizonal planes.

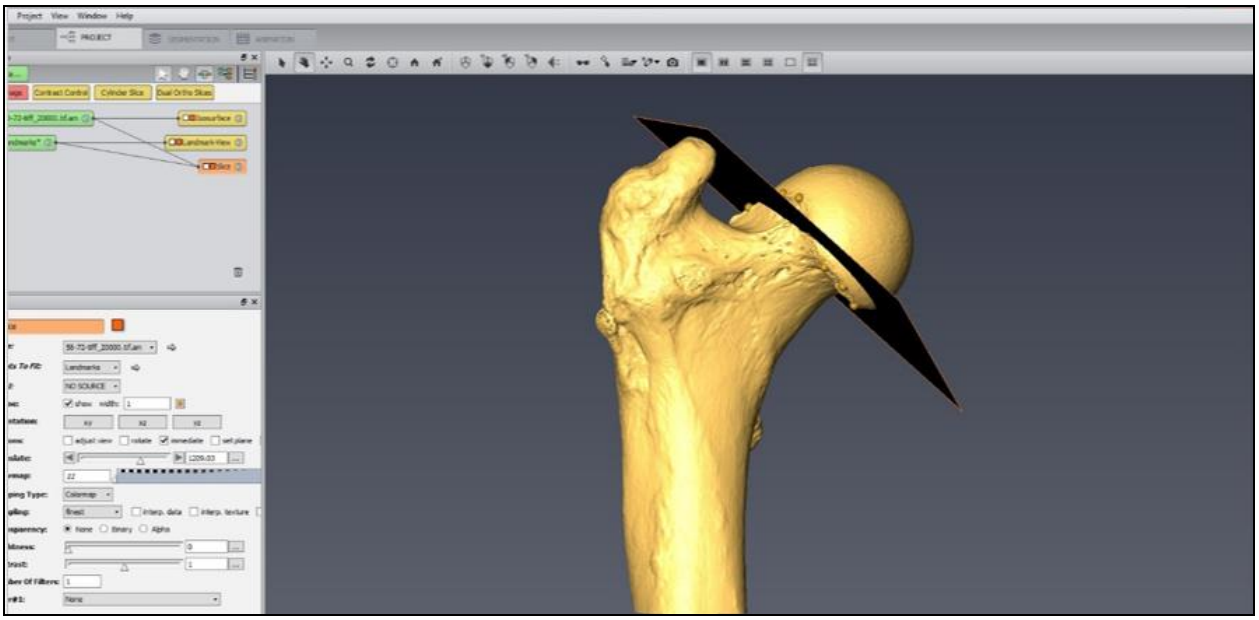

Figure 3.7: Landmarked specimen with slices that fit landmarks.

A new image stack was generated using the tool *Resampled Transformed Images* within the *Lanczos interpolation* and *extended mode*. This was done such that slices were re-aligned but retaining dimensions and voxel sizes even though the size seems different. Tiff stack was then exported and saved in Avizo as *transformed fil*e as well as with their *landmarks.* Through this process, it was ensured that all specimens were oriented in the same way and that the sections and volumes extracted are homologous.

3.2.4.2 Orientation of proximal tibia

Proximal tibial specimens were orientated such that the superior most tip of the intercondylar eminence was parallel with horizontal grids in the *global axes view* as illustrated (figure 3.8). This was done by using *Global axes* in the *View menu* and *grids*. *Global axes* allow the alignment of *grids* such that they are perfectly squared. This steep is followed by launching the *transform editor* from specimen file and *trackball* from *manipulato*r was selected. *Trackball* is used to move specimen around without moving *global axes* and *grids*, thereby aligning specimens in a desired position. *Resampled Transformed Images* were created without referencing *slices.* Specimens were interpolated to *Lanczos* and *extended* mode while preserving *voxel sizes.*

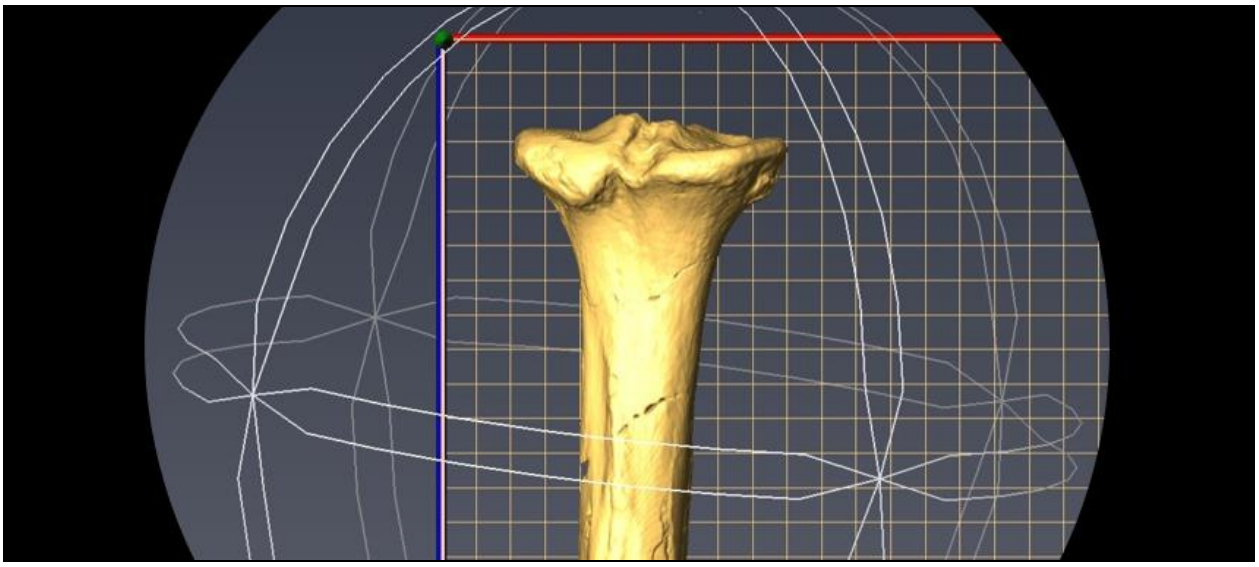

Figure 3.8: Posterior view within grids of global axes.

3.2.4.3 Orientation of calcanei

Just like proximal tibiae, calcanei were orientated such that the superior most tip of the posterior facet, calcaneal tuberosity and anterior talar articular surface were parallelly horizontal with *global axes grids* in the view menu as illustrated (figure 3.9). *Resampled Transformed Images* were created without *referencing source* as discussed in orientation of tibia above.

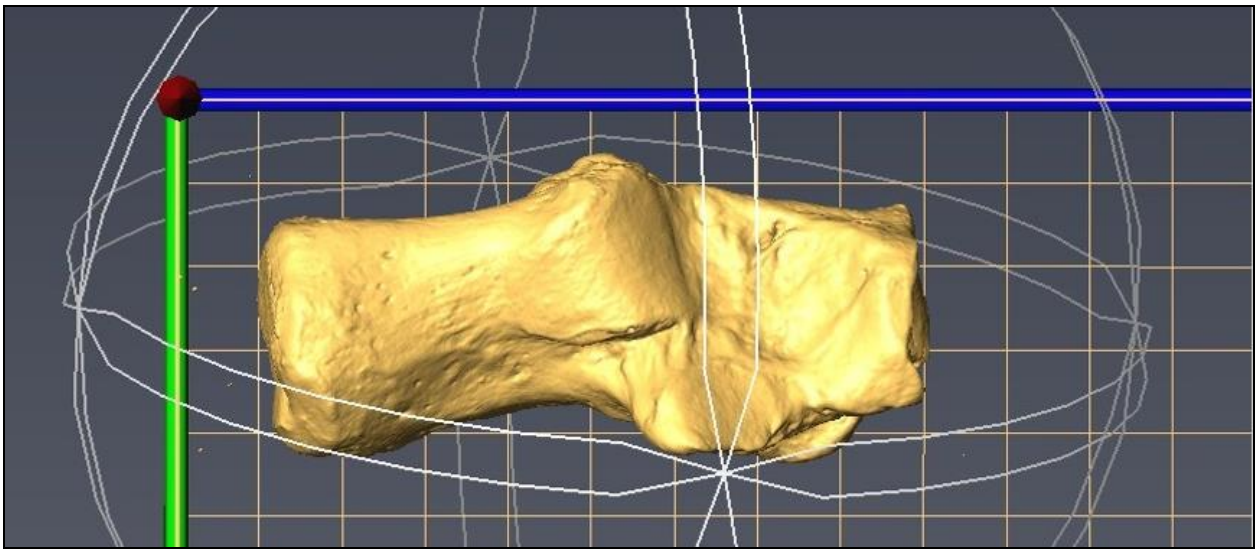

***Figure 3.9*:** Orientation of calcaneus within grids of global axes.

3.2.4.4. Orientation of humeri

Humeri were orientated such that the superior of humerus head and the most superior tip of its greater tubercles were verically aligned with g*rids* of *global axes* (figure 3.10). *Reasampled Transform Images* were created without *referencing slices* as discussed above in tibia section.

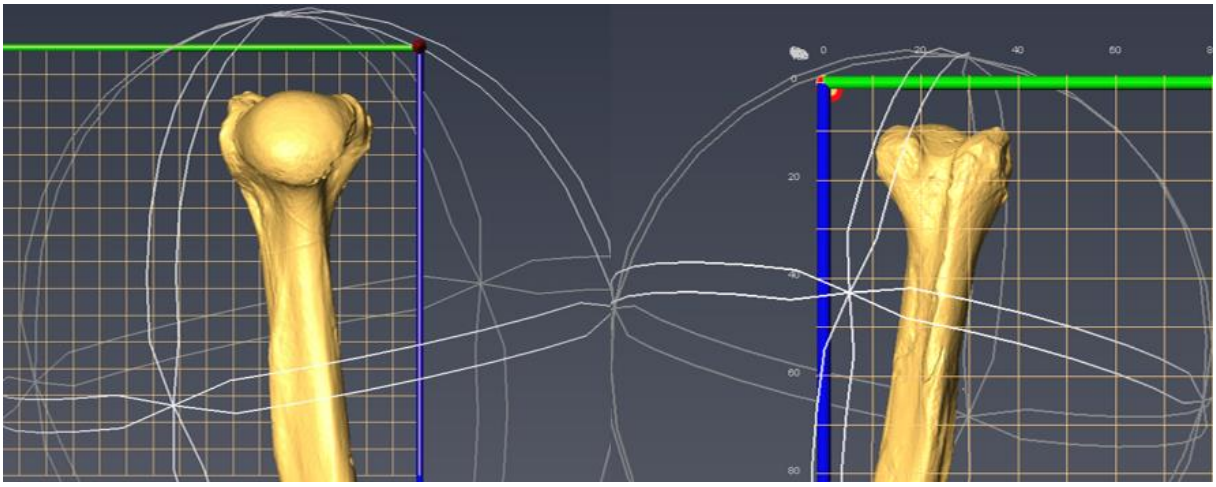

Figure 3.10 **:**Posterior (L) and anterior (R) views of humerus within grids of global axes and trackball.

3.2.5. Virtual segmenting sedimented specimens

Specimens that have sediments within their trabecular bone were manually segmented using Avizo. This was done to isolate trabecular bone from the sediments. However, this technique was not applied on all specimens with sediments because some specimen were fully sedimented with no trace of trabecular bone, while some specimen had trabecular bone that could be traced out of light grey sediments (figure 3.11.). Segmentation of specimens enables specimen to be quantitatively analysed.

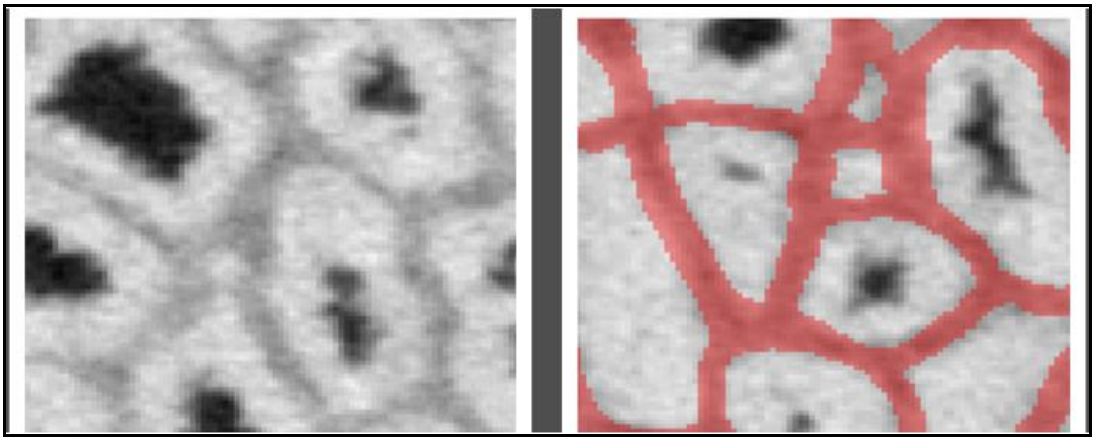

***Figure 3.11*:** Dark grey trabecular bone within light grey sediments (L) and segmented (isolated) trabecular bone in red colour (R).

3.2.6 Extraction of homologous 2D sections

Homologous 2 dimension (2D) sections were extracted in the mediolateral and anteroposterior planes. For mediolateral sections, coordinates of the anteroposterior view were used to locate the centre of concerned specimen (e.g proximal humerus head) while coordinates for mediolateral view were used to locate the centre of specimens in anteroposterior section.

New *isosurfaces* from *2D tiff* files were created. Coordinates from centres of slice numbers (previously calculated from the 6 different directions) were registered in the *threshold slice numbers* as shown in figures 3.12 and 3.13 and *Images* were extracted. Created files were saved as *Avizo transformed binary* file and *2D tiff* files. *Ortho slices* were concealed in the screen, resulting in the full view of cross sections.

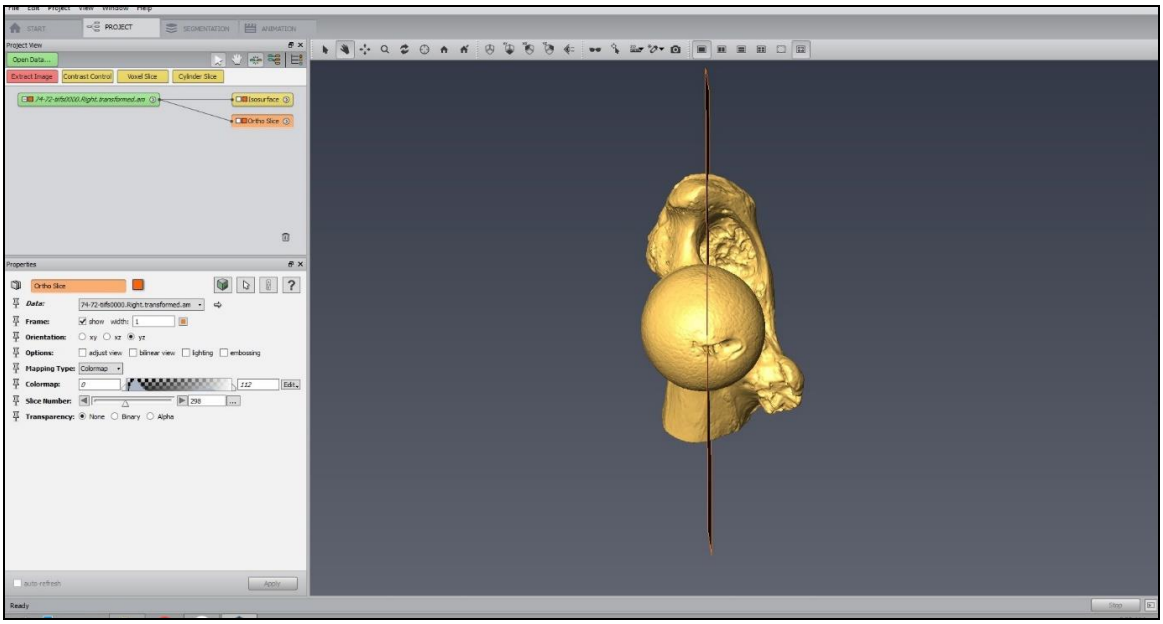

Figure 3.12: Extracting mediolateral 2D section.

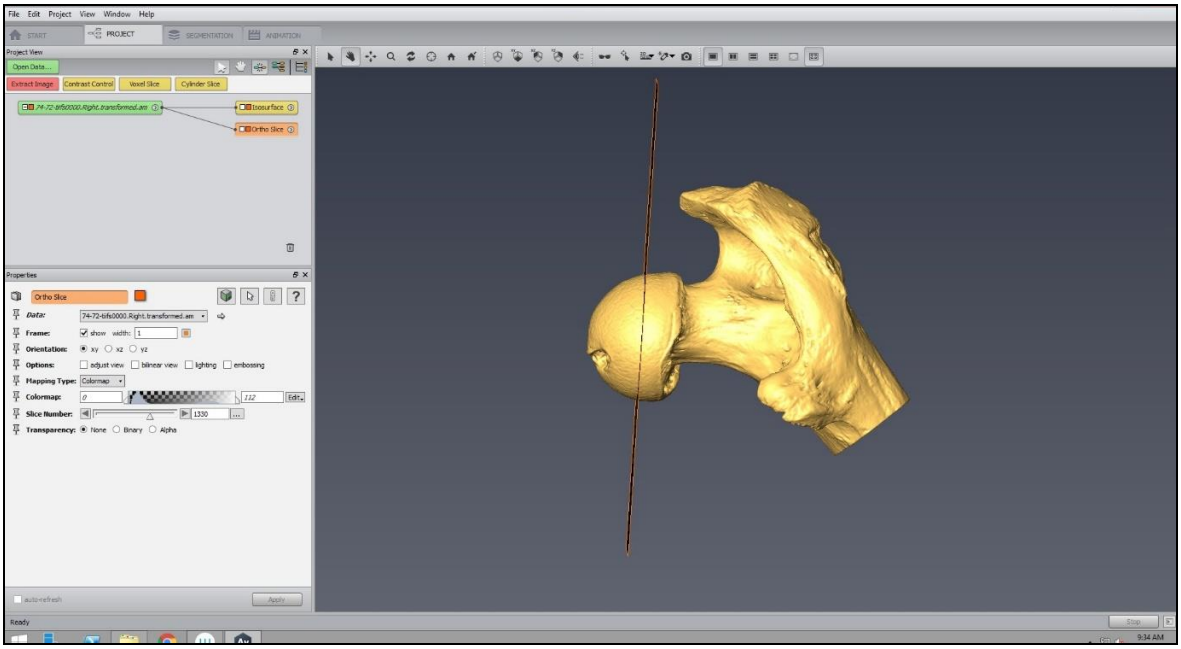

Figure 3.13: Extracting anteroposterior 2D section.

Cross section images were adjusted such that they were vertically and horizontally aligned with the computer screen. Images were scaled in mediolateral and anteroposterior cross sections as illustrated by figure 3.14 below and each cross section was screenshotted for every specimen, which were saved as *Jpeg* photographs.

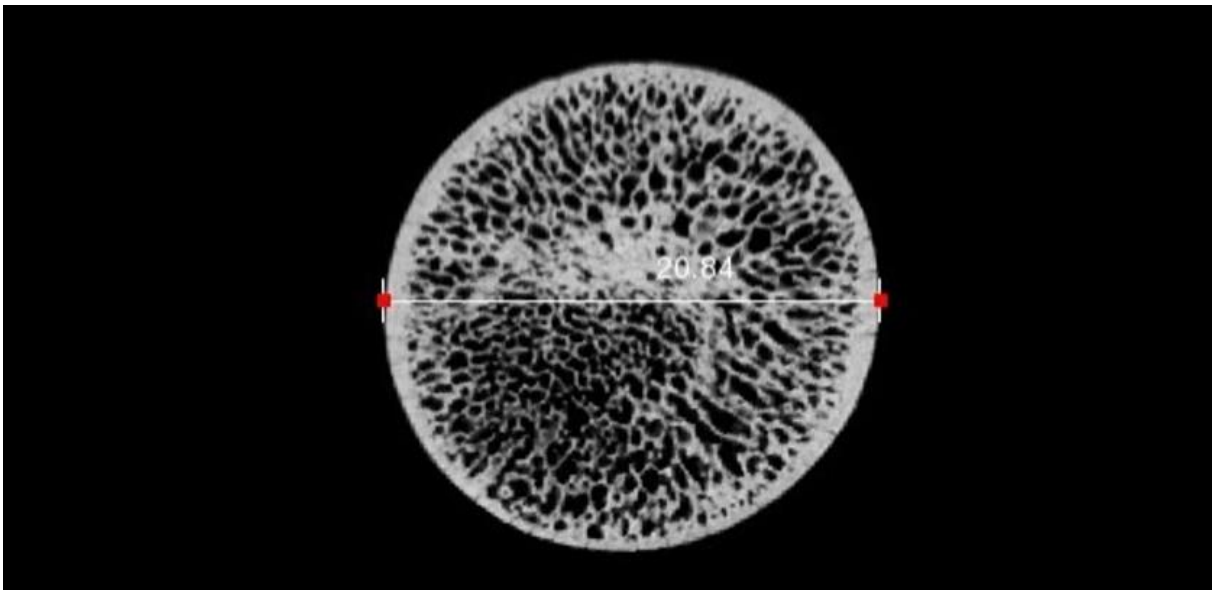

Figure 3.14: Medial view of anteroposterior cross section of femur head with scale.

3.2.7 Extraction of homologous volumes of interest (VOI)

A distinct spherical volume of interest (VOI) for each locomotor joint was extracted for the computation of trabecular bone parameters and analyses following after Ketcham and Ryan (2004). Trabecular bone parameters calculated include trabecular bone fabric anisotropy (DA), trabecular bone volume fraction (Bv/Tv), trabecular bone thickness mean (Tb.Th mean) and trabecular bone spacing mean (Tb.Sp mean)

Extraction of VOI of specimens in the study involves creating new *isosurfaces* from the *Transformed Avizo files* and coordinates of slices previously recorded in the Microsoft excel spread sheets were registered in the *Crop details box* as shown in figure 3.15 and figure 3.16 below.

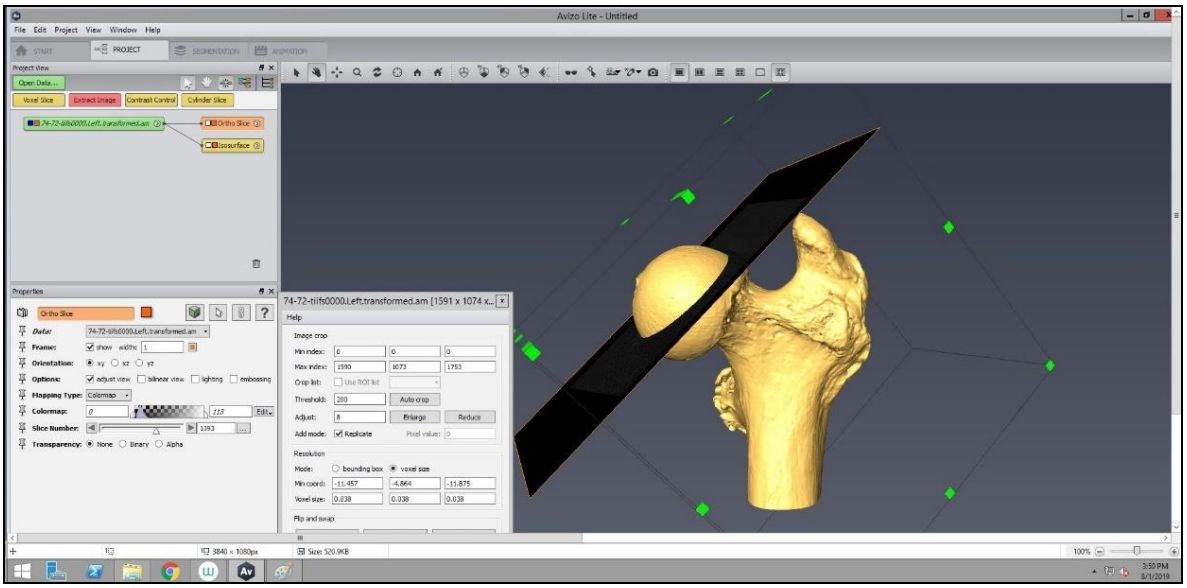

Figure 3.15: Extracting Volume of interests / 3D Volume. Note coordinates in the crop editor.

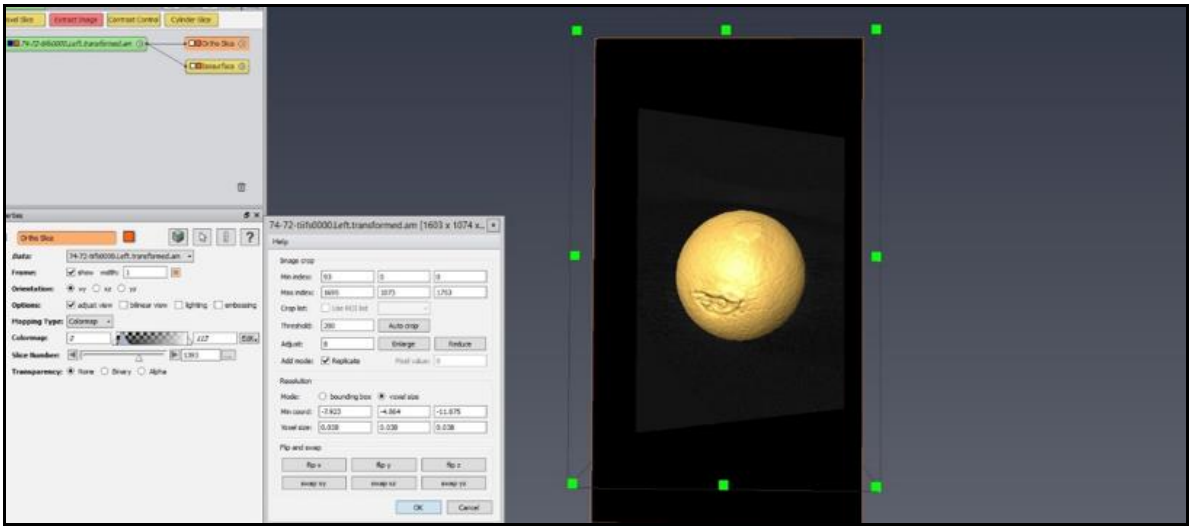

Figure 3.16: Extracting volume of interests / 3D Volume on femur head. Note coordinates in the crop editor.

Sizes of VOIs were calculated differently for each set of specimens. The size and location of VOI's were informed by shapes of specimen because some large ones VOI's (e.g 1/6) extruded cortical bone of tibiae and calcanei specimens.

Femoral and humeral heads: VOI were calculated as 1/6 of the total volume of head and was extracted in head nucleus (figure 3.15 and 3.16) above. However, in taking coordinates of humeral heads differ from that of femoral heads. The medial region of humerus head was taken as the boundary of the greater tubercle and the head while the anterior boarder is the most anterior of lesser tubercle (figure 3.17).

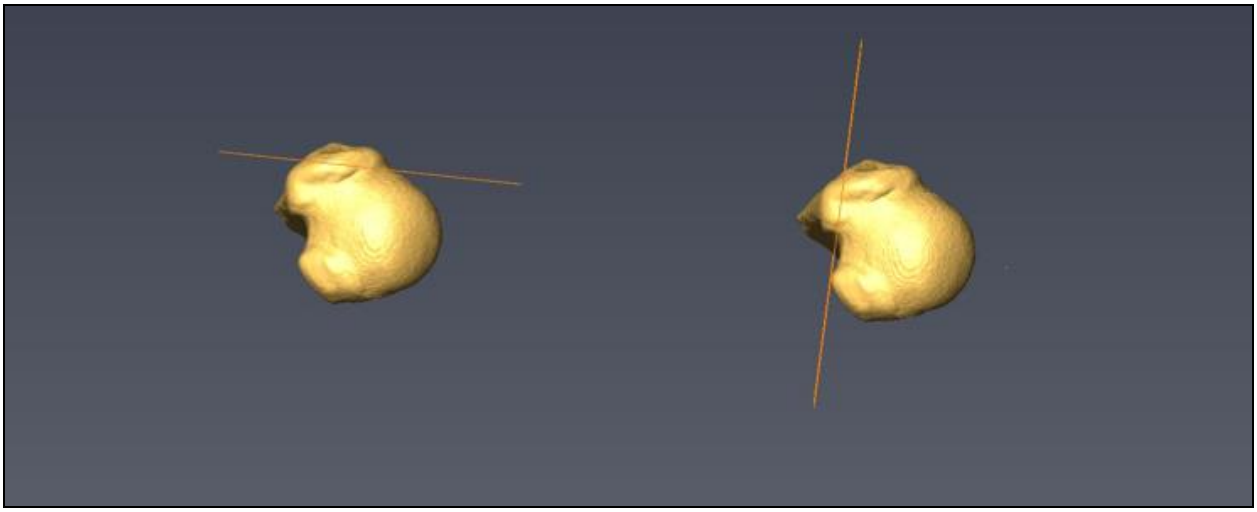

Figure 3.17: Recording coordinates on humerus head

Proximal tibiae: VOI were extracted on nucleus of entire proximal area, medial and lateral facets (figures 3.18). All VOIs were calacuated as 1/10 total volume of the concerned facets.

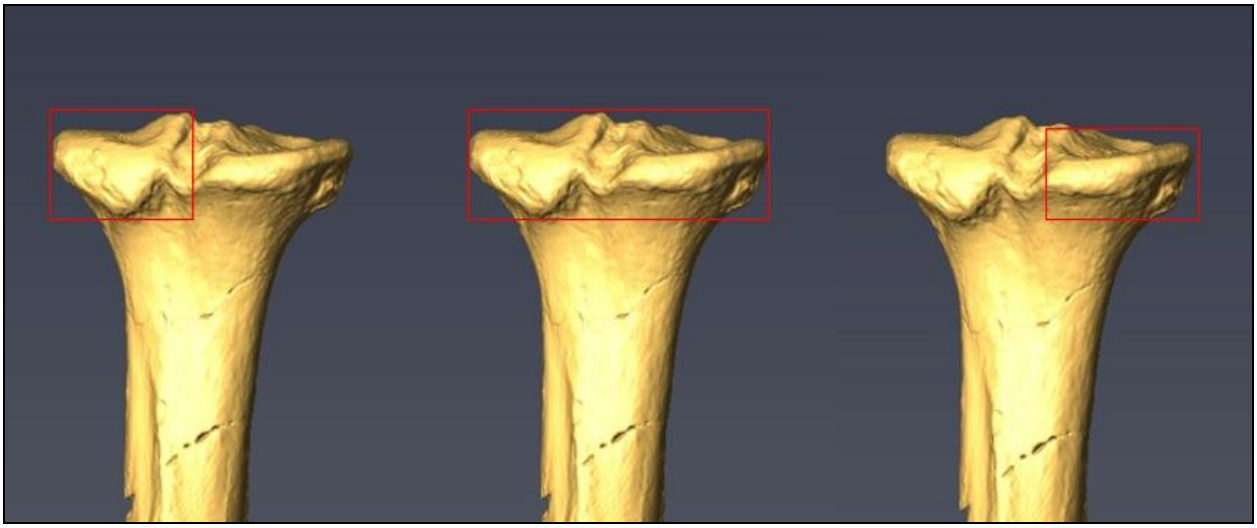

***Figure 3.18*:** Posterior view tibia showing regions where VOI was extracted. Medial facet (L), entire proximal volume (C) and medial facet (R).

Calcaneus: VOIs were extracted as 1/10 of the entire volume of specimens and was extracted at ¾ anterior (¼ posteriorly) of specimens as illustrated by figure 3.19 below.

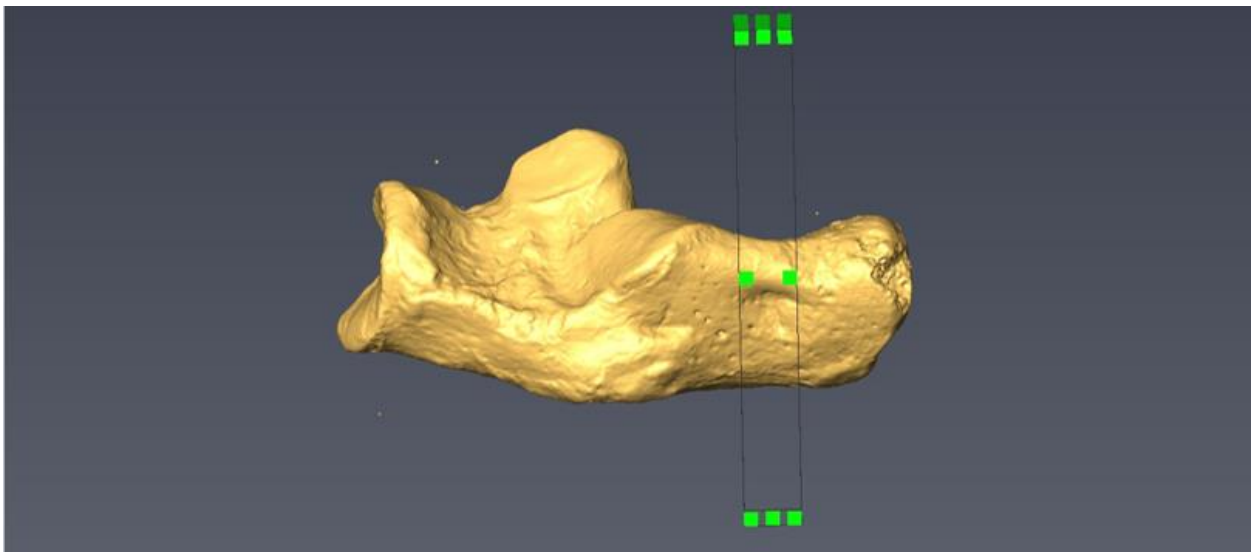

Figure 3.19: Extracting VOI posteriorly of calcaneus specimen.

Extracting volume of interest in posterior region of calcaneus was done so that the volume does not include a centrally located void called Neutral triangle or simply the Diard's area (Diard *et al*., 2007) as indicated by figure 3.20 below.

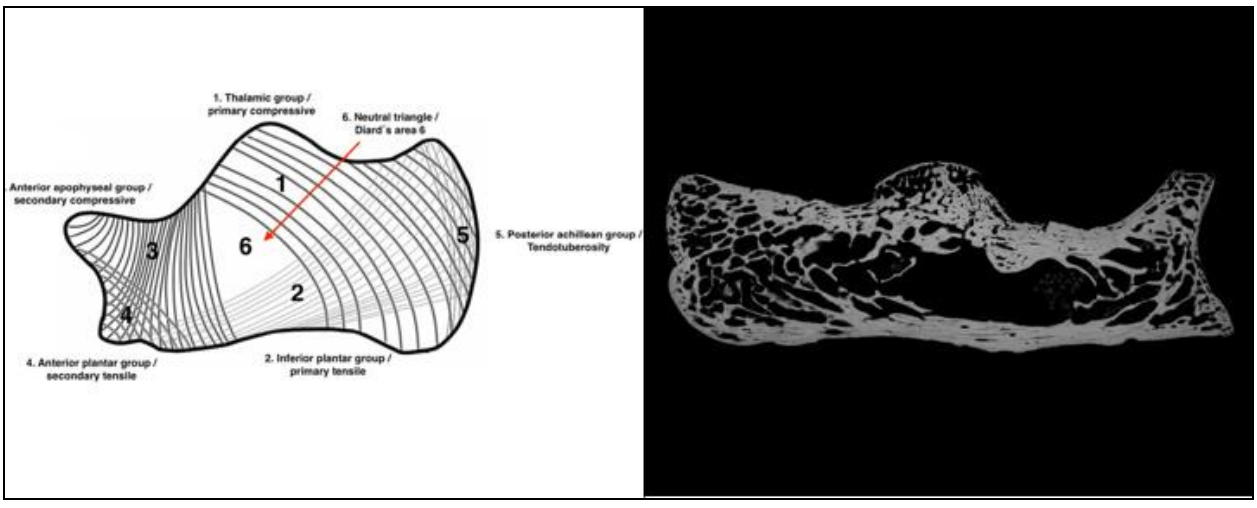

***Figure 3.20*:** A schematic diagram showing a void or an empty space in nucleus of calcaneus called Neutral triangle of Diard's area (picture adapted from Diard *et al.*, 2007).

3.2.8 Quantitative analysis of 3D volume

Parameters computed include the trabecular bone volume fraction (BV/TV), trabecular number (Tb.N), trabecular bone thickness (Tb.Th) and the trabecular bone fabric anisotropy (DA) (Ryan and Walker, 2010; Ryan *et al*., 2018), using ImageJ softwares.

Textural and structural properties of trabecular bone within VOIs were assessed following the protocol published in Doube *et al* (2010) using *ImageJ* software, and more particularly the *BoneJ plugin*, calculated as a table 3.9 below

Table 3.9: Trabecular bone structural properties calculated

Measurement	**Abbrevation**
Trabecular bone fabric anisotropy	DA
Trabecular bone volume fraction	BV/TV
Volume of selected area in specimen	BV
Total volume of entire specimen	TV
Trabecular bone thickness	Tb. Th
Trabecular bone spacing	Tb. Sp
Mean trabecular bone thicknesses	Tb. Th mean
Standard deviations of trabecular bone thickness	Tb. Th std dev
Mean trabecular bone spacing	Tb. Sp mean
Standard deviations of trabecular bone spacing	Tb. Sp std dev

The VOIs generated in Avizo as *image sequences* were imported into ImageJ. Resolutions and scales were set in the *Analyze bar* mode. This was done by assigning the *distance in pixel* to 1, with different resolution of individual specimen as *known distance* and *pixel aspect ratio* set to 1.

Thresholds were adjusted to *Otsu* on *Image* mode, so that image thresholds were automated. Images were then saved as *stack images* (*Image sequences*). Each image's threshold was calculated as in figure 3.21 below.

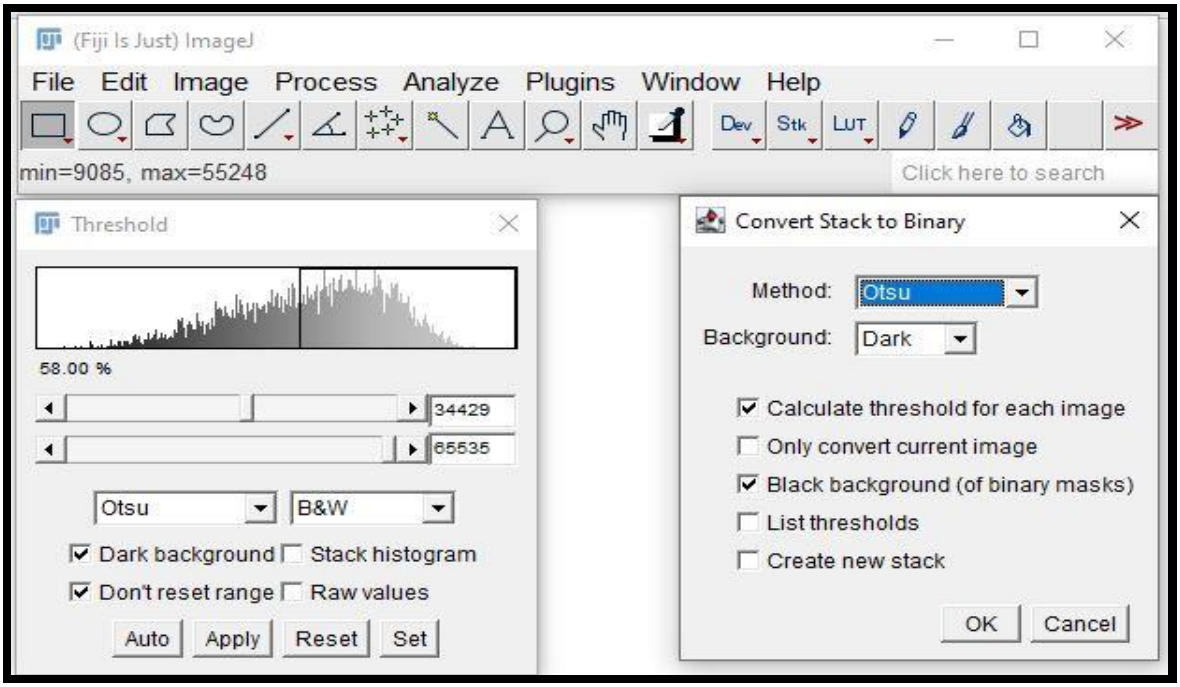

***Figure 3.21*:** Adjusting thresholds to dark backgrounds with white trabecular bone using *Otsu* methods**.**

Trabecular bone fabric anisotropy (DA) was computed by means of *BoneJ plugin*, which is an *automatic mode* (*default*) were recorded in a Microsoft excel file. Calculating trabecular bone volumes fraction or densities (BV/TV) were done in *BoneJ Plugin* by utilizing the *Fraction* menu. The *Area/Volume fraction* option was selected in the *fraction* menu. Trabecular bone volumes fraction (BV/BT), volumes of selected area in specimens (BV) and total volumes of entire specimens (TV), as in figure 3.22 were computed and recorded in Microsoft excel file.

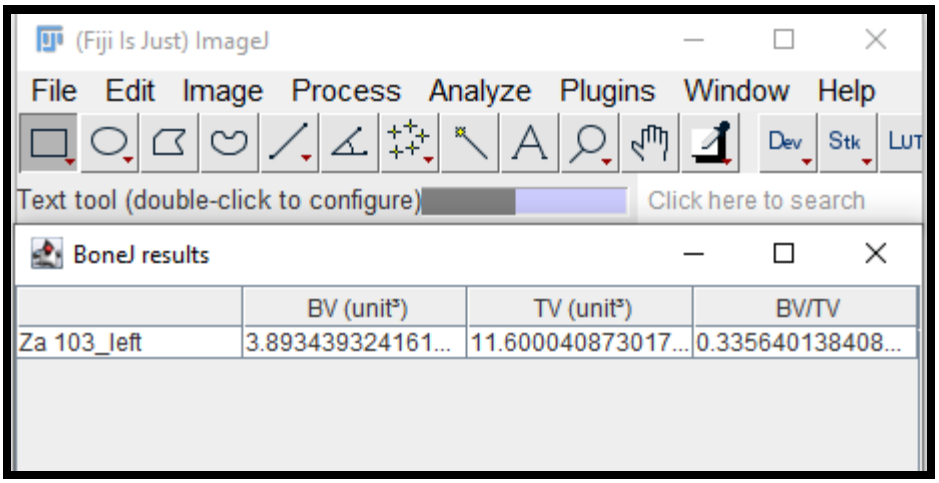

Figure 3.22: Computing trabecular bone volume fraction (BT/TV).

Trabecular bone thickness (Tb. Th) and trabecular bone spacing (Tb. Sp) were also calculated in *BoneJ* plugin *by* selecting the *thickness* option. *Thickness* and *Spacing* were activated in the *plugin options* as illustrated by figure 3.23 below. The mean trabecular bone thicknesses (Tb. Th mean), the standard deviations of trabecular bone thickness (Tb. Th std dev), the mean trabecular bone spacing (Tb. Sp mean) and the standard deviations of trabecular bone spacing (Tb. Sp std dev) were calculated and saved in Microsoft excel file with previously calculated parameters.

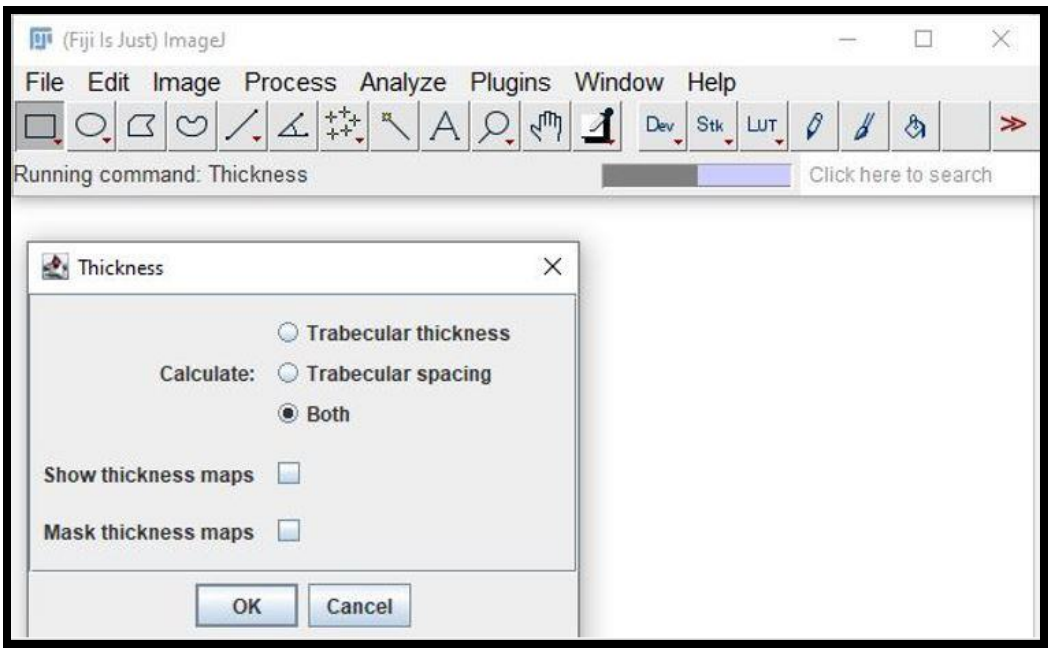

Figure 3.23: Computing trabecular bone thickness and trabecular bone spacing by ticking *both* option while deactivating mask and maps thicknesses.

3.2.9 Statistical analysis

Box plots of various trabecular bone parameters calculated during quantitative analysis in BoneJ were plotted to visualise fossil specimens against extant specimens. Furthermore, the student T-test was done so that means of specimens in box plots are compared for any difference. The use of a t-test was informed by data character I have. The data satisfy the following three (3) characters: (1) data is independent (2) data is normally distributed and (3) data has homogeneity of variance.

Chapter 4 - Results

4.1 External morphology

In this chapter, external morphology of fossil specimens is described. The description focuses on the locomotor joints only without long shaft bone even if they are preserved as is the case in some specimens. The description is centred on whether bone features like cortical are preserved on not.

4.1.1 Fossil femoral heads

14954M

This is a right proximal femur, the femoral head, neck and great trochanter are preserved but the lesser trochanter is missing. The femoral head is well preserved and of the fovea capitis is posteriorly elongated. The femoral neck is relatively short and the cortical bone is eroded in the in the head and neck junction area. The cortical bone of the femoral head is also eroded in the anterior region of the greater trochanter. The greater trochanter projects above the femoral head when viewed anteroposterioly (figure 4.1).

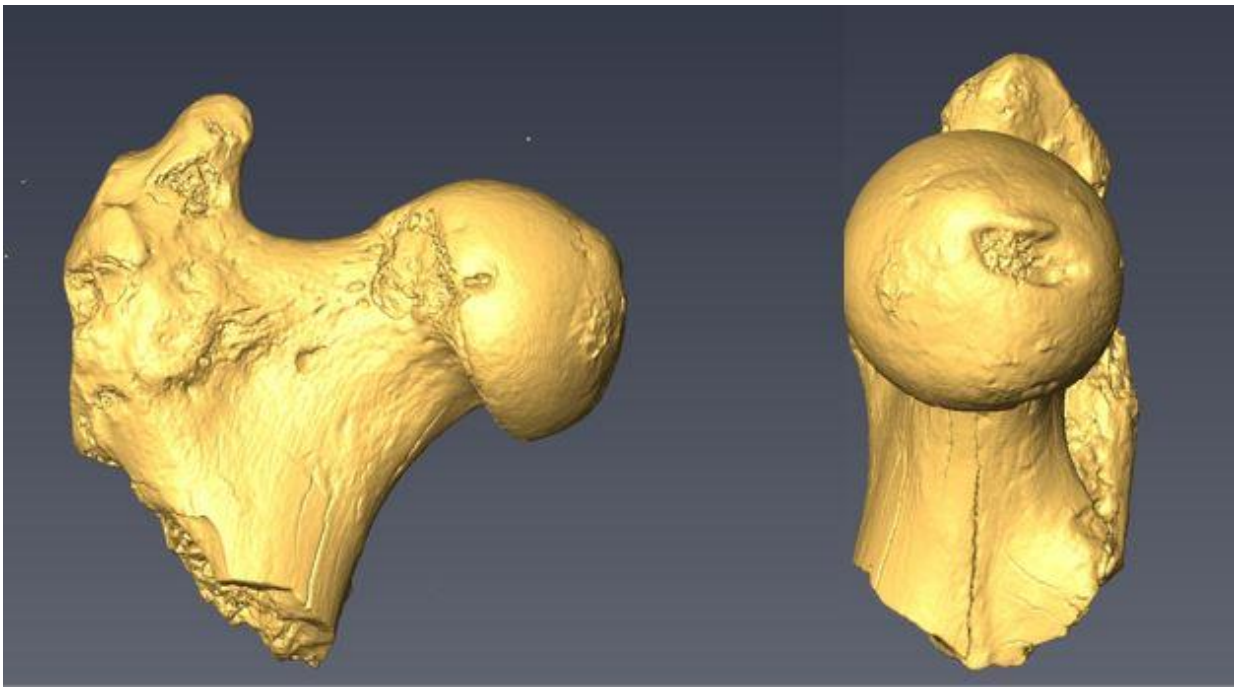

Figure 4.1: Specimen 14954M showing anterior view with eroded cortical on head-neck contact region (L) and posteriorly orientated fovea captis on medial view (R).

16383M

Specimen 16383 M is a well preserved left proximal femur. The femoral head has a wide fovea capitis with slightly eroded cortical bone posteriorly. The head also exhibits erosion on the anterior and posterior surfaces (figure 4.2). The femoral neck is relatively short. The greater trochanter is not preserved but the lesser trochanter is partial preserved with its most superior tip being eroded.

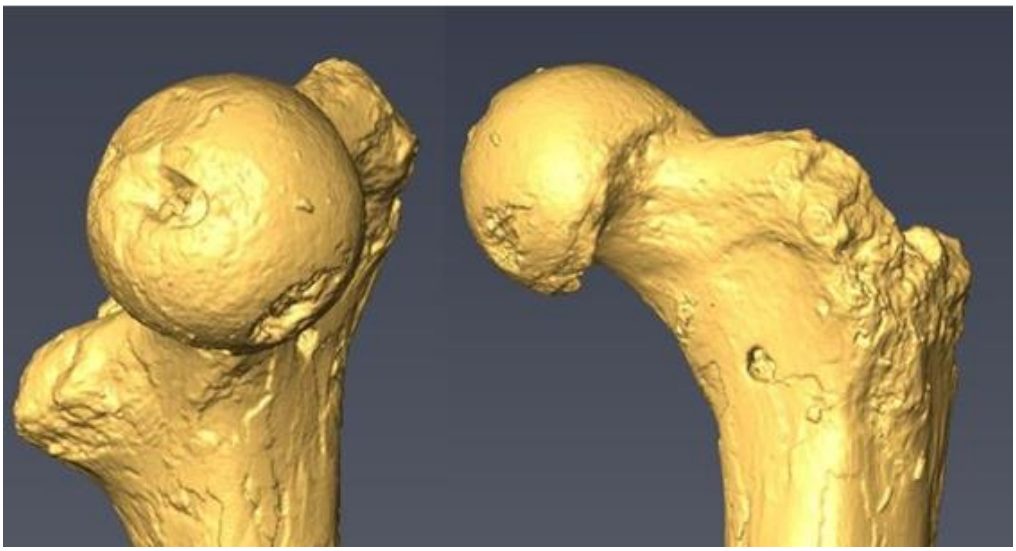

Figure 4.2: 16383 M with posterolateral orientated fovea captis (L) and eroded great trochanter (R).

SWP 526

This is a left proximal femur that preserves the femoral head, a portion of the neck and the lesser trochanter but the greater trochanter is missing. The femoral neck is relatively short and eroded posteriorly. Although the lesser trochanter is visible, the superior surface end tip is eroded. When viewed medially, the specimen exhibits a fracture that goes through the fovea capitis (figure 4.3).

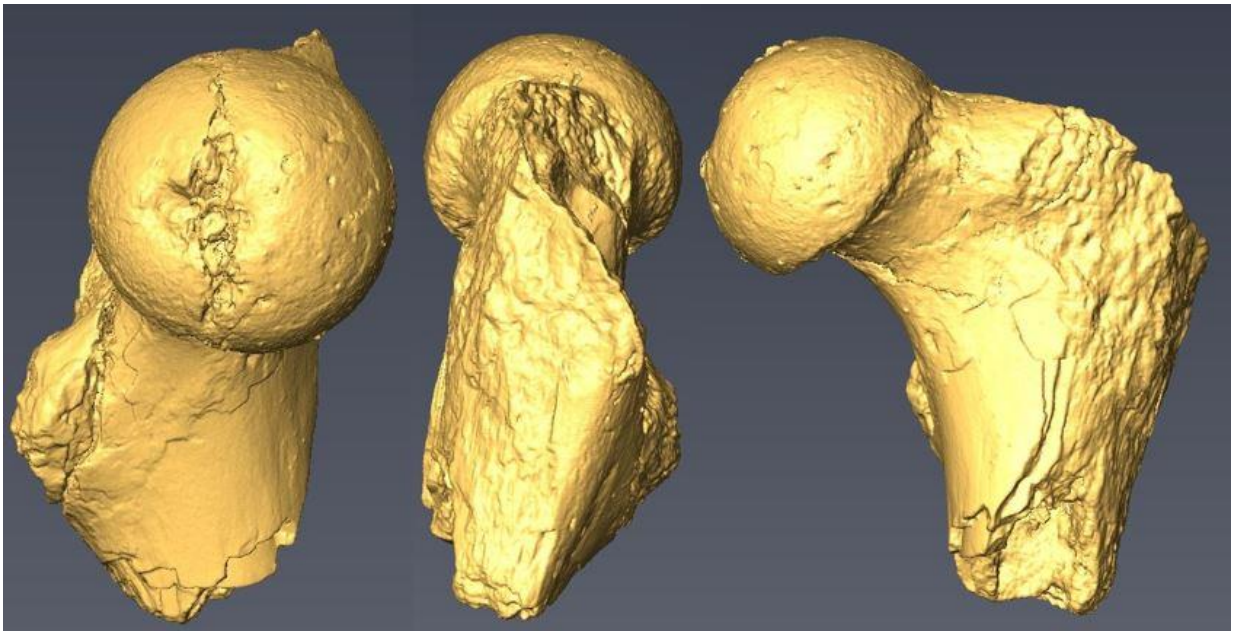

Figure 4.3: SWP 526 with fractured fovea captis (L), eroded great trochanter (C) and anterior view.

SWP 528

The specimen is a left proximal femur, with a very well preserved femoral head. The fovea capitis is well preserved and relatively circular. The femoral neck is relatively short with minor erosion affecting the femur head and femur neck junction area. The greater trochanter is partially preserved with cortical bone eroded away on the lateral surface, while the lesser trochanter is perfectly preserved. However, though the greater trochanter is partially preserved, the trochanteric fossa is visible (figure 4.4).

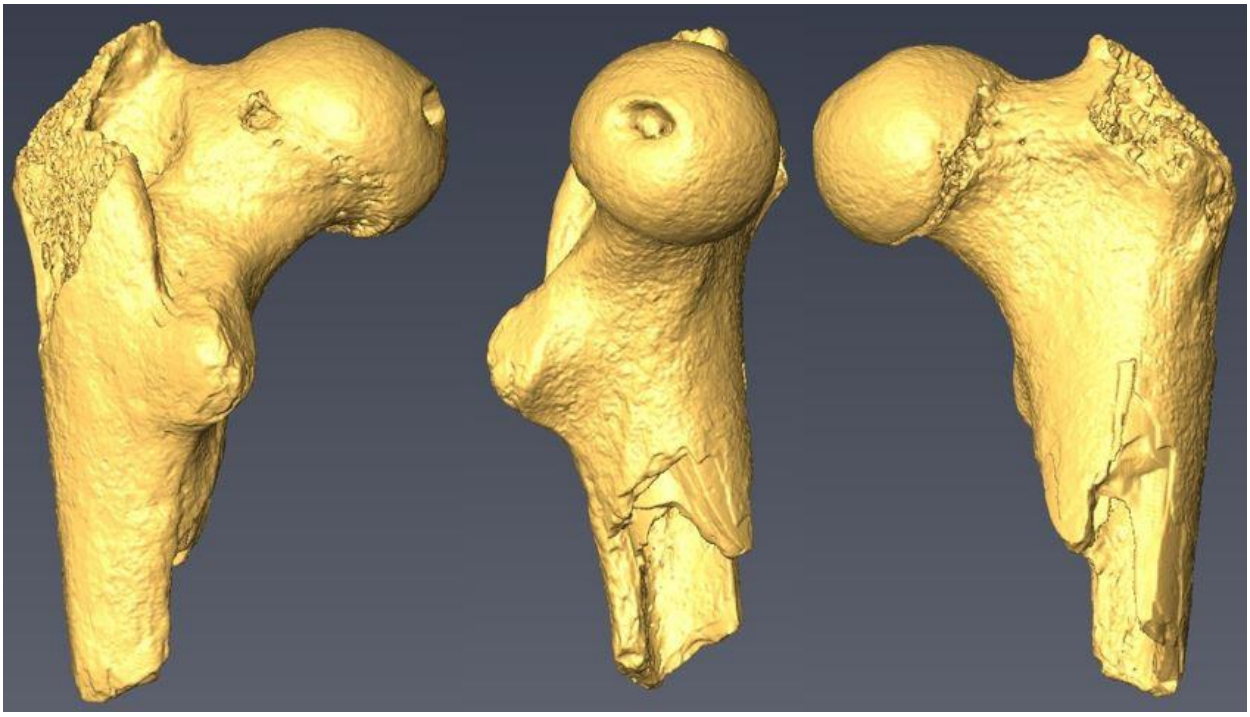

***Figure 4.4*:** Specimen SWP 528 showing recorded greater trochanter (L), perfectly fovea capitis (C) and anterior view.

SWP 529

This is a well preserved left femur. The head is completely preserved with relatively short neck and fovea capitis that is posteriorly orientated. Both lesser and greater trochanter are preserved. When viewed either mediolaterally or anteroposterioly, the greater trochanter projects above the femur head (figure 4.5).

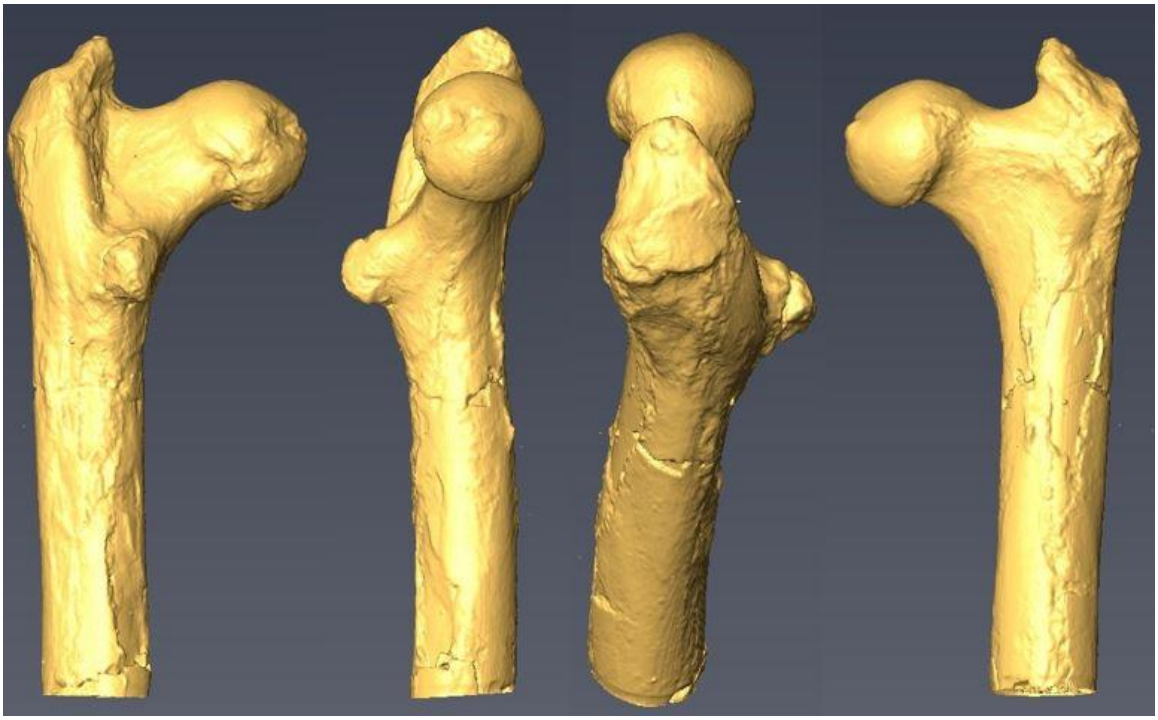

***Figure 4.5*:** Posterior, medial, lateral and anterior views of **SWP 529** showing a well preserved proximal femur features.

SWP 531

This is a right proximal femur with well-preserved femoral head and a circular fovea capitis. The lesser trochanter is missing but the greater trochanter is partially preserved and laterally eroded. The femoral neck is relatively short and consists of two distinct circular marks suspected to puncture marks from a predator (figure 4.6). The anterior view shows that the partially preserved greater trochanter is not projecting above the femoral head but placed below it instead.

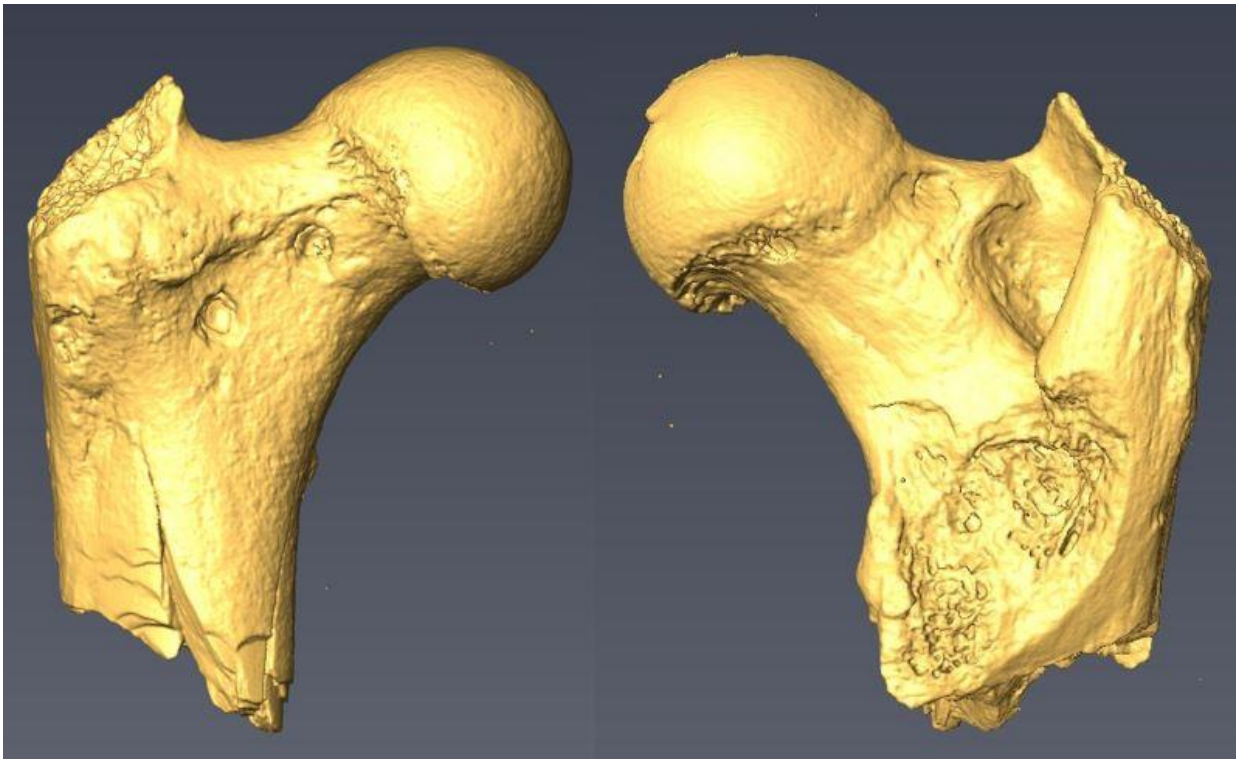

***Figure 4.6*:** Specimen SWP 531 with 2 Circular marks on femur neck (L) and partly preserved greater trochanter and trochanteric fossa (R).

SWP 532

The specimen is a well-preserved right femur. It preserves a semi-circular fovea capitis that is posteromedially orientated and a relatively short femur neck (figure 35). The greater trochanter is preserved. However, the superior part of the lesser trochanter is eroded and missing. The specimen is fractured around the shorter femur neck, below the greater trochanter as well as through the trochanteric fossa. When the specimen is viewed anteriorly, the greater trochanter projects above the femoral head (figure 4.7).

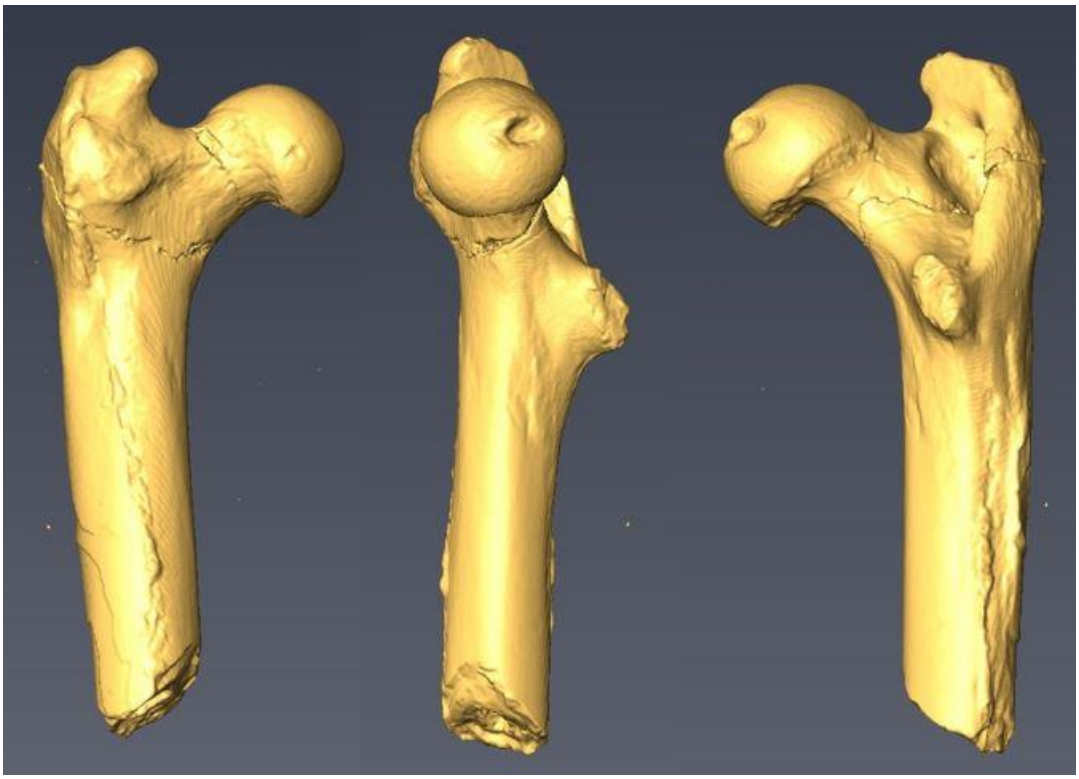

Figure 4.7: Fractured femur neck and post greater trochanter (L), preserved fovea captis (C) and preserved trochanteric fossa (R) of SWP 532.

SWP 533

The specimen is a right proximal femur and is highly weathered, particularly on the lateral region of the greater trochanter (figure 4.8). The posterior aspect of the lesser trochanter is missing. The specimen consists of a relatively long femoral neck, with the cortical bone being eroded away on the anterior aspect. Although the fovea capitis is preserved, it is not well defined due to a fracture running from anteromedially to anterolateral view (figure 4.8). Another fracture is observed below the lesser trochanter, going around the specimen as it divides the shaft from the proximal part. The partially eroded greater trochanter slightly projects above the femoral neck (figure 4.8). The femoral head and greater trochanter of the specimen are almost the same height when viewed anteroposterioly.

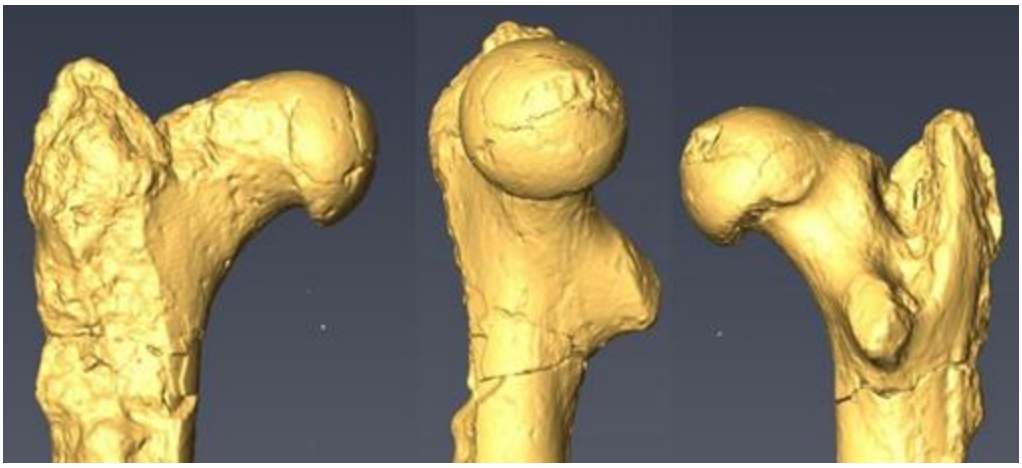

***Figure 4.8*:** Specimen SWP 533 exhibiting a highly eroded cortical bone (R), fractured femur head (C) and trochanteric fossa (L).

SWP 747

This is a right femur with a well preserved femoral head. The femoral head is perfectly spherical and comprises of fovea capitis that is enlarged posteroinferiorly. The greater and lesser trochanters are missing. The femoral neck is relatively short and damaged (figure 4.9).

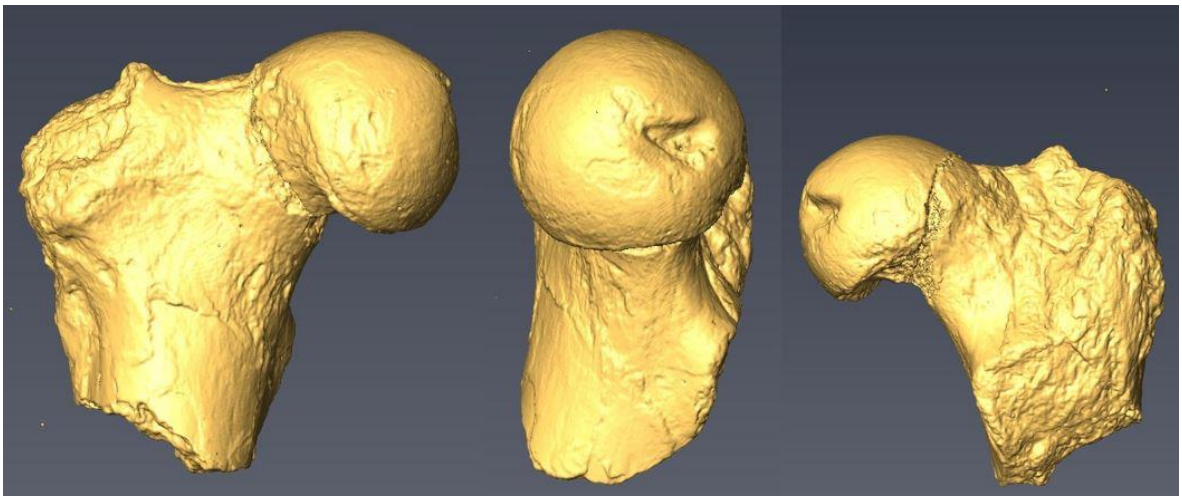

Figure 4.9: SWP 747 with fractured femur neck (R), preserved fovea captis (C) and highly eroded greater trochanter (L).

SWP 749

This specimen is a right femur head. The femur neck and the greater trochanter as well as the lesser trochanter are not preserved. The femoral head is spherically shaped with a well preserved fovea capitis (figure 4.10).

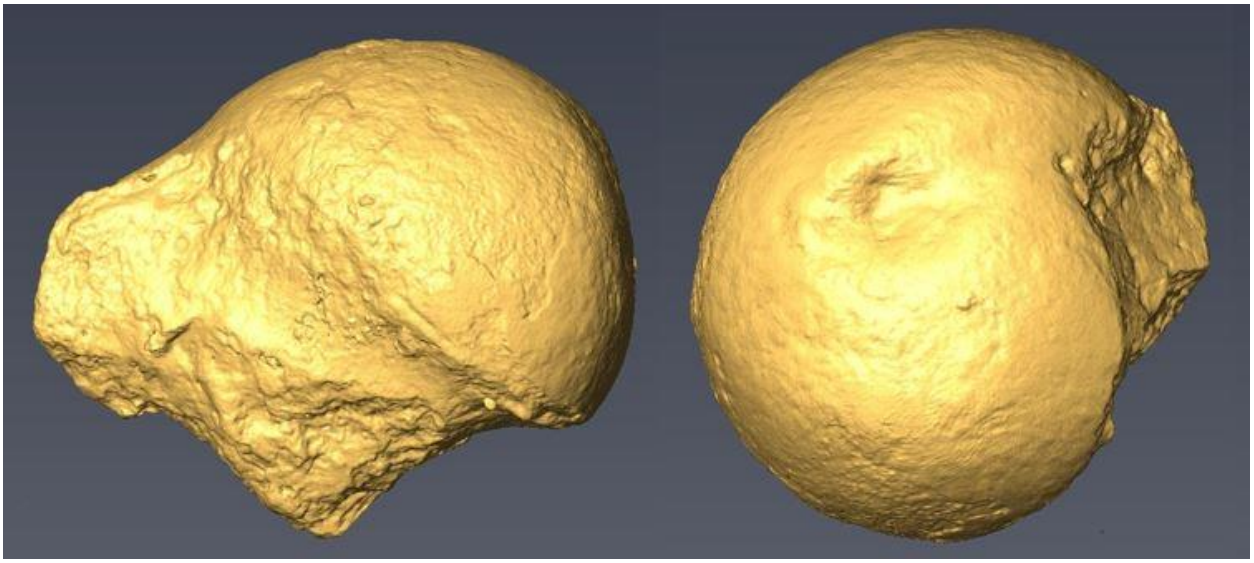

Figure 4.10: Anterior view (L) and fovea captis (R) in medial view of preserved femur head of SWP 749

SWP 753

This is a right proximal femur, which preserves the femur head and neck only. The neck is relatively short and the junction with the head is weathered. The greater trochanter and lesser trochanter are missing (figure 4.11). The femur head is not perfectly spherical owing to the eroded capitis fovea and cortical bone in the medial, the superior and lateral regions.

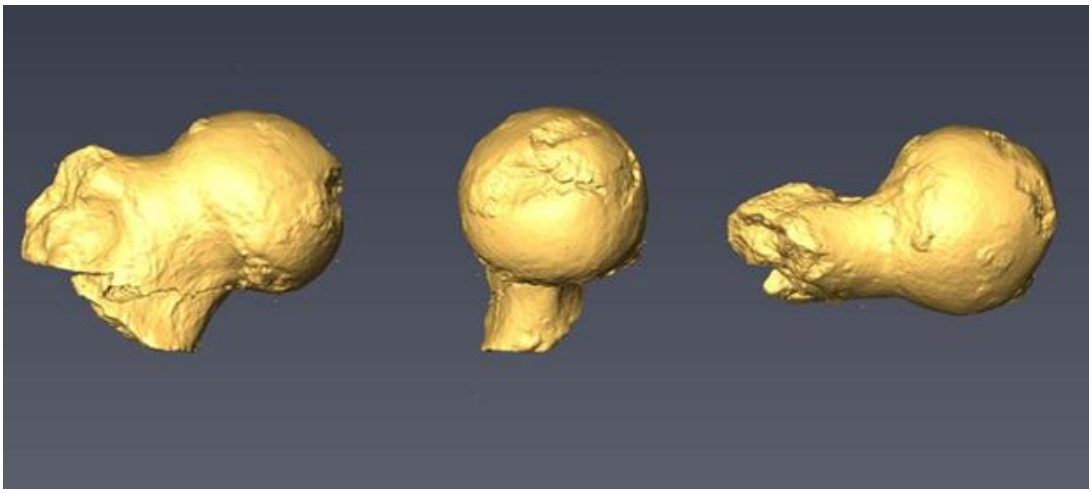

***Figure 4.11*:** SWP 753 showing femur neck and head (L), eroded fovea captis (C) and superior view (R).

SWP 756

Specimen SWP 756 is a femur head with a partial femur neck (figure 4.12). The femoral neck is relatively long and its anterior aspect is missing, leaving the posterior area as the only part of the neck preserved. The femoral head and the femoral neck junction lacks the cortical bone anteriorly. However, the fovea capitis is perfectly preserved and is medioposteriorly orientated. The greater trochanter, the lesser trochanter and trochanteric fossa are not preserved.

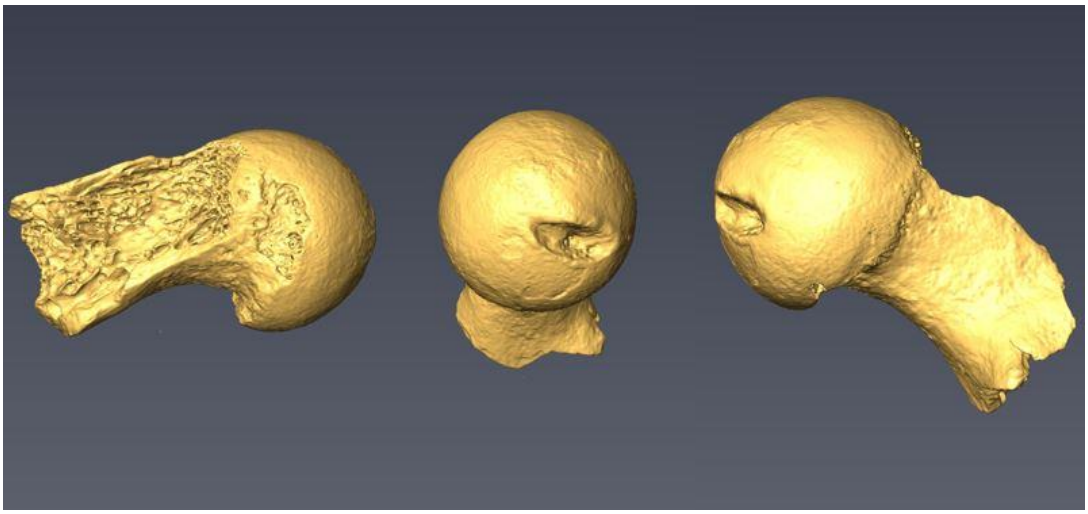

Figure 4.12: SWP 756 with a relatively long neck with exposed trabeculae (L), a perfectly mediolateral orientated fovea captis (C) and preserved spherical head viewed posteriorly (R).

SWP 1009

The specimen is a left proximal femur preserving the femur head (figure 4.13). The femoral head shows a posterolaterally damaged fovea capitis. The specimen consists in a relatively short neck and a partially preserved lesser .

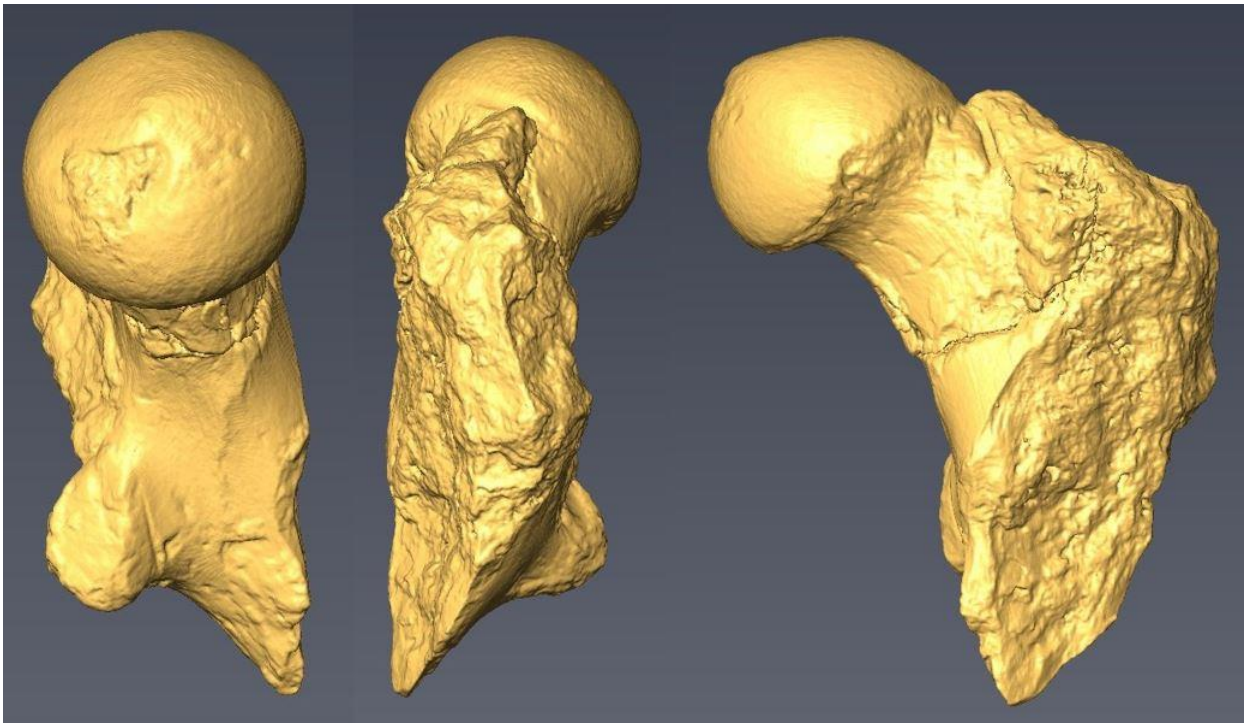

***Figure 4.13*:** A well preserved head with posterolateral damaged fovea captis (L), eroded greater trochanter in lateral view (C) and shorter neck visible in anterior view (R) of SWP 1009

SWP 1011

This specimen is a left proximal femur and it comprises of preserved proximal femur head, the femur neck and the lesser trochanter without the greater trochanter. The femur head consist of fovea captis that is posterolateraly and superoinferiorly eroded. The specimen is anteriorly fractured in the femur head (figure 4.14). This specimen consists of a relatively long femur neck, that is also mediolaterally fractured as illustrated by figure 4.14 below.

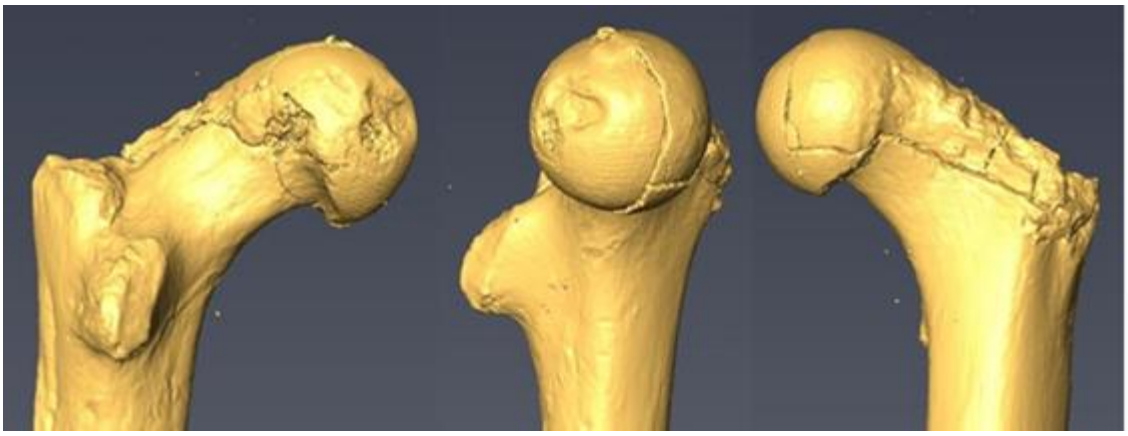

***Figure 4.14*:** Long and fractured femur neck (L, R) and posteriorly eroded fovea captis (C) of SWP 1011.

SWP 1203

This is a relatively well preserved left proximal femur with exception of the greater trochanter that has its most superior tip being eroded. It contains proximal femur head with fovea captis and relatively short neck as well as the lesser trochanter. Although the greater trochanter superior most tip end is eroded, trochanteric fossa is preserved. When viewed anteriorly, the remaining portion of the greater trochanter project slightly above the femur head as illustrated by figure 4.15.

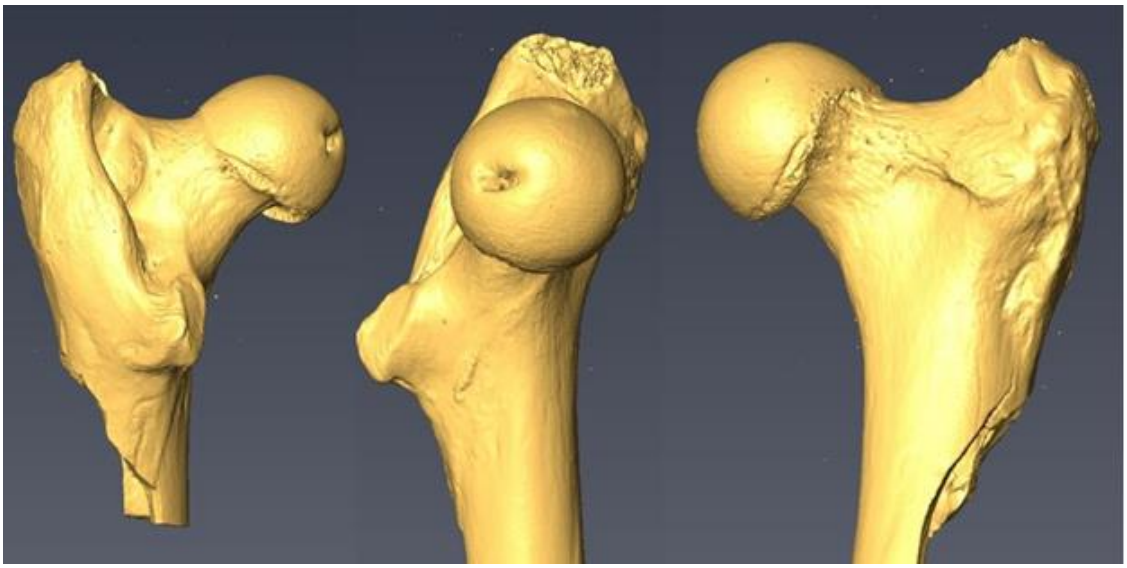

***Figure 4.15*:** SWP 1203 with a well preserved proximal femur with eroded greater chanter.

SWP 1384

This specimen is a right femur with preserved proximal femur head, a relatively long femur neck with greater trochanter and less trochanter are not preserved. The femur head comprises of slightly eroded fovea captis. The femur neck exhibit deep vertically concave cut superiorly, an action probably resulting in the removal of the greater trochanter (figure 4.16).

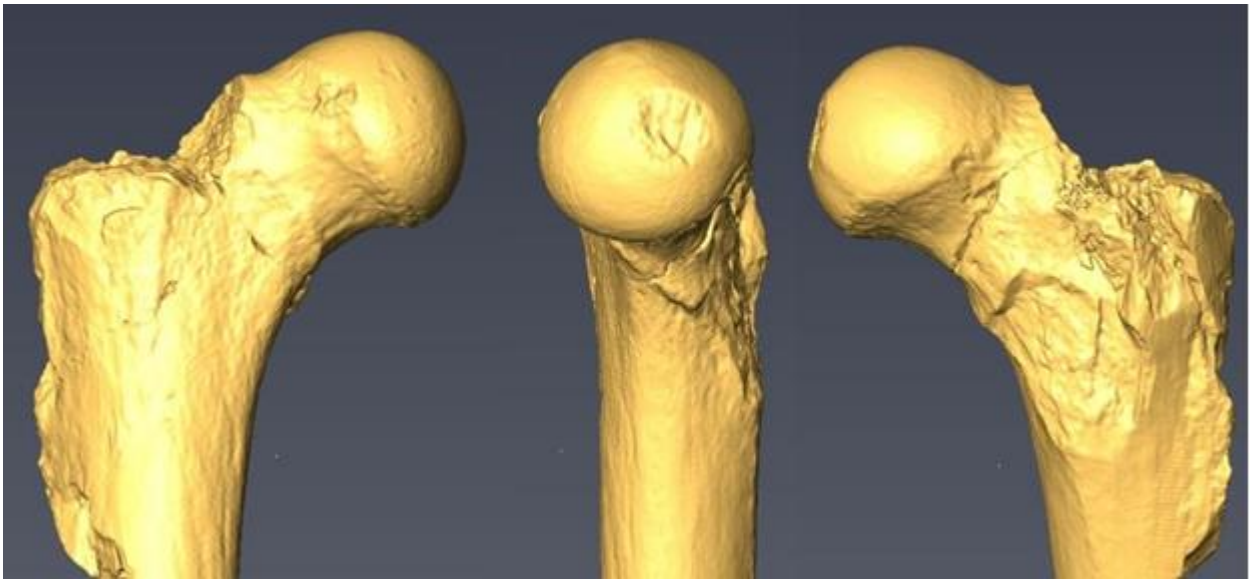

Figure 4.16: SWP 1384 femur neck with vertical concave cut (L) eroded fovea captis (C) and relatively long femur neck (R).

SWP 1698

This is a left side femur with proximal femur head exhibiting anteroposterioly orientated fovea captis. The greater trochanter and a relatively short femur neck are preserved while the lesser trochanter is missing. However, the greater trochanter exhibits cortical bone erosion on medial region as well are a fracture that tend to divide it with the rest of proximal femur features. An anterior view of the specimen shows that the greater trochanter project above the femur head as seen in figure 4.17 below.

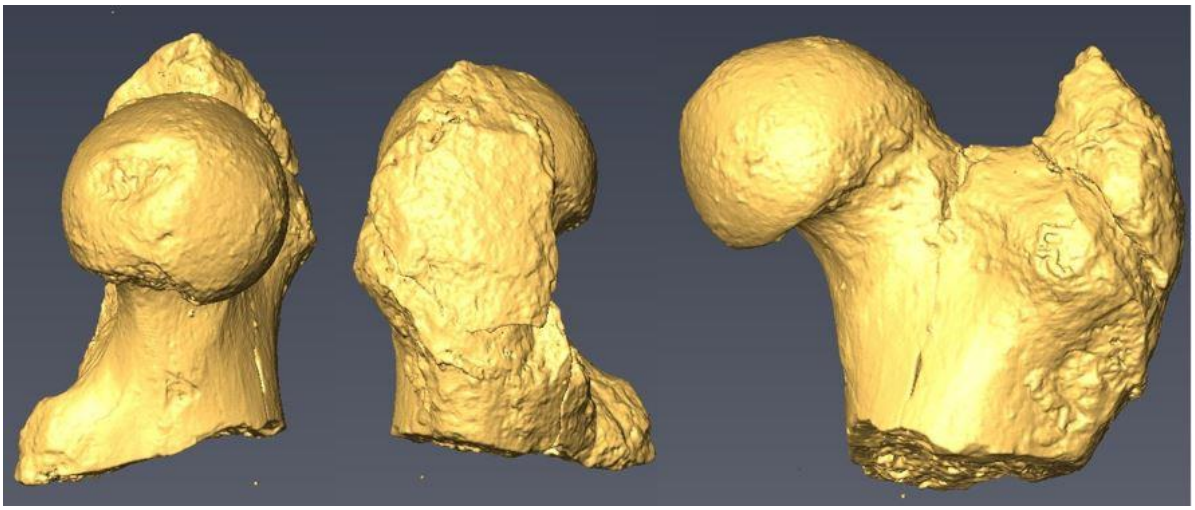

***Figure 4.17*:** Specimen SWP 1698 with greater trochanter projecting above the femur head (L) and lateral view illustrating cortical erosion (C) and anterior view (R).

SWP 1699

This specimen is a left proximal femur. The proximal femur head is preserved but its cortical bone is eroded posteriorly and this affected the fovea captis as well (figure 4.18). The greater trochanter is not preserved but the lesser trochanter is preserved even though its posterior most tip end is not preserved. The femur neck is preserved and is relatively short. Generally, the specimen's posterior and medially cortical bone is highly eroded as evidenced (figure 4.18).

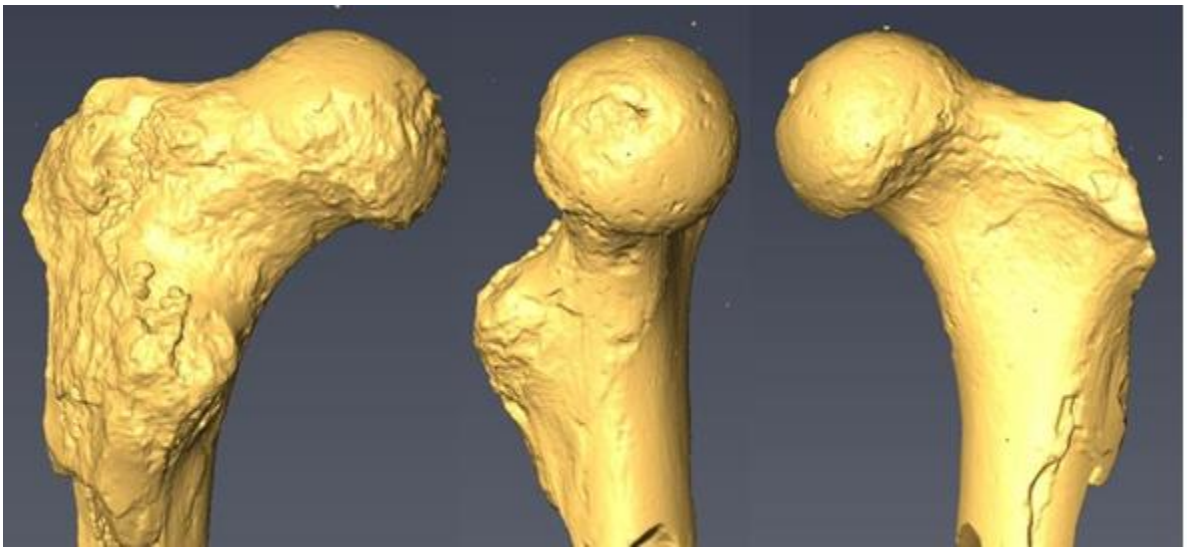

***Figure 4.18*:** Eroded cortical bone (L), fovea captis (C) and short neck (R) of SWP 1699.

Sts 2050

The specimen is a left proximal femur. Preserved features include femur head and its relatively long femur neck only the lesser and great trochanters (figure 4.19). This specimen consists of spherical femur head, with its fovea capitis partially sediments filled. The femur head has 'Y' shaped fracture, with the superior tip end of the fracture extending laterally towards the neck while the inferior end of the fracture extends superolateral (figure 4.19).

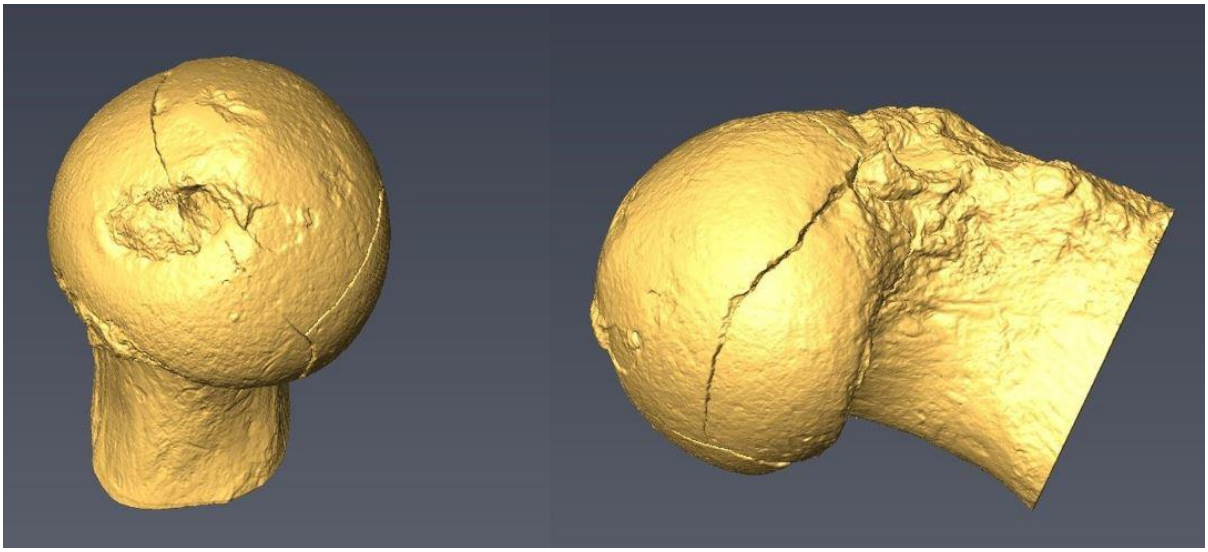

***Figure 4.19*:** Partially sedimented fovea captis (L) and fractured anterior aspect of femur head (R) of specimen Sts 2050.

Sts 2259

This is a left femur with a proximal femur head and the femur neck being the only preserved features of the proximal aspect (figure 4.20). The femur head is not spherical due to eroded fovea capitis. This erosion resulted in the development of a relatively large and intense collapse in the fovea captis region, removing most of cortical bone medially. The specimen consists of extremely short femur neck, which is highly weathered resulting to erosion of cortical bone as illustrated by figure 4.20 below. The greater trochanter as well as the lesser trochanter are not preserved, resulting in the trochanteric fossa not being preserved.

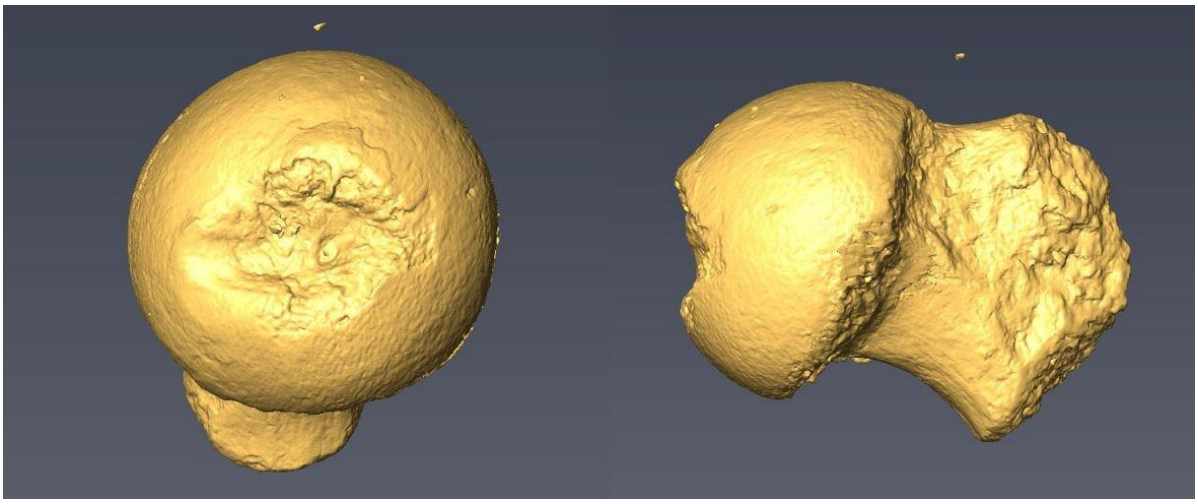

***Figure 4.20*:** Specimen Sts 2259 showing highly weathered fovea captis (L) and severely eroded femur neck (R).

Sk 605

This specimen is a left femur with preserved proximal femur head, femur neck, the lesser trochanter and partially greater trochanter (figure 4.21). The femur head is spherical and is attached to a relatively shorter neck The fovea capitis is rounded and well preserved. The specimen exhibit removed cortical bone anterosuperiorly of the femur head. The lesser and greater trochanters are preserved although the greater trochanter's superior most end is not preserved (figure 4.21).

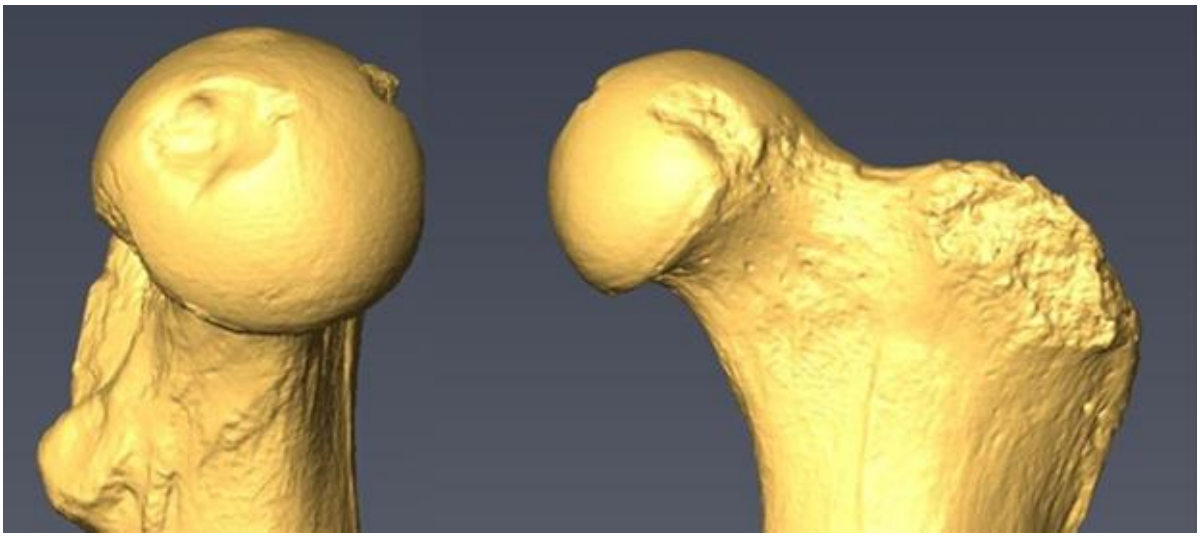

Figure 4.21: Preserved fovea captis (L) and eroded greater trochanter (R) of SK 605.

Sk 607

This specimen is a right femur and consist of proximal femur head, femur neck, lesser trochanter and part of the shaft (figure 4.22). The perfectly spherical femur head comprise of partially sediments filled fovea captis and is attached to its relatively long neck, which is superiorly cortically weathered and is mediolaterally fractured. Although the femur head is spherical, it is weathered on its junction with the neck. The lesser trochanter is preserved but the greater trochanter as well as trochanteric fossa are not preserved as seen in figure 4.22 below.

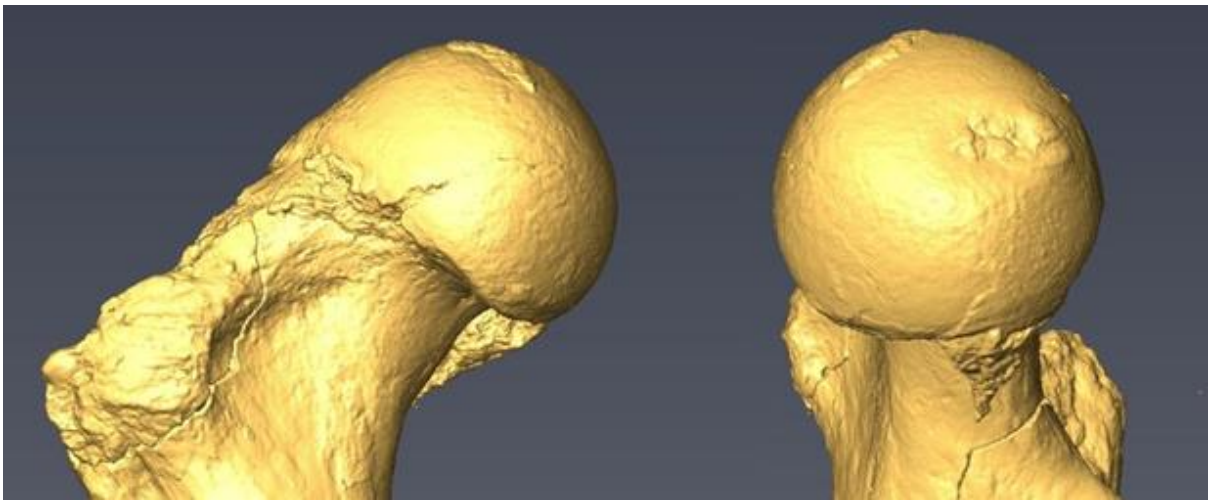

Figure 4.22: SK 607 with weathered and fractured neck (L) and spherical proximal head (R).

Sk 1513

This is a right proximal femur, with preserved femur head and its relatively short femur neck (figure 4.23). The femur head is not perfectly spherical due to eroded cortical bone, particularly along its junction with its femur neck. Erosion of cortical bone resulted in exposure of trabecular bone to external factors. The femur head is fractured anterosuperiorly, through the fovea capitis to the inferior region. The trochanteric fossa is not preserved due to eroded lesser and greater trochanters (figure 4.23).

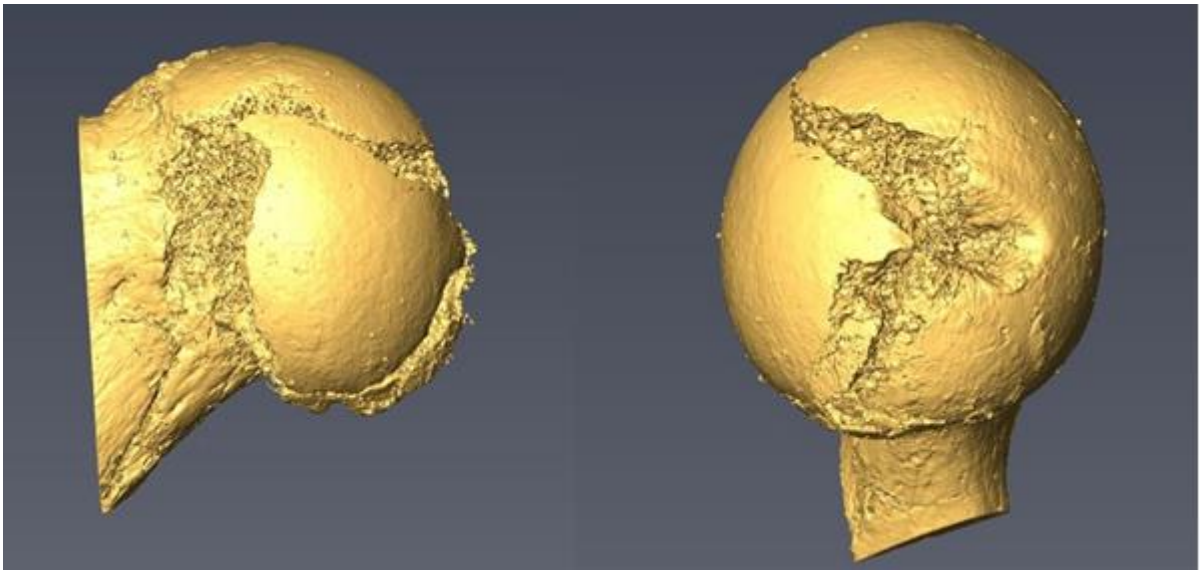

***Figure 4.23*:** SK 1513 with anteriorly eroded cortical bone (L) and fractured fovea captis (R).

Sk 2595

This specimen is a right proximal femur, consisting of femur head, femur neck and the greater trochanter (Figure 4.24). The femur head is spherical and is attached to a relatively short neck. Cortical bone in the medial aspect of femur head is slightly weathered, concealing the fovea capitis. Although the greater trochanter is preserved, it is superiorly weathered and eroded. Therefore, its height is reduced and is relatively level with the femur head as illustrated by figure 4.24 below.

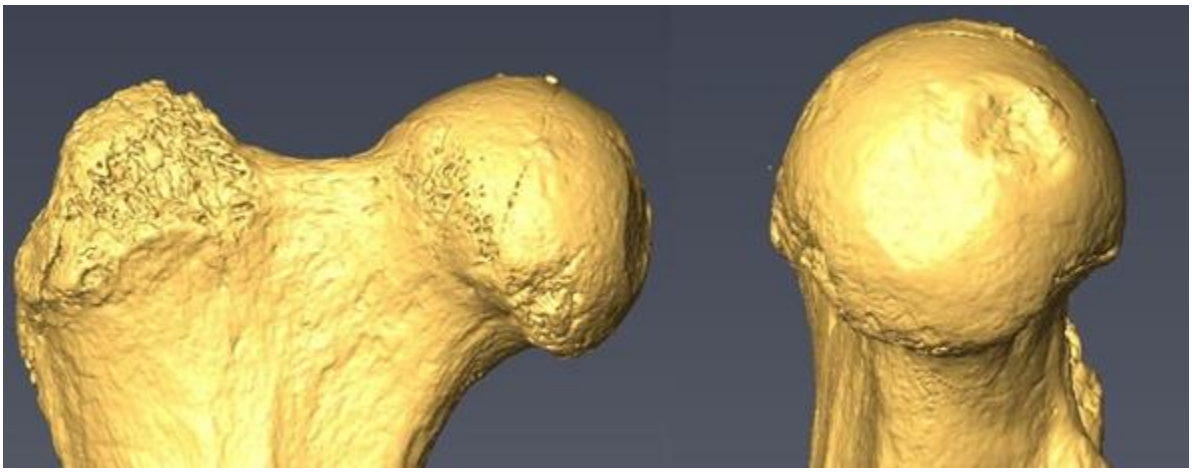

***Figure 4.24*:** SWP 2295 with a relatively short femur neck (L) and almost concealed fovea capitis area (R)

SK 14015

This specimen is a right proximal femur, consisting of femur head and the femur neck only (figure 4.25). The greater trochanter and lesser trochanter are both not preserved. It is difficult to determine the relative size of the femur neck because the specimen's femur neck was cut just below the femur head. The head is perfectly spherical but have a large linear and deep fovea capitis area. This may be attributed to eroded surface in the anteromedial views, eroding cortical bone and exposing the trabecular bone (figure 4.25 below).

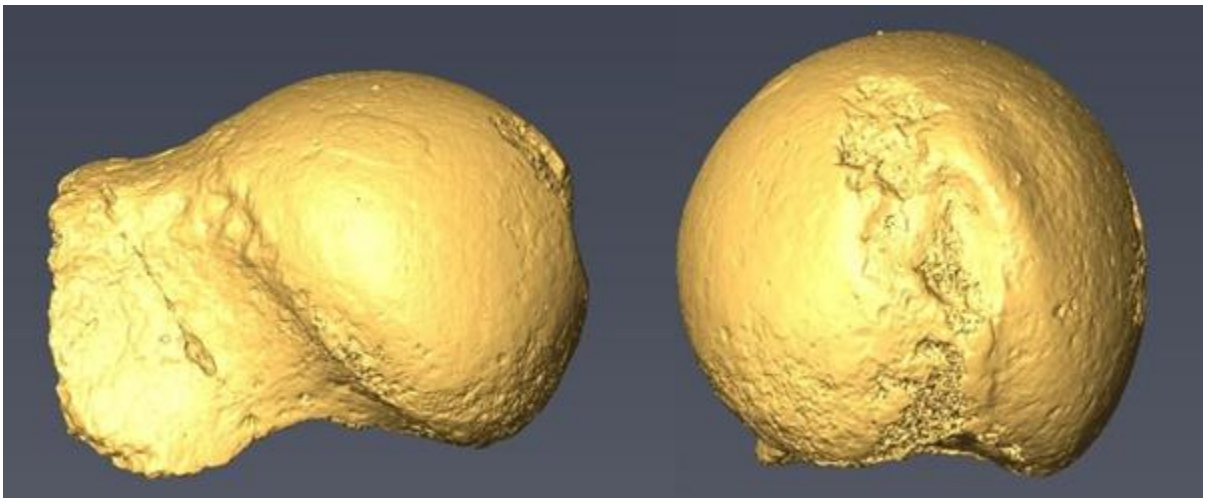

***Figure 4.25*:** Anterior view with a relatively spherical femur head (L) and a large linear capitis fovea area on medial section (R) of specimen SK 14015.

BF 36

This is a left proximal femur and is imbedded in a matrix that has also cemented its phalanges posteriorly as well as distal part of the femur shaft. The femur head is well-preserved, with relatively long neck, that is fractured around in a manner that it divide the femur head and trochanters as seen in figure 4.26 below. The proximal femur head is perfectly spherical with well-preserved and rounded fovea captis. (figure 4.26).

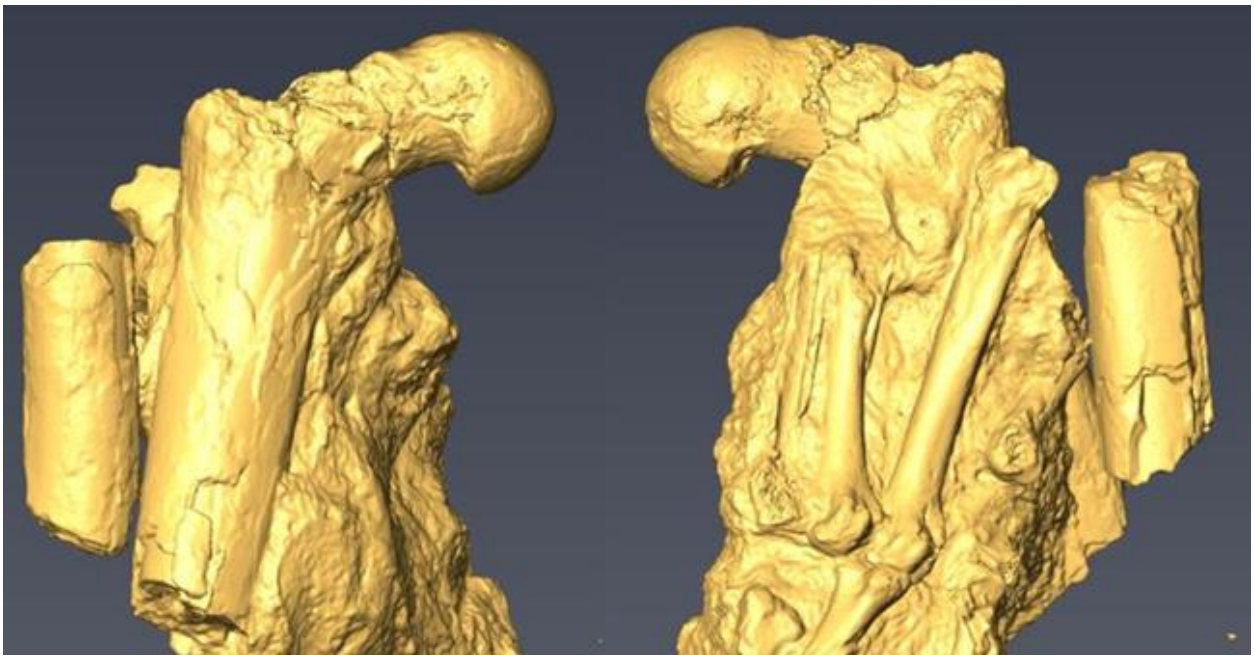

Figure 4.26: Specimen BF 36 showing proximal femur with laterally attached distal shaft (L) and cemented phalanges on the posterior region (R).

4.1.2 Fossil humeri

1930M

This specimen is a right proximal humerus, which preserves the humeral head (figure 4.27). The humeral neck is well developed and well defined. The greater and lesser tubercles are also preserved, with a well-defined sulcus intertubercularis.



***Figure 4.27*:** A well preserved specimen with defined tubercles and anatomical neck of 1930M

1934M

This specimen is a right proximal humerus (Figure 4.28). The greater and lesser tubercles are preserved observable, as well as a well-preserved sulcus intertuberclaris. Although the neck is preserved, it is mediolaterally marginally eroded.

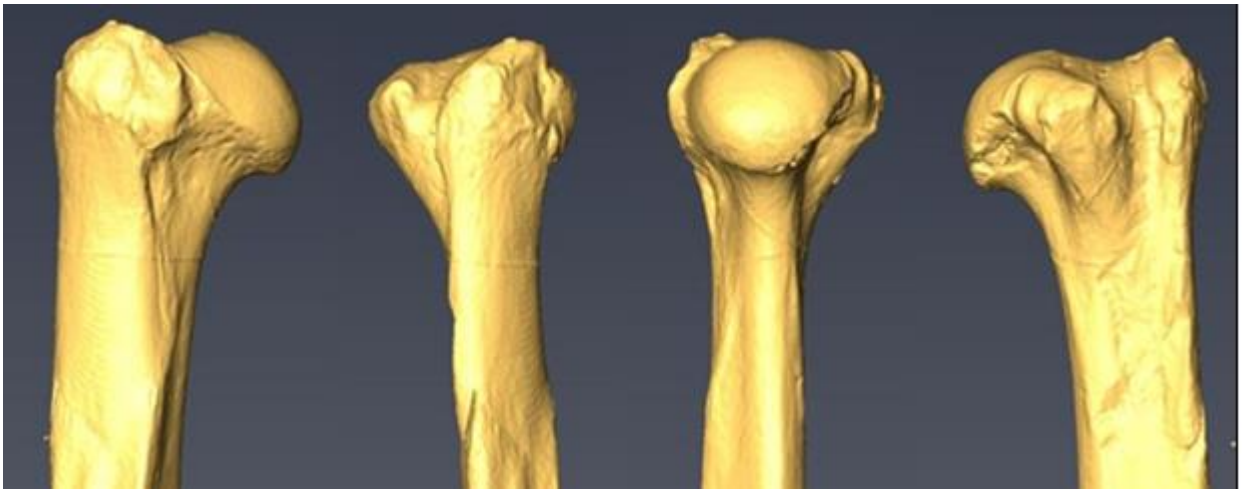

Figure 4.28: A well preserved humerus of 1934M with all its proximal features visible.

SWP 606

This specimen is a left humeral head that preserves the junction with the humeral shaft (figure 4.29). The head of the humerus is perfectly spherical, with thin eroded cortical bone. The lesser tubercle is partially preserved.

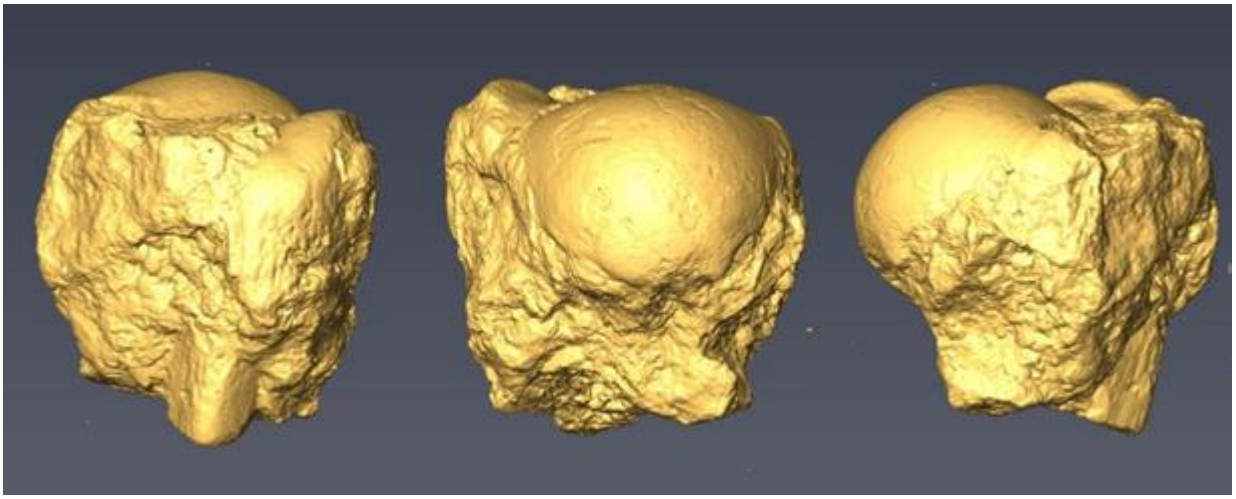

***Figure 4.29*:** Anterior view (L), a perfectly spherical head (C) and medial view (R) of SWP 606.

SWP 962

This is a right humerus with most of its proximal end preserved. The head and neck are preserved and well-defined (figure 4.30). Greater and lesser tubercles and the sulcus intertubercularis are preserved . The superior aspect of the humeri head has two distinct small circular marks that are oriented antero-superiorly. The head is fractured laterally and posteriorly. The cortical bone is weathered on the medial aspect and missing on the contact are between the head and the neck.



***Figure 4.30*:** Specimen 962 showing preserved greater and lesser tubercle with 2 small circular marks superiorly (L), removed cortical bone on the neck-head contact area (C) and fractured head (R).

SWP 1406

This is a well-preserved right proximal humerus. The humeral head is perfectly spherical. The greater tubercle is partially preserved and, when viewed laterally, the greater tubercle projects above the humeral head (figure 4.31). The cortical bone is eroded on the contact area between the head and shaft.

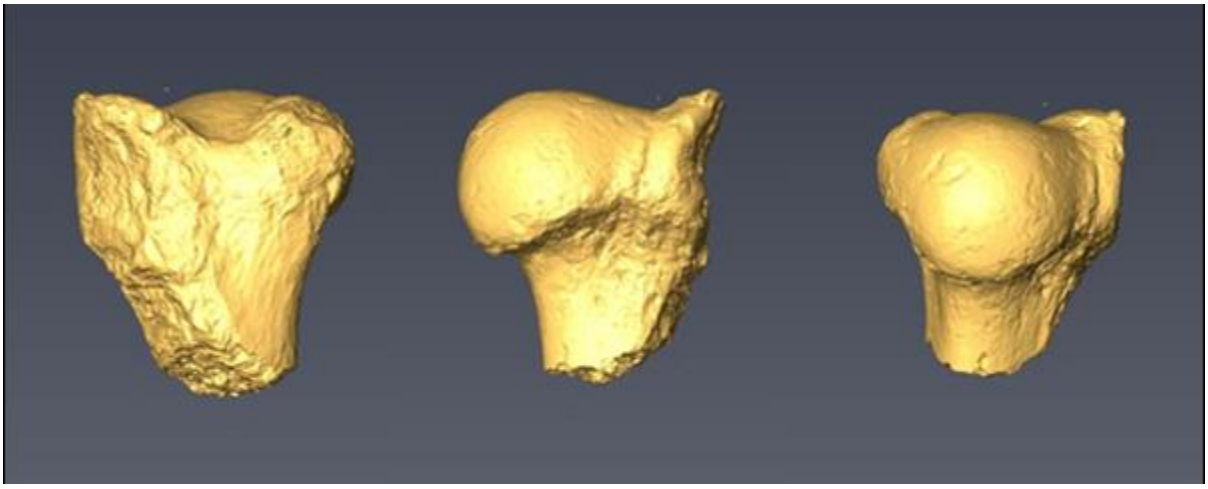

***Figure 4.31*:** Slightly preserved grater tubercle (L), greater tubercle projecting above humerus head (C) and spherical humerus head (R) of SWP 1406.

4.1.3 Fossil tibiae

SWP 1411

This is a left proximal tibia. with the area near the medial condyle and lateral condyle facets just below tibial plateau being eroded, exposing trabecular bone and sediment infiltration (figure 4.32). Both medial and lateral intercondylar eminences are preserved. The tibial tuberosity is partially preserved. The soleal line is not visible.

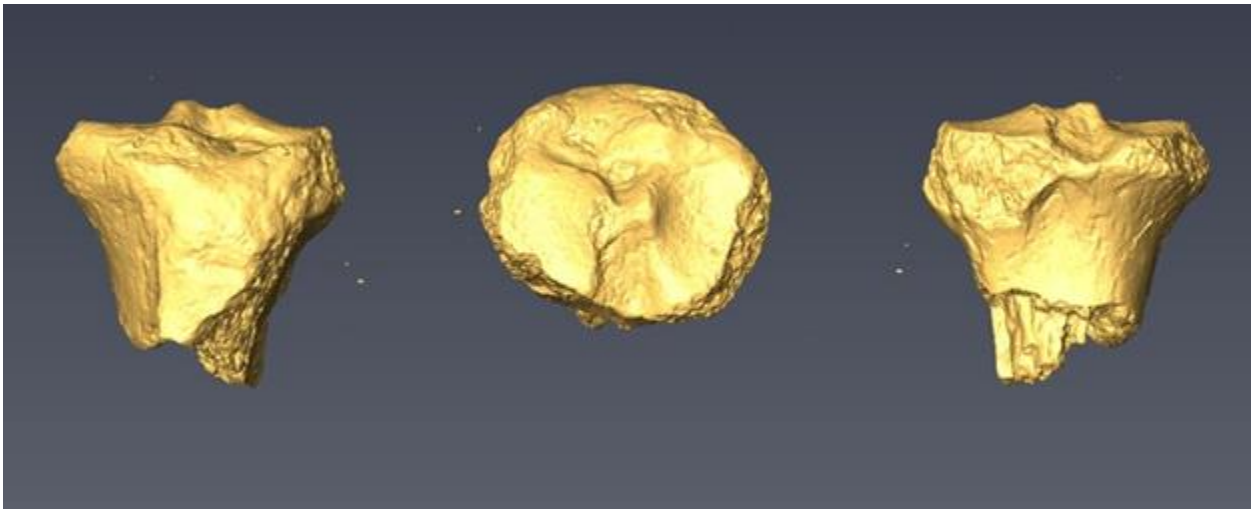

Figure 4.32: SWP 1411 with partially preserved tibial tuberosity (L), superior view showing eroded medial and lateral facets (C) and posterior view with no soleal line (R).

SWP 1546

This specimen is a left tibia with the proximal part and a portion of the shaft preserved (figure 4.33). Lateral and medial condyles are preserved as well as the intercondylar eminences, which are marginally eroded. The soleal line is also visible. The tibial tuberosity is preserved though is also eroded . Two fractures run around the soleal line and the tibial tuberosity, separating the epiphysis and the shaft .

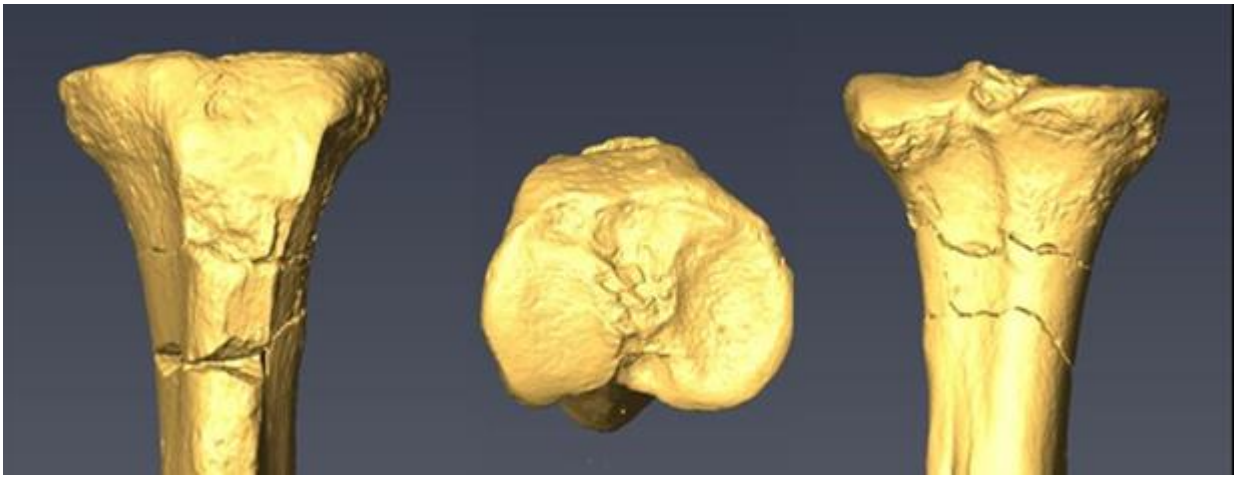

Figure 4.33: SWP 1546 with eroded and fractured tibial tuberosity (L), marginally removed intercondylar eminences (C) and fractured soleal line (R).

SWP 1596

This specimen is a right proximal tibia. It exhibits weathered cortical bone on lateral and medial condyles, but the intercondylar eminences are preserved. The tibial tuberosity is not preserved and there is a fracture running along the tibial tuberosity area, from the superior to the inferior parts. The fractures are observable in the medial area as well as in the tibial tuberosity region. The soleal line is preserved although some of adjacent cortical bone is eroded (figure 4.34).

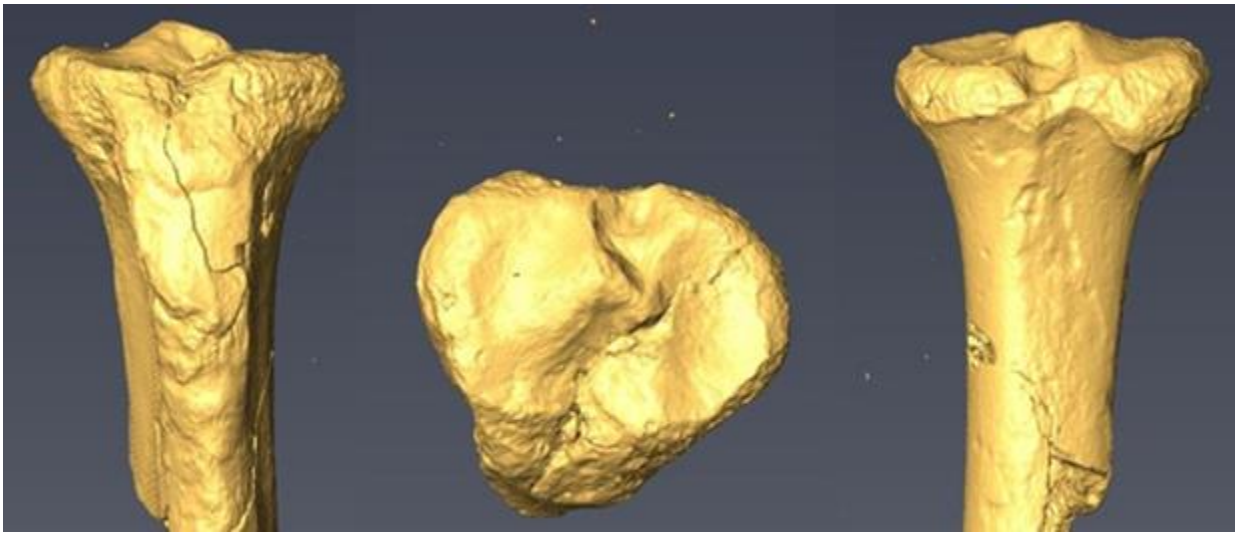

***Figure 4.34*:** Eroded and fractured tuberosity area (L), preserved condyles and intercondylar eminence (C) and preserved soleal line (R) of specimen SWP 1596.

TP 18

Specimen TP 18 is a right tibia with a well preserved proximal part. Preserved parts include lateral and medial condyles, intercondylar eminences, tibial tuberosity and soleal line (figure 4.35). The specimen has two fractures visible on the posterior surface of the shaft.



***Figure 4.35*:** Anterior view with tibial tuberosity (L) and two fractures posteriorly (R) of TP 18

4.1.4 Fossil calcanei

2222M

This specimen is a left calcaneus that is badly preserved. Most of the cortical bone is missing (figure 4.36). The superior aspect of the posterior facet, medial process of calcaneal tuberosity, the superior part of the calcaneal tuberosity are all missing. However, the inferior section, the sustentaculum tali and the anterior end of the contact facet with the cuboid are perfectly preserved (figure 4.36).

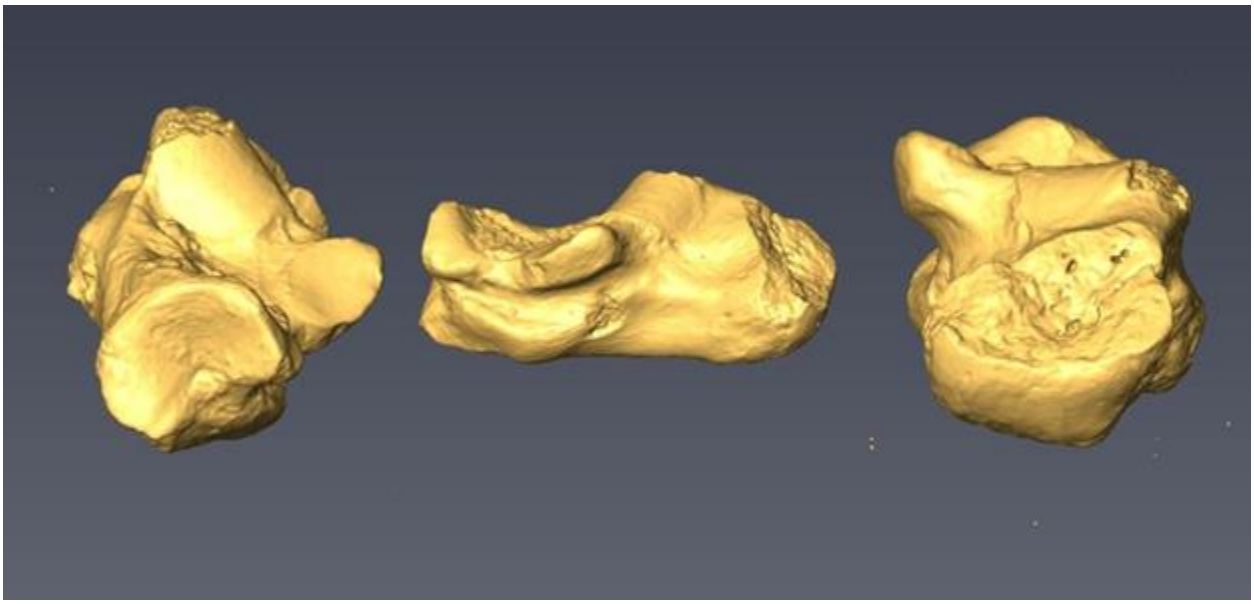

Figure 4.36: Anterior view (L), medial view (c) and posterior view (R) showing missing and preserved parts of 2222M.

SWP 537

This is a left calcaneus. Most of the anterior and superior parts are missing. The cortical bone is highly weathered (Figure 4.37). The facet for cuboid is preserved. The posterior facet is preserved with a well-defined calcaneal tubercle as well as calcaneal tuberosity.

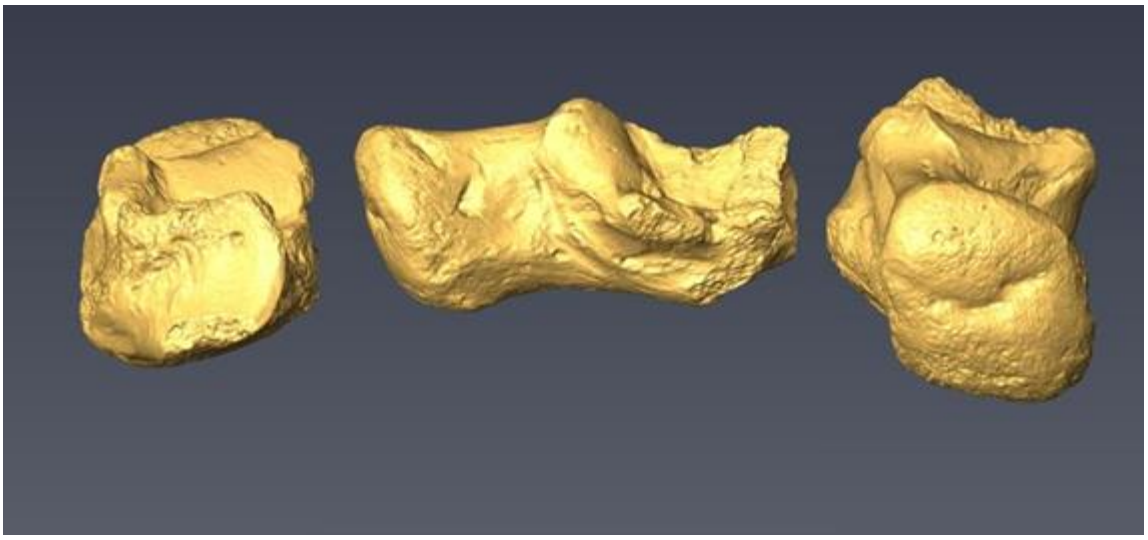

***Figure 4.37*:** Specimen SWP 537 showing facet for cuboid in anterior region (L), lateral view (C) and calcaneal tuberosity in the posterior area (R).

SWP 1146

This is left calcaneus specimen which is perfectly preserved. The contact facet with the cuboid, the calcaneal tubercle, the anterior facet, the sustentaculum tali, the sustentaculum facet, the posterior facet, the peroneal tubercle, and the calcaneal tuberosity are all preserved (figure 4.38). Although the specimen is generally well preserved, the cortical bone in the inferior area is slightly weathered.

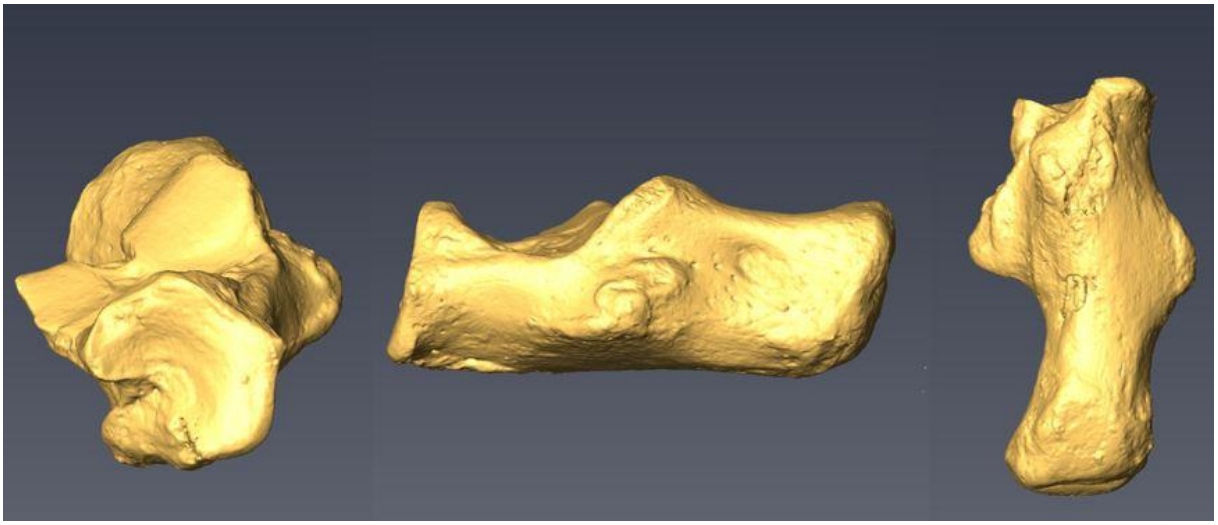

Figure 4.38: A perfectly preserved SWP 1146 showing anterior (L), lateral (C) and inferior (R).

SWP 1157

This specimen is a left calcaneus, which is fairly well preserved. The contact facet with the cuboid, the sustentaculum facet, the sustentaculum tali and the anterior process are preserved (figure 4.39). The anterior and posterior facets are preserved with a well-defined calcaneal tuberosity and peroneal tuberosity. However, the calcaneal tuberosity has minor cut in its superior region.

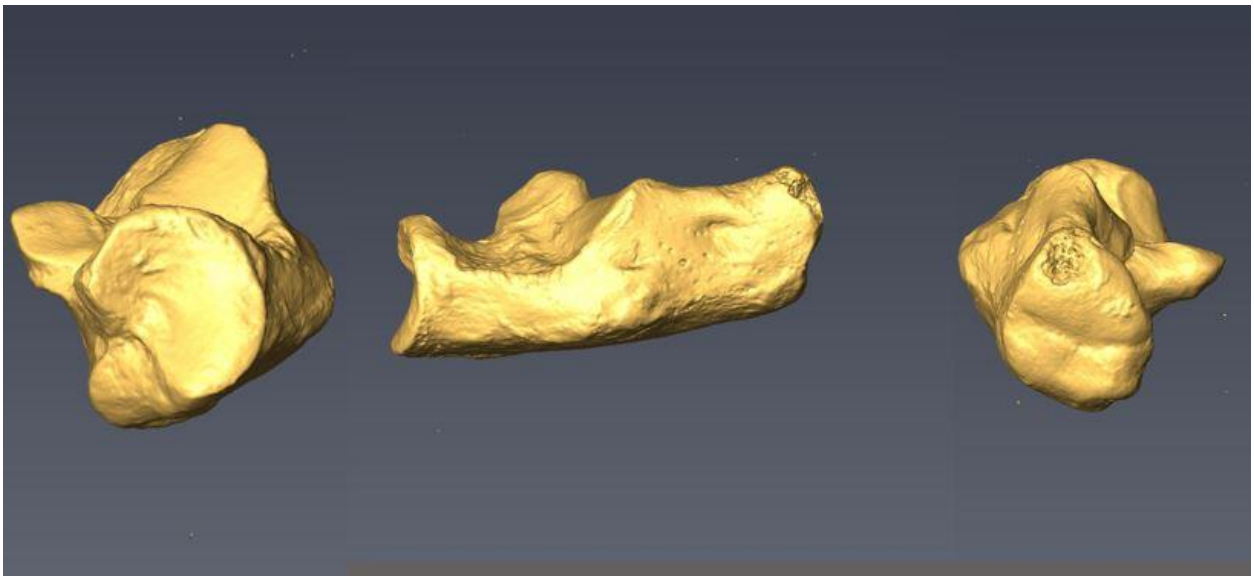

Figure 4.39*:* Facet for cuboid (L), preserved peroneal tuberosity (C) and eroded calcaneal tuberosity (R) of a fairly preserved specimen SWP 1157..

SWP 1161

The specimen is a right calcaneus and is fairly well preserved (Figure 4.40). However, the cortical bone is weathered in some areas and have sediment that resulted in several minute lumps on the surface (figure 4.40). Preserved parts include the contact facet with the cuboid, the anterior and posterior facets, the sustentaculum facet, sustentaculum tali, the anterior process, a well-defined calcaneal tuberosity and the peroneal tuberosity.

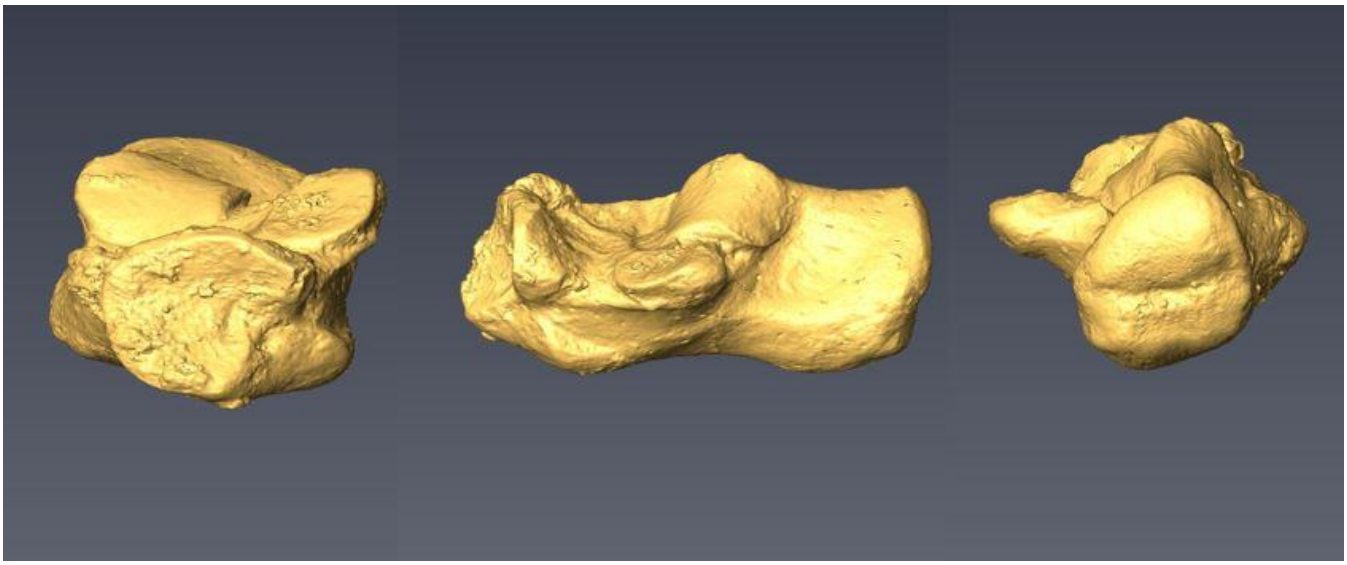

***Figure 4.40*:** SWP 1161 with a fairly preserved specimens showing minute lumps on the facet for cuboid in the anterior (L), lateral view (C) and a well-defined calcaneal tuberosity on the posterior (R).

SWP 1207

Specimen SWP 1207 is a right calcaneus (figure 4.41). With the exception of missing cortical bone in the inferoanterior region, this specimen is well preserved. The contact facet with the cuboid in the anterior section is preserved together with the anterior process, the posterior facet, the sustentaculum facet, the sustentaculum tali and the peroneal tuberosity. The specimen also consists in a well-defined calcaneal tuberosity in the posterior region.

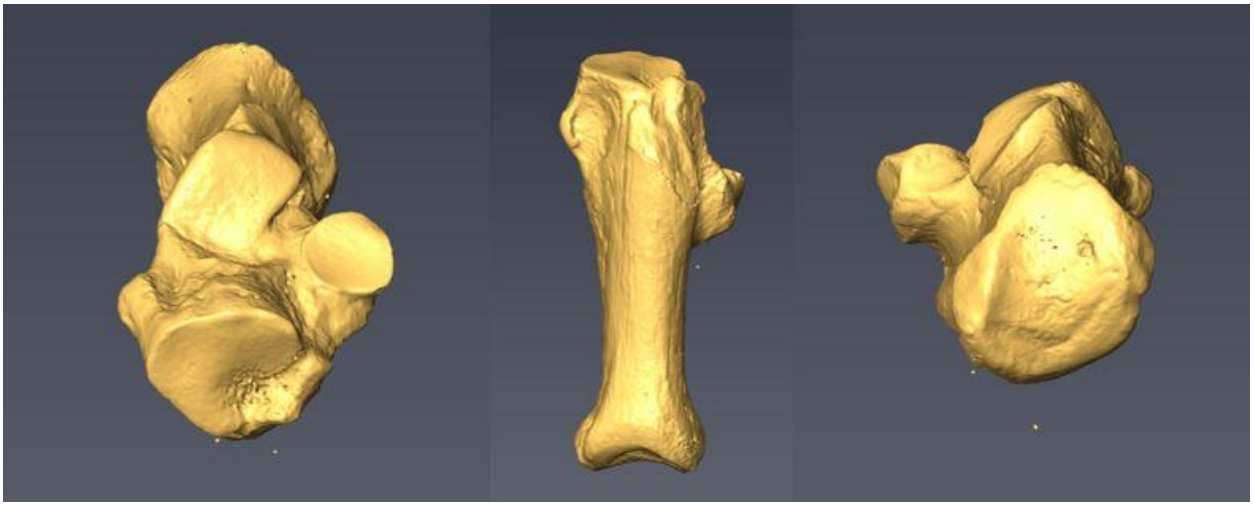

Figure 4.41: Well preserved anterosuperior view (L), eroded cortical bone on the inferoanterior (C) and preserved calcaneal tuberosity (R) of SWP 1207.

4.2 Description of homologous 2D sections

Cross sections (or 2D sections) are described here in order to track trabecular bone preservations and their organisation in each individual cercopithecid. They are informative in determining which specimens to be segmented for trabecular bone computation in ImageJ as well as determining the shape and pattern of trabeculae. This description includes both fossil and extant specimens.

4.2.1 Fossil femoral heads

14954M

The mediolateral section shows trabecular bone loaded with sediments. However, there are small amount of well-preserved trabecular bone found in the femoral shaft as well as few isolated trabeculae in the femoral head. The anteroposterior section reveals closed cells like trabecular structure on the medioinferior and lateral regions with no visible bundles (figure 4.42).

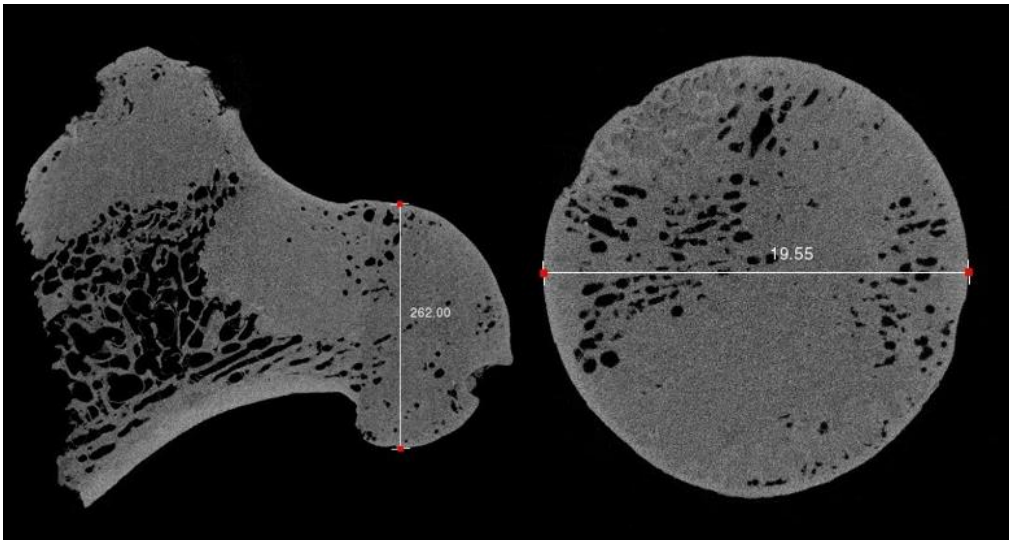

***Figure 4.42*:** Preserved trabecular bone in the shaft (L) and isolated closed cells trabecular anteroposterior section (R) of specimen 14954M.

16383M

most of the space in between trabeculae is filled up by sediment. Bone can be distinguished from the light grey coloured sediments by its dark grey colour. However, some preserved trabeculae are found to exhibit closed cells structures with no connectivity between them but more visible and connected in the femoral neck and below the trochanter area(figure 4.43).

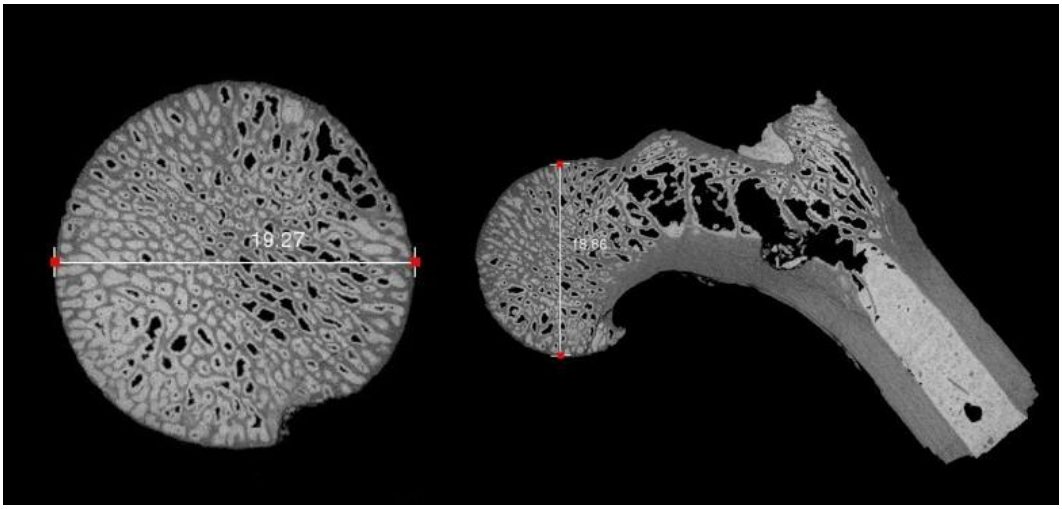

***Figure 4.43*:** 16383M showing anteroposterior section (L) and mediolateral section (R) showing dark grey sediments and light grey trabecular bone.

SWP 526

The anteroposterior section shows that although the specimen is sedimented, patterns of contrasting hue (light and dark grey) of sediments and trabecular bone respectively are clearly visible (figure 4.44). When viewed anteroposterioly, the specimen shows a fracture along the inferoanterior and superposterior regions. In the mediolateral cross section, the fracture runs from the fovea capitis area through to the femur neck

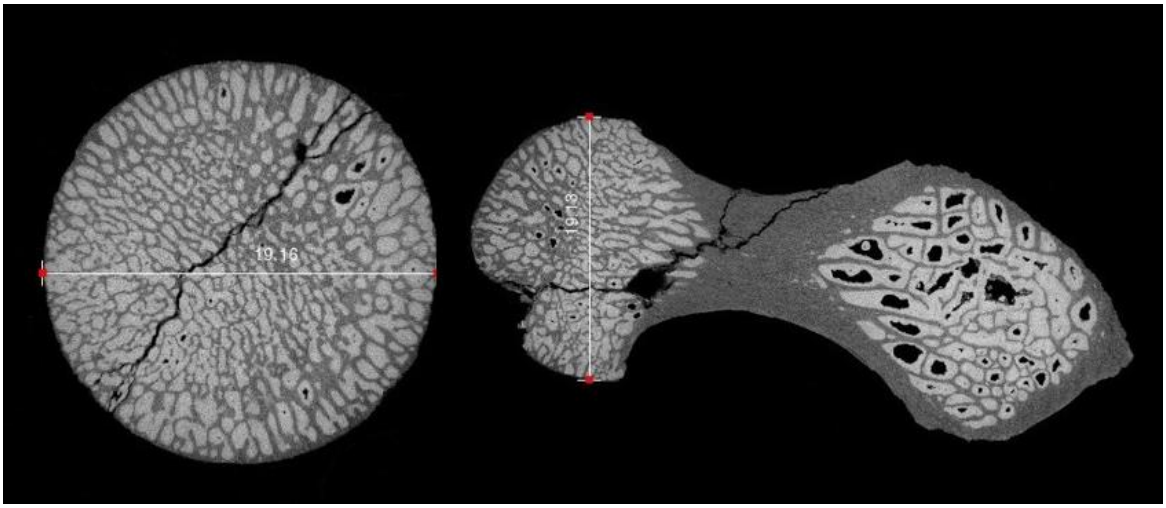

Figure 4.44: Specimen SWP 526 showing sediments filled trabecular bone (L) and fractured femur head and the neck (R).

SWP 528

The trabecular bone is well preserved. The anteroposterior section shows closed-cells like trabecular bone pattern together with a combination of rod-like trabeculae. The ML section shows vertical and arcuate bundles which intersect in the nucleus of the femoral head (figure 4.45).

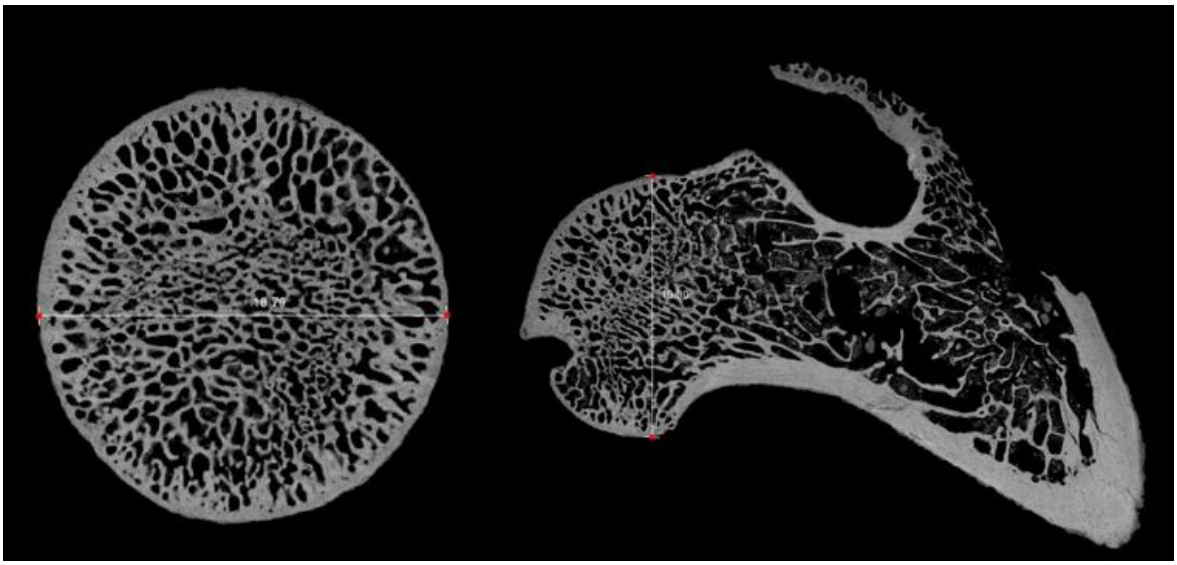

Figure 4.45: SWP 528 consisting of closed cells and rod like structure trabecular bone (L) in the anteroposterior section and vertical and arcuate bundles (R) in the mediolateral section.

SWP 529

The specimen is filled up with sediment, resulting in it being almost full. However, mediolateral cross section view shows few and isolated circular trabeculae on the posterior area (figure 4.46). The specimen is fractured in the shaft.

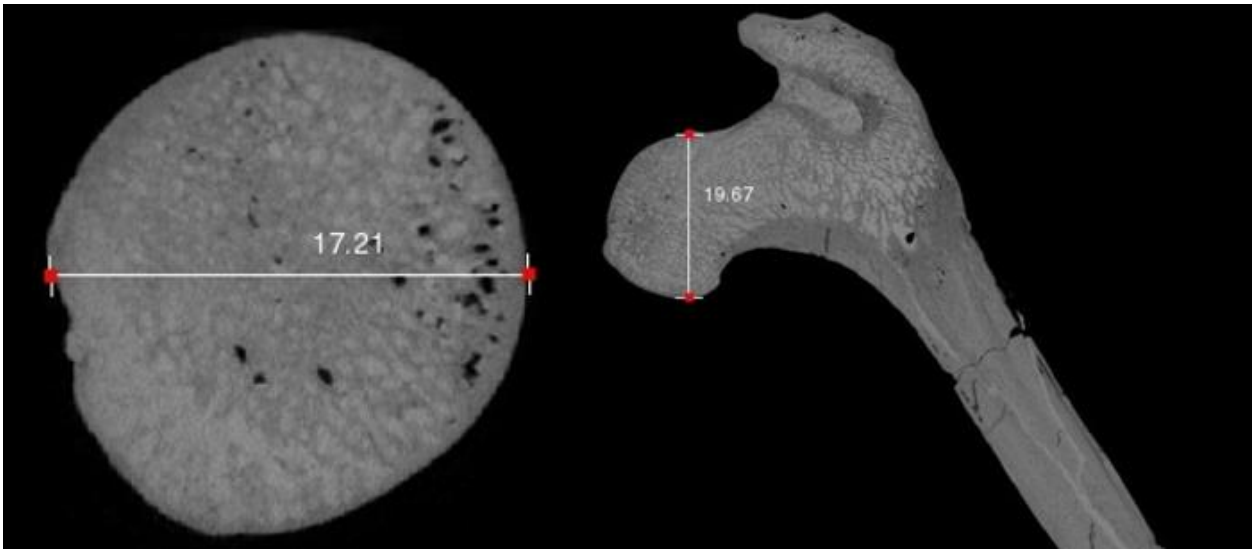

***Figure 4.46*:** Cross section of SWP 529 exhibiting compact and circular remotely trabeculae specimen with fractured femur neck.

SWP 531

The AP section shows of closed cells like structures trabecular bone. There are two patterns of trabecular bone observable on the mediolateral section. These are the superoinferior elongated as well as the anteroposterior elongated ones. The ML section displays well developed vertical and arcuate bundles which intersect in the centre of the femur head (figure 4.47).

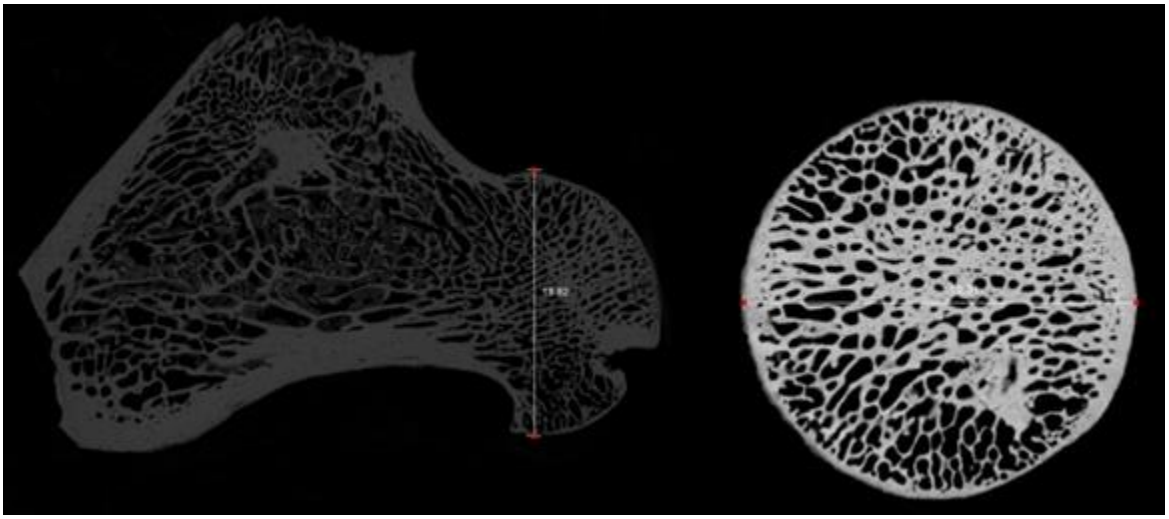

Figure 4.47: Arcuate and vertical bundles (L) elongated closed cells trabeculae (R) of SWP 531.

SWP 532

This specimen is filled in with sediment. It is fractured across the femur neck as well as in the inferior part of the greater trochanter. As explained above, it is filled up with sediments with few and minute isolated trabeculae on the superior region (figure 4.48).

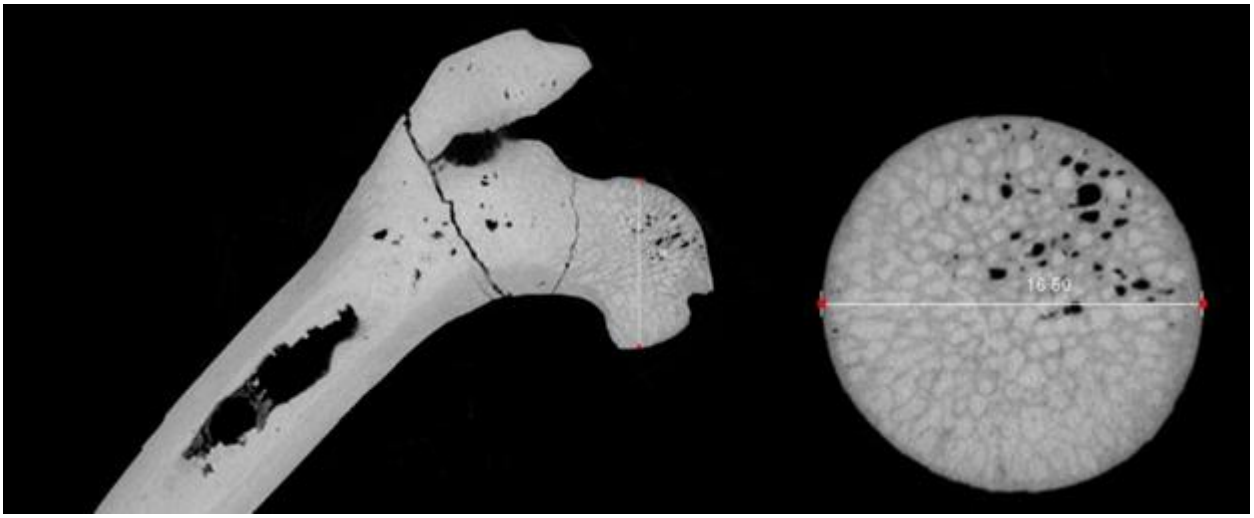

***Figure 4.48*:** Cross section of SWP 532 exhibiting fractured neck and shaft (L) and few and isolated trabecular bone (R).

SWP 533

The specimen is sedimented with few and remotely preserved trabeculae on the posterior region, when viewed anteroposteriorly. The ML section shows three fractures that are on the fovea captis region, the femoral neck and the inferior part of the great trochanter ((figure 4.49).

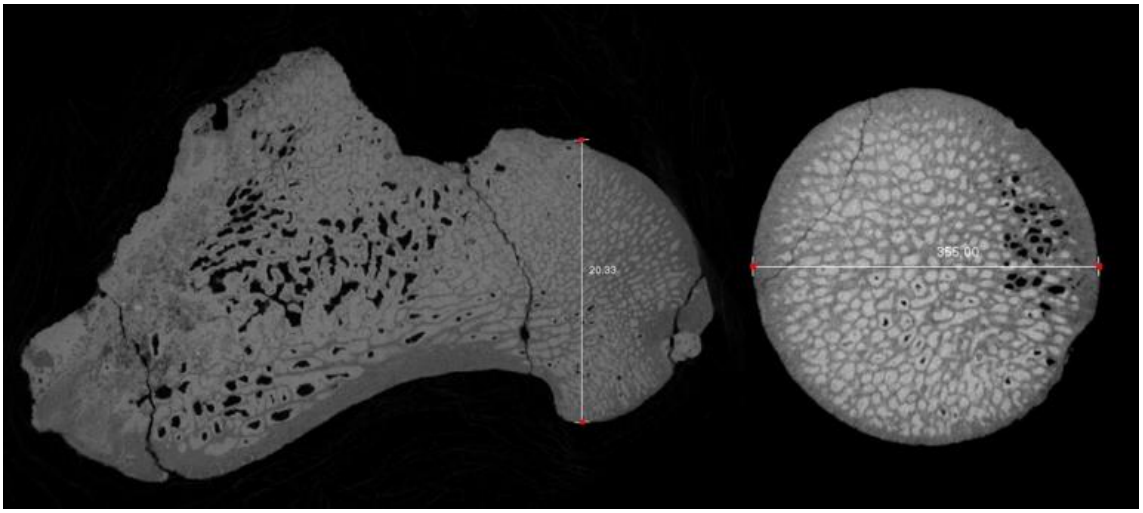

***Figure 4.49*:** 2D section of SWP 533 display highly fractures neck and shaft (L) and few remotely preserved trabecular bone (R).

SWP 747

The femoral head is entirely filled up with sediments. The ML section reveals a huge fracture in the femoral neck, dividing the femoral head and the entire femur shaft (figure 4.50). Although the specimen is filled with sediment, patterns of trabecular bone and sediments are differentiated by grey and white respectively.

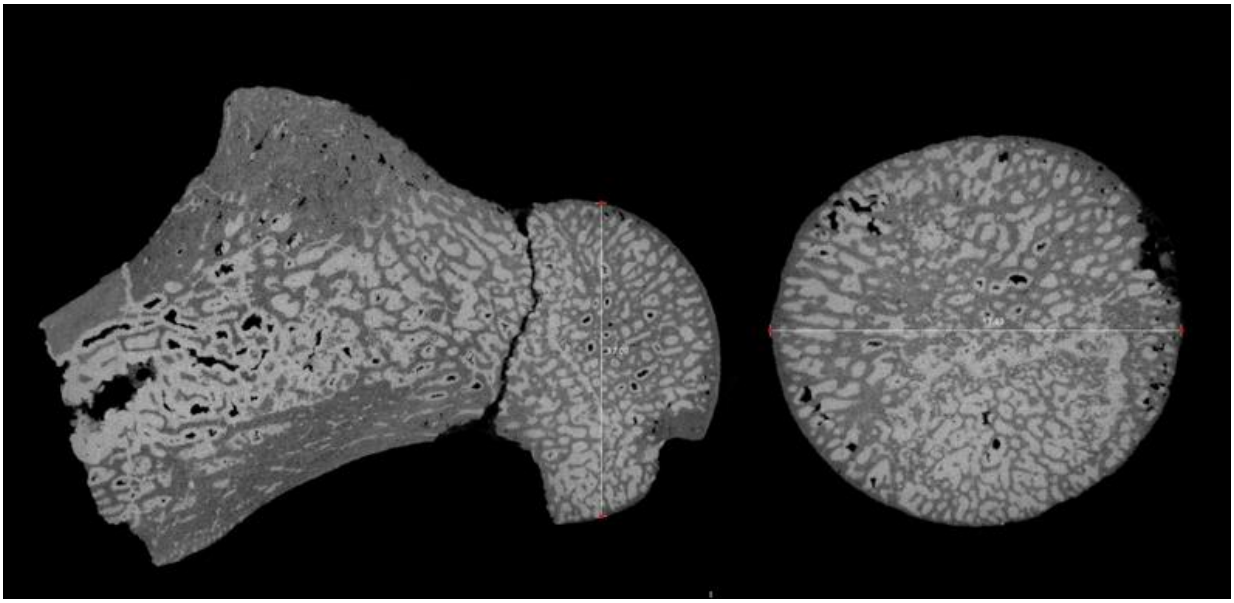

***Figure 4.50*:** 2D sections of SWP 747 displaying fractured femur neck (L) and mineralised anteroposterior section (R).

SWP 749

The ML section shows a small amount of preserved trabecular bone in the mediolateral direction, while the AP section contains preserved trabeculae that exhibit semi-circular structures (figure 4.51), leaving most of the specimen highly sedimented.

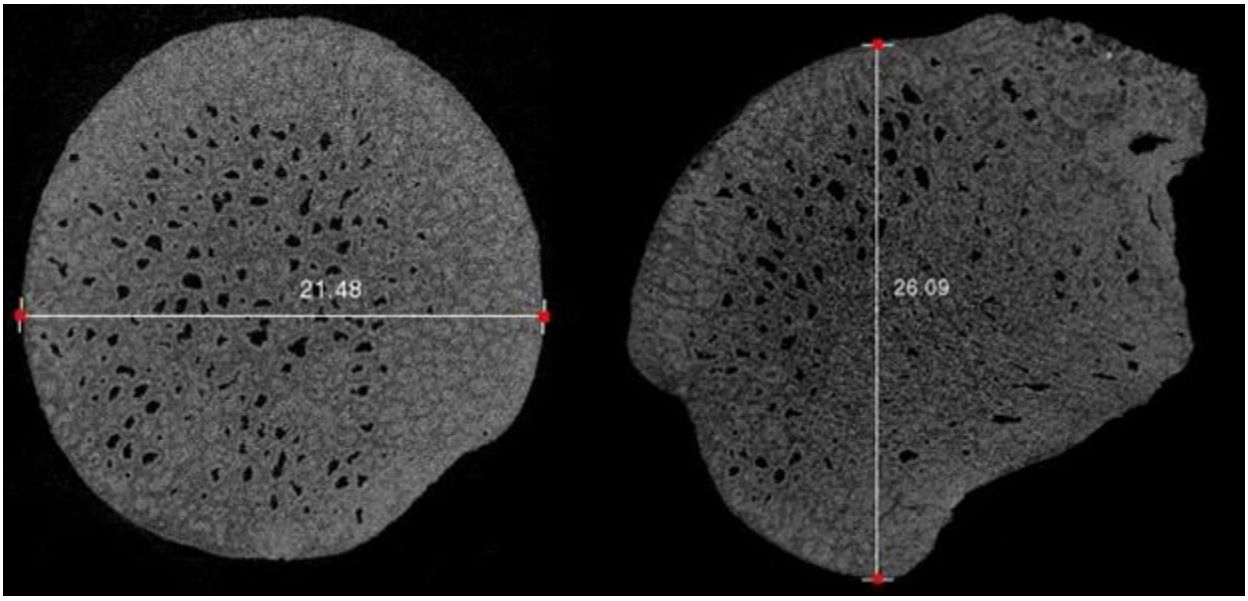

***Figure 4.51*:** SWP 749 showing isolated semi-circular trabecular bone.

SWP 753

The sections reveal that the trabecular bone is almost entirely preserved, particularly towards the nucleus of the femoral head. When viewed mediolaterally, sections indicate fractures in nucleus of the femoral head and in fovea capitis region (figure 4.52). open cell and rod like trabeculae are observed in the ML section. The AP section shows that fractures observed in the mediolateral section culminate into a huge void, surrounded by closed cells with plate like trabeculae.

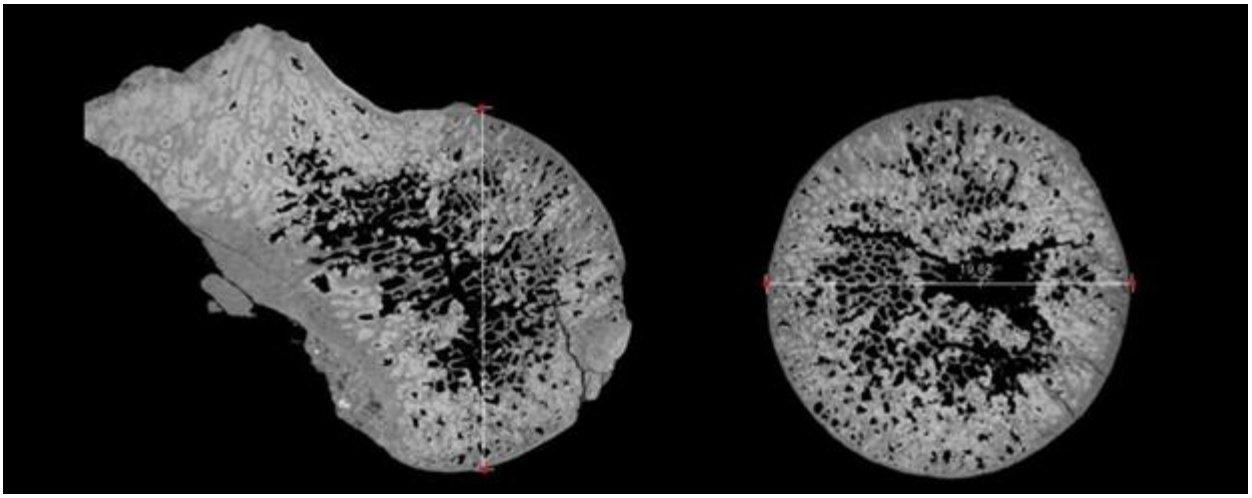

***Figure 4.52*:** Fractured mediolateral section (L) and preserved trabeculae in anteroposterior section (R) of specimen SWP 753

SWP 756

ML and AP sections show well preserved trabecular bone. The ML section shows open cells and rod like trabecular bone in the femoral neck which culminate into closed cells and honeycomb like trabecular bone in the femoral head (figure 4.53). When viewed anteroposteriorly, closed cell with honeycomb like structures are visible. Sediment is observed within trabeculae in both sections.

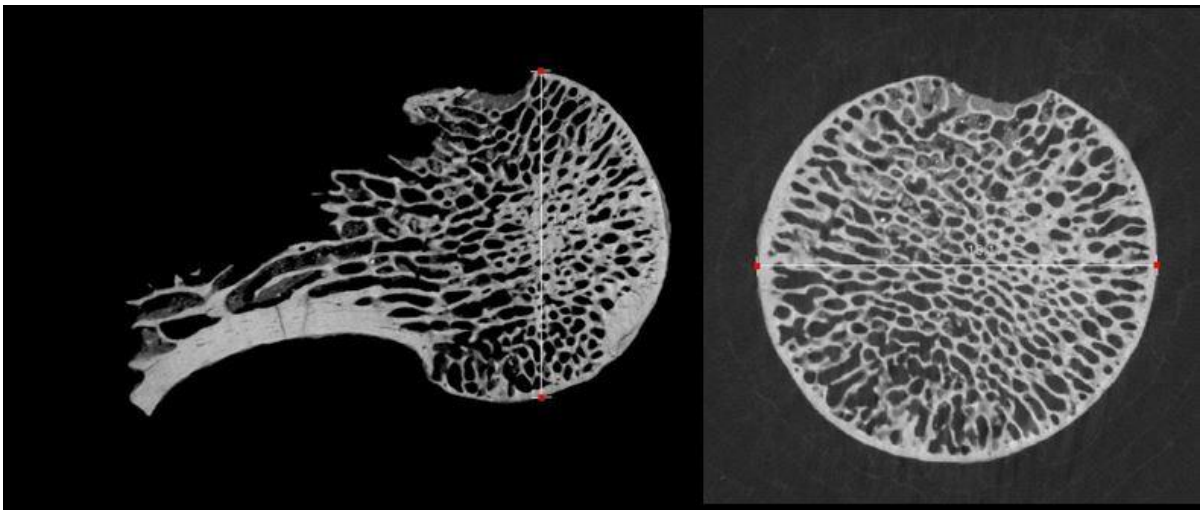

Figure 4.53 SWP 756 2D sections displaying open cells and rods like structure trabecular bone in the femur neck (L) and closed cells and honeycomb like structures (R).

SWP 1009

The specimen shows sediment with small amount of remotely preserved trabecular bone in the inferior and medial regions. This specimen is fractured in the neck, dividing the femur head and the shaft. Although the specimen is sedimented, vertical and arcuate bundle patterns can be seen when viewed mediolaterally. The AP section shows randomly arranged trabecular bone as shown by figure 4.54 below.

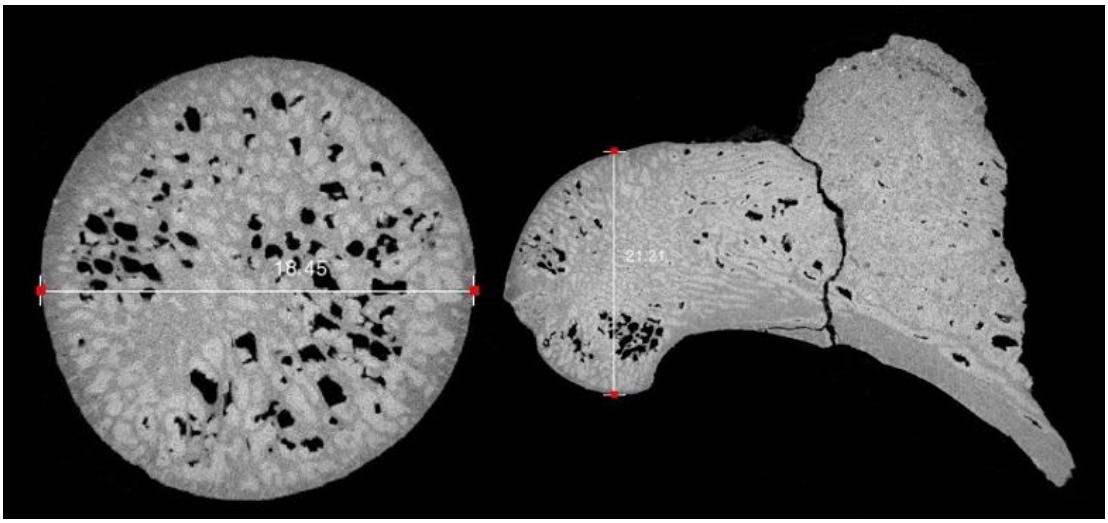

Figure 4.54: Cross sections of SWP 1009 displaying isolated trabeculae (L) and fractured femur neck (R).

SWP 1011

The trabecular bone is well-preserved. When viewed anteroposteriorly, a massive fracture along the superior-inferior direction, dividing the femoral head into almost two equal halves (figure 4.55). The specimen has closed-cells and honeycomb like trabecular bone structures in the AP section while the ML section shows open cells and rods like trabecular bone structures (figure 4.55).

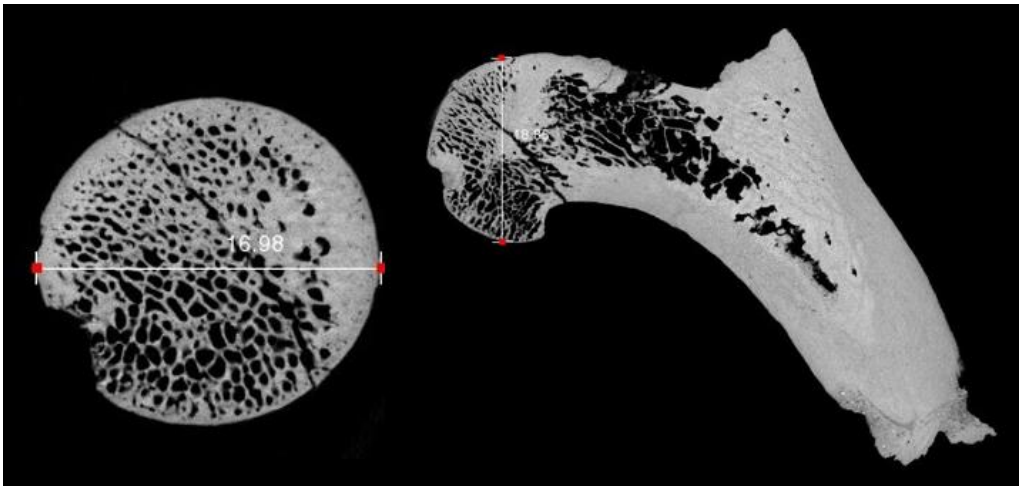

Figure 4.55: 2D sections of SWP 1011 showing closed cells and honeycomb structure (L) and open cells and rods like structure (R).

SWP 1203

The trabecular bone is well-preserved. The ML section reveals preserved vertical and arcuate bundles, intersecting in the nucleus of the femoral head (figure 4.56). Anteroposterior section exhibits closed-cells like trabecular bone structures, particularly on the superiorly among minute sediments in the femoral head. However, the nucleus of femur head consists of closed-cells like structures with honeycomb like trabecular bone while the presence of rod like trabecular structure is visible in the inferior region (figure 4.56).

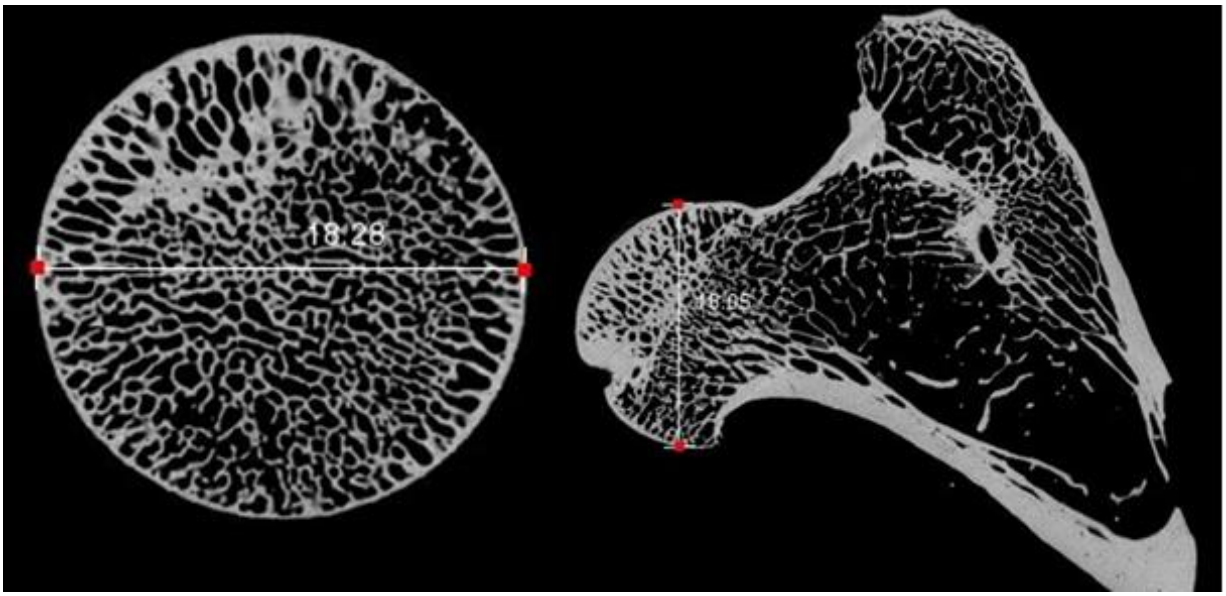

Figure 4.56: Cross sections of 1203 exhibiting a well preserved trabecular bone (L) and well-developed trabecular bundles (R).

SWP 1384

The femoral head is filled up by sediments. It is fractured in two regions; the first fracture separates the femoral head and the shaft while the other separates the great trochanter and the shaft. Although the specimen is filled with sediment, vertical and arcuate bundle patterns are preserved and visibly intersect in the centre of the femur head within surrounding sediment (figure 4.57 below).

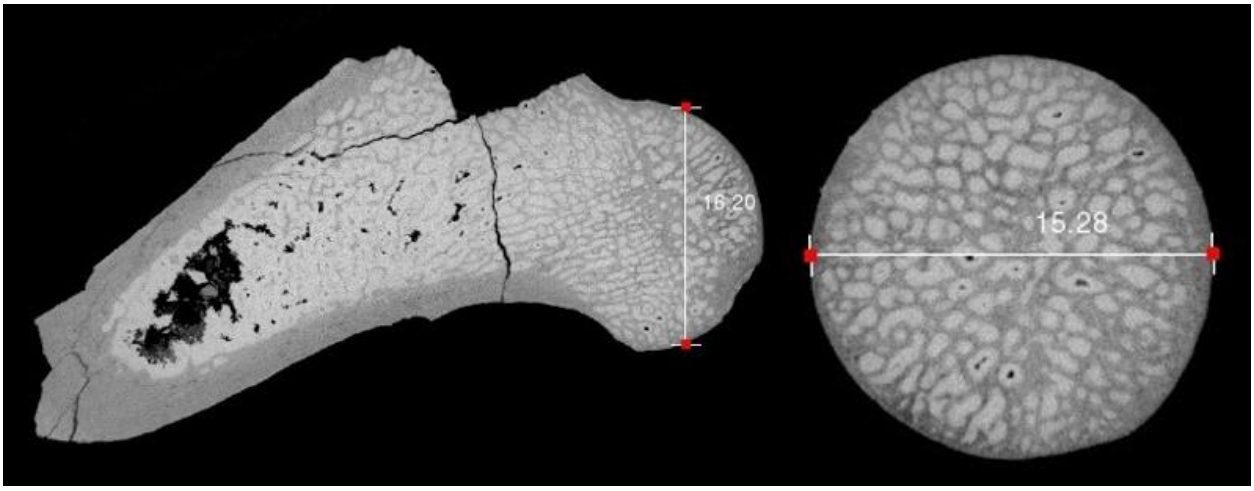

Figure 4.57: Mediolateral and anteroposterior of SWP 1384 with preserved bundles within sediments filled trabecular bone (L) and mediolateral section with completely filled up trabecular bone (R).

SWP 1698

Trabeculae are almost not preserved but small number of them are discernible in the anterior region. The ML section shows that the specimen is fractured in two regions: the tip most superior of the greater trochanter and the femoral neck, going down the shaft(figure 4.58).

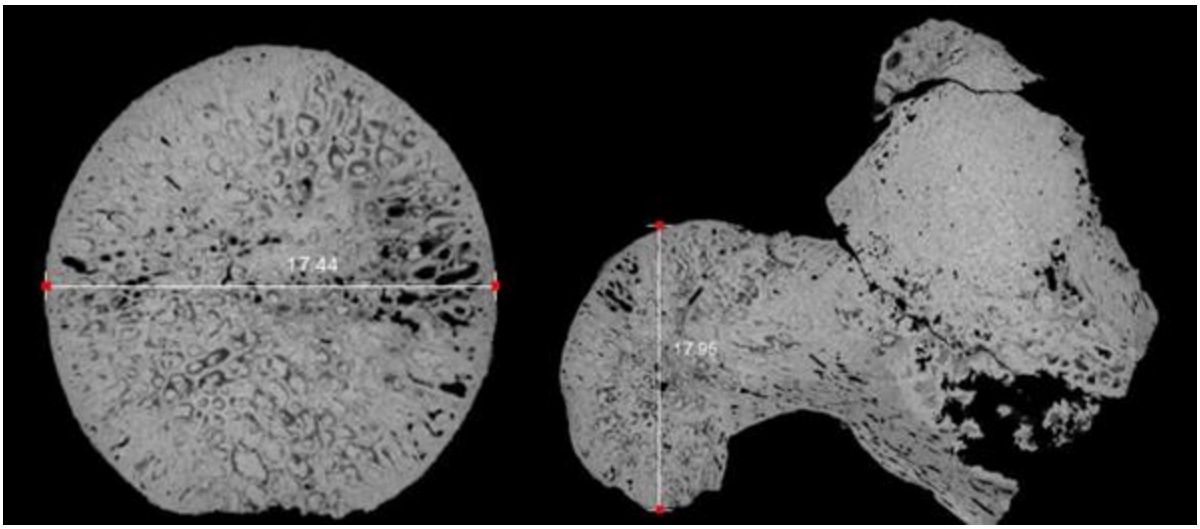

***Figure 4.58*:** Internal sections of SWP 1698 having sedimented and compact femur head (L) with fractured neck and trochanter (R).

SWP 1699

The trabecular bone is not preserved and filled with sediment. However, their pattern can be identified by their contrasting dark grey hue form light grey sediments. The ML section shows a small number and sporadic miniatured trabecular bone (figure 4.59).

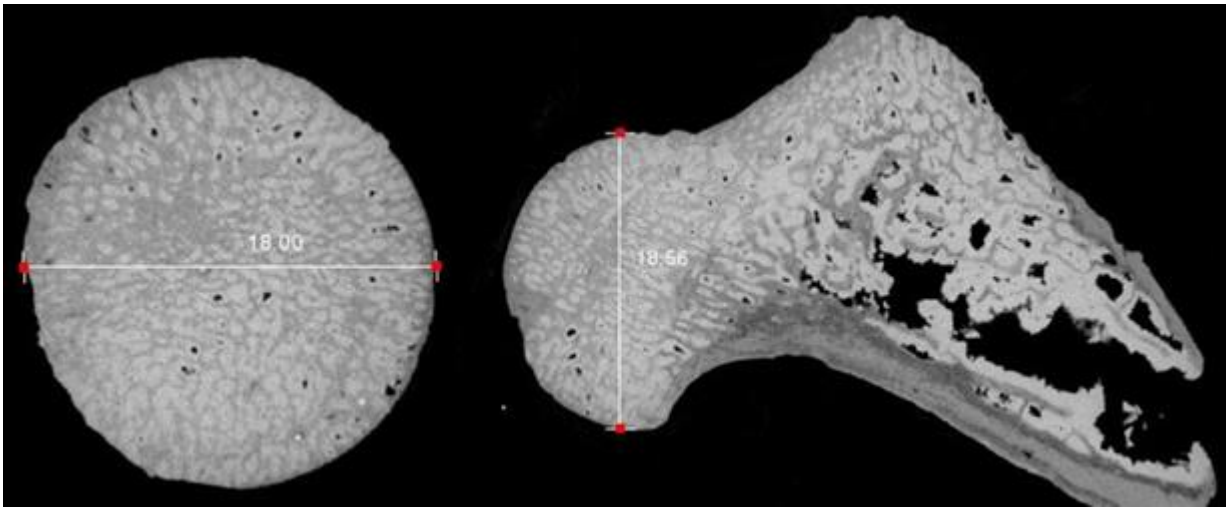

***Figure 4.59*:** SWP 1699 with **s**edimented femur head (L) and vertical and arcuate bundles (R)

Sts 2050

The specimen is entirely filled up with sediment without any discernible trabeculae, either in the femoral head or femur neck. As a result, it is difficult to discriminate cortical bone from trabecular bone. There are two fractures visible in both sections (figure 4.60).

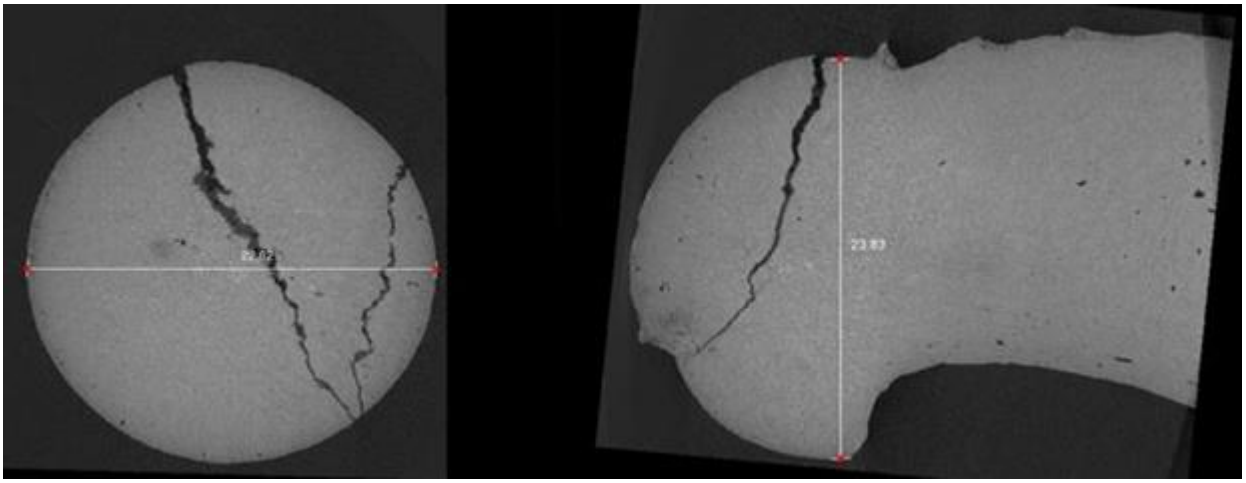

Figure 4.60: Fractured anteroposterior section (L) and mediolateral (R) of specimen Sts 2050.

Sts 2259

This specimen is almost completely filled up with sediments, but trabecular bone is distinguishable from the sediment due to their colour differences. Vertical and arcuate bundles are observed intersecting in the nucleus of the femur head (figure 4.61). Elongated plate like structures with open cells that are radially cortical bound are noticeable in the AP section, while the ML section displays preserved distinct arcuate bundle which have elongated cells. However, the specimen preserves no ward's triangle nor the trochanteric bundles due to sediments filling up trabecular bone pores (figure 4.61) also due to limited preserved femur neck.

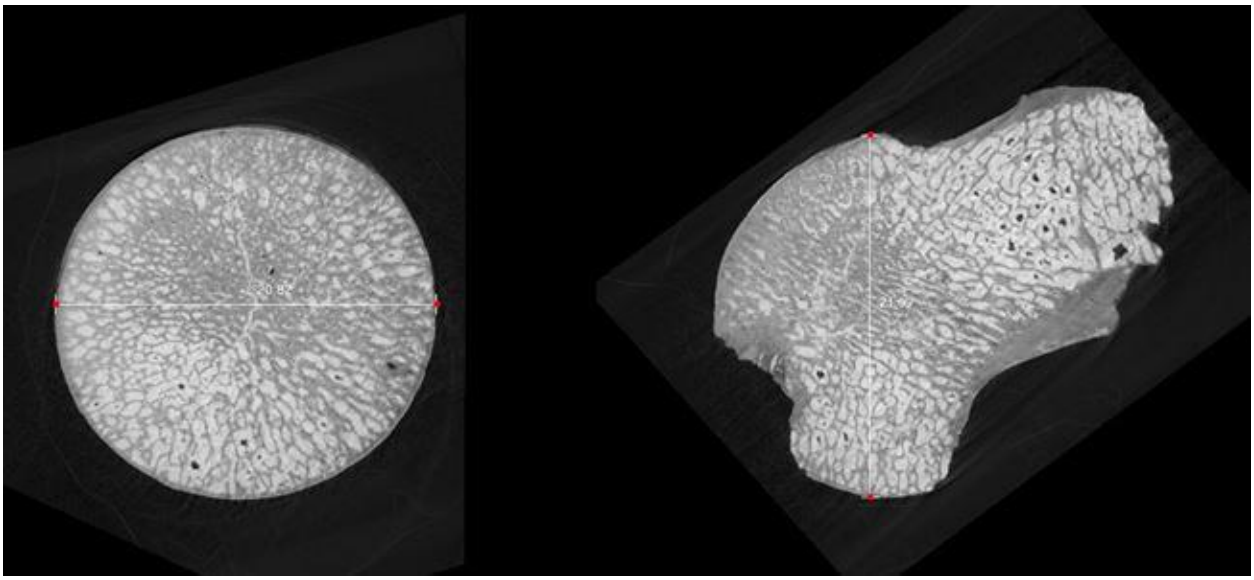

Figure 4.61: Medial view of anteroposterior cross section (L) and the mediolateral cross section of Sts 2259.

SK 605

The ML section shows sediment in the superolateral region, which extends to the nucleus of the femoral head. The vertical and arcuate bundles are preserved and observable in the superolateral as well as the inferolateral regions. However, they fade when approaching the nucleus of the femoral head (figure 4.62). The trochanteric bundle and the Ward triangle are not preserved possibly due to sediment infilling. The AP section shows preserved closed-cells like pattern and honeycomb like trabecular bone (figure 4.62).

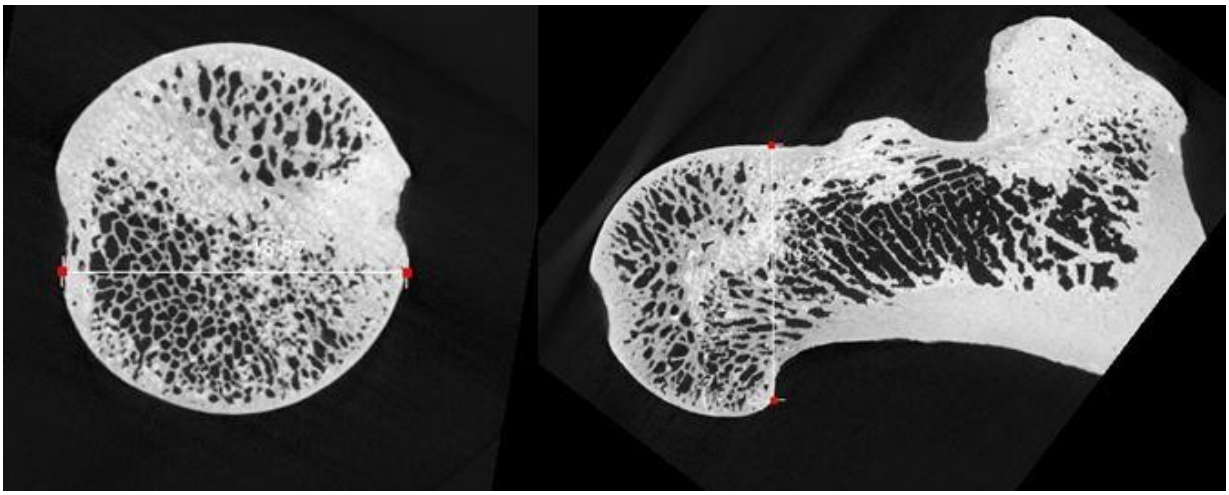

***Figure 4.62*:** Preserved trabeculae (L) with arcuate and vertical bundles (R) of SK 605 cross sections.

SK 607

This specimen is fairly filled up with sediment. Few and sporadically preserved trabeculae are observable in the femoral head as well as in the neck, particularly towards the cortical bone (figure 4.63). The AP section shows fracture in the anteroposteriorly, while ML section, is fractured from the greater trochanter through to the inferior of the shaft.

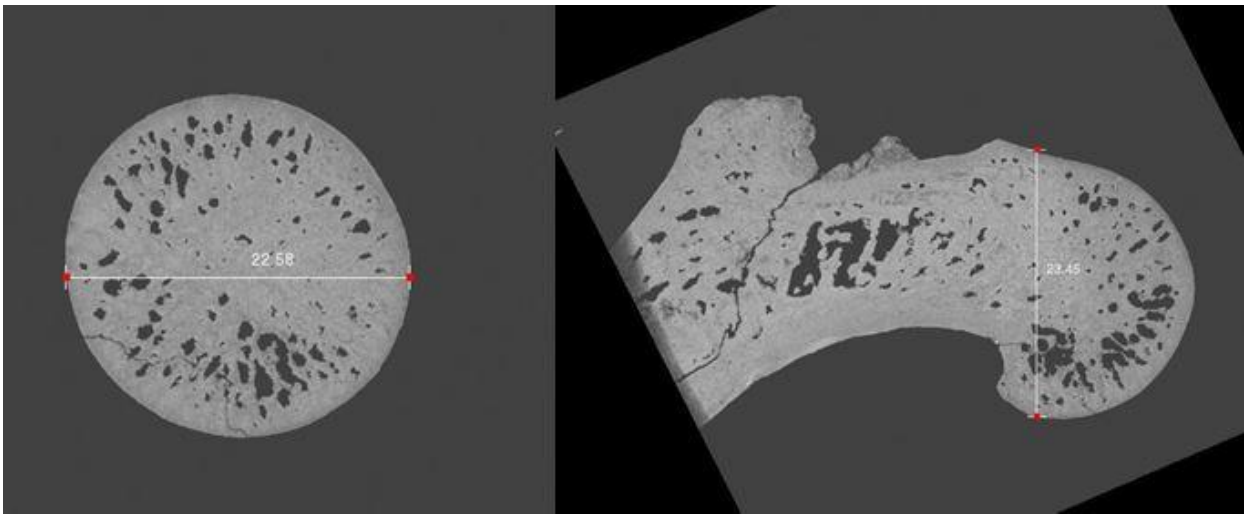

Figure 4.63: Anteroposterior cross section (L) and mediolateral cross section (R) of SK 607 showing sporadically preserved trabeculae.

SK 1513

The AP section shows open and closed cells in the trabecular bone. Preserved plate-like elongated trabecular structures are observed radiating from the nucleus of the femoral head to the cortical bone (figure 4.64). Some short and semi-circular trabeculae are preserved in the femoral head. ML section contains mediolaterally aligned elongated plate-like trabecular bone. Vertical and arcuate bundles are not well defined in anteroposterior section and completely not preserved in the femur neck. The trochanteric bundle and the Ward's triangle are not preserved. Anteroposterior section indicates a huge fracture (figure 4.64).

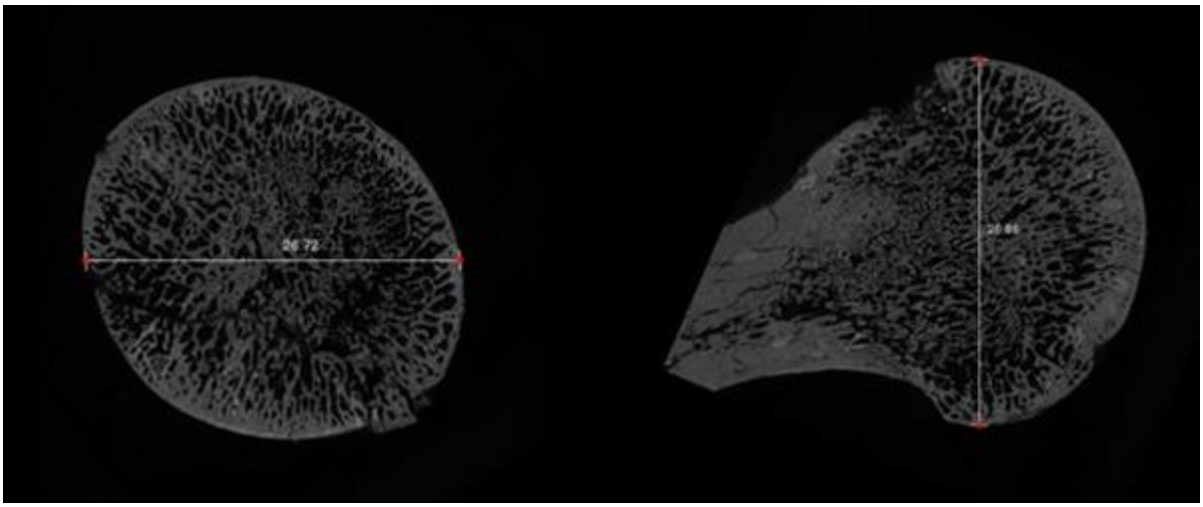

Figure 4.64: Plate and rod-like trabecular bone structure in the anteroposterior cross section (L) and mediolateral cross section (R) of SK 1513.

SK 2595

This specimen is almost completely filled up with sediments. However, like most specimens in this study, trabeculae can be distinguished from the rest of the sediment by their different colour. Therefore, this colour variation enables the identification of vertical bundle and arcuate bundle from the sediment (figure 4.65). The AP section shows preserved elongated plate-like structures trabecular bone with open cells that are radially cortical bound. The ML section, however, shows preserved distinct arcuate bundle with elongated cells and thick vertical bundle (figure 4.65). These bundles intersect in the nucleus of the femoral head. Like most of the specimens in the study, the Ward's triangle and the trochanteric bundle are not preserved probably due to

sediment filling up trabecular bone pores. AP section shows a fracture from the superoposterior to the inferoanterior areas while in the ML section, the fracture is seen to run from superomedial to the inferior (figure 4.65).

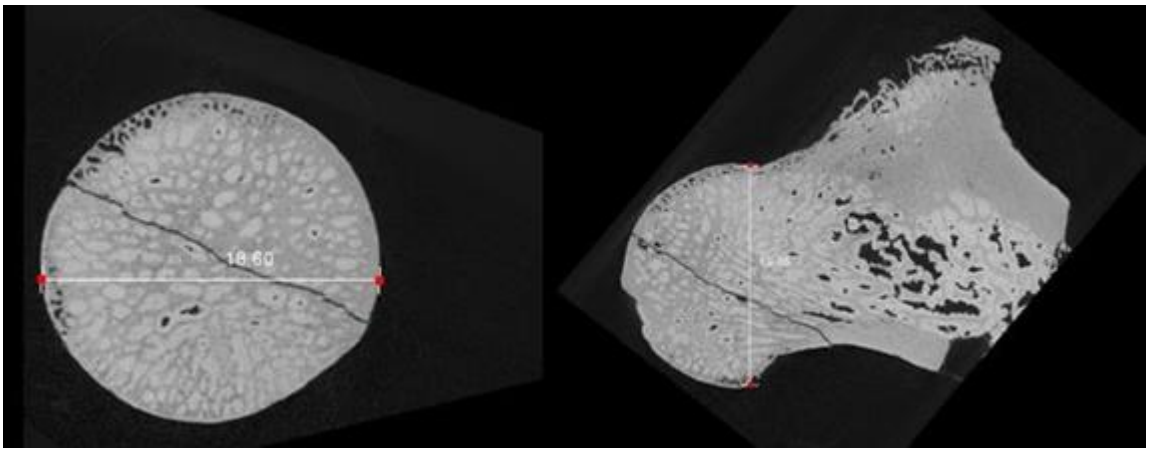

***Figure 4.65*:** Cross sections of SK 2295 displaying sedimented femur head (L) but bundles visible due to colour differences with sediments (R).

SK 14015

This specimen is almost entirely filled up with sediment, with few and irregular shaped trabeculae preserved. Preserved trabecular bone exhibits closed-cells like structures while some are mediolaterally orientated (Figure 4.66).

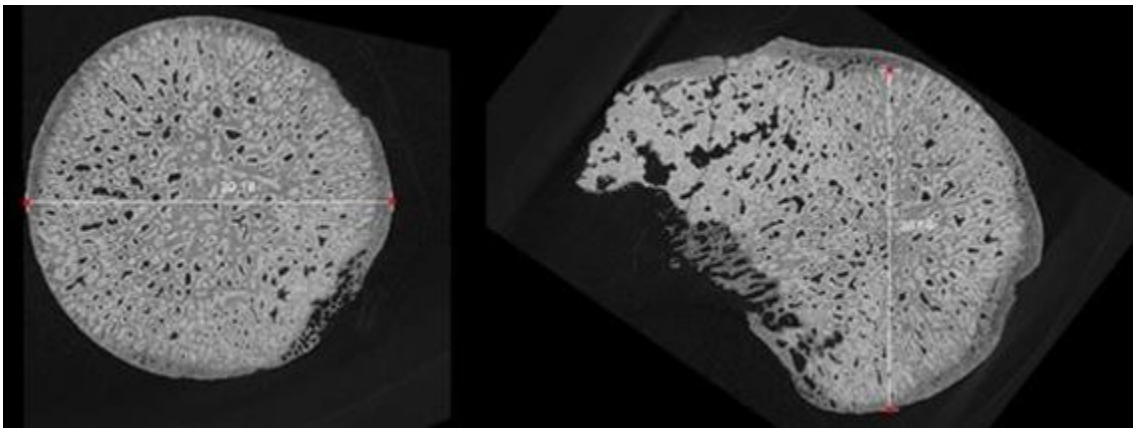

***Figure 4.66*:** Specimen SK 14015 showing irregular closed-cells like structure trabecular bone.

BF 36

Much of the specimen head is filled with sediment. The ML section shows a fractured neck, dividing the head and rest of the femur (figure 4.67). Few and isolated trabeculae are preserved from the neck and close to the fovea captis. The AP section exhibits isolated trabeculae (figure 4.67).

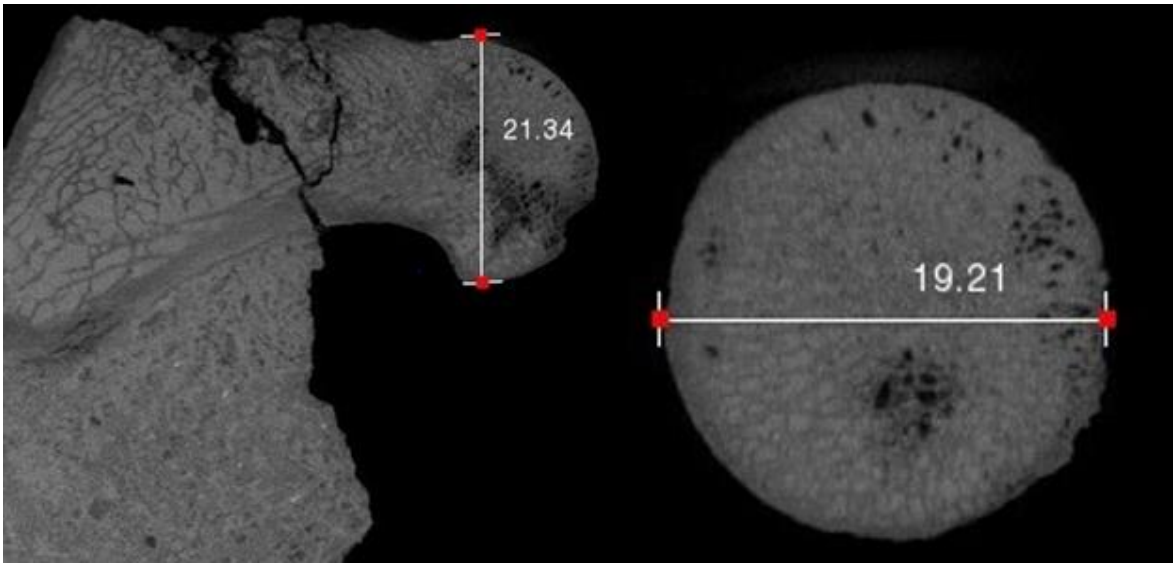

***Figure 4.67*:** Cross sections of BF 36 showing fractured neck (L) and cortically bound trabecular bone (R).

4.2.2 Fossil humeral heads

1930M

Trabecular bone in the humeral head is not preserved because it is filled with sediment. Both anteroposterior and mediolateral cross sections show a completely sedimented and mineralised trabecular bone without any view of trabeculae (figure 4.68).

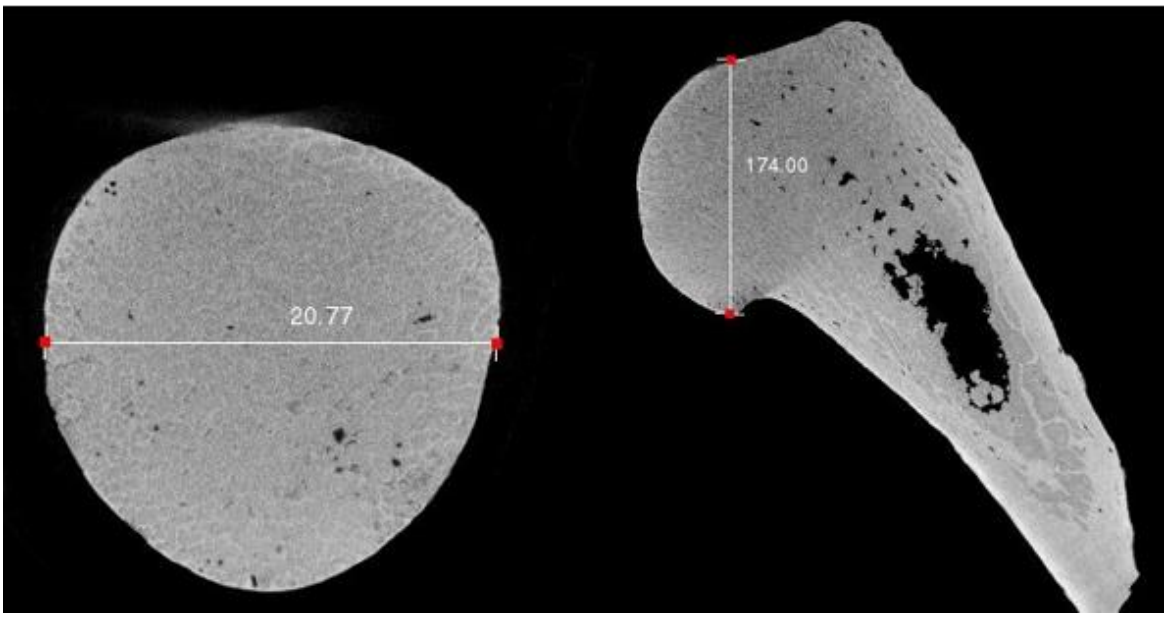

Figure 4.68: Anteroposterior and mediolateral cross sections of 1930M showing mineralised humerus head with no preserved trabecular bone.

1934M

The ML section shows preserved trabeculae in the inferomedial through the medial to the superolateral regions. AP section indicates the presence of trabecular bone in the superolateral and inferolateral regions (figure 4.69). These trabeculae are isolated due to the presence of sediment that fills most of the empty space.

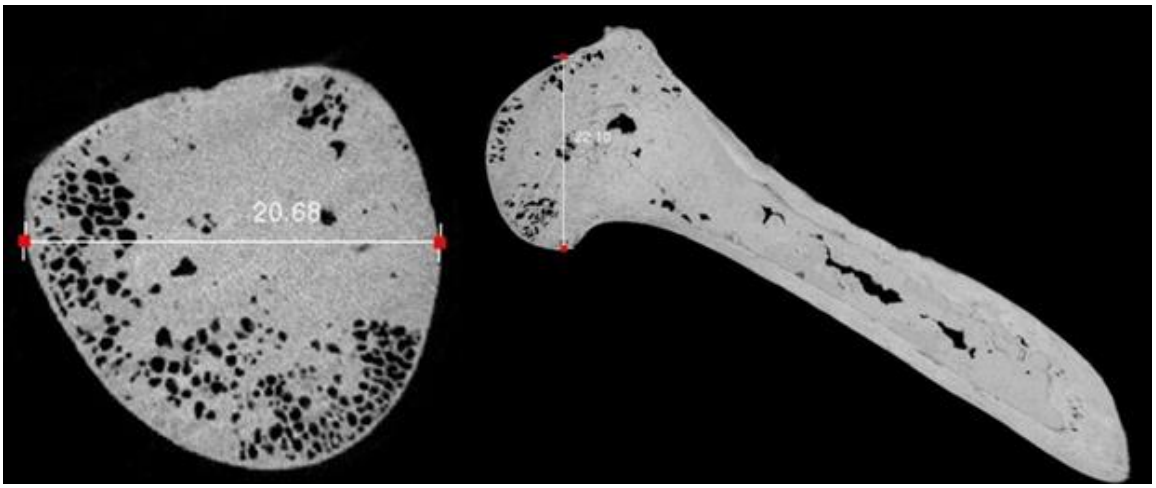

Figure 4.69**:** Mediolateral and anteroposterior cross sections of 1934M showing few remote trabeculae.

SWP 962

The 2D sections of this specimen reveal that it is almost completely filled with sediments. However, trabecular bone can be distinguished from the sediment by their colours (figure 4.70). The AP section shows few centrally localised trabeculae (figure 4.70).

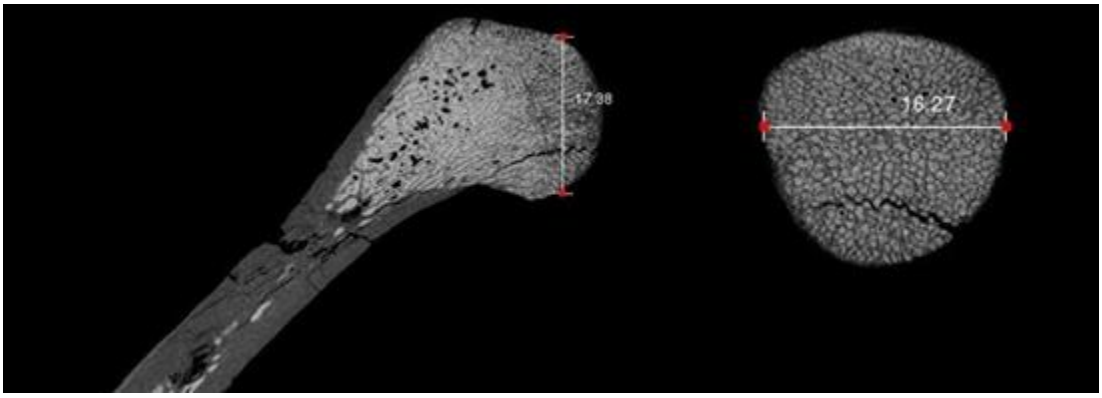

Figure 4.70: 2D sections of SWP 962 with few and isolated preserved trabecular bone (L) and fractured posteroinferior proximal head.

SWP 606

The trabecular bone contains sediment. The ML section shows minute, sporadic and isolated trabeculae medially. AP section does not show much, except that there is a huge opening on the head-neck contact region posteriorly (figure 4.71).

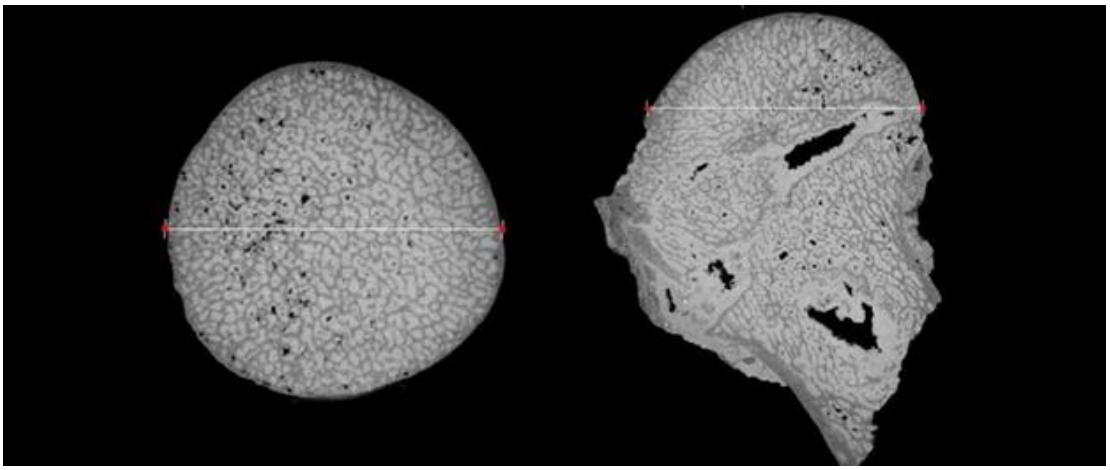

***Figure 4.71*:** SWP 606 with isolated trabecular bone on mediolateral section (L) and anteroposterior section with posteriorly void (R).

SWP 1406

Most of the space in between trabeculae is filled with sediment, leaving only small amount of preserved isolated trabeculae (figure 4.72).

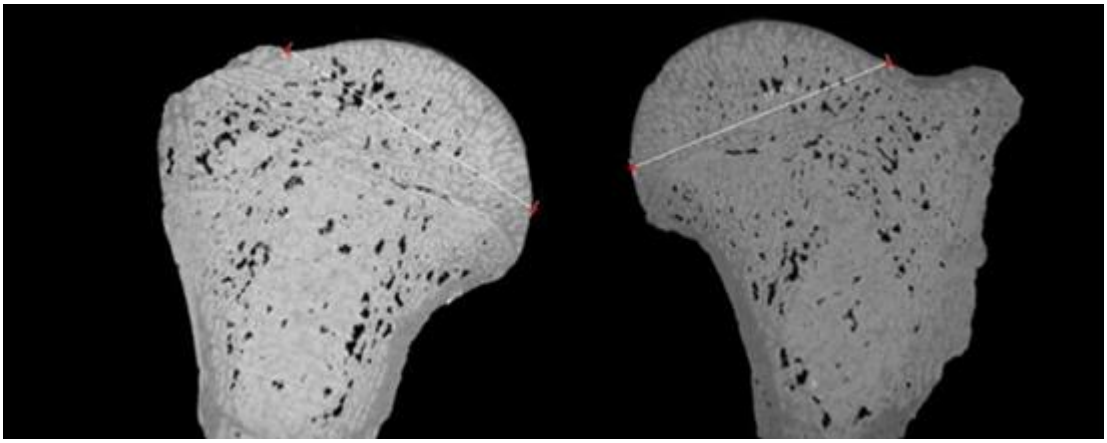

***Figure 4.72*:** Filled up trabecular bone with few isolated preserved trabecular bone.

4.2.3 Fossil proximal tibiae

SWP 1546

The ML section shows that the shaft is fractured in two areas below the tibial tuberosity (figure 4.73), separating the tibial plateau form the entire shaft. Although the specimen is highly sedimented, some few preserved trabeculae are observable, that form two patterns. One set of trabecular bone is oriented anteroposterioly while the other is oriented from the posterior particular area to the tibial tuberosity.(figure 4.73).

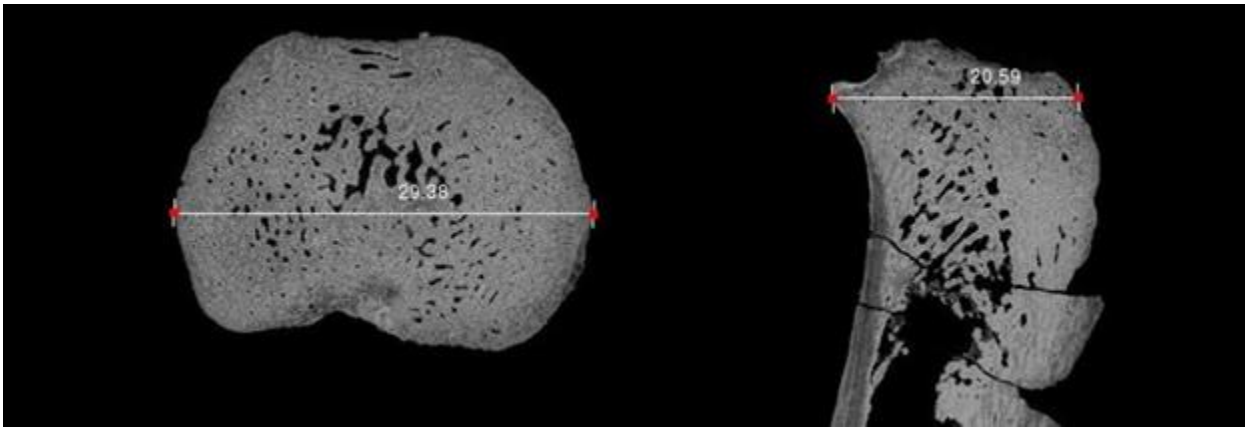

Figure 4.73: SWP 1546 with sporadic trabecular bone (L) and fracture tibial tuberosity (R).

SWP 1596

The ML section shows that the specimen is medially fractured and the medial facet is separated from the entire proximal aspect. This specimen is completely filled in with sediment but traces of trabecular bene are observed running from the anterior lateral (tibial tuberosity) to the medial facet (figure 4.74). When viewed superoinferiorly, the mediolateral 2D section illustrated the fracture described above running from tibial tuberosity, through the posterior of the medial facet (figure 4.74).

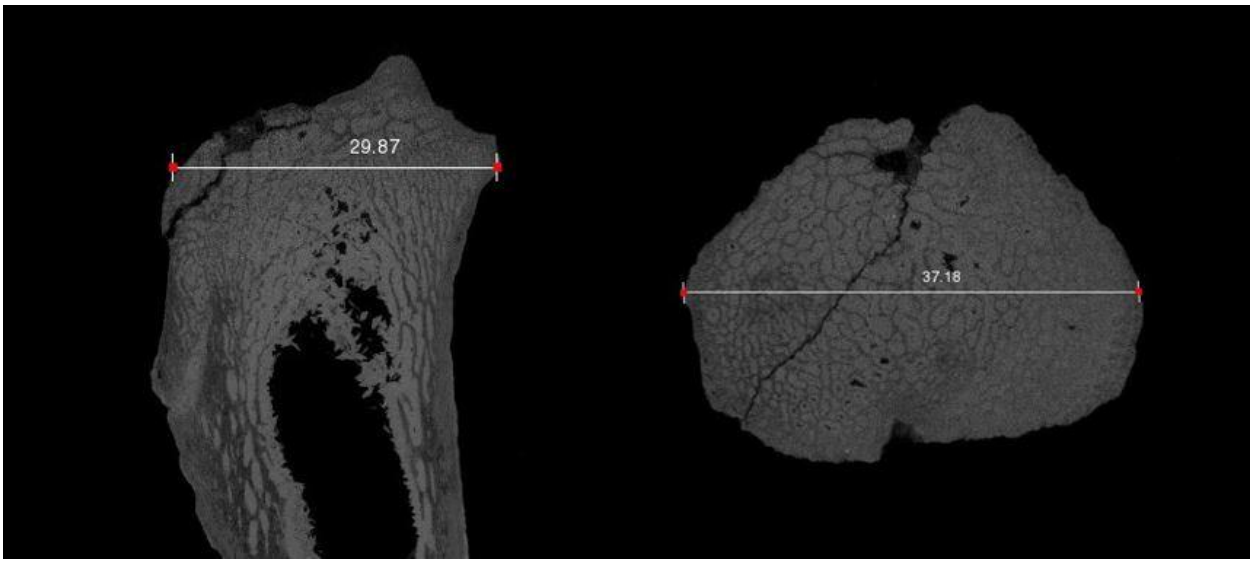

Figure 4.74: 2D sections of SWP 1596 showing tibial tuberosity to medial trabecular patterns with fractured medial facet (L) and anteroposterior fracture (R).

SWP 1411

The space in between trabeculae is filled with sediment, leaving sporadic and isolated openings. However, like most specimens in the study, trabeculae can be distinguished from the sediment by the dark grey colour compared to the light grey colour of sediment within trabecular bone spaces (figure 4.75).

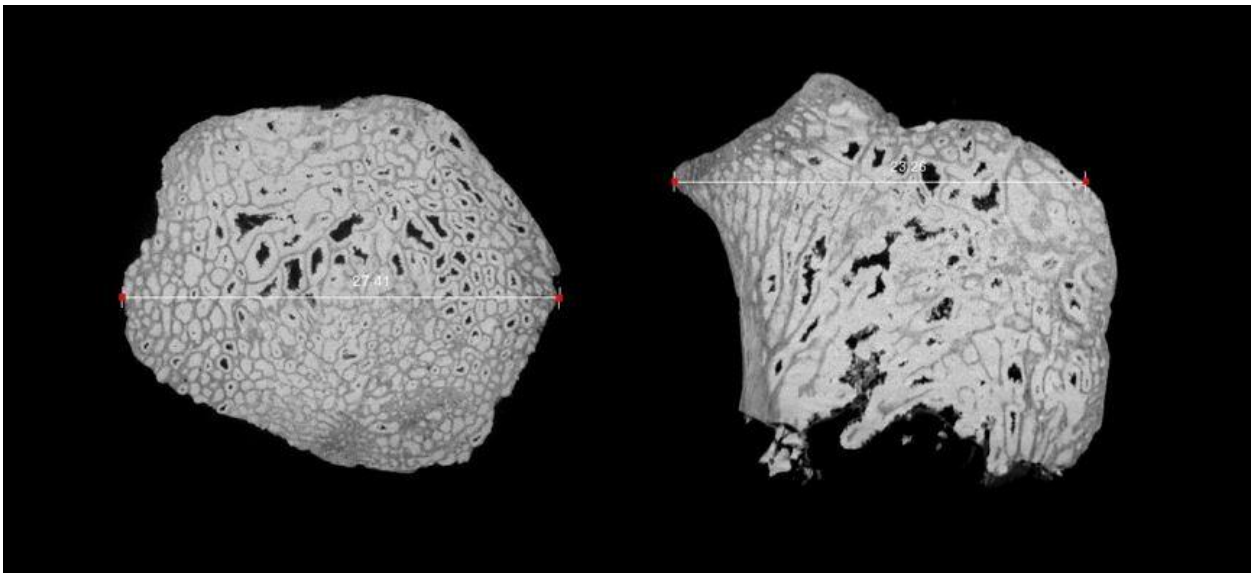

***Figure 4.75*:** Cross sections of SWP 1141 showing sediments within trabecular pores.

TP 18

The specimen's shaft is fractured on two areas: on tibial tuberosity and below it around the shaft. This specimen is completely filled with sediment resulting in no trabecular bone being preserved (figure 4.76).

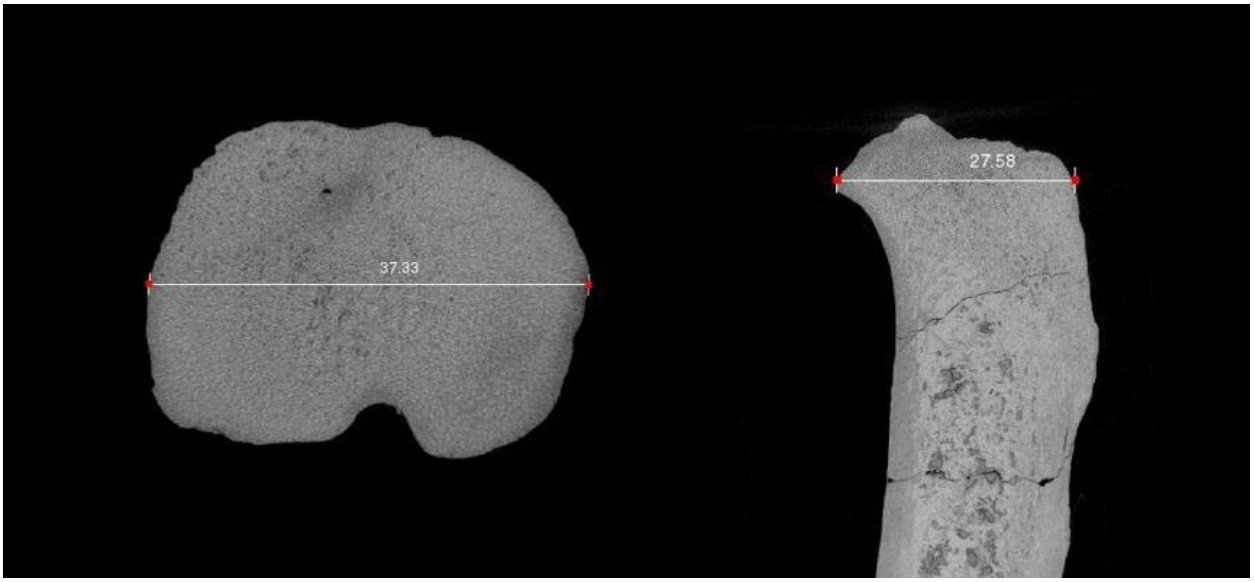

Figure 4.76: Cross sections of TP 18 showing a sediments filled up trabecular bone (R). Note fractures on the tibial tuberosity and just below it (L).

4.2.4 Fossil calcanei

2222M

This specimen is almost completely filled with sediments, resulting with few and sporadic trabeculae being preserved. The ML section shows a relatively anteroposteriorly elongated neutral triangle (Diard's area), situated directly below the posterior facet (figure 4.77). Though the specimen is sedimented, several isolated trabeculae are observable. The inferior plantar group of trabeculae also known as the primary tensile is visible in the posterior section (figure 4.77). The AP section does not show much except that the neutral triangle found in the ML section is in the centre of the specimen.

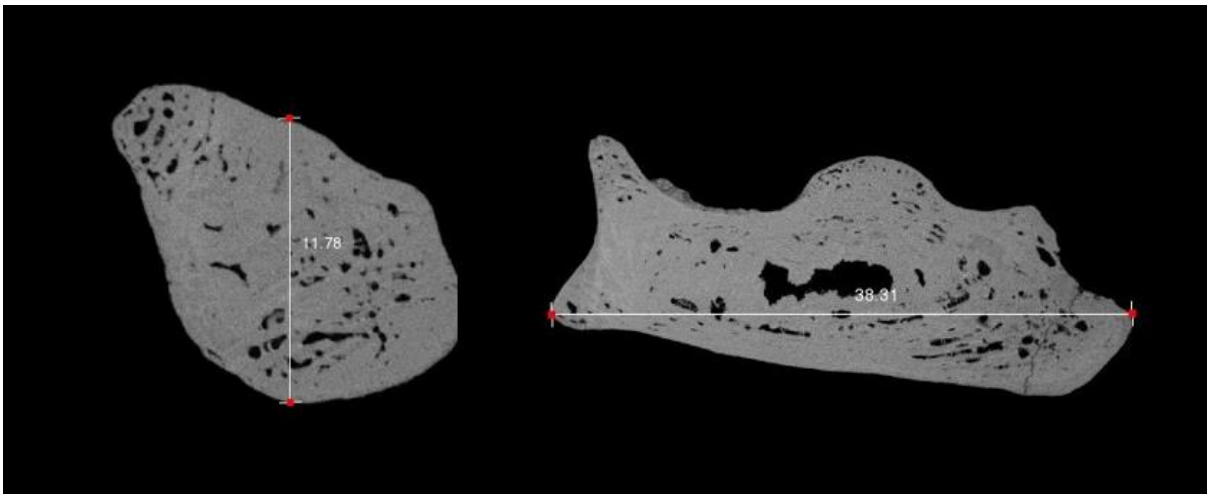

Figure 4.77: Mediolateral section with randomly isolated trabecular bone (R) and anteroposterior section showing neutral triangle in the centre (L) of 2222M.

SWP 537

This specimen is filled up with sediment, except the neutral triangle. However, patterns of trabecular bone and sediment are distinguishable by differences in colour hues of light and dark greys observable. The AP section shows that the neutral triangle is partly preserved and anteroposteriorly orientated with its most superior tip missing due to the presence of sediment (figure 4.78).

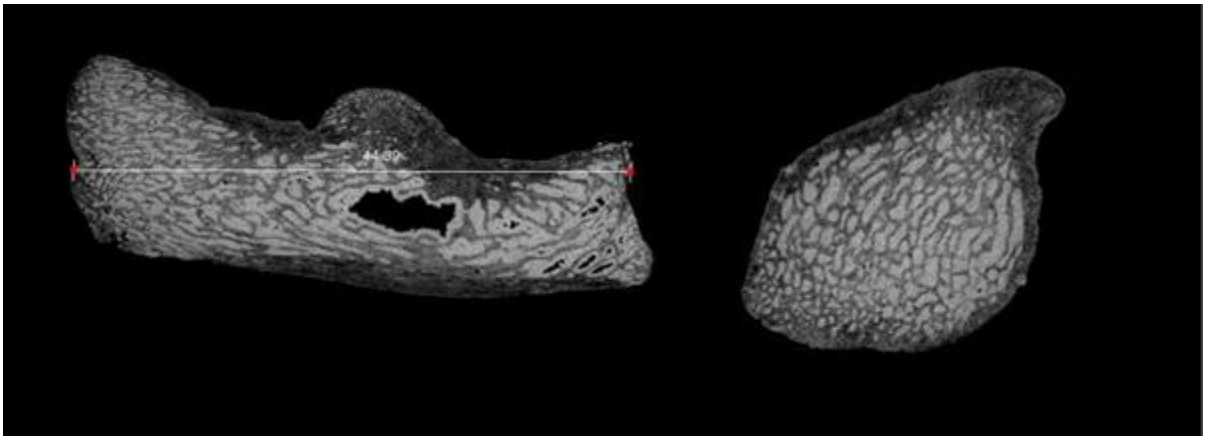

Figure 4.78: Anteroposterior section with centrally located Diard's area within sediments (L) and mediolateral section without preserved trabecular bone (R) of SWP 537.

SWP 1146

The ML section shows that the trabecular bone of this specimen consists of open and closed-cells. Open cells with honeycomb-like structures are visible radiating posteriorly while closed-cell with rods like structures are visible from the neutral triangle area to the anterior section (figure 4.79). The neutral triangle is present but not clearly defined. The anterior apophyseal group (secondary compressive trabecular bone) and the inferior plantar group are preserved. The AP section indicates well preserved closed-cells structures like trabecular bone in the posterior facet and around the neutral triangle (figure 4.79).

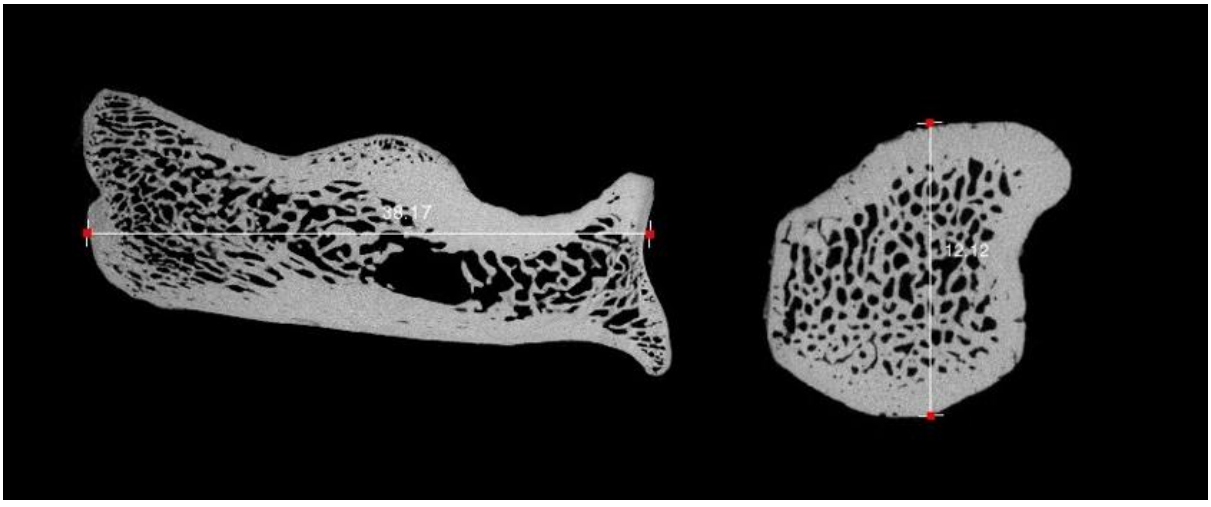

Figure 4.79: Open cells with honeycomb like structures on posterior region, rod like structures on the Diard's area (L) and closed cells trabecular bone (R) in 2D sections of SWP 1146

SWP 1157

This specimen has fairly preserved trabecular bone even though it has got sediment. The ML section reveals that trabecular bone shape is dominated by closed-cells that exhibit honeycomb lie structures but open cells with rods like structure trabecular bone (figure 4.80). The AP section shows that the neutral tringle is well preserved and is surrounded by well-defined thalamic group, posterior achillean group, anterior apophyseal group and the anterior planter group trabecular bone patterns. These trabeculae are open cell and rods like structures forming different patterns (figure 4.80).

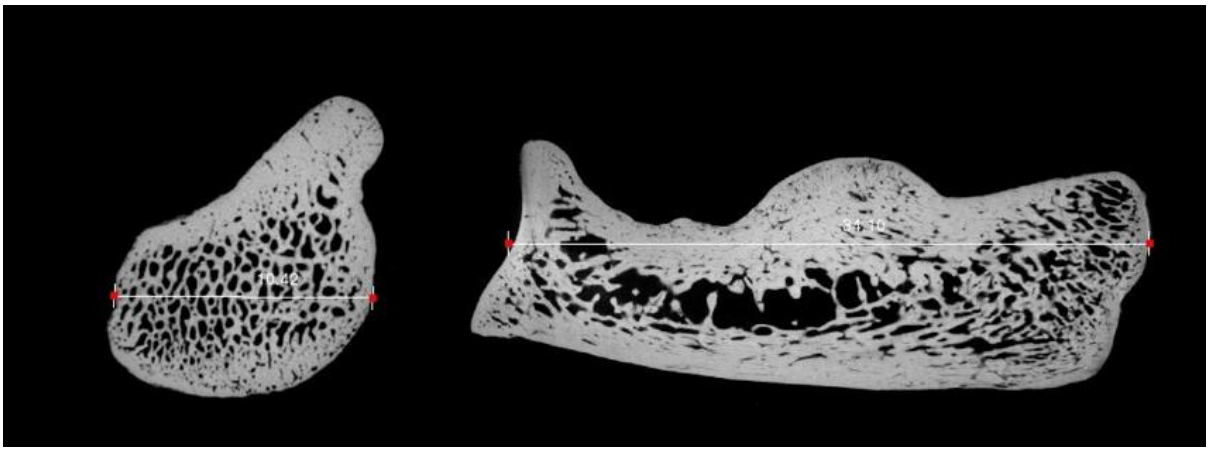

Figure 4.80**:** 2D sections of SWP 1157 showing closed-cells with honeycomb like structure (L) and elongated neutral angle sounded by open and rods like structure trabeculae forming different patterns**.**

SWP 1161

The ML section indicates that the trabecular bone consists of closed-cells with plate-like structures trabecular bone (figure 4.81). The anteroposterior cross section exhibits open cells with rods and plate-like structure trabecular bone. Furthermore, the neutral triangle is anteroposteriorly elongated and is surrounded by open cells with rods like structure trabeculae, forming anterior apophyseal group (figure 4.81).

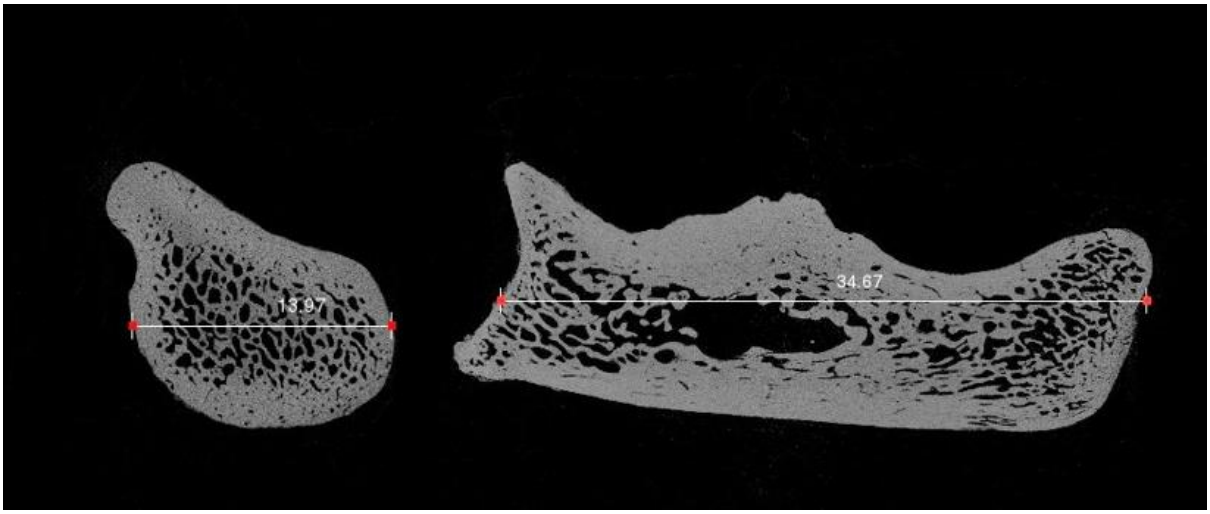

Figure 4.81: Cross sections of SWP 1161 displaying closed-cells preserved trabeculae (L) and open cell like structures forming trabecular bone groups (R).

SWP 1207

The ML section shows a well preserved open cells with rods as well as plate-like structure trabecular bone (figure 482). When observed on the AP section, the neutral triangle is found encompassed in anterior apophyseal, anterior planter, thalamic and inferior planter groups of trabecular bone. The anteroposterior trabeculae are open cells with plate-like trabecular bone structures as well as with few rods like structures (figure 4.82).

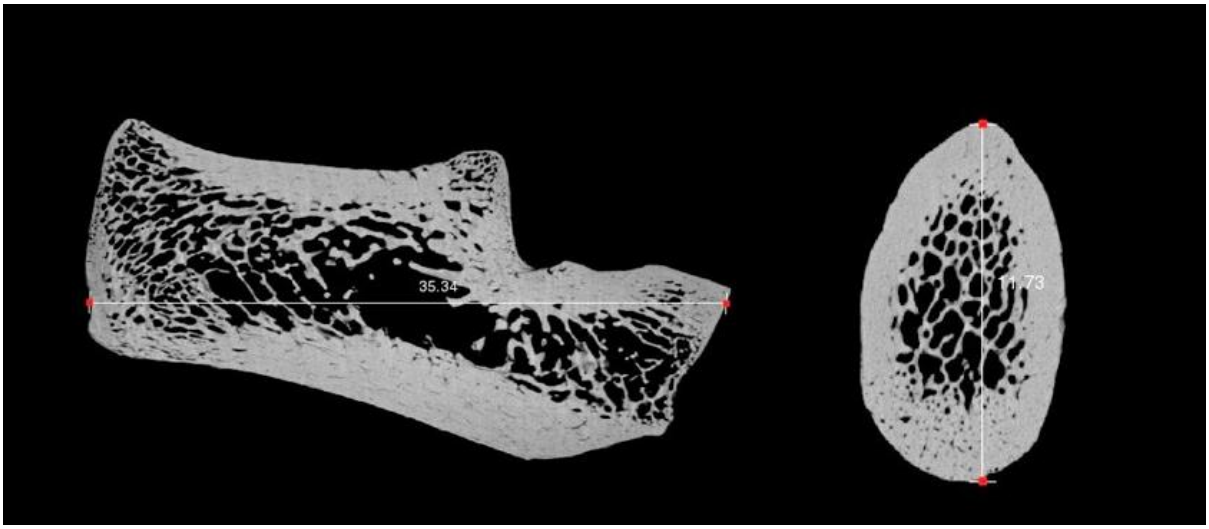

***Figure 4.82*:** Cross sections of SWP 1207 with large neutral triangle with rods-like structures trabeculae (L) and open cells like structures producing trabecular bone patterns (R).

Table 4.1: Summary of specimen extracted 2D sections or 3D volume of interest.

Specimens	**2D sections**	**3D Volume**	**Preserved or Segmented trabecular bone**
SWP 526	Yes	Yes	Preserved
SWP528	No	No	
SWP 529	No	No	
SWP 531	Yes	Yes	Preserved
SWP 532	No	No	
SWP 533	No	No	
SWP 537	No	No	
SWP 606	Yes	Yes	Segmented
SWP 747	No	No	
SWP 749	No	No	
SWP 753	No	No	
SWP 756	Yes	Yes	Preserved
SWP 962	Yes	Yes	Segmented
SWP 1009	No	No	
SWP 1011	Yes	Yes	Preserved
SWP 1411	Yes	Yes	Segmented
SWP 1146	Yes	Yes	Preserved
SWP 1157	Yes	Yes	Preserved
SWP 1161	Yes	Yes	Preserved
SWP 1203	Yes	Yes	Preserved
SWP 1207	Yes	Yes	Preserved
SWP 1384	No	No	
SWP 1406	No	No	
SWP 1546	Yes	Yes	Segmented
SWP 1596	No	No	
SWP 1698	No	No	
SWP 1699	No	No	

Sts 2050	No	No	
Sts 2259	No	No	
SK 605	No	No	
SK 607	No	No	
SK 1513	No	No	
SK 2595	No	No	
SK 14015	No	No	
1930 M	No	No	
1934 M	No	No	
2222 M	No	No	
14934 M	No	No	
16383 M	No	No	
BF 36	No	No	
TP 18	No	No	

4.3 Result of trabecular bone volumes of interest (3D VOI)

This section present results of quantification of the variation of the organisation and textural properties of the trabecular bone, presented in a tabular format as well as in box and whisker plots. Here, results of fossil specimens trabecular bone calculated parameters are presented in table format along with mean data of extant specimens because extant specimen's tables are presented as annextures (see annextures A1-A4). As discussed in chapter 3, a total of eighty one (81) specimens divided into forty one (41) fossils and forty (40) extant specimens were scanned. However, due to the preservation bias of some of the specimens, only eighteen (18) volumes of interest that derive from fifteen (15) fossil specimens are presented. Of the properties quantified are trabecular bone fabric anisotropy, trabecular bone thickness, trabecular bone volume fraction and trabecular bone spacing.

4.3.1: Trabecular bone fabric anisotropy

Femora

Most of fossil femoral heads (Four out of seven) fossil femora are more aligned than extant specimen in the study contain trabeculae that are highly aligned and generally have high fabric anisotropy when compared to extant specimens (*Chlorocebus* species and *Papio* species). Exception to this are specimens SWP 526 and SK 1513 because they have relatively low fabric anisotropy compared to extant specimens. A box plot of fabric anisotropy indicate that SK 1513 lies above the *Papio* range but below *Chlorocebus* (figure 4.83) with fabric anisotropy of 0.411 compared to 0.452 and 0.356 of *Chlorocebus* species and *Papio* species respectively while, specimen SWP 526 recorded fabric anisotropy of 0.339, the lowest trabecular bone fabric anisotropy on this locomotor joint (table 4.2).

Comparing Fossil means with *Chlorocebus* means show that they are statistically insignificant because they recorded p-value of 0.6587566, which is higher than 0.05 significancy level (have similar means). Fossils means compared to *Papio* means highly significant at 95% confidence level because they recorded p values of 0.0000000, indicating extremely significance with different means

Table 4.2: Trabecular bone parameters measured in fossil and extant femoral heads.

Specimen	**DA**	**BV (mm^3)**	TV (mm^3)	**BV/TV**	**Th.Th mean (mm)**	**Tb.Th sd (mm)**	**Tb.sp mean (mm)**	**Tb.Sp sd (mm)**
SWP 526	0.339	25.706	41.1	0.625	0.319	0.111	0.291	0.121
SWP 531	0.597	22.291	31.976	0.697	0.379	0.136	0.303	0.117
SWP 756	0.535	21.137	29.332	0.721	0.385	0.114	0.305	0.137
SWP 1011	0.637	30.345	38.841	0.781	0.828	0.52	0.339	0.146
SWP 1203	0.490	20.402	32.846	0.621	0.368	0.166	0.339	0.114
SK 605	0.497	5.098	7.813	0.653	0.429	0.181	0.37	0.199
SK 1513	0.411	55.731	124.85	0.446	0.337	0.201	0.256	0.086
Chlorocebus	0.452	4.993	9.989	0.503	0.250	0.068	0.358	0.126
Papio	0.356	38.711	67.706	0.564	0.394	0.157	0.471	0.178

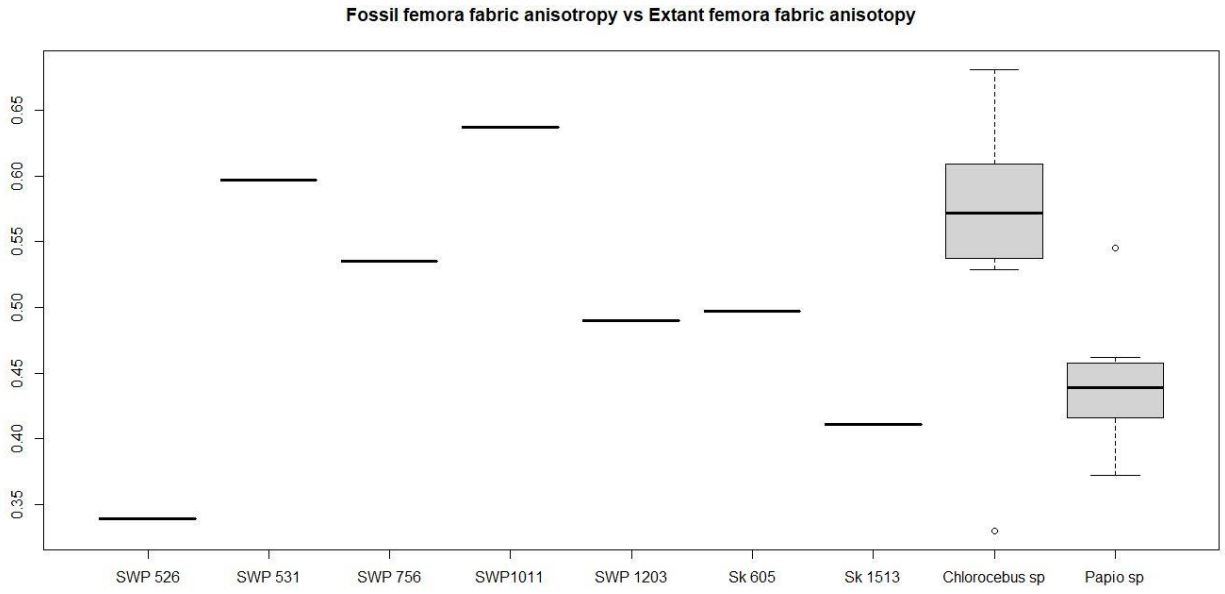

Figure 4.83: A plot of fossil femoral heads fabric anisotropy compared to fabric anisotropy of extant femoral heads**.**

Calcanei

Trabecular bone fabric anisotropy of fossil calcanei specimens is also plotted against the extant specimens in the study (figure 4.84). Here four (4) of the six (6) fossil specimens which have preserved trabecular bone were quantitatively analysed. The general trend is that fossil specimens have high fabric anisotropy than extant specimens because three (3) of the four (4) specimens (SWP 1146, SWP 1157 and SWP 1207) in a box plot lies above both positively skewed *Chlorocebus* and *Papio* species box plots as shown by figure 4.84. Specimens SWP 1146 and 1157 have similar value (0.649) and lies just above 50% of the variation of *Papio*. However, comparing means of Fossils specimens with extant specimens (*Chlorocebus* and *Papio*) show statistically insignificant means of 0.43 and 1.00 respectively. SWP 1207 has the highest trabecular bone fabric anisotropy, recording 0.728 while SWP 1161 has the lowest fabric anisotropy recording 0.580 compared to 0.589 and 0.668 of *Chlorocebus* and *Papio* (table 4.3).

Table 4.3: Summary of fossil calcanei trabecular bone parameters**.**

Specimen	**DA**	**BV (mm^3)**	TV **(mm^3)**	**BV/TV**	**Th.Th mean (mm)**	**Tb.Th sd (mm)**	**Tb.sp mean (mm)**	**Tb.Sp sd (mm)**
SWP 1146	0.649	3.919	6.756	0.58	0.351	0.106	0.411	0.154
SWP 1157	0.649	33.963	50.24	0.667	0.439	0.279	0.317	0.116
SWP 1161	0.58	5.628	7.172	0.785	0.655	0.322	0.419	0.266
SWP 1207	0.728	26.402	52.827	0.5	0.289	0.14	0.458	0.157
Chlorocebus	0.589	24.327	58.598	0.376	0.282	0.106	0.658	0.216
Papio	0.668	57.720	141.810	0.405	0.327	0.121	0.700	0.251

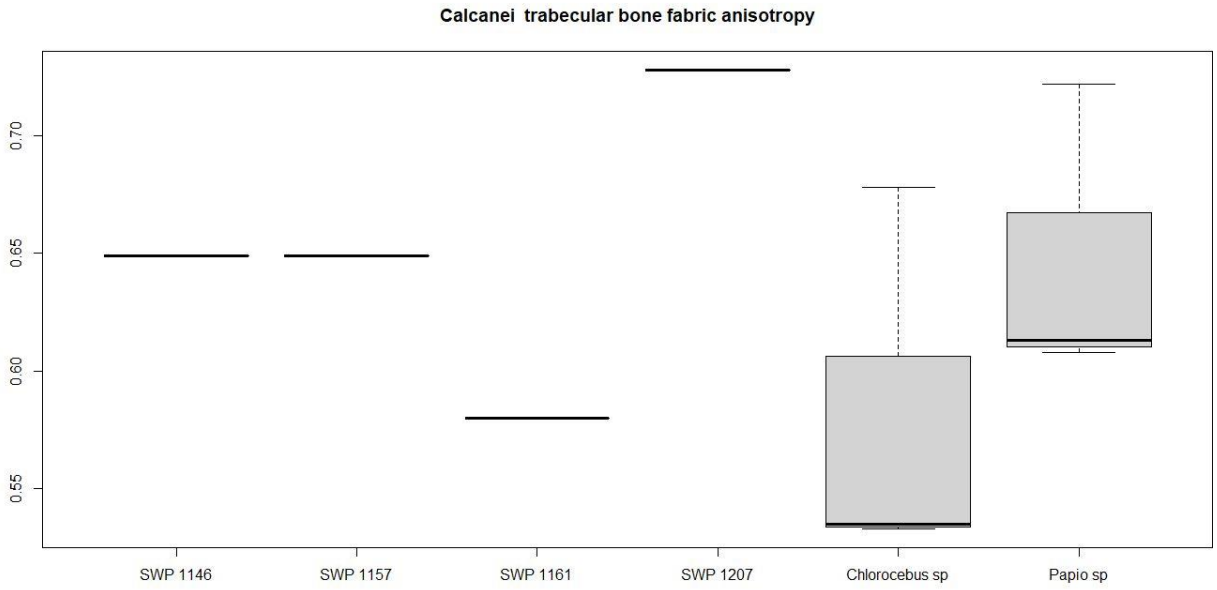

***Figure 4.84*:** Box plot showing fossil calcanei trabecular bone fabric anisotropy plotted against extant calcanei trabecular bone fabric anisotropy.

Tibiae

Two (2) fossil tibiae, SWP 1141 and SWP 1596 were quantitatively analysed. These specimens were further divided in to two (2) medial (M) and one (1) lateral (L) volumes, making a total of five (5) tibiae volumes. Although volumes of interest were extracted in centre (nucleus), medial and lateral facets, SWP 1596 lateral volume did not have preserved trabecular bone needed for computing fabric anisotropy and other related loading signals. Therefore the results presented here are devoid of SWP 1596 lateral facet volume (table 4.4).

Table 4.4: Summary of proximal tibiae trabecular bone parameters.

Specimen	**DA**	**BV (mm^3)**	**TV (mm^3)**	**BV/TV**
SWP 1141_Centre	0.476	13.039	15.519	0.744
SWP 1141_Medial	0.29	11.23	17.694	0.635
SWP 1141_Lateral	0.302	9.984	17.694	0.564
SWP 1596_Centre	0.347	10.47	12.535	0.835
SWP_1596_Medial	0.61	9.625	12.535	0.768
Chlorocebus centre	0.59	2.097	7.491	0.273
Chlorocebus Lateral	0.669	3.129	7.425	0.409
Chlorocebus medial	0.5935	3.143	7.425	0.417
Papio centre	0.324	4.945	18.001	0.275
Papio Lateral	0.528	7.00	18.059	0.387
Papio medial	0.289	6.778	18.059	0.376

A box plot of fossil tibiae against extant specimens (figure 4.85) indicates that trabeculae in fossil tibiae are less aligned as indicated by low trabecular bone fabric anisotropy compared to extant specimens. This is supported by t-test result that indicate a slightly significant means of 0.05 for Fossil specimen means compared to *Chlorocebus* means. However, when comparing means of Fossils to *Papio* it indicate that means of the group are similar with no difference since they recorded p-values of 0.97. Trabecular bone of specimens SWP 1596 extracted in proximal medial facet record the highest fabric anisotropy of 0.610 and is relatively in the same range as *Chlorocebus* (0.590) trabecular bone while trabecular bone extracted in the medial facet of SWP 1141 record the lowest trabecular bone fabric anisotropy of 0.290, almost similar to *Papio* at 0.289 (figure 4.85). However, trabeculae in the nucleus of SWP 1141 are more aligned than those of *Papio* but less aligned when compared to Chlorocebus.

Trabecular bone in medial of SWP 1596 recorded fabric anisotropy of 0.610 compared to 0.594 and 0.289 of *Chlorocebus* and *Papio* respectively. Trabecular bone from the lateral facet of specimen SWP 1141 has isotropic trabecular bone (less aligned) than extant specimens with 0.302 to 0.669 of *Chlorocebus* and 0.528 of *Papio* (table 4.4).

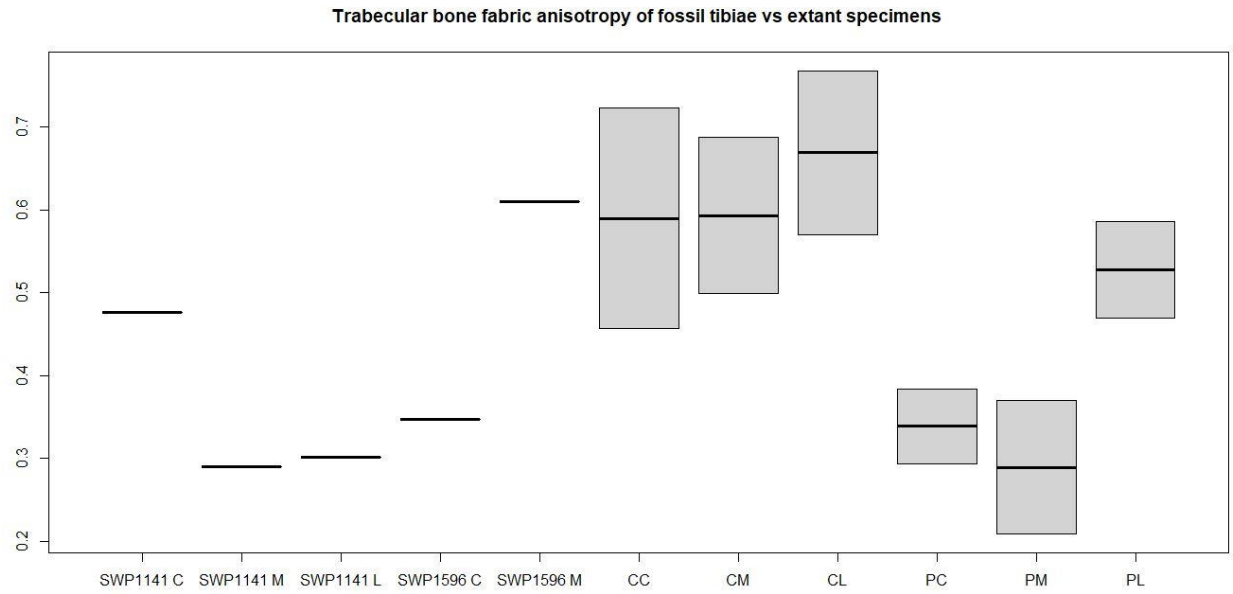

***Figure 4.85*:** A box plot of fossil tibiae trabecular bone fabric anisotropy compared to trabecular bone fabric anisotropy of extant specimens. (C, M, L) are centre, medial and lateral L facets of fossil specimens. (CC, CM, CL) are centre, medial and lateral facets of *Chlorocebus species* while (PC, PM, PL) are centre, medial and lateral facets of *Papio species*.

Fossil humeri fabric anisotropy were calculated and tabulated as in table 4.5. It was further plotted against extant humeri specimens as shown in figure 4.86 below. The box plot indicates trabeculae in fossil humeral heads are highly aligned as compared to their comparable extant humeri heads (figure 4.86). This is consistent with t-test results that recorded fossils and extant specimens difference in their means with p-values of Fossils to *Chlorocebus* specimens being 0.05 while Fossils to *Papio* is 0.04. *Papio*'s box plot is indicated as a line (single reading) because the two (2) readings used are the same. Specimens SWP 606 and SWP 962 respectively have 0.592 and 0.454 trabecular bone fabric anisotropy compared to 0.187 for *Chlorocebus* and 0.171 for *Papio* (table 4.5).

Table 4.5: Summary of fossil proximal humeri trabecular bone parameters.

Specimen	**DA**	**BV (mm^3)**	**TV (mm^3)**	**BV/TV**
SWP 962	0.592	39.521	60.080	0.658
SWP 606	0.454	51.406	81.430	0.631
Chlorocebus	0.187	7.0155	21.745	0.323
Papio	0.171	22.050	83.091	0.265

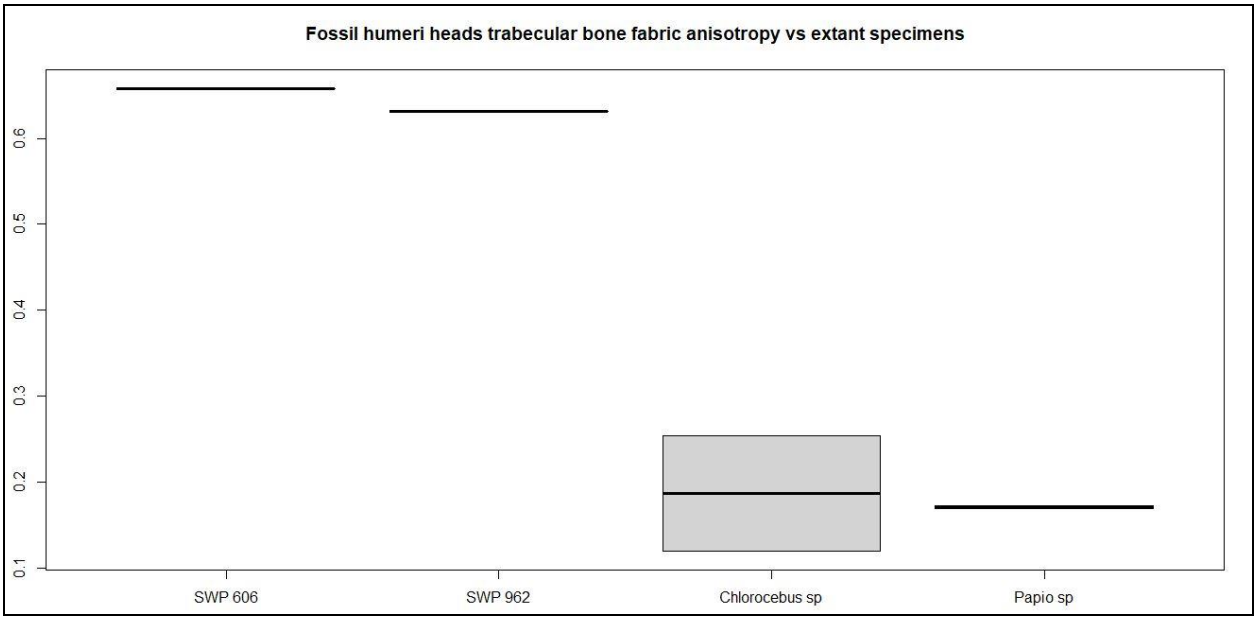

***Figure 4.86*:** Trabecular bone fabric anisotropy of fossil humeri compared to fabric anisotropy of extant humeri specimens.

4.3.2: Trabecular bone volume fraction

Observation from the trabecular bone volume fraction plot of fossil femora against extant specimens indicate that six (6) of the seven (7) specimens are denser and more connected than the extant groups, as shown by their high trabecular bone volume fraction (figure 4.87) even though extant specimens exhibit outliers in extreme lower and higher quartiles. This is consistent with student t-test results of Fossils specimen means compared to *Papio* specimens. The means are statistically significant because there are different with p-value of 0.00. However, when comparing Fossils to *Chlorocebus* specimens, the t-test recorded p-value of 0.66. This is statistically insignificant with no difference in means.

Specimen Sk 1513 has less dense and less connected trabecular bone with bone volume fraction of 0.446 (44.6%) compared to 0.503 (50.3%) for *Chlorocebus* and 0.564 (56.4%) for *Papio*, making it the specimen with less compact and less connected trabecular bone (table 4.6). However, on the contrary, SWP 1011 has the densest and well connected trabecular bone with its high trabecular bone volume fraction of 0.781 (78.1%) as seen in table 4.2 above. The rest of specimens lie above extant specimen's volume fraction.

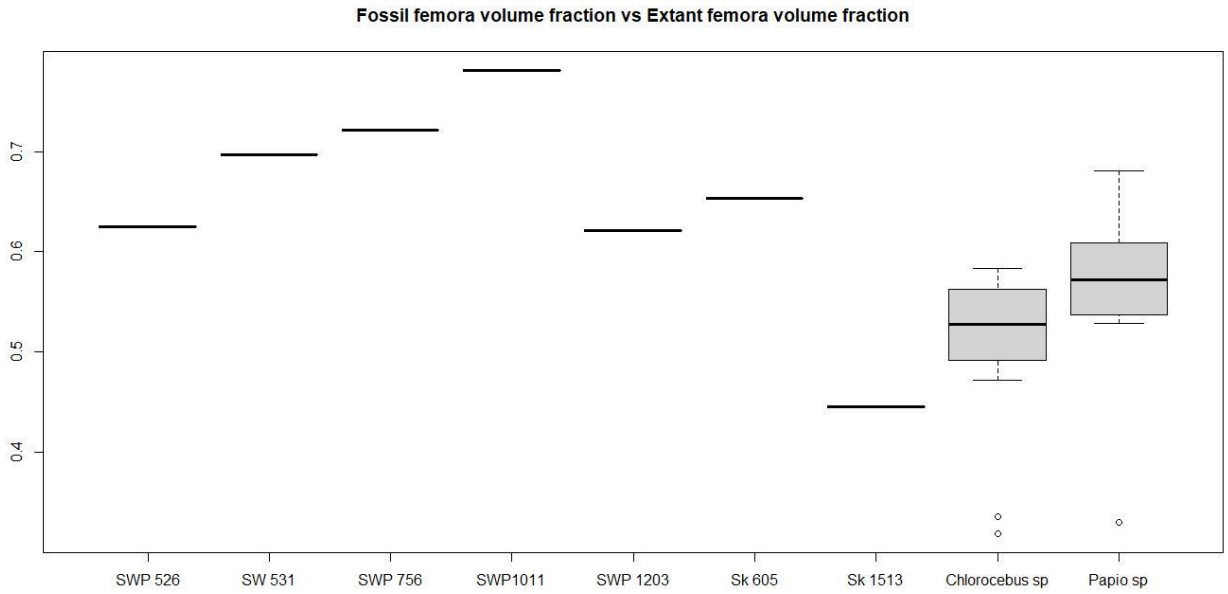

Figure 4.87: Trabecular bone volume fraction of fossil femoral heads compared to trabecular bone volume fraction of extant femoral heads.

Trabecular bone volume fractions of fossil calcanei are also compared to bone fractions of extant calcanei. Observations from the box plot below indicate that fossil calcanei have dense and well connected trabecular bone as indicated by their higher volume fraction compared to low bone volume fraction extant specimens (figure 4.88). This is consistent with student t-test recorded means that are higher than below 0.05 at 95% confidence level. Means of Fossils to *Chlorocebus* and *Papio* 0.01 and 0.04 respectively and this proved to be statistically significant with different means. Specimens SWP 1207 is the only one with trabecular bone structure close to the negatively skewed extant specimen's box plots, as it records bone volume fraction of 0.500 (50%) while SWP 1146 and SWP 1157 recorded 0.58 (58%) and 0.667 (66.7%) respectively (table 4.3). SWP 1161 is the densest specimen as it records 0.786 (78.6%) bone volume fraction compared to compared to 0.376 for *Chlorocebus* and 0.405 for *Papio* (table 4.3).

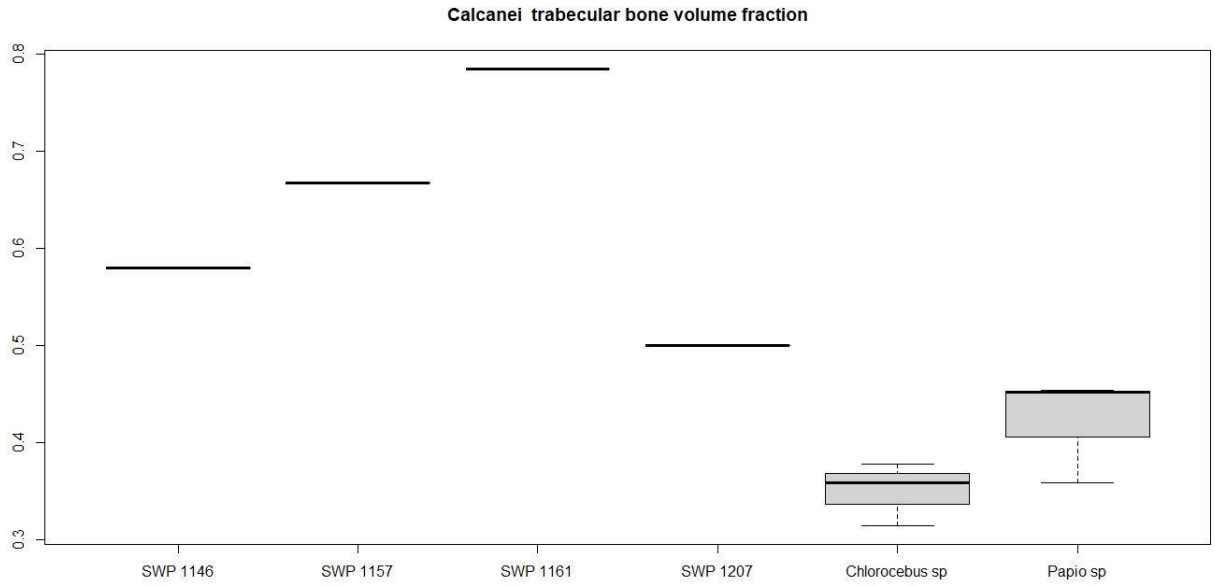

Figure 4.88: Trabecular bone volume fraction of fossil calcanei compared to trabecular bone volume fraction of extant calcanei specimens.

Another fossil cercopithecoids joint analysed for locomotor signal is humerus head. Just like trabecular bone fabric anisotropy of fossil humeri, trabecular bone volume fraction of fossil humeri is higher than those of the extant groups (figure 4.89), indicating that fossil humeri consist of dense and well connected trabecular bone compared to extant humeri. The findings are constant with statistical results of student t-test when comparing means of Fossils with that of extant specimens (*Chlorocebus* and *Papio*). The test yielded p-values of 0.00. This means that they are statistically significant since they are less than 0.05. Therefore, means are different. Fossil specimens SWP 606 and SWP 962 has a trabecular bone volume fraction of 0.631 (63.1%) and 0.658 (65.8%) respectively compared to 0.323 (32.3%) for *Chlorocebus* and 0.265 (26.5%) for *Papio* (table 4.5).

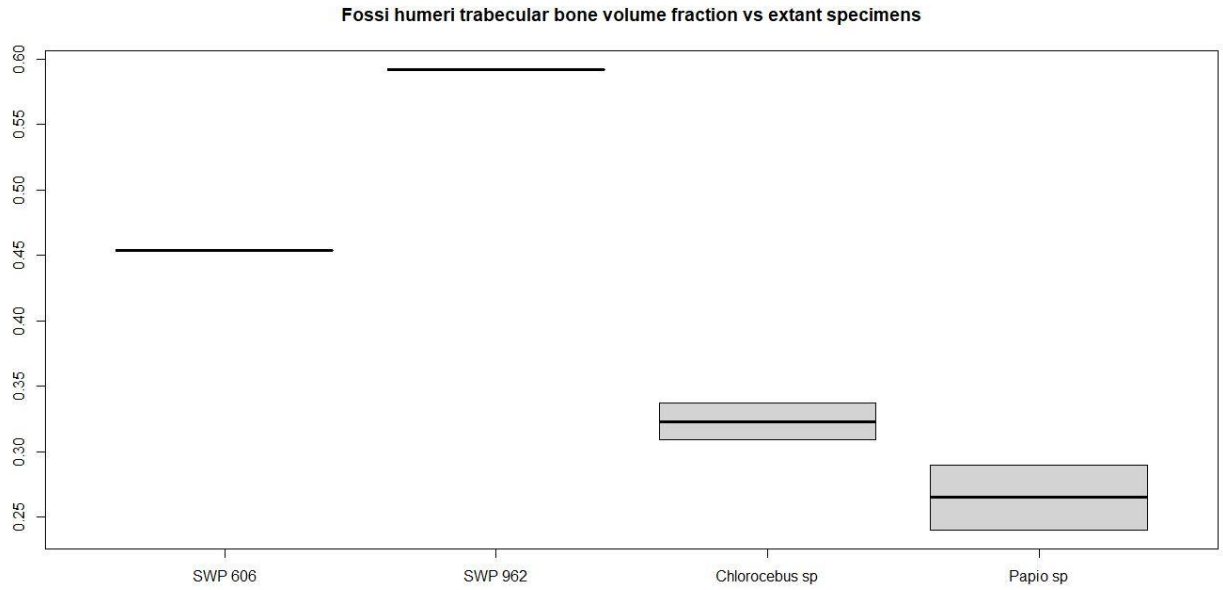

***Figure 4.89*:** Dense and well connected trabecular bone of fossil humeri heads shown by high bone volume fraction compared to less dense trabecular bone of extant humeri heads.

Trabecular bone volume fraction of fossil proximal tibiae extracted central (nucleus) (C), medial (M) and lateral (L) are presented in a box plot and compared to that of extant proximal tibiae. Observation of the box plot show that all fossil specimens have dense and well connected trabecular bone as indicated by their high bone volume fractions (figure 4.90). This is consistent with results of student t-test which yielded 0.00 p-values when Fossil specimens means are compared to extant specimens (*Chlorocebu*s and *Papio*), indicating that means of the group are not similar but different. This means that trabecular bone volume fraction extracted in centres (nucleus), medial and lateral sides all have high fabric anisotropy than the extant groups *Chlorocebus* and *Papio* (figure 4.90). Worth noting here is that trabecular bone of *Papio* extracted in the nucleus and lateral side of the tibia are presented as single lines because calculated parameters have similar reading.

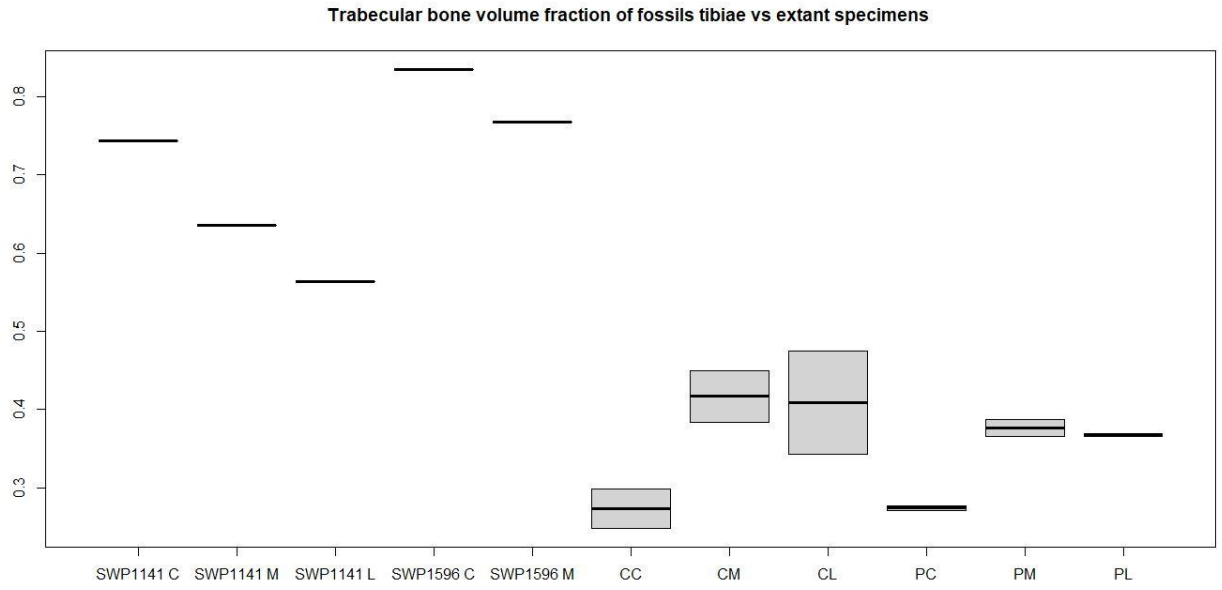

Figure 4.90: Dense and well connected trabecular bone of fossil proximal tibiae shown by high trabecular bone volume fraction compared to trabecular bone volume fraction of extant proximal tibiae specimens. (C, M, L) are centre, medial and lateral L facets of fossil specimens. (CC, CM, CL) are centre, medial and lateral facets of Chlorocebus species while (PC, PM, PL) are centre, medial and lateral facets of *Papio* species

4.3.3 Trabecular bone thickness

Trabecular bone thickness of fossil femora is presented in box plots as seen in figure 4.91 below. The plot shows that all fossil specimens have slightly thicker trabecular bone than *Chlorocebus*. However, when compared to *Papio*, five (5) fossil femora have trabeculae that are thin wile two (2) are thicker than all extant specimens (figure 4.91). Specimen SWP 1011 has thicker trabecular bone struts as shown by its high trabecular bone thickness mean of 0.828 mm compared to 0.250 mm for *Chlorocebus* and 0.394 mm for *Papio*, while specimen SWP 526 have thinner trabeculae with mean thickness of 0.319 mm (table 4.2). The rest of the specimens show trabecular bone thickness means that place them within the range of *Papio*. Comparing means of Fossils to means of *Chlorocebus* specimens, the means are statistically insignificant because they recorded p-values of 0.45, while fossil to *Papio* recorded p-values of 0.00 (a highly significant value where means of two groups are different.

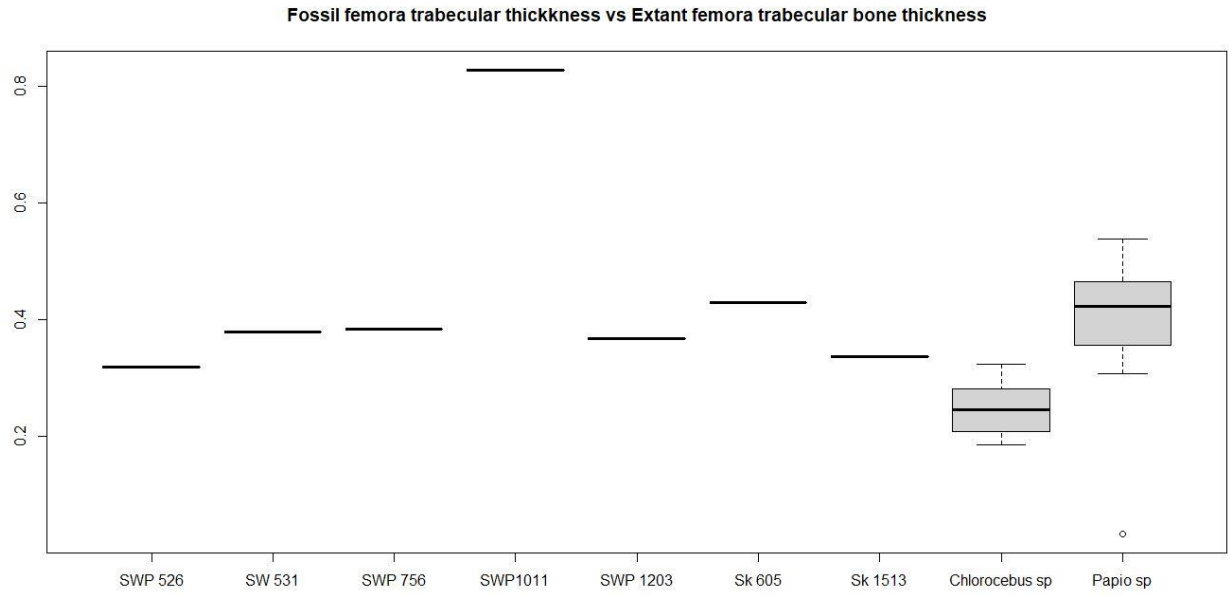

***Figure 4.91*:** Extant and fossil trabecular bone thickness.

Fossil calcanei trabecular thickness was also calculated and analysed in a box plot (figure 4.92). Trabecular bone thickness means of fossil calcanei shows most fossil calcanei have thick trabecular bone compared to extant specimens, with exception of specimen SWP 1207 (figure 4.92). This specimen has thin trabecular bone when compared to *Papio* but thicker than *Chlorocebus*. However, means of Fossils specimens compared to means of extant specimens (*Clorocebus* and *Papio*) show that the means of the groups are the same (statistically insignificant) with p-values of 0.15 and 0.47 respectively. SWP 1207 shows trabecular thickness mean of 0.289 mm trabecular bone thickness mean compared with 0.282 mm for and 0.327 mm for Papio. However, SWP 1146, SWP 1157 and SWP 1161 have thicker trabecular bone than extant specimens with 0.351mm, 0.439 mm and 0.655 mm respectively as illustrated by table 4.3 above.

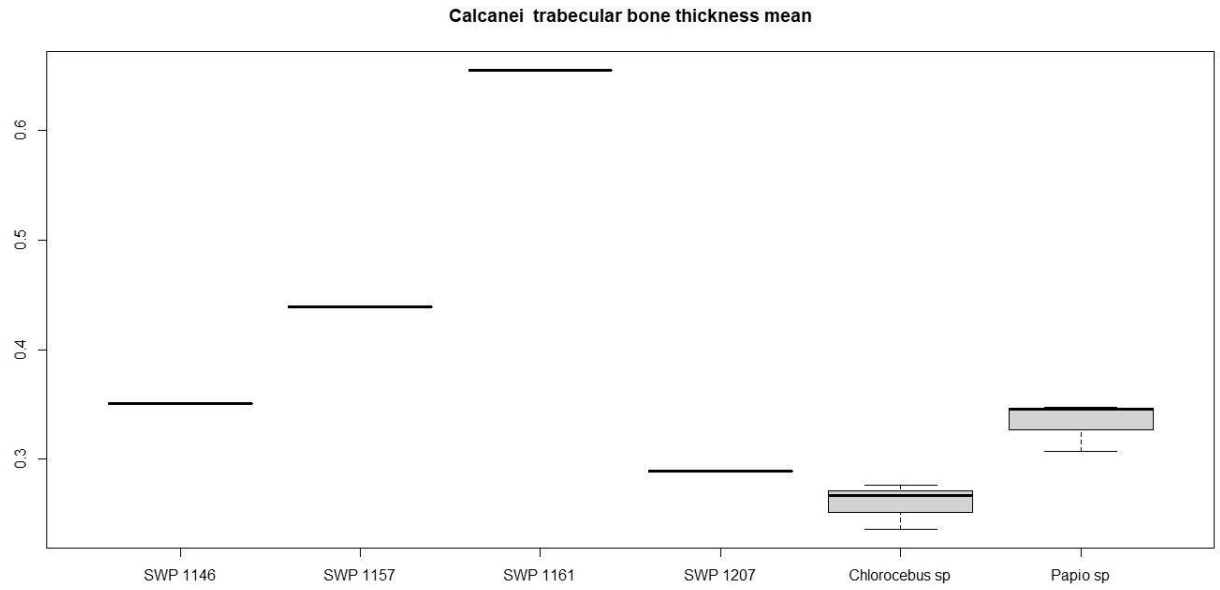

***Figure 4.92*:** Trabecular bone thickness mean of fossil calcanei compared with trabecular bone thickness mean of extant calcanei.

4.3.4 Trabecular bone spacing

Intertrabecular bone spacing of fossil femora were computed and analysed in box plot against their comparable extant femoral heads trabecular bone spacing. The box plot shows that all fossil femora have small intertrabecular bone spaces when compared to *Papio*. However, when compared to *Chlorocebus*, four (4) fossils lie below the range of the *Chlorocebus species* while three (3) fossil femora lie above the *Chlorocebus species* (figure 4.93). Generally, fossil specimens have small intertrabecular bone spaces than the extant specimens. This observation is supported by student t-test results because it yielded p-values of 0.00 for both Fossil means compared to *Chlorocebus* and *Papio* means. Statistically it means that the means of groups are different because they are all below 0.05 critical value at 95% confidence level. Specimen SK 605 is the only one with big trabecular bone spaces with lower values than extant specimens spaces with 0.370 mm of trabecular bone space mean while SK 1513 has the smallest intertrabecular bone space of 0.256 mm compared to 0.358 for *Chlorocebus* and 0.471 mm for *Papio* (table 4.2). The rest of the specimens have trabecular bone space means that are within the lower quartile (minimum or 25%) of extant specimens (figure 4.2).

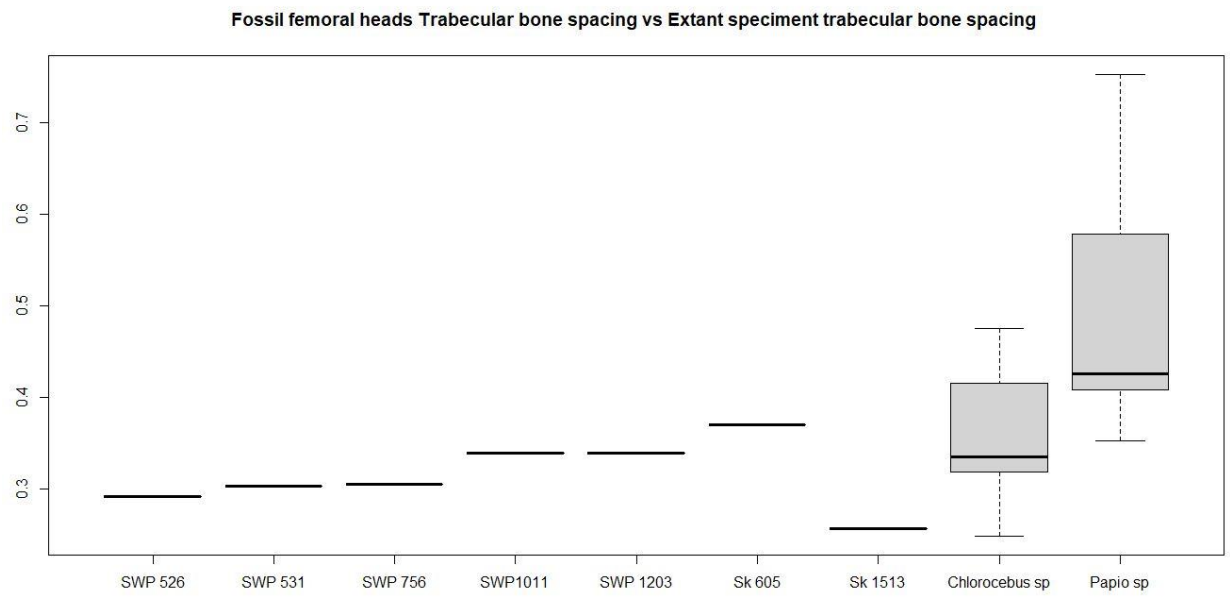

***Figure 4.93*:** Fossil femoral head trabecular bone spaces means plotted against trabecular bone spaces mean of extant specimens.

Space within trabecular bone of fossils and extant calcanei was also computed and presented in a box plot. When compared to extant calcanei, fossil specimens have less intertrabecular space (figure 4.94). This is supported by student t-test results that yielded significant means of Fossil specimens compared to extant specimens (*Chlorocebus* and *Papio*) as the recorded 0.00 respectively. This is highly significant because it is close to o (less than 0.05 critical value at 95% confidence level and means of the groups are different. Specimen SWP 1157 has the lowest intertrabecular space with 0.317 mm trabecular bone space mean, while SWP 1207 has higher intertrabecular space with 0.458 mm compared with 0.672 mm for extant calcanei. Specimens SWP 1146, SWP 1157 and SWP 1161 have trabecular bone spacing of 0.411 mm, 0.317 mm and 0.419 mm respectively compared to 0.658 mm for *Chlorocebus* and 0.700 mm for *Papio* (table 4.3).

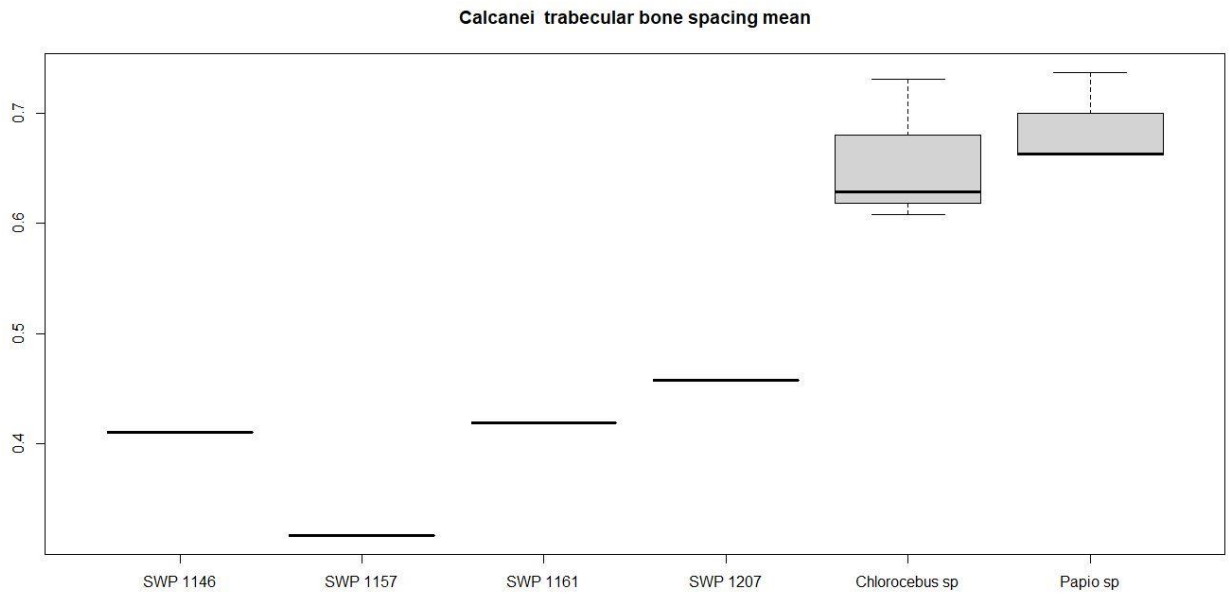

***Figure 4.94*:** Small intertrabecular bone space within fossil calcanei compared to well-spaced extant calcanei.

A summary of fossil trabecular bone computed parameters plotted against comparable extant specimens is presented in the following table 4.6. "+++" indicate high, “++" indicate low, “+" indicate lowest, while "-" indicate no reading.

Table 4.6: Summarised Fossil trabecular bone parameters vs extant specimens.

Parameters	**Fossil/Extant specimens**	**Femur**	**Calcaneus**	**Humerus**	**Tibia**
DA	Fossils	+ + +	+ + +	+ + +	+ +
	Extant	+ +	+ +	+ +	+ + +
Bv/Tv	Fossils	+ + +	+ ++	+ +	+ + +
	Extant	+ +	+ +	+	+ +
Tb.Th mean	Fossil	+ +	+ + +	-	-
	Extant	+	+	-	-
Tb.Sp mean	Fossils	+	+ +	-	-
	Extant	+ +	+ + +	-	-

Chapter 5 – Discussion and conclusion

The main aim of this research was to qualitatively and quantitatively analysing cercopithecoid's trabecular bone in key postcranial locomotor joints in search of locomotor signals which can be interpreted in terms of paleohabitats and palaeoenvironment. This is important because Plio-Pleistocene cercopithecoids shared their palaeoenvironment with contemporaneous hominins and as such they provide an excellent proxy in determining and reconstructing the late Pliocene-early Pleistocene palaeoenvironment. Several research studies analysing non-hominin fossil primates succeeded in defining locomotor and habitat activities of studied taxa based on their trabecular bone organisational structure, predominantly trabecular bone fabric anisotropy (e.g. Fajardo and Muller, 2001; Ryan and Ketcham, 2002a,b; Ryan *et al,* 2018).

5.1 Trabecular bone organisation in 2 dimensions (2D) and functional interpretations

Extant specimens possess trabecular bone with varying conventional and unpredictable trabecular bone structures such as open cells, short and closed-cells, plate-like as well as rod-like structure. Trabeculae networks are well-developed and thickened close to cortical bone with a well-developed vertical and arcuate bundle systems (Viola, 2002; Aiello and Dean, 1990).

Most of the fossil specimens used in this study are filled in by mineral deposits, resulting in trabecular bone not being preserved. This includes completely mineralised specimens such as Sts 2050 (femur) 1930 M (humerus) and TP 18 (tibia) as well as partially sedimented specimens e.g. SWP 537 (calcaneus), SWP 606 (humerus), SWP 749 (femur) etc. Partially sedimented specimens have preserved trabecular bone patterns, which allows tracing out trabecular bone from the sediment due to their colour contrasts (figure 5.1).

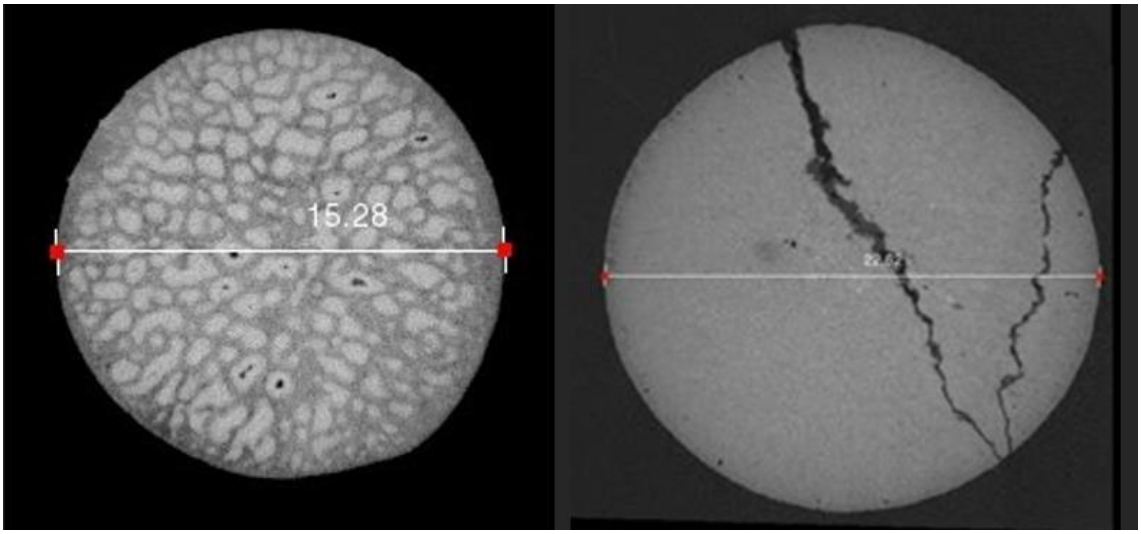

***Figure 5.1*:**Trabecular bone within sediments (R) and fully sedimented specimen (L).

However, few specimens e.g. SWP 526, SWP 1011, SWP 1203, SK 1513, etc. have excellent preserved trabecular bone. Preserved trabecular bone in femoral heads present visible vertical and arcuate bundles that intersect in nucleus of femoral heads. Vertical bundles spreads from inferolateral region (from neck) to superomedial of femoral heads and arcuate bundles spreads from inferomedial of femoral heads to superolateral regions (figure 5.2). Aiello and Dean (1990) as well as Viola (2002) interpreted vertical bundles as trabecular bone system that transmits main force through the femoral heads but arcuate bundles reduce tension in the femoral necks (Aiello and Dean, 1990: Viola, 2002).

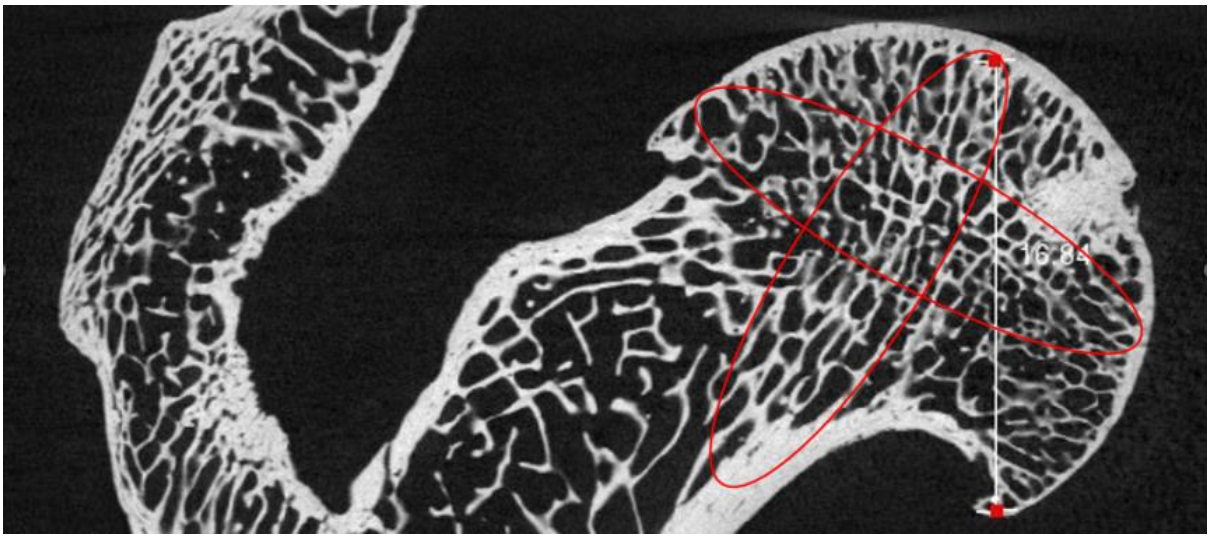

Figure 5.2: Illustration of vertical and arcuate bundles in femur head of extant specimen.

Trabecular bone in fossil femoral heads is comparable to extant specimens but differs in terms of thickness since fossil femoral heads are comparably thinner than extant specimens. Some specimens, for example SK 606, SWP 749, SWP 109 and SK 14015, present few observable and isolated trabecular bone. These specimens do not present preserved bundle systems but like most of the specimens in the study, present medially orientated trabecular bone that thickened close to cortical bone while becoming thin towards nucleus of the femoral heads (figure 5.2). In their study, Ito *et al*., (2000) described thickening of trabecular bone of hindlimbs towards cortical bone because of muscle attachment in quadrupeds, including in cercopithecoids (Ito *et al* 2000). It is considered that thickening of trabecular bone towards cortical bone replicate the role played by muscles and its link with locomotion, especially the gluteus medius muscle, because centre of gravitational force is located in between forelimbs and hindlimbs, thereby resulting in load distributed and scattered in all four legs (Ito *et al* 2000).

The calcanei SWP 1146, SWP 1157 and SWP 1207 have perfectly preserved trabecular bone, while specimen SWP 1161 also has preserved trabecular bone but slightly sedimented. However, these specimens exhibit combination of open cells with honeycomb and closed-cells with rods-like structures as well as a well-defined neutral triangle/Diard's area (Diard *et al*., 2007; Toepfer, 2017). Development of these structures is associated with compressive and tensile forces simultaneously acting on calcaneus of an individual, resulting in creation of thalamic, anterior, inferior plantar, anterior plantar and posterior achillean groups (Diard et al, 2007; Toepfer, 2017). In fact, the neutral triangle is a place of low stress since compressive and tensile neutralise each other. This is supported by Gibson (1985), who acknowledged that low-density, open cells and rod-like trabecular bone structures are found in areas dominated by low stress (Ultimately related to terrestrial locomotion), contrary to high-density with closed-cells and plate-like structures which usually develops in areas dominated by high stress (Gibson, 1985; Macchiarelli *et al*, 1998), related to arboreal locomotion.

The internal structures of fossil humeral heads and tibiae could not be described because all fossil humeral heads and tibiae specimens were filled with sediments. However, some fossil humeri such as SWP 962 and SWP 606 as well as some fossil tibiae specimens like SWP 1411 and SWP 1596 were manually segmented and quantitatively analysed.

5.2 Trabecular bone structural organisations in three (3) dimensions (VOI) and functional interpretations.

Fossil femoral heads in this study exhibit high fabric anisotropy compared to extant specimens, an indication of loading in a particular direction as a result of quadrupedal locomotion (Fajardo and Muller 2001; Fajardo *et al*., 2007, Ryan *et al*., 2018). The idea that high degree of alignment suggests efficient locomotor signal of action gait forces in a specific direction during locomotion is consistent with Takechi (1977), who suggested that trabecular position and directions is probably determined by tension applied on proximal femur head (Takechi (1977). Furthermore, Fajardo and Muller (2001) concluded that trabecular bone in proximal femoral heads develop high fabric anisotropy as a response to repeated force in the unilateral direction.

SWP 526 is the only specimen with the lowest fabric anisotropy with 0.339. The comparatively low fabric anisotropy could be attributed to presence of sediment, especially in nucleus of femoral head as explained in chapter 4.2 (description of homologous 2D sections). Furthermore, it could be due to monkeys primarily engaging in arboreal quadrupedalism locomotion but with occasional terrestrial quadrupedalism observed in nearly all extant cercopithecoids, resulting in variable loading (Fajardo and Muller, 2001). Schmidt (2010) and Fleagle (2013) observed that although extant monkeys are terrestrial quadrupeds, they spend quite a lot of time scavenging and napping on trees (Schmidt, 2010; Fleagle, 2013). Therefore, it seems that the isotropic state of SWP 526 and extant specimens are intricately linked to multidirectional loading, resulting in creation of isotropic locomotor signal structures related to terrestrial rather than arboreal locomotion.

Although trabecular bone volume fraction of fossil femoral heads is consistently higher than extant specimens, with exceptions of specimens SK 1513 which has 41.1%, extant specimens exhibit relatively high mean trabecular bone volume fraction (53.5%). The low trabecular bone volume fraction of specimen SK 1513 could either be attributed to the presence of sediment or the extent of compression and tension forces on proximal femoral heads by the weight of an individual animal (Takechi., 1977). It could also be attributed to an individual primarily walking terrestrially on its four limbs with the load evenly distributed and resulting in isotropic trajectories and low volume fraction (Fajardo and Muller, 2001; Schmidt, 2010; Fleagle, 2013). High amount of trabecular bone volume fraction of both fossil and extant specimens is an

indication of dense and well connected trabecular bone in proximal femoral heads (Ryan and Ketcham, 2002a,b).

Most fossil femoral heads have slightly thicker trabecular bone struts than in the extant sample even though they fall within the range of the extant specimens. Specimen SWP 526 is the only one that is slightly thinner at 0.319 mm compared to 0.328 mm of extant specimens. Intertrabecular bone spacing of proximal femoral heads indicate that fossil specimens have less or smaller intertrabecular bone spaces while extant femoral heads have well-spaced trabecular bone, with specimen SWP 1513 having the least intertrabecular space.

Trabecular bone fabric anisotropy of fossil calcanei specimens is relatively high than extant specimens with exception of specimen SWP 1161. This specimen has the least fabric anisotropy with 0.580 fabric anisotropy compared to 0.615 of extant specimens. However, this does not mean that its trabecular bone is not aligned since the alignment is close to one (1). Specimen SWP 1207 exhibits the most aligned trabecular bone with bone fabric anisotropy of 0.728. Generally, both fossils and extant calcanei in this study have fabric anisotropy more than 0.5 (50%). The highly anisotropic nature of calcaneus is noted by Diederichs *et al*, (2009) when assessing components of trabecular bone struts and texture of the calcaneus by clinical multi-detector row computed tomography (Diederichs *et al*, 2009). This means that both fossils and extant specimens possess trabecular bone that is highly aligned due to repetitive gait forces in particular direction (Takechi, 1977; Fajardo and Muller 2001; Fajardo *et al*., 2007, Ryan *et al*., 2018), a suggestion that cercopithecoids body weight was mainly loaded in hinge limbs than fore limbs.

Fossil calcanei trabecular bone volume fraction range of 50%-78.5% compared to 38.6% of extant specimens. In the study to assess relationship of trabecular bone phenotype and behaviour using human calcaneus, DeMars *et al* (2021) noted that high volume fraction was mainly due to repeated locomotion gait forces (DeMars *et al*., 2021). Saers *et al* (2019) indicated that trabecular bone volume fraction is raised by increasing thickness of trabecular bone and the higher bone volume fraction closely correlated with thicker as well as less intertrabecular spacing of bone (Saers *et al*, 2019), consistent with Lin *at al* (1998) which recorded high trabecular bone volume in the posterior region of the calcaneus (Lin *at al*, 1998).

Almost all fossil and extant calcanei specimens consist of thin trabecular bone because they are all below 0.5mm (ranges 0.289 mm-0.439 mm). However, the intriguing specimen SWP 1161 has thicker trabecular bone in its calcaneus, scoring 0.655 mmm. Its trabecular bone thickness could be attributed to the presence of sediment observed and described in chapter 4.2 (description of homologous 2D sections) or due to its density as suggested by Saers *et al* (2019).

Trabecular bone in fossil calcanei are less spaced, an indication of compact, dense and small intertrabecular spaces compared to large, well-spaced and less dense trabecular bone of extant specimens. Extant specimens recorded mean trabecular thickness (intertrabecular spaces) of 0.672 mm in contrast with to 0.317 mm-0.458 trabecular bone thickness indicating low intertrabecular space.

Volumes placed centrally and medially in fossil proximal tibiae exhibits variable trabecular bone fabric anisotropy compared to the centrally placed volumes of extant specimens. The central portion of specimen SWP 1141 has more aligned trabeculae than comparable extant specimens, while the central portion of SWP 1141 consists of less aligned trabecular bone compared to central portions of extant specimens. However, both fossils and extant specimen tibiae are generally less aligned with fabric anisotropy score below 0.5 with fossils scoring 0.347-0.476 and extant specimens scoring 0.430. Medial facet of specimen SWP 1596 has more aligned trabeculae than comparable extant specimens while medial facet of SWP 1141 has less aligned trabeculae as compared to extant specimens. The only lateral facet of fossil specimens studied in this work (the one of SWP 1141) contains less aligned trabeculae when compared with that of extant specimens.

Fossil proximal tibiae have high trabecular bone volume fraction, with central part of the specimen SWP 1596 recording an extremely high value of 0.835 (83.5%) compared to low trabecular bone volume fraction of extant specimens in the same facet, which recorded 0.274 (27,4%) of bone volume fraction. All fossil proximal tibiae recorded high bone volume fraction, ranging from 56.4% to 83.5% as compared to 27.4%-39.7% of extant specimens. As a general rule, high trabecular bone volume fraction reflects repeated gait forces of terrestrial quadrupedal locomotion (Fajardo and Muller, 2001; Schmidt, 2010; Fleagle, 2013; Ryan *et al*; 2018; Saers *et al*, 2019 DeMars *et al*, 2021) and the trabecular bone consists of dense and well connected trabecular bone. However, due to highly sedimented nature of specimens that necessitated

segmentation, the high trabecular bone volume fraction might be attributed to discrepancy during manual tracing of bone struts.

Fossil humeral heads show extremely high fossils fabric anisotropy of 0.592 and 0.454 in contrast to extremely low fabric anisotropy of 0.179 of extant specimens. Just like trabecular bone fabric anisotropy of this joint, trabecular bone volume fraction of these joints exhibits extremely high bone volume of fossil specimens to that of extant specimens. This is in contrast with the findings of Chirchir (2019), who found that upper limbs of cercopithecoids have consistently low trabecular bone volume that range from 32.0% to 41.5% (Chirchir, 2019). Fossil specimens in this study consist of bone volume fraction? that ranges 63.1%-65.8% compared to 29.4% in extant specimens. The high fabric anisotropy and trabecular bone volume fraction of fossil specimens might be due to an efficient locomotor gait forces in a specific direction during locomotion or extent of compression and tension forces on proximal humeral heads by the weight of an individual animal (Takechi., 1977; Fajardo and Muller 2001; Fajardo *et al*., 2007; Barak *et al*.,2011; Ryan *et al*., 2018). However, just like fossil proximal tibiae in this study, the high amount of sediment deposits and segmentation of trabecular bone struts might have influenced the actual trabecular bone volume fraction results.

5.3 Reconstruction of palaeoenvironment and palaeohabitats of the Cradle of Humankind World Heritage site.

Reconstructing palaeohabitats and palaeoenvironment of the Cradle of Humankind World Heritage site demonstrated to be a complex mission (Scott and Bonnefille 1986; Bamford *et al.,* 2010). This is attributed to hominin sites situated in caves occurring in calcareous outcrops of the Malmani Subgroup of the late Archaean (Button, 1973), consequently finding plant remains in calcareous rocks in a bid to reconstruct the palaeoenvironment is a challenge (Bamford *et al*., 2010). However, Bamford *et al* (2010) in the study that describe botanical remains from a coprolite recovered from Malapa hominin site discovered remains of *Podocarpus* (*Afrocarpus*) taxon, which is a conifer and dated approximately 2 Ma. This date is consistent with a recent study of Granger *et al* (2015), which suggested that Sterkfontein Member 5 is dated to 2.0-1.7 Ma, with Kuman *et al* (2021) dating Swartkrans Member 1 to 2.22 Ma (Kuman *et al*, 2021). Delson (1988) compared Taung Limewok site with East African sites and suggested its age to 2.3 Ma (Delson, 1988). Dupont (2006) dated pollen of this plant from Namibian marine deposits

to 2 Ma (Dupont, 2006). Surviving *Podocarpus* species are found in high rainfall areas, comparable to the one currently experienced in the Magaliesburg area and this suggests Afromontane Forest during the Pleistocene epoch in the Cradle of Humankind World Heritage sites, with cool and wet climatic conditions (Tappen, 1968; Mackee, 1991; Bamford, 1999; Bamford *et al*., 2010).

Hominin fossil sites in the Cradle of Humankind World Heritage site produced a substantial amount of *Parapapio* species, particularly *Parapapio jonesi (*Jones, 1937; Broom, 1940; Freedman, 1957, 1960, 1961; Brain, 1981; de Ruiter, 2003; Fourie *et al*, 2008; Mokokwe, 2016). The species is believed to signify a primitive form of papionins (Mackee, 1991). Features of *Parapapio* species suggest adaption to variable palaeoenvironment similar to savanna and open woodland (Eisernhart, 1974). Furthermore, the presence of *Cercopithecoides williamsi* in Sterkfontein Members 2, 4 and 5 (Broom, 1940; Brain, 1960, 198; Freedman, 1957; Tappen; 1968; Wilkinson 1983; Mackee, 1991, 1993; de Ruiter, 2003; Fourie *et al*, 2008) suggested more open savanna type of environments, consistent with studies like Elton (2001), that concluded that contrasts to its extant form, *Cercopithecoids williamsi* was more of terrestrial than arboreal primate. This colobine (leaf consuming) monkey is widely known to prefer moist habitat as shown by its extant form, strongly suggesting an open woodland savanna form of environment with widespread grassland and tall trees (Vrba, 1975, Mackee, 1991, Reed, 1997) suitable for arboreal and terrestrial quadrupedalism. Habitat transformation from thicket woodland to open woodland is recorded in Swartkrans Member 1 by the small number of available arboreal specimens Reed, 1997; Elton, 2001), consequently reducing woodland arboreal cercopithecoids (Elton, 2001).

Three dimensional (3D) results show a relatively high trabecular bone fabric anisotropy in femoral heads, calcanei and humeral heads with contrasting low fabric anisotropy of proximal tibial trabecular bone. High trabecular bone fabric anisotropy, coupled with thick as well as denser and well connected trabecular bone is closely related to loading in a particular direction (Takechi,1977; Fajardo and Muller 2001; Fajardo *et al*., 2007, Ryan *et al*., 2018; Saers *et al.*, 2018), an indication of arboreal locomotion in which the monkey's feet does not entirely rest on the substrate resulting in the load not evenly distributed on all four limbs but concentrated on hindlimbs. However, high trabecular bone volume fraction with relatively thin trabeculae is

consistent with the idea that environment was an open woodland savanna, with cercopithecoids occasionally engaging in terrestrial quadrupedalism, resulting in body loads consistently distributed on fore and hindlimbs. The load is consistently distributed in terrestrial quadrupedal locomotion because the foot entirely contact substate unlike a specific potion of a foot contacting substrate in arboreal locomotion, resulting in non-uniform loading. Saers *et al*, 2018

5.4 Inferences and implications for human evolution

Trabecular bone inner structural organisation were analysed utilizing imaging technique that includes utilisation of micro-focus X-ray computer tomography (CT) scans, CT Pro 3D, VGStudio, Avizo and ImageJ software. Postcranial remains of Plio-Pleistocene cercopithecoids record locomotor signals that indicate a more arboreal environment with occasional terrestrial locomotion than their comparable extant specimens.

However, environmental inferences and its implications on human evolution in the African context has been subjected to inconsistent findings (Reed, 2007), with early studies like Dart (1925) suggesting an open savanna type of palaeoenvironment while recent studies (e.g. Vrba, 1985, 1988; Demenocal, 1995; Pavia, 2020) are consistent with this conclusion and furthermore suggested an African Plio-Pleistocene palaeoenvironment that experienced environmental transformation from mesic and closed woodland to a more open habitat with arid climatic conditions (Vrba,1985, 1988; Demenocal, 1995; Pavia, 2020) and results of this study appear to acquiesce with suggested palaeoenvironment. This transitional palaeoenvironment from trees with cool climatic conditions to a more open grass land savanna type environment with dry climatic conditions, which are believed to have contributed significantly to the extinction of early humans and the emergence of the successful *Homo (*Vrba, 1985, 1988; Demenocal, 1995; Pavia, 2020).

5.5 conclusion

The primary goal of the study is to reconstruct the Plio-Pleistocene palaeoenvironment of southern African hominin. In trying to address the hypothesis, this study quantitatively analysed the structural arrangement of the trabecular bone of cercopithecoid locomotor key joints in search of functional signal that can be helpful in reconstruction of locomotor repertoire and palaeohabitats of fossil cercopithecoids as well as the palaeoenvironment shared with hominins.

2D and 3D results point to a more arboreal quadrupedal locomotion with occasional terrestrial quadrupedal locomotion. This is because fossil specimens have high trabecular bone fabric anisotropy with high trabecular bone volume fraction, thick trabecular bone and less spaced trabecular bone. These locomotor signals are useful in inferring locomotor behaviour because high fabric anisotropy is associated with loading in certain direction (arboreal locomotion). Furthermore, thick and less spaced trabecular bone are also associated with arboreal locomotion while high trabecular bone volume fraction with relatively thin trabeculae is associated with terrestrial locomotion.

The degree of sedimentation within trabecular bone of specimens included in this study are potential constraints to achieving best desired results. Forty (40) fossil specimens were scanned but only eighteen (18) volumes of interest derive from fifteen (15) specimens were analysed. This limitation is attributed to taphonomic issues and were highlighted by Ryan and Ketcham (2002a,b), that they affected bones post individual's death as well as diagenesis processes (Ryan and Ketcham., 2002a,b). Some specimens are fully sedimented while some are partially sedimented. Sedimentation of specimens cause isolation of some trabecular bone and affects trabecular thickness, spacing and compactness. The presence of high density minerals within sediments can also lead to overlapping trabecular bone density or volume fraction (Ryan and Ketcham, 2002a,b). As such, this present potential of negatively impacting results.

Presence of weathered and eroded external surfaces of cortical bone of fossil specimens, especially femoral heads presented a challenge. This is because femoral necks and femoral heads contact region of most fossil specimens were removed and the region was important particularly during landmarking stage. Therefore, locating and placing landmarks became a complicated exercise to conduct since the contact was removed and sometimes it was inferred for landmarking necessary for homologous volume of interest.

Some earlier studies on trabecular bone strands indicated that variations of trabecular bone structural arrangement can exist within the same specimen (e.g. Ryan and Ketcham, 2002b; Ryan and Krovitz, 2006; Fajardo *et al.*, 2007) and variation might be attributed to various techniques applied in a particular study. For instance, manual segmentation of some specimens like humeral heads and proximal tibiae in this study might have contributed to high trabecular bone fabric anisotropy as well as high bone volume fraction. This is because the size or shape of may have

been misrepresented when tracing them from the sediment. Therefore, it is desirable to conduct another study that employing automated segmentation techniques (e.g. Veneziano *et al*, 2021).

There is need to carry out study that uses automatic segmentation (e.g. Veneziano *et al*, 2021) to segregate trabecular bone from the rest of sediments because manual segmentation of some specimens (humeral heads and proximal tibiae) in this study might have negatively contributed some inaccuracies in our parameter's calculations. This is because size or shape may have been misrepresented when tracing trabecular bone from the rest of sediment. Therefore, it is desirable to conduct another study that employing automated segmentation techniques to curb against misrepresenting trabecular bone shapes and sizes. Furthermore, there is need to increase locomotor set specimen to include hind and forelimbs phalanges as well as vertebrae column (cervical, thoracic, lumbar, sacrum, and Caudal).

The findings of this study will augment the existing knowledge of hominins evolution. This is because this study present the Plio-Pleistocene palaeoenvironment, a period in which warm and aridic climatic condition set in. This is often regarded as the main cause for ,extinction of pre-existing hominin species but radiation of successful *Homo sapiens*.

References

Aiello L. and Dean C., 1990. *An introduction to human evolutionary anatomy*. Academic Press.

Bamford M., 1999. Pliocene fossil woods from an early hominid cave deposit, Sterkfontein, South Africa. *South African Journal of Science*, **95**: 231-237.

Bamford M. K, Neumann F. H, Pereira I. M, Scott I, Dirks P. H. G. M and Berger I. R., 2010. Botanical remains from a coprolite from the Pleistocene hominin site of Malapa, Sterkfontein Valley, South Africa. *Palaeontologia Africana*, **45**: 23-28.

Barak M. M, Weiner S and Shahar R., 2008. Importance of the integrity of trabecular bone to the relationship between load and deformation of rat femora: an optical metrology study. *Journal of Materials Chemistry*, **18**: 3855-3864.

Barak M. M, Lieberman D. E and Hublin J. J., 2011. A Wolff in sheep's clothing: trabecular bone adaptation in response to changes in joint loading orientation. *Bone*, **49**: 1141-1151.

Berger L.R, Tobias P.V., 1996. A chimpanzee-like tibia from Sterkfontein, South Africa and its implications for the interpretation of bipedalism in Australopithecus africanus. *Journal of Human Evolution*, **30**: 343–348

Berger L.R., Lacruz R and De Ruiter D.J., 2002. Brief communication: Revised age estimates of *Australopithecus*-bearing deposits at Sterkfontein, South Africa. *American Journal of Physical Anthropology*, **119**: 192-197.

Begun D. R. and Kivell T. L., 2011. Knuckle-walking in Sivapithecus? The combined effects of homology and homoplasy with possible implications for pongine dispersals. *Journal of Human Evolution*, **60**: 158–170.

Bobe R., Behrensmeyer A. K and Chapman R. E., 2002. Faunal change, environmental variability and late Pliocene hominin evolution. *Journal of Human Evolution***, 42**: 475-497.

Brain C. K., 1981. *The hunters or the hunted?: an introduction to African cave taphonomy*. University of Chicago Press.

Brain C.K., 1993b. Structure and stratigraphy of the Swartkrans Cave in the light of the new excavations. In: Brain C.K (edition), Swartkrans. Swartkrans; a cave's chronicle of early man. *Transvaal Museum, Pretoria*, pp, 23-33.

Brock A, McFadden P. L and Partridge T. C., 1977. Preliminary palaeomagnetic results from Makapansgat and Swartkrans. *Nature,* **266**: 249-250.

Broom R., 1938. The Pleistocene anthropoid apes of South Africa. *Nature,* **142:** 377-379.

Broom R., 1940. The South African Pleistocene cercopithecoid apes. *Annals of the Transvaal Museum,* **20**: 89-100.

Broom R., 1946. The occurrence and general structure of the South African ape-men. Part 1. The South African fossil Ape-Men, the Australopithecinae. *Transvaal Museum Memoir*, **2**: 11-153.

Broom R., 1947. Discovery of a new skull of the South African ape-man, Plesianthropus. *Nature,* **159:** 672-672.

Button A.,1973. The stratigraphic history of the Malmani Dolomite in the eastern and north-eastern Transvaal. *South African Journal of Geology*, **76**: 229-247.

Cadman A and Rayner R. J., 1989. Climatic change and the appearance of Australopithecus africanus in the Makapansgat sediments. *Journal of Human Evolution,* **18**: 107-113.

Cardiff P., 2012. *Development of the finite volume method for hip joint stress analysis* (Doctoral dissertation, University College Dublin).

Chirchir H., 2019. Trabecular bone fraction variation in modern humans, fossil hominins and other primates. *The Anatomical Record*, **30**: 288-305.

Ciochon R. L., 1993. *Evolution of the Cercopithecoid Forelimb. phylogenetic and functional implications from morphological analyses.* Berkeley, University of California Press.

Clarke R. J., 1994. On some new interpretations of Sterkfontein stratigraphy. *South African Journal of Science*, **90**: 211-214.

Cooke H. B. S., 1938. The Sterkfontein bone breccia: a geological note. *South African Journal of Science*, **35**: *204-208.*

Cooke H. B. S., 1970. Notes from members. Canada: Dalhousie University, Halifax. *Society of Vertebrate Palaeontology Bulletin*, **90**: 2.

Cooke H. B. S., 1991. *Dinofelis barlowi* (mammalia, carnivora, felidae) cranial material from bolt's farm, collected by the University of California African Expedition. *Palaeontologica Africana*, **28**: 9-21.

Cowin S. C. 1997. Remarks on the paper entitled 'Fabric and elastic principal directions of cancellous bone are closely related'. *Journal of Biomechanics*, **30**: 1191–1192.

Cowin S. C., 2001. *Bone mechanics handbook*. CRC press.

Currey J., 1968. The adaptation of bones to stress. *Journal of Theoretical Biology*, **20:** 91–106.

Dart R. A., 1925. Australopithecus africanus: The man ape of South Africa. *Nature*, **115**: 195-199.

Dart R. A., 1940. The status of *Australopithecus Africanus*. *American Journal of Physical Anthropology*, **26**: 167-186.

Delson E., 1988. *Chronology of South African australopithecine site units*. In "*Evolutionary History of the Robust Australopithecines*" (F.G Grange, ED), pp. 317-324. *De Gruyter, New York.*

DeMars L. J, Stephens N. B, Saers J. P, Gordon A, Stock J. T and Ryan T. M., 2021. Using point clouds to investigate the relationship between trabecular bone phenotype and behavior: An example utilizing the human calcaneus. *American Journal of Human Biology*, **33**:234 268.

Demenocal P. B., 1995. Plio-Pleistocene African climate. *Science*, **270**:53-59.

Demenocal P. B., 2004. African climate change and faunal evolution during the Pliocene–Pleistocene. *Earth and Planetary Science Letters*, **220**:3-24.

de Ruiter D. J., 2003. Revised faunal lists for Members 1-3 of Swartkrans, South Africa. *Annals of the Transvaal Museum***, 40**: 29-41.

Diard F, Hauger O, Moinard M, Brunot S, Marcet B., 2007. Pseudo-cysts, lipomas, infarcts and simple cysts of the calcaneus: are there different or related lesions? *JBR-BTR*, **90**: 315–324.

Diederichs G, Link T. M, Kentenich M, Schwieger K, Huber M. B, Burghardt A. J, Majumdar S, Rogalla P and Issever A. S., 2009. Assessment of trabecular bone structure of the calcaneus using multi-detector CT: correlation with micro CT and biomechanical testing. *Bone,* **44**: 976-983.

Disotell T. R, Honeycutt R. L and Ruvolo M., 1992. Mitochondrial DNA phylogeny of the Old-World monkey tribe Papionini. *Molecular biology and evolution*, **9**:1-13.

Disotell T. R., 1996. The phylogeny of Old-World monkeys. Evolutionary Anthropology: *Issues, News, and Reviews,* **5**: 18-24.

Doube M, Kłosowski M. M, Arganda-Carreras I, Cordelières F. P, Dougherty R. P, Jackson J. S, Schmid B, Hutchinson J. R and Shefelbine S. J., 2010. BoneJ: free and extensible bone image analysis in ImageJ. *Bone,* **47**: 1076-1079.

Dupont L. M., 2006. Late Pliocene vegetation and climate in Namibia (southern Africa) derived from palynology of ODP Site 1082. *Geochemistry, Geophysics, Geosystems*, **7**.

Edwards T. R, Pickering R, Mallett T. L and Herries A. I. R., 2020. Reconstructing the depositional history and age of fossil-bearing palaeokarst: A multidisciplinary example from the terminal Pliocene Aves Cave Complex, Bolt's farm, South Africa. *Results in Geophysical Sciences,***1–4**: 100005

Eisenhardt W. L., 1974. *The fossil cercopithecoids of Makapansgat and Sterkfontein (*Doctoral dissertation).

Elton S., 2001. Locomotor and habitat classifications of *cercopithecoid* postcranial material from Sterkfontein Member 4, Bolt's Farm and Swartkrans Members 1 and 2, South Africa. *Palaeontologia Africana,* **37**:15-126.

Elton S., 2006. Forty years on and still going strong: the use of hominin-cercopithecid comparisons in palaeoanthropology. *Journal of the Royal Anthropological Institute*, **12:** 19-38.

Elton S., 2007. Environmental Correlates of the Cercopithecoid Radiations. *Folia Primatologica*, **78**: 344–364.

Fajardo R. J, Muller R., 2001. Three-dimensional analysis of nonhuman primate trabecular architecture using micro-computed tomography. *Journal of Physical Anthropology*, **115**: 327–336.

Fajardo R.. J., Muller R., Ketcham, R. .A., Colbert M., 2007. Nonhuman anthropoid primate femoral neck trabecular architecture and its relationship to locomotor mode. *Anatomical Record*, **290**: 422-436.

Fleagle J. G., 2013. *Primate adaptation and evolution*. Academic press.

Fourie N. H, Lee-Thorp J. A and Ackermann R. R., 2008. Biogeochemical and Craniometric Investigation of Dietary Ecology, Niche Separation, and Taxonomy of Plio-Pleistocene Cercopithecoids from the Makapansgat Lime works. *American Journal of Physical Anthropology* **135**: 121–135.

Freedman L., 1957. The fossil cercopithecoidea of South Africa. *Annals of the Transvaal Museum*, **23**: 121-262.

Freedman L., 1960. Some new fossil Cercopithecoid specimens from Makapansgat, South Africa. *Palaeontologia Africana*, **7**: 7-45.

Freedman L., 1961. New Cercopithecoid fossils, including a new species, from Taung, Cape Province, South Africa. *Annual South African Museum*, **46**: 1-14.

Freedman L., 1970. A new check-list of fossil Cercopithecoidea of South Africa. *Palaeontologia Africana*, **13**: 109-110.

Freedman L., 1976. South African Fossil Cercopithecoidea: A Re-assessment Including a Description of New Material from Makapansgat, Sterkfontein and Taung. *Journal of Human Evolution*, **5:** 297-315.

Gear J. H. S., 1926. Preliminary account of the baboon remains from Taungs. *Southern African Journal of Science*, **23**: 731-747.

Gibson L. J., 1985. The mechanical behaviour of cancellous bone. *Journal of biomechanics*, **18**: 317-328.

Gibbon R. J, Pickering T. R, Sutton M. B, Heaton J. L, Kuman K, Clarke J. R, Brain C. K and Granger D. E., 2014. Cosmogenic nuclide burial dating of hominin-bearing Pleistocene cave deposits at Swartkrans, South Africa. *Quaternary Geochronology*, **24**: 10–15.

Gilbert C. C, Takahashi Q, M and Delson E., 2016. Cercopithecoid humeri from Taung support the distinction of major papionin clades in the South African fossil record. *Journal of Human Evolution*, **90:** 88-104.

Gosman J. H and Ketcham R. A, 2009. Patterns in ontogeny of human trabecular bone from SunWatch Village in Pre-historic Ohio Valley: general features of microarchitectural change. *American Journal of Physical Anthropology*, **138:** 318-332.

Granger D. E, Gibbon R. J, Kuman K, Clarke R. J, Bruxelles L and Caffee M.W., 2015. New cosmogenic burial ages for Sterkfontein member 2 Australopithecus and member 5 Oldowan. *Nature*, **522**: 85-88.

Granger D. E, Stratford D, Bruxelles L, Gibbon R. J, Clarke, R. J and Kuman K., 2022. Cosmogenic nuclide dating of Australopithecus at Sterkfontein, South Africa. *Proceedings of the National Academy of Sciences*, **119:** (27), p.e2123516119

Haughton S. H., 1925. Note on the occurrence of a species of baboon in limestone deposits near Taungs. *Transactions of the Royal Society of South Africa*, **12**: 68.

Heaton J. L., 2006. Taxonomy of the Sterkfontein fossil Cercopithecinae: the Papionini of members 2 and 4 (Gauteng, South Africa) (Doctoral dissertation, Indiana University).

Herries A. I. R., 2003. Magnetostratigraphic seriation of South African hominin palaeo caves (Doctoral dissertation, *University of Liverpool*).

Hodgskinson R, Currey J.D. 1990a. Effects of structural variation on Young's modulus of non-human cancellous bone. *Journal of Engineering in Medicine*, **204**: 43–52.

Hodgskinson R, Currey JD. 1990b. The effect of variation in structure on the Young's modulus of cancellous bone: a comparison of human and non-human material. *Journal of Engineering in Medicine*, **204:** 115–121.

Hople K. G and Lovejoy C. O. 1971. The distal femoral anatomy of Australopithecus. *American Journal of Physical Anthropology*, **35**: 75–84.

Hopley P. J, Herries A. I. R, Baker S. E, Kuhn B. F and Menter C. G., 2013. Beyond the South African cave paradigm–*Australopithecus africanus* from Plio-Pleistocene paleosol deposits at Taung. *American Journal of Physical Anthropology*, **15**: 316–324.

Huiskes R., 2000. If bone is the answer, then what is the question? *Journal of Anatomy 2000*, **197**: 145–156.

Ito J, Shiraishi N, Umino M, Kimura T and Akita H., 2000. Morphological evaluation of the Baboon hind limb muscles based on relative weight. Okajimas Folia Anatomica Japonica., **77:** 161-166.

Jablonski N. G., 2002. *Fossil Old World monkeys: the late Neogene radiation.* In The *Primate Fossil Record (Hartwig WC, ed.),* pp 255–299. Cambridge, Cambridge University Press.

Jablonski N. G and Frost, S., 2010. *Cercopithecoidea. In L. Werdelin & W. J. Sanders (Eds.), Cenozoic Mammals of Africa* (pp. 393-428). Berkeley, CA: University of California.

Jones T.R., 1937. A new fossil from Sterkfontein, Krugersdorp, Transvaal. South African Journal of Science, **33**: 709-728.

Ketcham R. A and Ryan TM. 2004. Quantification of anisotropy in trabecular bone. *Journal of Microscopy*, **213**: 158–171.

Kivell T. 2016. A review of trabecular bone functional adaptation: What have we learned from trabecular analyses in extant hominoids and what can we apply to fossils? *Journal of Anatomy*, **228**:569–594.

Kuganenthira N, Zhao D and Anandarajah A., 1996. Measurement of fabric anisotropy in triaxial shearing. *Géotechnique*, **46**: 657-670.

Kuhn B. F, Herries A. I. R, Price G. J, Baker S. E, Hopley P. J, Menter C. G and Caruana M. V., 2016. Renewed investigations at Taung; 90 years after the discovery of *Australopithecus africanus. Palaeontologia Africana,* **51**: 10–26.

Kuman K and Clarke R. J., 2000. Stratigraphy, artefact industries and hominid associations for Sterkfontein, Member 5. *Journal of Human Evolution*, **38**: 827-847.

Kuman K, Granger D. E, Gibbon R. J, Pickering T. R, Caruana M. V, Bruxelles L, Clarke, R. J, Heaton J. L, Stratford D and Brain C. K., 2021. A new absolute date from Swartkrans Cave for the oldest occurrences of *Paranthropus robustus* and Oldowan stone tools in South Africa. *Journal of Human Evolution,* **156**: 03000.

Latimer B and Lovejoy C. O., 1989. The calcaneus of *Australopithecus afarensis* and its implications for the evolution of bipedality. *American Journal of Physical Anthropology*,**78**: 369–386.

Latham A. G McKee J. K and Tobias P. V., 2007. Bone breccias, bone dumps, and sedimentary sequences of the western Lime works, Makapansgat, South Africa. *Journal of human evolution,* **52**: 388-400.

Lin J. C, Amling M, Newitt D. C, Selby K, Srivastav S. K, Delling G, Genant H. K, Majumdar S0, 2998. Heterogeneity of trabecular bone structure in the calcaneus using magnetic resonance imaging. *Osteoporosis International* , **8**: 16-24.

Lovejoy C. O, Heiple K. G and Burstein A. H., 1973. The gait of Australopithecus. *American Journal of Physical Anthropology*, **38**: 757–779.

Lovejoy C. O, McCollum M. A, Reno P. L and Rosenman B. A., 2003. Developmental biology and human evolution. *Annual Review of Anthropology,* **32**: 85–109.

Macchiarelli R, Bondioli L, Galichon V, Tobias P. V., 1999. Hip bone trabecular architecture shows uniquely distinctive locomotor behaviour in South African australopithecines. *Journal of Human Evolution*, **36**: 211-232.

Maguire J. M., 1985. Recent geological, stratigraphical and paleontological studies at Makapansgat limeworks. Ancestors: *The Hard Evidence,* 151-164.

Marker M. E., 1975. On Taung Revisited. *Current Anthropology,* **16**: 295-296.

Maslin M. A, Brierley C.M, Milner A.M, Shultz S, Trauth M.H and Wilson K. E. 2014. East African climate pulses and early human evolution. *Journal of Human evolution,* **101**: 1-17.

McKee J.K., 1991. Palaeo-ecology of the Sterkfontein hominids: A review and synthesis. *Palaeontologia Africana,* **28**: 4l-51.

McKee J. K., 1993. Faunal dating of the Taung hominid fossil deposit. *Journal of Human Evolution,* **25**: 365-375.

McKee J. K., 2010. Taphonomic Processes of Bone Distribution and Deposition in the Tufa Caves of Taung, South Africa. *Journal of Taphonomy,* **8**: 203-213.

McKee J. K and Kuykendall K. L., 2016. The Dart deposits of the Buxton Limeworks, Taung, South Africa, and the context of the Taung Australopithecus fossil. *Journal of Vertebrate Paleontology*. DOI:10.1080/02724634.2015.1054937.

Mokokwe D. W., 2016. Taxonomy, taphonomy and spatial distribution of the cercopithecoid postcranial fossils from Sterkfontein caves (Doctoral dissertation).

Morbeck M. E., 1977. Positional behavior, selective use of habitat substrate and associated non-positional behavior in free-ranging Colobus guereza (Rüppel, 1835). *Primates,* **18**: 35-58.

Odgaard A, Kabel J, van Rietbergen B, Dalstra M, Huiskes R.., 1997. Fabric and elastic principal directions of cancellous bone are closely related. *Journal of Biomechanics,* **30**: 487-495.
Oftadeh R, Perez-Viloria1 M, Villa-Camacho J. C, Vaziri A and Nazarian A. 2015. *Journal of Biomechanical Engineering,* **137 /** 010802-15

Partridge T. C., 1973. Geomorphological dating of cave opening at Makapansgat, Sterkfontein, Swartkrans and Taung. *Nature*, **246**: 75-79.

Partridge, T. C, 1978. Re-appraisal of Lithostratigraphy of Sterkfontein hominid site. *Nature,* **275**: 282-287.

Partridge T. C., 1979. Re-appraisal of lithostratigraphy of Makapansgat Limeworks hominid site. *Nature*, **279:** 484-488.

Partridge T. C, Latham A. G. and Heslop D., 2000. Appendix on magnetostratigraphy of Makapansgat, Sterkfontein, Taung and Swartkrans. *The Cenozoic of Southern Africa. Oxford Monographs on Geology and Geophysics*, **40**: 126-129.

Pavia M., 2020. Palaeoenvironmental reconstruction of the Cradle of Humankind during the Plio-Pleistocene transition, inferred from the analysis of fossil birds from Member 2 of the hominin-bearing site of Kromdraai (Gauteng, South Africa). *Quaternary Science Reviews,* **248**: 106532.

Peabody F. E., 1954. Travertines and cave deposits of the Kaap escarpment of South Africa, and the type locality of *Australopithecus Africanus* Dart. *Bulletin of the Geological Society of America,* **65**: 671-706.

Pickering R and Kramers J. D., 2010. Re-appraisal of the stratigraphy and determination of new U-Pb dates for the Sterkfontein hominin site, South Africa. *Journal of Human Evolution*, **59**: 70-86.

Pickering T. R, Heaton J. L, Clarke J. R, Sutton B. M, Brain C. K and Kuman K., 2012. New hominid fossils from Member 1 of the Swartkrans formation, South Africa. *Journal of Human Evolution*, **62**: 618-628.

Rayner R. J, Moon B. P and Masters J. C., 1993. The Makapansgat australopithecine environment. *Journal of Human Evolution,* **24**: 219-231.

Reed K. E., 1997. Early hominid evolution and ecological change through the African Plio-Pleistocene. *Journal of Human Evolution***, 32**: 289–322.

Rose D. M., 1973. Quadrupedalism in Primates. *Primates*, **14**: 337-357.

Rose M. 1988. Another look at the anthropoid elbow. *Journal of Human Evolution,* **17**: 193–224.

Ruff C, Holt B, Trinkaus E., 2006. Who's afraid of the big bad Wolff?: "Wolff's law" and bone functional adaptation. *American Journal of Physical Anthropology*, **129**: 484–498.

Ryan T. M and Ketcham R. A., 2002. The three-dimensional structure of trabecular bone in the femoral head of strepsirrhine primates. *Journal of human evolution*, **43**: 1-26.

Ryan TM and Van Rietbergen B. 2005. Mechanical significance of femoral head trabecular bone structure in Loris and Galago evaluated using micromechanical finite element models. *Journal of Physical Anthropology*, **126**: 82–96.

Ryan T. M and Walker A, 2010. Trabecular Bone Structure in the Humeral and Femoral Heads of Anthropoid Primates. *The anatomical record*, **293**: 719–729.

Ryan, T.M. and Shaw, C.N., 2012. Unique suites of trabecular bone features characterize locomotor behavior in human and non-human anthropoid primates. *PloS one*, **7:** 41037.

Ryan M. T, Carlson J. K, Adam D. G, Jablonski N, Shaw N. C and Stock T. J., 2018: Human-like hip joint loading in *Australopithecus africanus* and *Paranthropus robustus*. *Journal of Human Evolution*, **121**: 1-13.

Saers, J. P, Ryan T. M and Stock J. T., 2019. Trabecular bone functional adaptation and sexual dimorphism in the human foot. *American journal of physical anthropology*, **168**: 154-169.

Schmidt M., 2011. Locomotion and postural behaviour. *Advances in Science and Research*, **5**:23-39.

Scott L and Bonnefille R. 1986. A search for pollen from the hominid deposits of Kromdraai, Sterkfontein and Swartkrans: some problems and preliminary results. *South African Journal of Science*, **82**: 380–382.

Sissons H. A and O'Connor P., Quantitative histology of osteocyte lacunae in normal human cortical bone. *Calcified Tissue Research*., **22**: 530, 1977.

Singh I., 1978. The architecture of cancellous bone. *Journal of Anatomy*, **127**: 305-310.

Sloggett G. C., 2016. An Analysis of the Plio-Pleistocene Paleoecology of Makapansgat, Limpopo Province, South Africa. Vis-à-vis: *Explorations in Anthropology*, **13:** 54-77.

Stanley S. M., 1992. An ecological theory for the origin of *Hom*o. *Paleobiology*, **18**: 237-257.

Stratford J. D and Caruana V. M., 2017. The Long-Term Conservation of the Australopithecus-bearing Member 4 Excavation Walls at the Sterkfontein Caves, South Africa. *Studies in Conservation*, **63**: 201-214.

Sukhdeo S, Parsons J, Niu X. M and Ryan T. M., 2020. Trabecular bone structure in the distal femur of humans, apes, and baboons. *The Anatomical Record*, **303:** 129-149.

Susan O. M., 2018. Cortical or Trabecular Bone: What's the Difference? *American Journal of Nephrology*, **47**: 373–375.

Sutton B. M, Pickering R. T, Pickering R, Brain C. K, Clarke R. J, Heaton J. L and Kuman K., 2009. Newly discovered fossil- and artefact-bearing deposits, uranium-series ages, and Plio-Pleistocene hominids at Swartkrans Cave, South Africa. *Journal of Human Evolution*, **57:** 688–696.

Takechi H., 1977. Trabecular architecture of the knee joint. *Acta Orthopaedica Scandinavica*, **48**: 673-681.

Tobias P. V, Vogel J. C, Oschadleues D, Partridge T. C and McKee J. K., 1993. New Isotopic Sedimentological Measurements of the Thabaseek Deposits (South Africa) and Dating of Taung Hominid. *Quaternary research*, **40**: 360-367.

Tosi A. J, Detwiler K. M and Disotell, T. R. 2005. X-chromosomal window into the evolutionary history of the guenons (Primates: Cercopithecini). *Molecular Phylogenetics and Evolution*, **36**:58-66.

Veneziano A, Cazenave M, Alfieri F, Panetta D and Marchi D., 2021. Novel strategies for the characterization of cancellous bone morphology: Virtual isolation and analysis. *American Journal of Physical Anthropology*, **175**: 920-930.

Viola T. B., 2002. Locomotion dependent variation in the proximal femoral trabecular pattern in primates M.Sc. Thesis, University of Vienna, Vienna, Austria.

Vrba E.S., 1975. Some evidence of chronology and paleoecology of Sterkfontein, Swartkrans and Kromdraai from the fossil Bovidae. *Nature*, **254**: 301-304.

Vrba E. S., 1985. Early hominids in southern Africa: updated observations on chronological and ecological background. Hominid Evolution: *Past, present and future*, **195**: 200.

Vrba E. S., 1988. *Late Pliocene climatic events and hominid evolution. In (F. E. Grine, Ed.) Evolutionary history of the "robust" australopithecines*, pp405-426. New York: Aldine de Gruyter.

Ward F.O., 1876. *Outlines of human osteology*. H. Renshaw.

Ward C. V., 2002. Interpreting the posture and locomotion of *Australopithecus afarensis*: where do we stand? *American Journal of Physical Anthropology*, **119**: 185–215.

Warwick R and Williams P. L., 1973. *Gray's Anatomy, 35th ed*., p. 216. Edinburgh: Longman.

Wilkinson M.J., 1983. Geomorphic perspectives on the Sterkfontein australopithecine breccias. *Journal of Archaeological Science*, **10**:515-529.

Wolff J., 1892. Das Gesetz der Transformation der Knochen. Berlin A. Hirchwild. *The Law of Bone Remodelling*.

Wolff J., 1986. *Concept of the law of bone remodelling*. *In The law of bone remodelling* (pp. 1-1). Springer, Berlin, Heidelberg.

Wood B and Boyle E. K. Hominin Taxic Diversity: Fact or Fantasy.2016. *Yearbook of Physical Anthropology***, 159**:537–578.

https://industry.nikon.com/en-us/products/x-ray-ct

Annexture

Table A1: Extant femoral heads structural parameters.

Specimens	**DA**	**BV (mm^3)**	**TV (mm^3)**	**BV/TV (%)**	**Tb.Th mean (mm)**	**Tb.Th sd (mm)**	**Tb.Sp mean (mm)**	**Tb.Sp sd (mm)**
Za 103 Left	0.425	3.893	11.600	0.336	0.200	0.067	0.467	0.156
Za 103 Right	0.458	3.685	11.548	0.319	0.186	0.056	0.475	0.151
Za 118 Left	0.396	63.055	110.920	0.568	0.492	0.166	0.579	0.204
Za 118 Right	0.250	64.393	111.880	0.576	0.516	0.2	0.578	0.208
Za 127 Right	0.332	26.436	49.406	0.535	0.332	0.087	0.430	0.154
Za 127 Left	0.367	34.962	60.024	0.582	0.424	0.196	0.419	0.165
Za 128 Left	0.403	6.693	11.827	0.566	0.308	0.095	0.415	0.136
Za 128 Right	0.372	8.254	14.147	0.583	0.325	0.1	0.416	0.141
Za 168 Left	0.486	44.843	65.812	0.681	0.538	0.293	0.352	0.138
Za 168 Right	0.309	51.100	83.941	0.609	0.423	0.152	0.408	0.160
Za 182 Left	0.398	14.477	43.854	0.330	0.308	0.103	0.753	0.264
Za 182 Right	0.473	59.993	105.556	0.568	0.463	0.156	0.596	0.240
Za 787 Right	0.422	4.293	8.389	0.512	0.239	0.061	0.329	0.125
Za 787 Left	0.416	4.522	8.666	0.522	0.241	0.06	0.341	0.119
Za 791 Left	0.545	5.243	9.287	0.565	0.273	0.069	0.318	0.106
Za 791 Right	0.454	4.577	8.359	0.548	0.280	0.069	0.352	0.126
Za 792 Left	0.462	4.782	8.530	0.561	0.283	0.081	0.321	0.105

Za 792 Right	0.453	4.857	9.094	0.534	0.250	0.076	0.248	0.141
Za 793 Left	0.495	5.015	9.713	0.516	0.219	0.045	0.301	0.104
Za 793 Right	0.517	4.107	8.709	0.472	0.198	0.041	0.318	0.105
za 891 Left	0.335	25.258	47.773	0.529	0.356	0.116	0.411	0.154
Za 891 Right	0.373	25.000	45.385	0.551	0.365	0.122	0.405	0.150
Za 1226 Left	0.285	33.708	55.306	0.609	0.377	0.133	0.373	0.142
Za 1226 Right	0.308	26.077	48.583	0.537	0.034	0.085	0.434	0.159
Za 1227 Left	0.358	32.898	56.317	0.584	0.426	0.196	0.422	0.166
Za 1227 Right	0.318	39.758	63.121	0.630	0.465	0.188	0.432	0.184

Table A2: Extant calcanei structural parameters

Specimens	**DA**	**BV ($mm^{3)}$**	**TV (mm^3)**	**BV/TV**	**Tb.Th mean (mm)**	**Tb.Th sd (mm)**	**Tb.sp mean (mm)**	**Tb.sp sd (mm)**
Za 103 Left	0.535	12.953	34.239	0.378	0.267	0.107	0.608	0.203
Za 103 Right	0.533	9.923	31.555	0.314	0.276	0.12	0.731	0.231
Za 182 Left	0.722	48.951	136.655	0.358	0.307	0.123	0.737	0.251
Za 182 Right	0.613	66.489	146.964	0.452	0.346	0.118	0.663	0.25
Za 791 Left	0.678	7.753	21.634	0.358	0.236	0.079	0.629	0.182
Za 891 Left	0.608	66.678	146.964	0.454	0.347	0.118	0.662	0.249

Table A3: Extant tibiae structural parameters. Letters (C), (M) and (L) denote centre, medial and lateral facets.

Specimens	**DA**	**BV ($mm^{3)}$**	**TV (mm^3)**	**BV/TV (%)**	**Tb.Th mean (mm)**	**Tb.Th sd (mm)**	**Tb.Sp mean (mm)**	**Tb.Sp sd (mm)**
Za 103 Right (C)	0.457	2.710	9.089	0.298	0.290	0.119	0.827	0.245
Za 103 Right (L)	0.570	4.209	8.867	0.475	0.313	0.123	0.457	0.134
Za 103 Right (M)	0.499	3.990	8.867	0.450	0.326	0.148	0.555	0.225
Za 791 Left (C)	0.723	1.483	5.892	0.248	0.253	0.063	1.156	0.449
Za 791 Left (L)	0.768	2.049	5.982	0.343	0.277	0.077	0.716	0.273
Za 791 Left (M)	0.688	2.296	5.982	0.384	0.262	0.058	0.589	0.185
Za 891 Left (C)	0.294	4.657	16.814	0.277	0.301	0.134	0.762	0.228
Za 891 Left (L)	0.586	6.078	16.484	0.369	0.295	0.089	0.635	0.191
Za 891 Left (M)	0.370	6.387	16.484	0.387	0.340	0.171	0.576	0.202
Za 891 Right (C)	0.384	5.520	20.374	0.271	0.283	0.109	0.790	0.272
Za 891 Right (L)	0.469	7.922	19.633	0.404	0.304	0.088	0.587	0.202
Za 891 Right (M)	0.208	7.168	19.633	0.365	0.353	0.175	0.633	0.216

Table A4: Extant humeri structural parameters.

Specimens	**DA**	**BV ($mm^{3)}$**	**TV (mm^3)**	**BV/TV (%)**	**Tb.Th mean (mm)**	**Tb.Th sd (mm)**	**Tb.Sp mean (mm)**	**Tb.Sp sd (mm)**
Za 103 Left	0.254	7.099	21.054	0.337	0.193	0.054	0.496	0.219
Za 103 Right	0.12	6.932	22.435	0.309	0.178	0.048	0.484	0.199
Za 891 Left	0.173	19.666	81.826	0.24	0.175	0.058	0.501	0.143
Za 891 Right	0.169	24.433	84.356	0.29	0.208	0.069	0.494	0.152

Table A5: Fossil femoral heads scan resolutions

Specimen	**Resolution**	**Specimen**	**Resolution**
14954M	0.0296	SWP 1207	0.0257
16383 M	0.0374	SWP 1384	0.0402
BF 36	0.0653	SWP 1698	0.0345
SAP 756	0.0257	SWP 1699	0.0413
SK 14015	0.024	SWP 526	0.0362
SK 2595	0.025	SWP 528	0.0579
Sk 607	0.025	SWP 529	0.0293
SK 6O5	0.028	SWP 531	0.0345
SK1513	0.021	SWP 532	0.0579
sts 2050	0.018	SWP 533	0.0484
sts 2259	0.018	SWP 747	0.0294
SWP 1009	0.0353	SWP 749	0.0231
SWP 1011	0.0413	SWP 753	0.028
SWP 1203	0.0402	-	-

Table A6: Fossil calcaneus, humerus and tibia scan resolutions

Calcaneus specimens	
Specimen	**Resolution**
2222M	0.0329
SWP 537	0.0296
SWP 1146	0.0285
SWP 1157	0.0258
SWP 1161	0.0231
SWP 1207	0.0257

Humerus specimens	
Specimen	**Resolution**
1930M	0.0398
1934M	0.0597
SWP 606	0.0258
SWP 962	0.047
SWP 1406	0.0258

Tibia specimens	
Specimen	**Resolution**
SWP 1411	0.0258
SWP 1546	0.0397
SWP 1596	0.047
TP 18	0.0547

Table A7: Extant femoral heads scan resolutions

Specimen	Resolution	Specimen	Resolution
Za 103-Left	0.0441	787-Right	0.0381
Za 103-Right	0.0381	791-Left	0.0441
Za 118-Left	0.0635	791-Right	0.0369
Za 118_Right	0.0695	792-Left	0.0441
Za 127-Left	0.0615	792-Right	0.0441
Za 127-Right	0.0615	793-Left	0.0381
Za 128-Left	0.0441	793-Right	0.0381
Za 128-Right	0.0441	891-Left	0.0615
Za 168-Left	0.0695	891-Right	0.0615
Za 168-Right	0.0695	1226-Left	0.0635
Za 182-Left	0.0687	1226-Right	0.0553
Za 182-Right	0.0695	1227-Left	0.0615

Table A8: Extant humerus tibia, and calcaneus resolutions.

Humerus	Resolution
Za 103 Left	0.0443
Za 103 Right	0.0443
Za 891 Left	0.0443
Za 891 Right	0.0443

Tibia	Resolution
Za 103 Right	0.0509
za 791 left	0.0509
Za 891 Left	0.0509

Calcaneus	Resolution
Za 103 left	0.0216
za 103 Right	0.0316
Za 182 left	0.0316
Za 182 Right	0.0316
Za 791 right	0.0216

Table A9: Project budget.

Item	**Year 1**	**Year 2**
Tuition Fees	R34 290	R34 290
Scanning fees	N/A	R3 450
Transport to scan facility	N/A	R4 000
United kingdom trip	N/A	R50 000
Total	R 34 290	R 91 740
Grant total	**R 126 030**	